TECHNISCHE UNIVERSITÄT MÜNCHEN

Department Chemie

Lehrstuhl für Biotechnologie

Analysis of small heat shock proteins and their interaction with substrate proteins

Marina Angelika Kreuzeder

Vollständiger Abdruck der von der Fakultät für Chemie der Technischen Universität München zur Erlangung des akademischen Grades eines Doktors der Naturwissenschaften (Dr. rer. nat.) genehmigten Dissertation.

Vorsitzender:	Prof. Dr.	Bernd Reif
Prüfer der Dissertation	1. Prof. Dr.	Johannes Buchner
	2. Prof. Dr.	Michael Sattler

Die Dissertation wurde am 18.09.2017 bei der Technischen Universität München eingereicht und durch die Fakultät für Chemie am 02.11.2017 angenommen.

Für meine Eltern

Contents

1. Introduction

1.1 Protein folding

Proteins are a major class of bio-macromolecules. They are essential building blocks in all living organisms and play central roles in almost all cellular processes. The primary structure of proteins consists of an amino acid sequence of variable length and is composed of the 20 natural amino acids. The amino acids are covalently linked via peptide bonds connecting alpha-carboxy- and alpha-amino-groups of two neighboring amino acids.

After translation at the ribosome, each polypeptide chain has to adopt a unique three dimensional structure in order to fulfill its specific function in the cell (Ellis and Hartl, 1999). This process, which leads to the native form of the protein, is termed protein folding (Dobson and Karplus, 1999). In Anfinsen's experiment on ribonuclease A in the 1960s, he was able to show that ribonuclease did refold into its native structure *in vitro* and regained its catalytic activity. He demonstrated that protein folding is a reversible process and that the specific three dimensional structure is already determined by the linear amino acid sequence of the polypeptide chain, which, in turn, is already encoded in the DNA sequence of the correspondent gene via the genetic code (Anfinsen et al., 1961, Anfinsen, 1973).

Protein folding is a highly complex process with a vast number of different possible conformations that a polypeptide chain can adopt. The pathway of folding varies among the different proteins and there are several stable folding intermediates possible. The folded structure of a protein cannot be found by an exclusively statistical search for the native conformation as this search would take much too long to be biologically relevant. For a polypeptide of 100 amino acids in length, for example, there would be 10^{30} possible conformations (Levinthal, 1968). Reaching the one native conformation would therefore take more than one billion years. In contrast to that, most proteins adopt their native structure within a time scale of milliseconds to minutes under physiological conditions (Anfinsen, 1973, Baldwin, 1996, Creighton, 1988). This discrepancy is described as the "Levinthal's Paradox" (Levinthal, 1969).

The general idea of protein folding is that proteins adopt a thermodynamically stable state by reaching a global minimum of free energy. In the beginning of the folding process, single folding nuclei can develop in the polypeptide chain, leading to a hydrophobic collapse and a preliminary structure. The energy landscape of the folding polypeptide chain can nicely be visualized by a funnel (Dobson and Karplus, 1999, Dinner et al., 2000, Dobson et al., 1998, Dill et al., 1995). The upper edge of the funnel represents the states of high free energy of unfolded proteins whereas the native structure culminates in the global minimum (Figure 1).

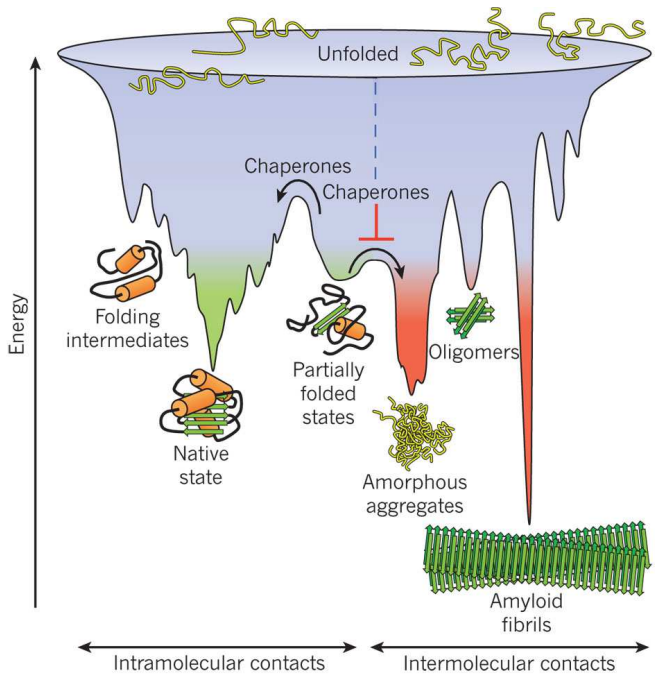

Figure 1: Scheme of the funnel-shaped free-energy surface that proteins explore as they move towards the native state (green) by forming intramolecular contacts. The ruggedness of the free-energy landscape results in the accumulation of kinetically trapped conformations that need to traverse free-energy barriers to reach a favourable downhill path. *In vivo*, these steps may be accelerated by chaperones. When several molecules fold simultaneously in the same compartment, the free-energy surface of folding may overlap with that of intermolecular aggregation, resulting in the formation of amorphous aggregates, toxic oligomers or ordered amyloid fibrils (red). Fibrillar aggregation typically occurs by nucleation-dependent polymerization. It may initiate from intermediates populated during *de novo* folding or after destabilization of the native state (partially folded states) and is normally prevented by molecular chaperones. Reprinted with the permission of the Nature Publishing Group (Hartl et al., 2011), ©2011

Proteins can adopt their native structures on many parallel downhill routes in this funnel. The wall of the funnel represents the difference in free energy ΔG which is traversed during the folding process. The free-energy surface if often rugged and local minima exist which lead to intermediate conformational states, partially folded states or even misfolded states, fibrils and protein aggregates (Udgaonkar, 2008).

Misfolded proteins or protein aggregates often impair important cellular functions and are therefore associated with ageing as well as several diseases like neurodegenerative diseases, myopathies or cancer (Morimoto, 2008).

Not only newly synthesized proteins have to find their way to the correct native conformation but also previously functional proteins, which unfold and aggregate under stress conditions in the cell. To maintain proteostasis, a huge protein quality control network consisting of different signaling pathways and components has evolved (Balch et al., 2008, Powers et al., 2009).

1.2 Cell stress and heat shock proteins

During life, all organisms have to face different types of stress conditions ranging from heat stress and oxidative stress over ethanol to heavy metals or other toxic substances. The resulting effects on the cell can be deleterious (Figure 2) and besides the unfolding of different proteins also damages and disruption of the cytoskeleton leading to a loss on intracellular structures and mislocalization of organelles and failure in transport processes have been described upon heat stress (Szalay et al., 2007, Toivola et al., 2010, Welch and Suhan, 1985, Welch and Suhan, 1986). Some organelles like the Golgi or ER become fragmented, others are decreased in their numbers as it was observed for lysosomes and mitochondria together with a harsh drop in ATP levels (Welch and Suhan, 1985, Lambowitz et al., 1983, Patriarca and Maresca, 1990). Also processes in the nucleus, like RNA splicing or processing of ribosomal RNAs are affected (Vogel et al., 1995, Welch and Suhan, 1985). In the cytosol, stress granula are formed containing components of failed translation processes including RNA (Nover et al., 1989, Buchan and Parker, 2009). But also membrane fluidity and integrity is changed (Kruuv et al., 1983, Vigh et al.,

2007). A combination of those effects leads to cell cycle arrest and furthermore to a stagnation in growth and cell proliferation (Lindquist, 1980, Yost and Lindquist, 1986, Piper et al., 2003). In terms of long and severe stress exposure, the cell finally faces cell death (Fulda et al., 2010).

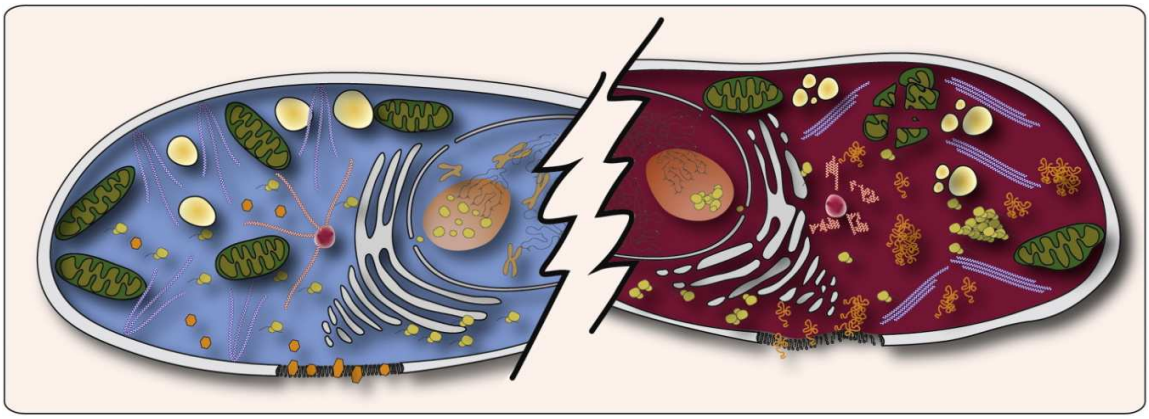

Figure 2: Effects of Heat Shock on the Organization of the Eukaryotic Cell
An unstressed eukaryotic cell (left) is compared to a cell under heat stress (right). Heat stress leads to damage to the cytoskeleton, including the reorganization of actin filaments (blue) into stress fibers and the aggregation of other filaments (microtubuli, red). Organelles like the Golgi and the endoplasmic reticulum (white) become fragmented and disassemble. The number and integrity of mitochondria (green) and lysosomes (yellow-white gradient) decreases. The nucleoli, sites of ribosome (yellow) assembly, swell, and large granular depositions consisting of ribosomal proteins become visible. Large depositions, the stress granula (yellow), resulting from assemblies of proteins and RNA, are found in the cytosol in addition to protein aggregates (hexagonal versus spaghetti style, orange). Finally, there are changes in the membrane morphology, aggregation of membrane proteins, and an increase in membrane fluidity. Together, all these effects stop growth and lead to cell-cycle arrest as indicated by the oncondensed chromosomes in the nucleus. Reprinted with the permission of Elsevier (Richter et al., 2010), ©2010

To overcome the deleterious effects of stress the cells have developed a heat shock response. The heat shock response was first discovered in the early 1970's in experiments with Drosophila (Ritossa, 1996). General functions of the heat shock response are for example the removal of misfolded and aggregated proteins from the cell via proteolysis, repair of RNA and DNA damages, restoration of the cell's energy supply by adjusting metabolic pathways, regulation of expression of further stress response pathways, maintenance of cellular structures and rehabilitation of the membrane stability but also the refolding of unfolded proteins (Ellis et al., 1989, Jantschitsch and Trautinger, 2003, Bugl et al., 2000, Malmendal et al., 2006, Voit and Radivoyevitch, 2000, Al Refaii and Alix, 2009, Welker et al., 2010, Richter et al.,

2010). According to their function, the heat shock proteins can be divided into different classes. The so called “molecular chaperones” make the biggest class of the heat shock proteins (Richter et al., 2010).

1.3 Molecular chaperones

Molecular chaperones are an evolutionary old protein class that can be found in all kingdoms of life. Representatives of this protein class have important functions in the maintenance of proteostasis by either refolding unfolded or aggregated proteins under stress conditions or by assisting de novo protein folding in co- and posttranslational processes under physiological conditions (Walter and Buchner, 2002, Buchner, 1996, Mogk and Bukau, 2004).

Especially under molecular crowding conditions in the cell, where the cytosolic protein concentration can amount for about 300 to 400 mg/ml (Ellis, 2001), molecular chaperones are important to assist the folding of newly synthetized proteins and prevent the aggregation of nonnative protein chains (Hartl and Hayer-Hartl, 2002).

Mild stress conditions in the cell can lead to the induction of chaperones and a phenomenon called hormesis, which then allows the tolerance of more harsh stress conditions lateron (Wiegant et al., 2012, Yost and Lindquist, 1986).

One feature by which molecular chaperones can discriminate between native and nonnative proteins seem to be hydrophobic amino acids that are increasingly exposed to the protein surface upon protein unfolding (Richter et al., 2010).

According to their molecular weight, molecular chaperones are classified into highly conserved families: Hsp100, Hsp90, Hsp70, Hsp60, Hsp40 and small heat shock proteins (sHsps) (Buchner, 1996, Richter et al., 2010). Except for small heat shock proteins, all those families bind their substrates in an ATP-dependent manner and are referred to as “foldases”, whereas small heat shock proteins are often referred to as “holdases”, which interact with their substrates ATP independently (Richter et al., 2010).

1.4 ATP- dependent chaperones

Substrate binding and chaperone activity of ATP-dependent chaperones relies on binding and hydrolysis of the nucleoside ATP whereby the conformational state of the chaperone is regulated and the binding affinity towards substrates or clients is mediated. The energy is provided by the hydrolysis of ATP and the release of ADP and phosphate (P).

An overview of the different molecular chaperone classes is depicted in figure 3. The chaperonin GroE machinery in bacteria consists of two heptameric rings in cylindric composition with the heptameric cochaperone GroES constituting the lid for this complex (Grallert and Buchner, 2001, Horwich et al., 2006). Nonnative proteins are bound inside the cylinders and therein are able to refold to their native structure in an isolated environment preventing any disturbing interactions with other nonnative proteins (Horwich et al., 2006, Hartl and Hayer-Hartl, 2002, Todd et al., 1994). In mitochondria closely related proteins are found: Hsp60 and Hsp10 (Richter et al., 2010).

For Hsp70 and Hsp90 there are stress-induced isoforms as well as constitutively expressed versions. The constitutively expressed Hsc70 for example mainly assists in the folding of newly synthesized proteins and their translocation and secretion, whereas the stress-induced version Hsp70 prevents aggregation and supports the refolding of nonnative proteins after the impact of stress (Mayer and Bukau, 2005).

Hsp70 proteins contain an ATPase domain and a peptide binding domain with a peptide binding cleft where typically target sequences of about 7 residues length are bound (Zhu et al., 1996). Those target peptides usually contain hydrophobic residues in their central region and occur statistically every 40 residues in proteins (Bukau and Horwich, 1998, Zhu et al., 1996). The Hsp70 system works together with a nucleotide exchange factor (NEF) and, as an activating protein, a cochaperone for example Hsp40 or J-proteins to fulfill its function (Kampinga and Craig, 2010). In prokaryotes, Hsp70 and Hsp40 are referred to as DnaK and DnaJ respectively (Richter et al., 2010, Qiu et al., 2006, Tilly et al., 1983).

Hsp90 is one of the most abundant proteins and makes about 1 % of all cellular proteins (Buchner, 1999, Catelli et al., 1985). In the presence of different stress conditions the expression of Hsp90 can even be further upregulated (Richter et al., 2010). Hsp90 consists of three domains: a highly conserved N-terminal domain which contains the ATP binding site, a middle domain, and a C- terminal domain which is needed for the dimerization of the protein (Pearl and Prodromou, 2006, Harris et al., 2004). In its functional form Hsp90 exists as a homodimer which is able to switch between open and closed conformation (Mayer, 2010, Li et al., 2012). The middle domain was shown to be essential for interaction with substrate proteins and the regulation of the ATP hydrolysis (Meyer et al., 2003, Retzlaff et al., 2010, Koulov et al., 2010). Hsp90 features a variety of interesting substrates like transcription factors (e.g. heat shock factor-1, Hsf1) steroid hormone receptors and kinases (Pratt et al., 2006, Zou et al., 1998, Hartl et al., 2011) and is therefore an interesting target in therapeutic approaches. Hsp90 closely interacts with the Hsp70 system. Together with the help of NEFs and co-chaperones, Hsp70 transfers substrate proteins to Hsp90 (Brychzy et al., 2003). For the yeast Hsp90 system, important cochaperones are Sti1/Hop and p23, by which the substrate transfer, ATPase activity and substrate release are regulated (Figure 3) (Rohl et al., 2015, Schopf et al., 2017).

The Hsp100 proteins (Clp protein in bacteria) are able to disassemble protein aggregates and are therefore often designated as unfoldases or disaggregases (Saibil, 2013). As members of the AAA+ ATPases they form hexameric rings and pull misfolded proteins through the central pore unwinding them (Neuwald et al., 1999, Hanson and Whiteheart, 2005). Some Hsp100 representatives like ClpB from *E. coli* or Hsp104 from yeast contain tandem ATPase domains and are able to completely reverse proteins aggregation together with the help of their respective Hsp70 chaperone system (Glover and Lindquist, 1998, Goloubinoff et al., 1999, Miot et al., 2011).

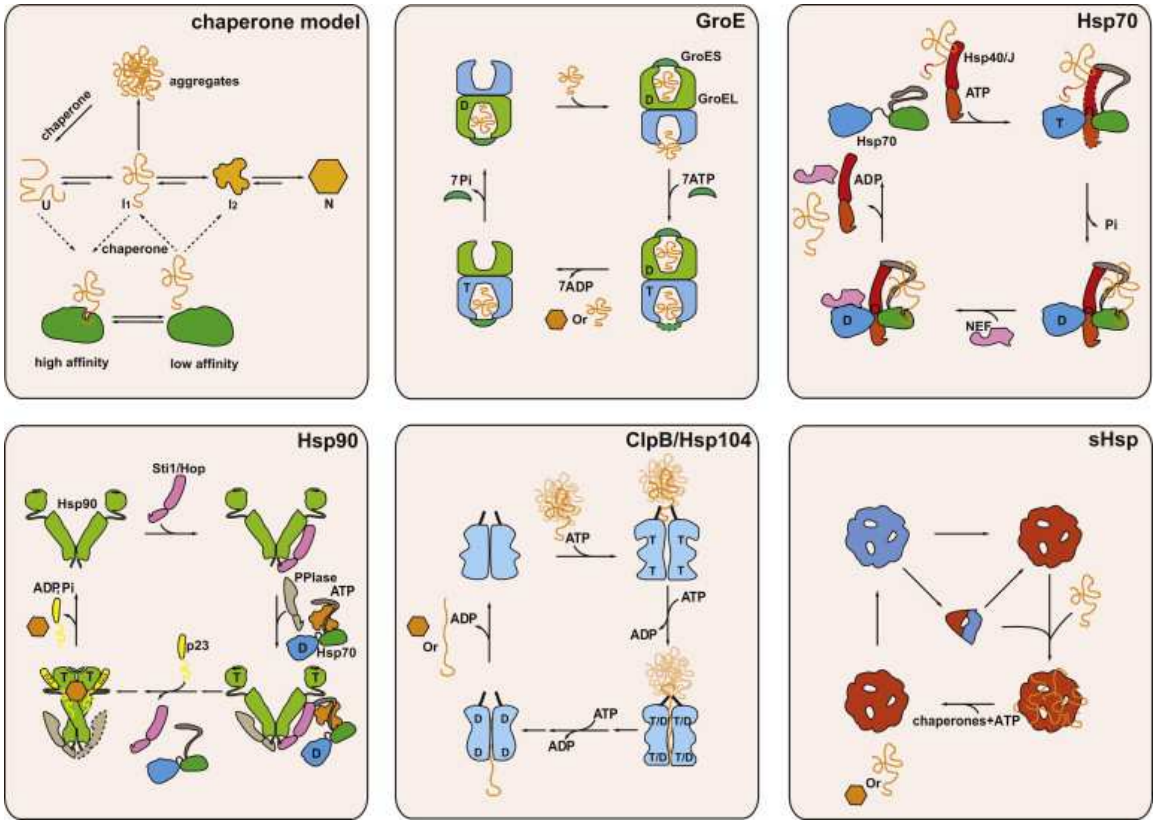

Figure 3: Molecular Chaperone Mechanisms
Chaperone model: In general, proteins fold via increasingly structured intermediates (I_1, I_2) from the unfolded state (U) to the folded state (N). Under heat shock conditions, this process is assumed to be reversed. Molecular chaperones bind proteins in nonnative conformations. The shift from the high-affinity binding state to the low-affinity release state is often triggered by ATP binding and hydrolysis.GroE: The GroE machinery in bacteria, mitochondria, and chloroplasts consists of two identical rings that enclose a central cavity each. Nonnative protein is bound by the apical domains of the rings, and upon binding of ATP and the cochaperone GroES, the protein is encapsulated and released into the cavity. Whether a complex consisting of GroEL and two GroES cochaperones or just one GroES bound is controversial; therefore the second GroES is shown with dashed lines. ATP hydrolysis in one ring results in the release of GroES and substrate protein from the opposite ring. During encapsulation the protein may fold partially or completely, depending on the characteristics of the respective substrate protein.
Hsp70: The Hsp70 system comprises two cochaperones, an activating protein (Hsp40/J-protein) and a nucleotide exchange factor (NEF). The activating protein can bind the nonnative protein and deliver it to Hsp70. It forms a complex with Hsp70 and stimulates its ATPase. The dashed line in the Hsp70-ATP complex indicates a transient interaction. It may also modulate the conformation of Hsp70 to stabilize a substrate protein-accepting state. Hsp70 binds a stretch of seven amino acids in the substrate protein. The NEF will induce the exchange of nucleotide. This further accelerates the ATPase cycle. The substrate protein is released presumably in a nonnative form.
Hsp90: In this chaperone system a large number of proteins work together. First, for a number of substrate proteins, Hsp70 delivers the substrates to Hsp90. It is not clear whether this is true for all substrate proteins and whether this occurs also under stress conditions. More than a dozen cochaperones of Hsp90 exist in eukaryotes, which seem to modulate the system. One of them, Sti1/Hop, binds both Hsp70 and Hsp90 and at the same time inhibits Hsp90s ATPase (in yeast). In this complex, which also contains an additional PPIase cochaperone, the substrate protein is transferred from Hsp70 to Hsp90. Sti1/Hop is released once Hsp90 binds nucleotide and a further cochaperone (p23). In contrast to other chaperones, the protein in complex with Hsp90 is assumed to be bound and released as a structured intermediate (such as I_2, see general chaperone scheme).
ClpB/Hsp104: In bacteria and yeast, this chaperone is able to dissolve aggregates by actively pulling proteins through a central channel of the hexameric structure. Each protomer contains two ATPase

sites, which have quite distinct characteristics concerning turnover and function. During passage through the chaperone complex, the substrate protein is unfolded. Refolding can occur upon release, and, to some extent, it can also occur in cooperation with other chaperones.
sHsps: sHps are oligomeric complexes that are often activated, e.g., by heat or modifications. Many are believed to dissociate into smaller oligomers to become active. sHsps can bind many nonnative proteins per complex. Release requires cooperation with other ATP-dependent chaperones such as Hsp70. Reprinted with the permission of Elsevier (Richter et al., 2010), ©2010

1.5 Small heat shock proteins

Small heat shock proteins (sHsps) constitute the so-called „first line of defense“ by binding to unfolding proteins in the cell and are often referred to as „holdases“. In their function as “holdases” they bind nonnative substrates in an ATP-independent manner and prevent the formation of cytotoxic aggregates (Eyles and Gierasch, 2010, Horwitz, 1992, Jakob et al., 1993). sHsps were first discovered in Drosophila in 1974 as proteins with a small molecular mass that are induced after heat shock (Tissieres et al., 1974). In general, sHsps are among the most upregulated proteins in the cell under conditions of proteotoxic stress (Stengel et al., 2010). For IbpA and IbpB of *E. coli*, for example, an upregulation of up to 300 fold after heat induction was observed (Schumann, 2006). Even though the concentration of many sHsps is strongly increased under stress conditions, there are also members of this family that are constitutively expressed and constitutively active in many organisms and tissues (Basha et al., 2012, Haslbeck et al., 2005a, Narberhaus, 2002).

1.5.1 Structure of Hsps

Primary structure

In general, the size and sequence of sHsps are very heterogeneous and poorly conserved, which was shown by a comparative analysis of 8700 identified putative sHsps in a bioinformatical approach (Kriehuber et al., 2010). The molecular weight of monomers ranges between 12 and 43 kDa, which led to the name “small heat shock proteins” (Haslbeck et al., 2005a). The most important criterion for the classification of proteins as sHsps is the presence of the conserved alpha-crystallin domain (ACD) (Kappe et al., 2010). The name of this special domain refers to the

most prominent family member: the alpha-crystallin from the mammalian eye lens (Horwitz, 2003). The ACD contains approximately 90 amino acid residues and folds into an immunoglobulin-like β-sheet sandwich consisting of up to nine antiparallel β-strands (MacRae, 2000, Horwitz, 2003). Aside of the ACD, sHsps show very little sequence similarity but they exhibit a common domain organization. The ACD is flanked by long variable N-terminal domain and a shorter C-terminal domain with the largely conserved tripeptide Ile-XXX-Ile, the so-called IXI motif (Figure 4A) (Caspers et al., 1995, de Jong et al., 1998, Kriehuber et al., 2010, Poulain et al., 2010). The N-terminal domain shows an average length of 56 aa but large variations are found herein (Kriehuber et al., 2010). In Hsp12 proteins from *C. elegans*, for example, the N-terminal domain is restricted to 25 amino acids, whereas in yeast Hsp42 this domain contains 247 residues (Haslbeck et al., 2005a). The C-terminal domain is remarkably shorter with 10 amino acids in average and exhibits the conserved IXI-motif, which is supposed to be important for inter-dimer interactions (Basha et al., 2012, Haslbeck et al., 2005a, Hilton et al., 2013).

Secondary Structure, Dimerization and Oligomerization

As described above, the ACD of sHsps folds into a β-sheet sandwich, the N-terminal domain however seems to be very flexible. The monomers of sHsps tend to form large dynamic oligomers with varying number of subunits and symmetries (Haley et al., 2000, Basha et al., 2010). Aside of the very heterogeneous homo-oligomers even the formation of hetero-oligomers consisting of different sHsps has been shown (Bova et al., 1997, Bova et al., 2000, den Engelsman et al., 2009). Hybrid approaches combining EM, NMR, crosslinking, molecular modelling, SAXS etc. are therefore used to get an idea about the structure of such polydisperse proteins (Braun et al., 2011). To further simplify the work on those heterogeneous proteins, often truncation mutants are used for structural analysis, sometimes even the isolated ACD (Chen et al., 2010).

In addition to oligomers, some sHsps have been reported to be active as dimers. For Hsp17.7 from *Deinococcus radiodurans* and AtHsp18.5 from *Arabidopsis thaliana*, for example, a stable dimer formation has been observed and chaperone activity of

those dimers could be shown *in vitro* in aggregation assays with model substrates (Bepperling et al., 2012, Basha et al., 2013).

The basic building blocks for sHsps oligomers are thought to be dimers. Here, two different modes for dimer-formation have been observed so far (Figure 4B). For bacteria, archaea and plants a dimer formation via domain-swapping is suggested. An example for this is Hsp16.9 from *T. aestivum* (wheat), where dimerization occurs by reciprocal swapping of the β6-strand into the β-sandwich of the adjacent monomer (van Montfort et al., 2001). In contrast to that, an antiparallel arrangement of the dimer was found in metazoans. In the structure of human HspB5 it could be shown that the β6 and β7 strand are fused and form an elongated β6+7 strand, which lies in antiparallel direction to the β6+7 strand of the other monomer, thereby building a dimer interface (Bagneris et al., 2009, Jehle et al., 2009, Laganowsky et al., 2010).

So far, the structures of only a few sHsps have been solved by high resolution X-ray crystallography. Among them, for example, Hsp16.9 from *T. aestivum* (van Montfort et al., 2001), Hsp16.5 from the hyperthermophile archaeon *Methanocaldococcus jannaschii* (Kim et al., 1998), Hsp17.7 from *Deinocuccus radiodurans* (Bepperling et al., 2012) and Sip1 from *C. elegans (Fleckenstein et al., 2015)*. Hsp16.5 forms a spherical complex containing 24 subunits with octahedral symmetry along with eight triangular and six square openings into the hollow center whereas Hsp16.9 is a barrel shaped dodecamer, comprised of two hexameric discs that are build up of trimers of dimers (Figure 4C). The oligomerization state of Sip1 was shown to be pH dependent. The 3.6 Å crystal structure of full-length Sip1 consists of 32 subunits forming a hollow sphere (Figure 4C). The hollow sphere is build up of two identical hemispheres consisting of antiparallel homodimers. In contrast to that, Hsp17.7 has been shown to form only dimers.

Structure, arrangement and symmetries of oligomers can vary a lot. As a common feature in the aforementioned examples, the composition out of dimers and the importance of the C-terminal IXI-motif for the stabilization of the oligomers can be named. The main differences seem to be caused by the very variable N- and C-terminal domains (Hilton et al., 2013).

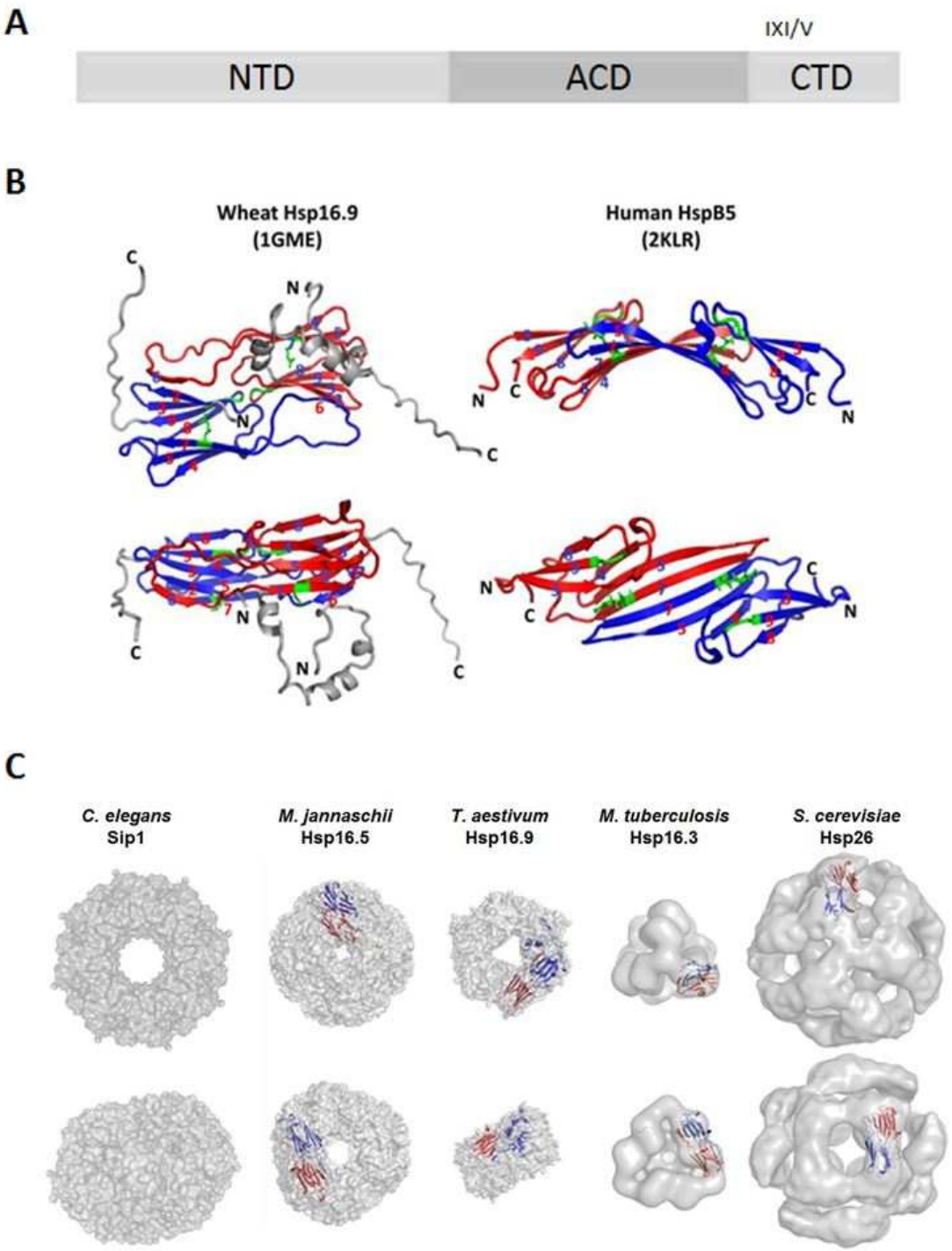

Figure 4: Structural features of small heat shock proteins.
A: Primary structure of small heat shock proteins with the conserved alpha-crystallin domain (ACD), a long variable N-terminal domain (NTD) and a short C-terminal domain (CTD) with the conserved IXI motif. B: Dimer structure of the alpha-crystallin domain of wheat Hsp16.9 (1GME; left) and human HspB5 (2KLR; right). Individual monomers are colored in red or blue. Regions outside the ACD in wheat Hsp16.9 are in gray C: Diversity of sHSP oligomer architecture. sHSP oligomeric structures derived from X-ray and EM data. Surface representations are shown in two orientations rotated by 90°. Ribbon diagrams of a single dimer structure are superimposed, although the wheat dimer (Hsp16.9) was used for the dimer structures of *Mycobacterium tuberculosis* and yeast.
B and C reprinted and adapted with the permission von Elsevier (Basha et al, 2012), © 2012

1.5.2 Function of sHsps

Small heat shock proteins exist in low and high affinity states (Haslbeck et al., 2005a). They bind to nonnative substrates in an ATP-independent way to prevent the formation of cytotoxic protein aggregates. Upon substrate binding, stable sHsp-substrate complexes are formed to keep the substrates in a refolding competent state (Stromer et al., 2003, McHaourab et al., 2009, Cheng et al., 2008). Refolding of substrates is achieved with the help of ATP-dependent chaperones (Figure 5) (Lee and Vierling, 2000, Ehrnsperger et al., 1997, Mogk and Bukau, 2004, Haslbeck et al., 2005b, Veinger et al., 1998). sHsps show a high substrate binding capacity compared to other molecular chaperones. They are able to bind one substrate molecule per subunit (Haslbeck et al., 1999, Lee et al., 1997). Therefore they are also called molecular sponges (Eyles and Gierasch, 2010).

How sHsps recognize their substrates is not clear so far. A common theory is that they recognize unfolding substrates via the exposure of hydrophobic patches on the surface. A specific recognition pattern is not known to date. Also a common substrate binding site in the sHsp itself could not be identified yet although different approaches were used (Ahrman et al., 2007, Ghosh et al., 2007, Jaya et al., 2009).

sHsps are not only involved in refolding of substrates but they were also shown to directly and indirectly iteract with the proteasome and were found to be part of ubiquitin ligase complexes (Lanneau et al., 2010, Garrido et al., 2006, Andrieu et al., 2010, Boelens et al., 2001, den Engelsman et al., 2003). Therefore sHsps seem to maintain proteostasis by mediating the coordination between refolding and degradation.

In vitro, the chaperone activity of sHsps can nicely be monitored using model substrates, whereby aggregation is followed via light scattering (Haslbeck and Buchner, 2015). In the cell, sHsps are supposed to have a rather broad substrate spectrum. Experiments with yeast showed that approximately one third of the cytosolic proteins was found in sHsp-substrate complexes upon stress (Haslbeck et al., 2004a). In some organisms more than just one sHsp is expressed at the same time in the same tissue, which leads to the assumption that in addition to a broad

overlapping substrate spectrum there might be specific substrates or functions of the different sHsps that cannot be overtaken by another sHsp.

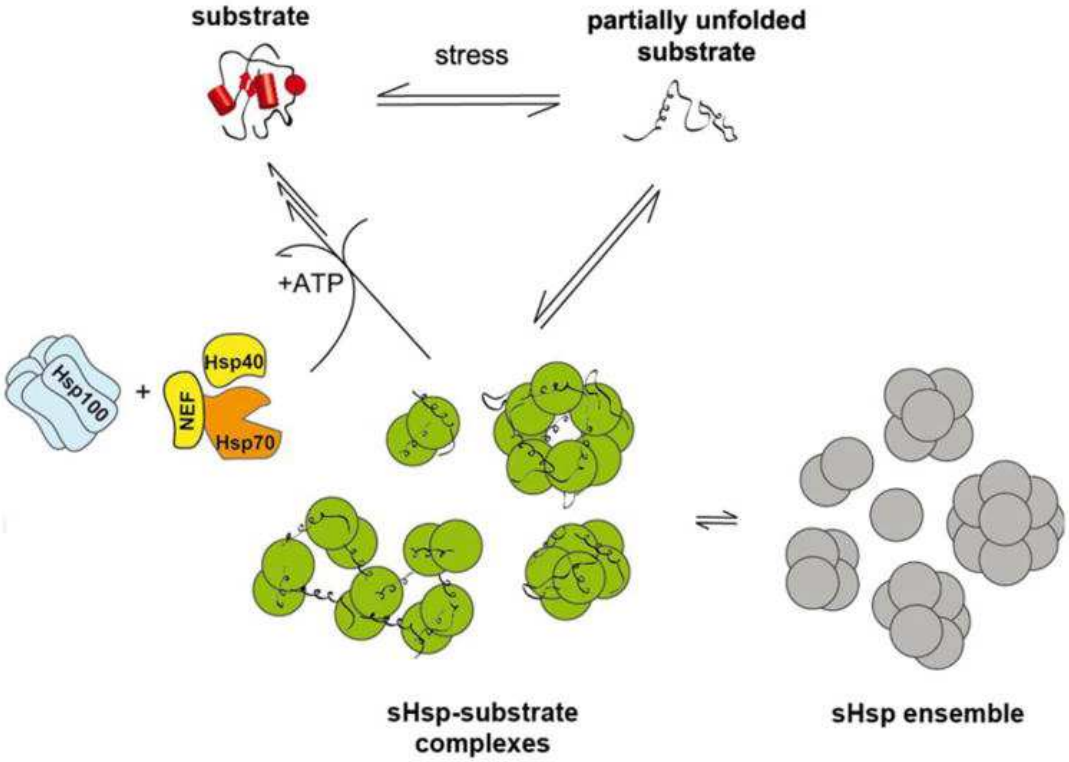

Figure 5: Model for the chaperone function of sHsps. Under stress conditions when substrate proteins are destabilized and begin to unfold, sHsps bind these partially unfolded substrates in an energy-independent manner and keep them in a folding-competent state. The physiologic ensemble of sHsp oligomers (grey) are activated (green) by a shift to a higher content of smaller species (often dimers). The substrate is stabilized by this activated ensemble of sHsps (green) and may reactivate spontaneously or is captured in stable sHsp/substrate complexes (of still enigmatic organization). Bound substrates are subsequently refolded by the ATP-dependent Hsp70 chaperone system (composed of Hsp70, Hsp40 and a nucleotide exchange factor; NEF) and may involve the Hsp100/ClpB chaperone system in cells and cellular compartments where it is found. Reprinted with the permission of Elsevier (Haslbeck et al, 2015), © 2015

1.6 sHsps in different organisms

Small heat shock proteins are ubiquitous and occur in all organisms with only a few exceptions like *Helicobacter pylori* or *Mycoplasma genitalium* (Haslbeck et al., 2005a). The origin of sHsps can be dated back quite early in evolution as they were already found in the last common ancestor of prokaryotes and eukaryotes (Kappe et al., 2002, Waters, 1995).

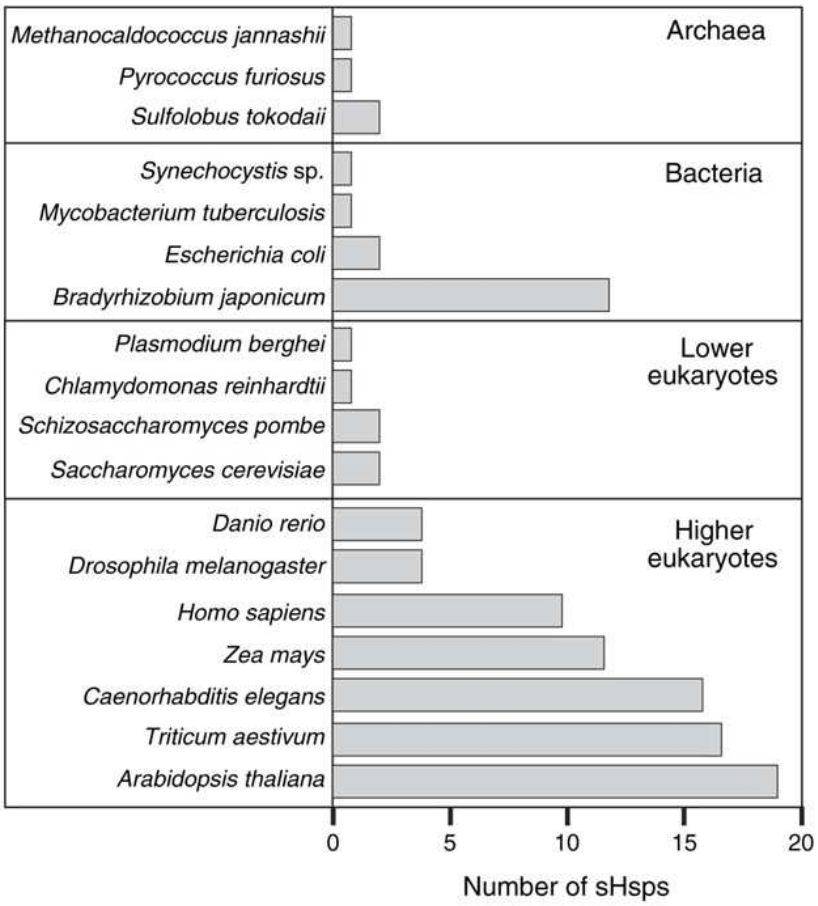

Figure 6: Schematic overview of the number of representatives of the sHsp family in different organisms. In general, from bacteria to higher eukaryotes, a substantial increase in the number of sHsps per organism is observed. Rhizobia are a notable exception to this trend. Reprinted with the permission of Nature Publishing Group (Haslbeck et al, 2005), © 2005

Archaea, prokarya and lower eukaryotes in general possess less sHsps than higher eukaryotes and plants (Figure 6). *E. coli*, *S. cerevisiae* and *S. pombe* for example contain two sHsps, *Drosophila melanogaster* and *Danio rerio* contain four sHsps and

10 sHsps are found in humans. In *C. elegans* there are 16 sHsps reported and in plants there are even more, as for example 18 sHsps in *A. thaliana*.

The occurance of high numbers of sHsps in an organism raises the question on specific functions, expression profiles and substrate spectra.

1.6.1 sHsps in *S. cerevisiae*

A popular model organism for the analysis of the stress response in lower eukaryotes is *Saccharomyces cerevisiae*, the baker's yeast. Major advantages of this organism are the easy cultivation and short generation time, accessibility of the complete genome sequence information, easy techniques for genetic manipulation and the presence of a diploid and haploid state.

Aside of ATP-dependent molecular chaperones like Hsp82, Ssa1 and Hsp104, there are two cytosolic sHsps present in *S. cerevisiae*: Hsp26 and Hsp42. Hsp42 is the larger one of the two sHsps and is constitutively expressed (Haslbeck et al., 2004a) whereas expression and activation of Hsp26 is strongly induced at elevated temperatures (Haslbeck et al., 1999). Together, Hsp26 and Hsp42 are able to suppress the aggregation of one-third of the cytosolic proteins under heat shock conditions by binding to unfolding substrates and thereby maintaining proteostasis in the cell (Haslbeck et al., 2004a). The two sHsps were shown to share a substrate spectrum of about 90% (Haslbeck et al., 2004a). However, the two cytosolic sHsps seem to execute quite distinct functions in the cell as well. Recent studies revealed an "aggregase" function of Hsp42 showing that Hsp42 can actively sequester misfolded proteins and promote the formation of cytosolic aggregates at defined deposition sites in the cell (Specht et al., 2011, Escusa-Toret et al., 2013). This function is specific for Hsp42 and cannot be taken over by Hsp26 (Specht et al., 2011). There are speculations about the role of the prion-like domain in the N-terminal extension of Hsp42 conferring this special function (Mogk and Bukau, 2017). Hsp26 instead seems to fulfill the classic function of a sHsp by binding to unfolding substrates and promoting their refolding (Ungelenk et al., 2016).

Hsp26 has a molecular mass of 23.88 kDa and consists of 214 amino acids. Residues 95-195 comprise the conserved alpha crystallin domain. The alpha crystallin domain is flanked by a short C-terminal elongation with the IXI-motif and a long N-terminal segment. The N-terminal part is separated by a glycine-rich linker into a middle domain containing the residues 31-95 and an N-terminal extension comprising residues 1-30 (White et al., 2006). Size exclusion chromatography and electron microscopy showed that the N-terminal extension is not essential for the oligomerization of the protein and also the chaperone function was not affected in the deletion mutant. However, the N-terminal domain seems to stabilize substrate complexes (Haslbeck et al., 2004b). The middle domain of Hsp26 has been shown to act as a thermosensor leading to the activation of the protein under heat stress conditions (Franzmann et al., 2008). After heat activation, Hsp26 is able to suppress aggregation of a large number of model substrates (Haslbeck et al., 2005b, Haslbeck et al., 1999, Haslbeck et al., 2004b, Franzmann et al., 2008).

Like many sHsps, Hsp26 assembles into large oligomers. The oligomeric state of Hsp26 was originally described as a 24mer based on SEC, AUC and EM analysis (Bentley et al., 1992, Haslbeck et al., 1999, Franzmann et al., 2008, White et al., 2006). A mass spectrometry-based approach published in 2010 describes the existence of different oligomeric states with up to 42 subunits (Benesch et al., 2010). Further studies on the oligomerization state of Hsp26 revealed a broad heterogeneity and a strong dependency on the ionic strength of the buffer conditions as well as the temperature (Kriehuber, 2012). Still, the arrangement of dimers into oligomers and the principles of dimer formation itself remain elusive (Chen et al., 2010).

Also, the way of activation is not solved to date. It has been shown that the Hsp26 oligomer is destabilized by heat stress (Haslbeck et al., 1999, Benesch et al., 2010) but this obviously is not essential for the chaperone function of the protein (Franzmann et al., 2005). For other sHsps, the regulation of oligomerization and chaperone activity via posttranslational modifications like phosphorylation and glycosylation is described (Nagaraj et al., 2003, Oya-Ito et al., 2006, Narberhaus, 2002). Indeed, for Hsp26 several phosphosites are already identified (Ficarro et al., 2002, Smolka et al., 2007, Albuquerque et al., 2008, Schreiber et al., 2012, Soroka et

al., 2012). Experiments with phosphomimetic mutants revealed a stronger chaperone activity without heat activation and the formation of smaller oligomers compared to the wildtype as shown by AUC and negative stain EM analysis (Kriehuber, 2012).

1.6.2 human sHsps

A search for the conserved alpha-crystallin domain in the human genome revealed the presence of 10 sHsps (Kappe et al., 2003, Seal et al., 2011). A sequence alignment (Figure 7) displays the alpha-crystallin domain, which stretches approximately from residue 118-203, as the only homologous region. The N- and C-terminal parts show high variations and only short sequence motifs e.g. positions 56-67 and 219-223 (Kappe et al., 2003).

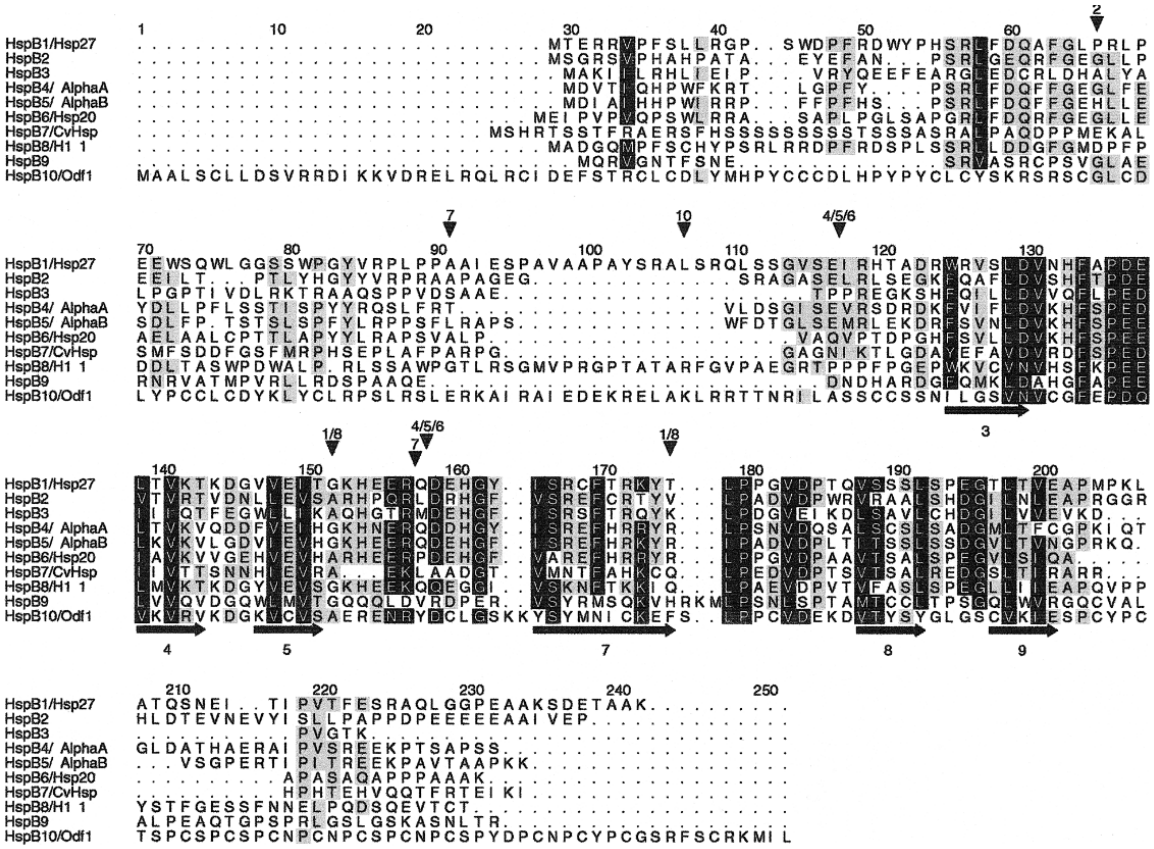

Figure 7: Alignment of the 10 human small heat shock proteins (sHsps). Intron positions and predicted secondary structure elements are indicated by arrowheads above and arrows (for ß strands) below the alignment, respectively. The α-crystallin domain is approximately located between positions 118 and 203. The alignment is made with ClustalW and manually edited in GeneDoc. Residues in black are conserved in 8 or more sHsps and those in gray in 5–7. The secondary

structure was predicted from the 10 aligned sequences with PHD (Rost and Sander 1994); predicted ß-strands are numbered according to the approximate location of the corresponding ß strands in the crystal structures of *M jannaschii* Hsp16.5 (Kim et al 1998) and wheat Hsp16.9 (van Montfort et al 2001). Numbers above the arrowheads correspond to the HspB1–10 numbering: thus, in the HspB1 and HspB8 genes, 2 introns are present at the same positions, 152 (phase 1) and 175 (phase 2); HspB2 has a single phase 1 intron, at position 66; HspB3 and HspB9 are intronless; HspB4, HspB5, and HspB6 have 2 phase 0 introns at identical positions, between 117 and 118 and between 158 and 159; HspB7 has 2 introns, at positions 91 (phase 1) and between 157 and 158 (phase 0); HspB10 has 1 phase 2 intron, at position 107. Adopted from Kappé et al. 2003 (Kappé et al, 2003)

The ten human sHsps can be divided into two classes. Some of them are ubiquitously expressed and are therefore assigned to Class I sHsps. Class I sHsps are believed to play a general role for cell survival under stress conditions. Other sHsps are expressed in specific tissues and most likely take over some more specific functions in cell differentiation or tissue development. Those sHsps belong to the Class II sHsps.

Table 1: Nomenclature, distribution and functions of human small heat shock proteins (see (Taylor and Benjamin, 2005) and references therein for details). Adapted from Bakthisaran et al., 2015 (Bakthisaran et al., 2015).

Name	Subunit MW (kDa)	pI	Tissue distribution	Stress inducibility	Class	Function
HspB1 (Hsp27)	22.8	6.4	Ubiquitous, high levels in heart, striated and smooth muscle	+	I	Chaperone activity, stabilization of cytoskeleton, anti-apoptotic and anti-oxidant function
HspB2 (MKBP)	20.2	4.8	Heart, skeletal and smooth muscle	-	II	Chaperones DMPK and enhances its kinase activity. Target protein-dependent chaperone activity, myofibrillar integrity, anti-apoptotic function, mitochondrial energetic, anti-apoptotic
HspB3	17.0	5.9	Heart, brain, skeletal and smooth muscle	-	II	Target protein-dependent chaperone activity, Maintaining myofibrillar integrity
HspB4 (αA-crystallin)	19.9	6.2	Abundant in eye lens, skeletal muscle, liver, spleen, adipose tissue (low level)	-	II	Chaperone activity, genomic stability, eye lens refractive index

Name	Subunit MW (kDa)	pI	Tissue distribution	Stress inducibility	Class	Function
HspB5 (αB-crystallin)	20.2	7.4	Ubiquitous, abundant in eye lens, High levels in heart and muscle	+	I	Chaperone activity, stabilization of cytoskeletal and nucleoskeletal matrix, cell cycle, cardioprotection, eye lens refractive index, regulation of muscle differentiation, anti-apoptotic function
HspB6 (Hsp20)	16.8	6.4	Ubiquitous, abundant in muscle	-	I	Smooth muscle relaxation, cardioprotection, chaperone activity, anti-apoptotic
HspB7	18.6	6.5	Heart and skeletal muscle. Adipose tissue (low level)	-	II	Chaperone activity, maintaining myofibrillar integrity
HspB8 (Hsp22	21.6	4.7	ubiquitous	+ (cell type dependent)	I	Chaperone activity, induction of autophagy
HspB9	17.5	9.0	Testis	-	II	Role in cancer/testis antigen
HspB10	28.3	8.4	Testis	-	II	Elastic cytoskeletal structure

The most prominent members of the human sHsps are Hsp27 (HspB1), αA-crystallin (HspB4) and αB-crystallin (HspB5). αA-crystallin and αB-crystallin constitute about 30 % of the total eye lens protein and play an important role in the prevention of cataract (Swamy and Abraham, 1991, Horwitz, 2003, Quinlan, 2015). The sHsp with the broadest distribution in different tissues is Hsp27, which seems to be the most essential of the human sHsps (Sugiyama et al., 2000). In addition to that, also very specifically expressed sHsps are found, like HspB9 and HspB10, which are only found in testis (Kappe et al., 2001, Gastmann et al., 1993).

For several human sHsps, interactions with components of the cytoskeleton have been reported. Binding of Hsp27, αB-crystallin and Hsp20 to actin has been shown, as well as interaction of Hsp20 with the actin-crosslinking protein actinin (Tessier et al., 2003). Hsp27 has been shown to interact with keratin (Kayser et al., 2013), whereas αB-crystallin associates with intermediate filaments like vimentin and desmin (Nicholl and Quinlan, 1994, Song et al., 2008). Besides the regulation of cytoskeleton dynamics and prevention of aggregation of the different cytoskeleton components, sHsps further assist in filament-filament interactions (Garrido et al., 2012, Perng et al., 1999), display important anti-apoptotic functions and play an important role in cell differentiation. Loss of function of human sHsps leads to severe diseases like cataract, myopathies and neurodegenerative diseases (Acunzo

et al., 2012, Balch et al., 2008, Sun and MacRae, 2005, Shinohara et al., 1993, Renkawek et al., 1994, Mymrikov et al., 2011).

1.6.3 sHsps in *C. elegans*

A BLAST-Search revealed 16 potential sHsps in the *C. elegans* genome with a molecular mass between 12 and 45 kDa. Based on their alpha-crystallin domains, a sequence alignment was performed (Figure 8) which shows the *C. elegans* sHsps in relation to each other (Weinfurtner, 2008). The Hsp16 core family is highlighted in red, consisting of two subfamilies Hsp16.11/Hsp16.2 and Hsp16.41/Hsp16.48. In blue the extended Hsp16 protein family is depicted which includes the embryo specific Sip1 and the two proteins F08H9.3 and F08H9.4. All Hsp16 and Hsp17 genes are located on chromosome V, except for sip1, which is located on chromosome III (WormBase 2017).

F08H9.3 and F08H9.4 are still named after their gene locus on chromosome V. They share 50 % sequence identity with the Hsp16 core family and are therefore the closest relatives of the the Hsp16 proteins. F08H9.3 and F08H9.4 contain one intron each and are regulated by one or two HSEs respectively (Shim et al., 2003). Both proteins are expressed constitutively in all developmental stages in a tissue- specific manner. Expression of F08H9.3 is observed in the pharynx of *C. elegans* whereas F08H9.4 is found in the excretory channel, in some neurons and under heat stress conditions in the gut cells as well (Shim et al., 2003). Under heat stress conditions, RNAi knockdown of F08H9.4 led to increased lethality whereas under non-stress conditions no effect of the knockdown was observed (Shim et al., 2003).

Sip1 is a 17.8 kDa protein in *C. elegans* and is the largest member of the extended Hsp16 protein family. Sip-1 exhibits a basic isoelectric point (pI) of 7.9, which is higher than the intracellular pH of *C. elegans* of 6.3 (Wadsworth and Riddle, 1988). Sip1 is exclusively expressed in developing oocytes and embryos and in the gonads of adult nematodes (Candido, 2002, Levin et al., 2012, Linder et al., 1996, Tabuse et al., 2005, Kohara, 2005). Thermotolerance assays with a sip1 deletion strain showed that Sip1 is essential in adults and embryos for the survival of heat shock (Fleckenstein et al., 2015). By electron microscopy and X-ray crystallography Sip1

could be determined to form a range of well-defined globular assemblies of two half-spheres consisting of dimeric building blocks (Fleckenstein et al., 2015). Interestingly, the oligomeric state and the chaperone activity of Sip1 seems to be regulated by changes in the pH. Under slightly acidic conditions, consistent with the lower pH in oocytes, Sip1 was found to be more active and formed smaller oligomers (Fleckenstein et al., 2015).

Aside of the Hsp16 protein family there is the Hsp12 protein family in *C. elegans* consisting of Hsp12.1, Hsp12.2, Hsp12.6 and Hsp12.3 with an average size of 12 kDa. Expression studies showed that Hsp12.6 is mainly expressed in early larval stages. Expression in adult worms is limited to cells in the vulva and spermatheca (Ding and Candido, 2000a). Compared to other sHsps, this protein family has strongly shortened N- and C-terminal regions and the members of this protein family are not able to form large oligomers. For Hsp12.1, Hsp12.2 and Hsp12.3 a tetrameric organization was reported *in vitro* (Kokke et al., 1998, Krause, 2013). Hsp12.6 is even reported to be monomeric (Leroux et al., 1997a). The Hsp12 family also seems to lack chaperone activity in assays with model substrates (Leroux et al., 1997b, Kokke et al., 2001, Leroux et al., 1997a).

Hsp25 is a 23.5 kDa protein which is expressed in all developmental stages and located to the body wall muscle cells and the pharynx (Ding and Candido, 2000b). Binding of Hsp25 to vinculin and α-actinin but not to actin has been shown (Candido, 2002) and localization to the M-lines and myofibrils has been reported (Ding and Candido, 2000b). Knockdown of Hsp25 by RNAi did not disclose any phenotype (Ding and Candido, 2000b).

Hsp43 is the only sHsps in *C. elegans* that is located on chromosome X. With a molecular mass of 43.2 kDa it is the largest of the sHsps in *C. elegans*. It is expressed constitutively in all developmental stages and expression is not increased upon heat stress (Ding and Candido, 2000c). In adult worms, localization of Hsp43 is observed in vulva and spermathecal cells. Also localization in body wall muscles was observed (Ding and Candido, 2000a). RNAi experiments did not show any phenotype (Ding and Candido, 2000c, Candido, 2002).

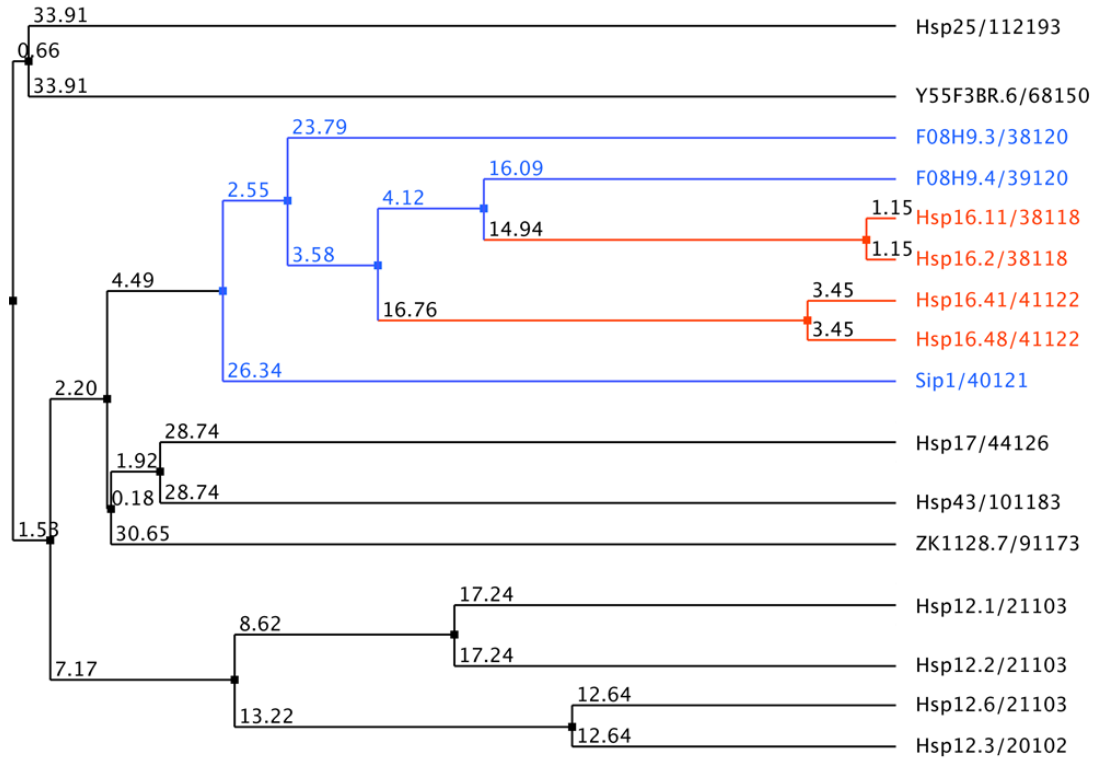

Figure 8: The sHsps in *C. elegans*. Relation of the 16 sHsps in *C. elegans* based on their alpha-crystallin domain. Depicted in blue is the extended Hsp16 protein family with the Hsp16 core family in red. Figure adapted from Weinfurtner (2008).

1.6.3.1 The Hsp16 core family

The Hsp16 genes are organized as tandem pairs in two inversely oriented gene loci named hsp16.1/48, hsp16.11/49 and the hsp16.2/41 locus respectively (Russnak and Candido, 1985, Jones et al., 1986). The gene loci contain overlapping promotor regions with two regulatory heat shock elements (HSE) each 15 nucleotides upstream of the TATA-box (Candido, 2002). The two HSEs are able to induce expression of the hsp16 gene pairs bidirectionally (Stringham et al., 1992).

Each gene consists of an exon of 42-46 amino acids which encodes the variable N-terminal region followed by an intron of 46-58 base pairs and another exon which encodes the alpha-crystallin domain and the C-terminal extension. The gene pair hsp16.1/48 is present twice on chromosome V in exactly opposite directions, which may originate from a former gene duplication or conversion (Jones et al., 1986).

Expression of all four members of the core family is induced by heat stress whereas mRNA and the corresponding proteins are not detectable in worms under non-stress conditions (Russnak et al., 1983, Weinfurtner, 2008, Candido, 2002, Kohara, 2005). Expression takes place in all developmental stages after gastrulation (Candido, 2002) but is highest in L1 larvae and is continuously reduced towards older stages (Stringham et al., 1992, Candido, 2002). Under heat stress conditions the four Hsp16 proteins were ubiquitously expressed in almost all tissues with a maximum expression of hsp16.1/48 in gut cells and pharynx. It has also been shown that expression can be induced by alternative stressors like oxidizing agents, alcohols, heavy metals and fungicides (Jones et al., 1996, Shin et al., 2011, Jones and Candido, 1999, Candido, 2002). Under chemical stress conditions the expression pattern was tissue specific especially in cells that were particularly exposed to the reagents, for example gut and pharynx (Stringham and Candido, 1994).

Proteins of the two Hsp16 subfamilies share 93 % sequence identity and 70 % sequence identity between the two subfamilies. The best studied representative of the Hsp16 family is the protein Hsp16.2. Hsp16.2 was shown to form oligomers *in vitro* and *in vivo* (Hockertz et al., 1991, Leroux et al., 1997b). Size exclusion chromatography revealed oligomers of about 500 kDa, whereas based on sedimentation experiments with AUC two smaller oligomeric populations of 239 and 395 kDa, which would hint to a 24 mer, were reported (Leroux et al., 1997b). These differences might indicate the formation of a hollow sphere, leading to different sedimentation behavior depending on the compactness of the oligomer (Weinfurtner, 2008). The Hsp16.2 oligomers were shown to have chaperone activity in thermally or chemically induced aggregation assays with citrate synthase. Deletion of 15 amino acids from the C-terminus were shown to form slightly larger oligomers whereas the chaperone activity remained unchanged. Deletion of the amino acid residues 15-44 of the N-terminal region (Hsp16.2Δ15/ Hsp16.2Δ44) lead to the disruption of the oligomeric species to monomers, dimers and trimers accompanied with a loss in chaperone function (Leroux et al., 1997b).

Comparative analysis of the Hsp16 core family showed less chaperone activity for Hsp16.41 and Hsp16.48 in *in vitro* assays with the model substrate citrate synthase compared to Hsp16.11 and Hsp16.2 when aggregation during thermal unfolding was

monitored (Weinfurtner, 2008, Fleckenstein, 2014). However aggregation of model substrates at lower temperatures (20 °C) after chemical unfolding could effectively be suppressed by Hsp16.41 and Hsp16.48 (Weinfurtner, 2008). Oligomeric associations were observed for all four proteins of the Hsp16 core family in analytical size exclusion and ultracentrifugation experiments. The oligomeric size was in the range of about 360-500 kDa, suggesting the formation of 22-30mers (Weinfurtner, 2008). The analysis of those oligomers via electron microscopy revealed spherical molecules with an average diameter of 12 nm. Three-dimensional reconstruction suggested 24 subunits per oligomer (Weinfurtner, 2008, Kastenmüller, 2011). Subunit exchange between Hsp16.11 and Hsp16.2 was observed by FRET experiments and even the formation of hetero-oligomers was possible (Weinfurtner, 2008). RNAi experiments revealed that both Hsp16 subfamilies are essential for thermotolerance in ΔHsf1-worms. Loss of one member of the subfamily can be rescued by the other member, but complete knockdown of a subfamily leads to lethality under heat stress conditions. This leads to the assumption that both subfamilies have essential distinct functions that cannot be fulfilled by other proteins (Weinfurtner, 2008).

Hsp16.11, together with Hsf1, has been shown to play an important role in the mediation of higher heat-stress tolerance by maintaining Ca^{2+} homeostasis under heat stroke (Tavernarakis, 2012). Hsp16.2 has been shown to directly interact with Aβ peptides *in vivo*, and thereby reducing Aβ toxicity (Fonte et al., 2008).

1.7 Objectives

Small heat shock protein constitute a very old and diverse protein family that is found in all domains of life. In this work sHsps of the three different organisms *S. cerevisiae*, *H. sapiens* and *C. elegans* were analyzed.

In the first part of this thesis, Hsp26, one of the two cytosolic sHsps in *S. cerevisiae*, was investigated. So far, the structural organization of Hsp26 is not completely understood. To reduce complexity, truncation mutans of Hsp26 were cloned, purified and analyzed for their structural propensities. The truncation mutants were used for NMR experiments with the aim to elucidate the mode of dimerization of Hsp26. With the knowledge of the dimer-interface and in combination with cryo- EM experiments a structural model of Hsp26 should be determined. Furthermore the regulation of Hsp26 via phosphorylation was assessed by the investigation of Hsp26 phosphomimetic mutants.

In the second part of this thesis, the substrate spectra of human sHsps were analyzed. The ten human sHsps differ in their expression pattern, activity and biochemical properties (Mymrikov et al., 2017). This leads to the question if they fulfill individual functions in the cell or if they work together redundantly and to some extent share the same substrates. With a mass spectrometric analysis after co-immunoprecipitation the substrate spectra of the human sHsps were identified and subjected to a bioinformatical analysis.

The third part of this thesis focused on the Hsp16 core family in *C. elegans*. Here, a comparative analysis regarding the structure and chaperone activity of Hsp16.11, Hsp16.2, Hsp16.41 and Hsp16.48 was performed. Chaperone activity was assessed with the help of model substrates *in vitro*, but also in *C. elegans* lysates. A sophisticated LFQ mass spectrometry approach allowed the determination of substrate spectra of the four different proteins after co-immunoprecipitation experiments with *C. elegans* lysate.

2. Material

2.1. Chemicals and media components

^{13}C-Glucose	Cambridge Isotope Laboratories
^{15}N-Ammoniumchloride	Cortecnet
2-Iodoacetamide	Merck
2-Mercaptoethanol	Roth
2-Propanol	Roth
Acetic acid	Roth
Acetonitrile LiChrosolv®	Merck
Acrylamid/Bis solution 38:2 (40% w:v)	Serva
Agar Agar	Serva
Agarose	Serva
Ammonium persulfate (APS)	Roth
Ampicilin sodium salt	Roth
Bromphenolblue	Serva
$CaCl_2$	Merck
Dan Klorix	Dan Klorix
Cholesterol	Sigma
Citric acid monohydrate	Merck
Coomassie Brilliant Blue R-250	Serva
$CuSO_4$*5H_2O	Merck
D_2O	Euriso-top
Deoxynucleoside triphosphates (dNTPs)	Roche
Dithiothreitol (DTT)	Roth
Ethylenediaminetetraacetic acid disodium salt (EDTA)	Merck
Formic Acid	Sigma
Glycerol	Roth
Glycine	Roth
Guanidinium chloride (GdnCl)	Merck
H_2O LiChrosolv®	Merck
HCl	Merck

Hepes	Roth
Iodoacetamide	Merck
Isopropyl β-D-1-thiogalaktopyranoside (IPTG)	Serva
K_2HPO_4	Merck
Kanamycin sulfate	Roth
KCl	Roth
KH_2PO_4	Merck
KOH	Roth
LB medium	Serva
MES	Roth
Methanol	Roth
$MgSO_4$	Merck
Milk powder	Roth
$MnCl_2*4H_2O$	Merck
MOPS	Roth
$Na_2HPO_4*2H_2O$	Merck
NaCl	Merck
NaOH	Merck
NaH_2PO_4	Merck
Sodium deoxycholate	Sigma
NH_4HCO_3	Fluka
Nonidet P-40 Substitute	Roche
Pepstatin A	Roth
Peptone	BD
Phenylmethanesulfonyl fluoride (PMSF)	Sigma
Protease Inhibitor Mix G	Serva
Sodium dodecylsulfate (SDS)	Serva
Stain Clear G	Serva
TEMED	Roth
Tetracyclin Hydrochloride	Roth
Tri-potassium citrate monohydrate	VWR Chemicals
Tris	Roth
Triton-X100	Merck

Tween-20	Merck
Urea	Merck
WesternBright™ ECL-Spray	Advansta
$ZnSO_4*7H_2O$	Sigma

2.2 Consumables

Amicon Ultra-15 Centrifugal Filter Units	Millipore
Amicon Ultra-4 Centrifugal Filter Units	Millipore
Blotting paper	Whatman
Centrifuge Filter, 0.22 µm	Merck Millipore
Chromacol Vials, 9mm, Polypropylene, 300 µl	Thermo Scientific
Chromacol Closures, 9mm, white Silicone/Red PTFE	Thermo Scientific
Cuvettes, plastic, 1 ml	Brand
Cuvettes, plastic, semi-micro	Brand
Dialysis membranes Spectra/Por (various MWCOs)	Spectrum Laboratories
Glass beads, 0.25-0.5 mm	Roth
Roti®-Fluoro PVDF, 0.2 µm	Roth
Ultracel Ultrafiltration disc 3 kDa NMWL, 76 mm and 44.5 mm	EMDMillipore
Ultracel Ultrafiltration disc 10 kDa NMWL, 76 mm and 44.5 mm	EMDMillipore
PCR tubes	BioRad Laboratories
PE tubes, 15 and 50 ml	Greiner Bio One
Petri dishes, PS, 94 mm und 60 mm	Greiner Bio One
pH indicator	Merck
Protein G Sepharose 4 Fast Flow	GE Healthcare
Reaction tubes, 0.5 ml, 1.5ml and 2 ml	Sarstedt
Reaction tubes, 0.5 ml	Eppendorf
SERVAGel™ TG PRiME™ 4-20%, 15 sample wells	Serva

Solid Phase Extraction Disk, C18, 47 mm	Empore™
UV cuvettes, plastic, micro	Brand
Xpress Micro Dialyzer MD300	Scienova

2.3 Oligonucleotides

Hsp26 Primer:

alphaM2(76-194)_fwd	GCAGATCCCATGGGAAATGACTTGTCCCTG
alphaM2(76-194)_rev	GATCTGCGCGGCCGCTTACTGAGGCTTC
alphaM3(76-201)_rev	GATCTGCGCGGCCGCTTAGACGTGGTTCTTACC
26(76-206)_rev	GATCTGCGCGGCCGCTTAAACCTCAATCTTC
26(95-206)_fwd	GCAGATCCCATGGGAGTTGATATTTTGGACC

2.4 Substrate proteins

In chaperone activity assays following proteins were used as model substrates:

Malate dehydrogenase (MDH), from pig heart mitochondria	Roche
Citrate synthase (CS)	Roche

2.5 Antibodies

Antibody	Host	Source
anti-human HspB1	mouse monoclonal	StressMarq
anti-human HspB2	rabbit polyclonal	abcam
anti-human HspB3	rabbit	Sigma-Aldrich
anti-human HspB4	mouse monoclonal	StressMarq
anti-human HspB5	mouse monoclonal	StressMarq
anti-human HspB6	mouse monoclonal	Prof. A. Katrukha
anti-human HspB7	rabbit monoclonal	abcam
anti-human HspB8	mouse	Prof. A. Katrukha
anti-CeHsp16.48	rabbit	Pineda
anti-rabbit IgG- Peroxidase	goat	Sigma- Aldrich
anti-mouse IgG-Peroxidase	rabbit	Sigma- Aldrich

2.6 Enzymes, standards and kits

1 kb DNA Ladder	NEB
100 bp DNA Ladder	NEB
5x Bradford Reagent	Serva
DNaseI	AppliChem
Gel Filltration Standard	BioRad
NcoI-HF®	NEB
NotI-HF®	NEB
Pierce™ BCA Protein Assay Kit	Thermo Scientific
Protein-Marker IV (Prestained)	Peqlab
Pwo DNA polymerase	Roche
T4 DNA Ligase	Promega
Trypsin (Sequencing Grade Modified Trypsin)	Promega
Wizard® Plus SV Minipreps DNA Purification System	Promega
Wizard® SV Gel and PCR Clean-Up System	Promega

2.7 Strains

E.coli		
Strain	**Genotype**	**Origin**
BL21-CodonPlus® (DE3) RIL	F$^-$ *ompT hsdS*(r_{B^-} m_{B^-}) *dcm*+ Tetr *gal endA* Hte [*argU proL* Camr]	Stratagene
HB101	thi-1, hsdS20 (r_{B^-},m_{B^-}), supE44, recA13, ara-14, leu B6, pro A2, lacY1, rpsL20 (strr), xyl-5, mtl-1	Promega
Mach1	F– Φ80*lac*ZΔM15 Δ*lac*X74 *hsd*R(rK–, mK+) Δ*rec*A1398 *end*A1 *ton*A	Invitrogen
OP50	Unknown	CGC (Minneapolis, USA)
HT115 (DE3)	F-, mcrA, mcrB, IN(rrnD-rrnE)1, rnc14::Tn10	CGC (Minneapolis, USA)
C. elegans		
Strain	**Genotype**	**Origin**
N2	WT	Caenorhabditis Genetics Center (CGC)
sy441	Hsf1-226STOP	Caenorhabditis Genetics Center (CGC)
tm1221	ΔHsp16.11	Shohei Mitani
VC475	ΔHsp16.2	Caenorhabditis Genetics Center (CGC)
tm1093	ΔHsp16.41	Shohei Mitani
RB791	ΔHsp16.48	Caenorhabditis Genetics Center (CGC)

2.8 Chromatography materials and columns

Acclaim PepMap RSLC C18 trap column, 75µm x 20 mm, 3 µm, 100 Å	ThermoFisher Scientific
PepMap RSLC C18 column,75 µm x 150mm, 2 µm, 100Å	ThermoFisher Scientific
PepMap RSLC C18 column,75 µm x 500mm, 2 µm, 100Å	ThermoFisher Scientific
Resource-Q, 6 mL	GE Healthcare
Superdex 200 26/60	GE Healthcare
Superdex 75 16/60	GE Healthcare
Superdex75 26/60	GE Healthcare
Q Sepharose Fast Flow	GE Healthcare
SP Sepharose Fast Flow	GE Healthcare
TSK G4000PW HPLC gel filtration	Tosoh Bioscience

2.9 Devices

Amicon Bioseparations Stirred Cells	EMD Millipore
Autoclave Varioclav EP-Z	H+P
Bead Mill MM400	Retsch
Cell Disruption Apparatus Basic Z	Constant Systems
Centrifuges	
Avanti J25 and J26 XP	Beckman Coulter
Optima XL-I	Beckman Coulter
Rotina 420R	Hettich
Tabletop centrifuge 5418	Eppendorf
Tabletop centrifuge 5415 C	Eppendorf
Chromatography systems	
ÄKTA FPLC P-920	GE Healthcare
equipped with	
UPC-900 UV-detecor	GE Healthcare
Frac-900/950 fraction collectors	GE Healthcare
Superloops (various volumes)	GE Healthcare

Circular dichroism spectropolarimeters	
J710 (with PTC 343 Peltier device)	Jasco
J715 (with PTC 343 Peltier device)	Jasco
Thermomixer comfort	Eppendorf
Gel documentation system Biodoc II	Biometra
Gel electrophoresis and blotting devices	Hoefer
Homogeniser Ultra Turrax DIAX900	Heidolph
HPLC system	
LC-20AT liquid chromatograph	Shimadzu
equipped with	
SIL-20AC autosampler	Shimadzu
SPD-20A detector	Shimadzu
RF-10A XL detector	Shimadzu
Ice maker	Ziegra
ImageQuant 300 Imager	GE Healthcare
ImageQuant LAS4000 system	GE Healthcare
Incubator	mytrom
Incucell	MMM Medcenter
Magnetic stirrer Heidolph Hei-Standard	Heidolph
Mass spectrometers	
LTQ Orbitrap XLTM Hybrid Ion Trap MS	ThermoFisher Scientific
Orbitrap Fusion Tribrid MS	ThermoFisher Scientific
Ultraflex II MALDI ToF/ToF	Bruker Daltonics
Microscope Stemi 2000 with a CL1500 Eco cold light source	Zeiss
pH meter	WTW
Polymax 2040	Heidolph
Power amplifiers EPS 301	amersham pharmacia
Power amplifiers GPS 200/400	Pharmacia
Rotator SB3	Stuart
Savant™ DNA120 SpeedVac™ Concentrator	Thermo Scientific
Scales	
SI-4002	Denver Instrument

SI-234	Denver Instrument
Thermoblock TB 1	Biometra
Ultrasonic cleaner USC-T	VWR
UV-Vis spectrophotometers	
Ultrospec 1100 pro	Amersham Biosciences
Varian Cary 50 Bio	Agilent
NanoDrop1000	Peqlab
Vortex Genie 2	Scientific Industries
Water bath F12	Julabo

2.10 Software

Adobe Illustrator CS5	Adobe Inc.
Chromeleon	Thermo Fisher Scientific
DCDT+	John Philo
EndNote Web	Thomson Reuters
Image J	Rasband, W.S.
ImageQuant LAS 4000	GE Healthcare
ImageQuant TL	GE Healthcare
MassMatrix	Hua Xu
MaxQuant 1.5.3.8	Jürgen Cox
Microsoft Office 2010	Microsoft
MMass	Open Source
Origin 8.6	OriginLab Corp.
Perseus 1.5.3.2	Jürgen Cox
Proteome Discoverer 1.4	Thermo Scientific
Pymol	Schrödinger
RawMeat	Vast Scientific
SedFit	Peter Schuck
Sednterp	John Philo
SedView	Hayes, Stafford

UltraScan	Borries Demeler
Xcalibur	Thermo Fisher Scientific

2.11 Databases

BioGRID	https://thebiogrid.org/
PaxDB	www.pax-db.org
PDB	www.rcsb.org/pdb
PubMed	www.ncbi.nlm.nih.gov/pubmed
UniProt	www.uniprot.org

2.12 Web-based tools

ClustalW2	http://ebi.ac.uk/Tools/msa/clustalw2/
NCBI Blast	http://blast.ncbi.nlm.nih.gov/
ProtParam	http://web.expasy.org/protparam/
Idt OligoAnalyzer	http://eu.idtdna.com/calc/analyzer
PantherDB	http://pantherdb.org
GRAVY Calculator	http://gravy-calculator.de

3. Methods

3.1 Molecular biology

3.1.1 Polymerase chain reaction

Polymerase chain reaction (PCR) is used to amplify DNA *in vitro*. In a first step, the DNA double strand is denatured, then the primers anneal to the DNA region with the corresponding complementary sequence and in a final step the DNA strand is elongated by a polymerase.

PCR was performed to amplify DNA for analytical or preparative use. The reaction mixture and conditions are shown below.

PCR reaction mixture:

10x Polymerase Buffer	5 µl
dNTPs (10 mM per dNTP)	2 µl
Template DNA	0.5 µl
5'-Primer (10 pmol/µl)	1 µl
3'-Primer (10 pmol/µl)	1 µl
Pwo DNA Polymerase (5U/µl)	1 µl
ddH2O	39.5 µl

PCR reaction conditions:

Cycles	Temperature	Time
1x	95°C	5 min
30x	95°C	30 s
	55°C	45 s
	72°c	1 min
1x	72°C	5 min

Hsp26 fragments were amplified by using forward primer containing a 5‘ NcoI- and reverse primer containing a 3‘ NotI restriction site. Primer were designed with a low GC content and analyzed for hairpin structures using Idt OligoAnalyzer (https://eu.idtdna.com/calc/analyzer). As polymerase the Pwo DNA Polymerase (Roche) from the hyperthermophilic archaebacterium *Pyrococcus woesei* was used.

The success of the polymerase chain reaction was assessed using agarose gel electrophoresis.

3.1.2 Agarose gel electrophoresis

For analytical or preparative reasons DNA samples were separated by agarose gel electrophoresis.
1g Agarose was dissolved in 100 ml TAE buffer and 4 µl DNA stain clear G (Serva) solution was added to allow for detection via UV light. DNA loading dye was added to the samples prior loading them on the gel. To estimate the size of the separated DNA fragments 5 µl of 1 kb DNA ladder or 100 bp DNA Ladder (NEB) were loaded as a standard to the gels.
Agarose gel electrophoresis was performed for 20 min at a constant power of 100 V in TE buffer. The gels were analyzed under UV-light in an ImageQuant 300 Imager (GE Healthcare).

TAE (50x):	Tris/Acetate pH 8.0	2 M
	EDTA	50 mM
DNA loading dye (5x):	Glycerol	50 % (v/v)
	EDTA (pH 8.0)	10 mM
	Bromphenolbue	0.2 % (v/v)

3.1.3 Isolation of DNA fragments from Agarose gels

To isolate DNA fragments from agarose gels the corresponding bands were excised using a scalpel and were further treated with the Wizard® SV Gel and PCR Clean-Up System (Promega) according to the manufacturer's protocol. The obtained DNA was stored in nuclease-free water at -20 °C or directly used for further cloning.

3.1.4 Restriction digest and ligation

To ligate the PCR product of interest into the target vector, both, purified PCR product and vector have to be digested in separate reactions with the specific restriction enzymes. Restriction digest was performed for 5 h at 37 °C. The composition of the reaction mixture is shown below.

Digestion mixture:

DNA	50 µl
CutSmart buffer (NEB)	6 µl
NcoI HF (NEB)	2 µl
NotI HF (NEB)	2 µl

Both digests were purified using the Wizard® SV Gel and PCR Clean-Up System (Promega) according to the manufacturer's protocol. For ligation, the digested and purified vector and PCR product were combined in a 1:5-ratio in a total volume of 20 µl and 1 µl T4 DNA Ligase (Promega) was added with the corresponding buffer. Ligation was performed at 4 °C overnight.

Ligation mixture:

Vector	1µl
Insert	5 µl
10x Ligase Buffer	1µl
T4 DNA Ligase (Promega)	1µl
H_2O	2µl

The ligation product was used to transform chemically competent Mach1 cells. Mach1 cells were used to amplify the cloned plasmid. Plasmids were isolated from Mach1 cells and checked for the right sequence as described in chapter 3.1.6 and 3.1.7.

3.1.5 Transformation of *E.coli*

For the transformation of *E. coli,* 200 µl of chemically competent Mach1 cells and 20 µl of PCR or ligation product or 200 µl of chemically competent BL21 cells and 1 µl of plasmid solution were incubated on ice for 20 min. The mixtures were heat-shocked at 42 °C in a water bath and immediately cooled down on ice again. The transformed cells then were diluted with 1 ml LB_0 and incubated for 1 h at 37 °C and 850 rpm in a table top incubator. The cell suspension was either directly used to inoculate liquid cultures or harvested, resuspended in 100 µl LB_0 and subsequently plated on LB-Agar plates with the corresponding antibiotic for selection and incubated overnight at 37 °C.

3.1.6 Preparation of plasmid DNA from *E. coli*

Preparation of plasmid DNA from *E. coli* was performed using the Wizard® Plus SV Minipreps DNA Purification System (Promega) according to the manufacturers' protocol. The DNA was stored in nuclease-free water at -20°C.

3.1.7 DNA-sequence analysis

The correct sequence of all plasmids used in this work was verified by sequence analysis. DNA sequencing was carried out by GATC Biotech AG (Konstanz, Germany) or Eurofins (Ebersberg, Germany). A DNA concentration between 50-100 ng/µl was used.

3.2 Protein analytics

3.2.1 Determination of protein concentration

3.2.1.1 Bradford-Assay

To determine the protein concentration of protein mixtures, e.g. in cell lysates, a Bradford Assay was performed (Bradford, 1976). This assay is based on a shift of the absorption maximum of the coomassie dye when it binds to proteins in an acidic environment. The 5x Bradford reagent (Serva) was diluted in a 1:5 ratio in H_2O. 1 ml of diluted Bradford reagent was mixed with 100 µl of the unknown protein solution or BSA (Pierce™ Bovine Serum Albumin Standard, Thermo Fisher Scientific) solutions with defined concentrations. The samples were incubated for exactly 10 min at room temperature. Then the absorbance at 595 nm was determined. The BSA samples were used to generate a standard curve. The protein concentration of the unknown protein samples was determined with the help of the BSA standard curve.

3.2.1.2 BCA-Assay

To determine the protein concentration in presence of detergents the Pierce™ BCA Protein Assay Kit (Thermo Scientific) was used. The assay allows for colorimetric detection and quantification of the total protein amount in the sample using a reagent containing bicinchoninic acid. The working reagent and BSA standard protein solutions were prepared according to the manufacturer's protocol. A volume of 50 µl BCA standard solution or protein solution to be determined was mixed with 1 ml of working reagent and incubated for 30 min at 37°C in a water bath. All samples were cooled down to room temperature and analyzed in a spectrophotometer at 562 nm within 10 min. The protein concentration of the unknown sample was determined with the help of the plotted BSA standard curve.

3.2.2 SDS-Polyacrylamid-Gelelectrophoresis (SDS-PAGE)

To separate proteins according to their molecular mass, discontinuous SDS-PAGE was performed using a modified protocol of Laemmli (Laemmli, 1970). Depending on the molecular mass of the proteins 12.5 %, 15 % or 18 % separation gels were used in combination with a 5 % stacking gel. Samples were mixed with Laemmli sample loading buffer and denatured at 95 °C for 5 min. Separation of proteins was carried out at 30 mA for 35-50 min in Laemmli running buffer. To estimate the size of the separated proteins 4 µl of prestained Protein-Marker IV (Peqlab) were loaded as a size standard to the gels.

Separation gel buffer (2x):	Tris/HCl, pH 8.8	1.5 M
	SDS	0.8 % (w/v)
Stacking gel buffer (4x):	Tris/HCl, pH 6.8	250 mM
	SDS	0.4 % (w/v)
Laemmli sample loading buffer (5x):	Tris/HCl, pH 6.8	300 mM
	SDS	10 % (w/v)
	Glycerol	50 % (v/v)
	2-Mercaptoethanol	5 % (v/v)
	Bromphenol bue	0.05 % (w/v)
Laemmli running buffer (10x):	Tris/HCl	250 mM
	Glycine	2 M
	SDS	1 % (w/v)

3.2.3 Staining of SDS-PAGE gels according to Fairbanks

To visualize the separated proteins, the SDS-PAGE gels were stained with Fairbanks A and destained with Fairbanks D solution (Fairbanks et al., 1971). The Coomassie dye binds unspecifically to proteins whereas the gel itself can be destained by 10 % acetic acid. To reduce the incubation time the gels were heated up in the respective solution.

Fairbanks A:	2-Propanol	25 % (v/v)
	Acetic acid	10 % (v/v)
	Coomassie Blue R 250	0.05 % (w/v)
Fairbanks D:	Acetic acid	10 % (v/v)

3.2.4 Western-blotting

Proteins that were separated by SDS-PAGE can be transferred to a PVDF membrane by semi dry western blotting and afterwards be detected by specific antibodies. Therefore, a Semi Dry Blot Apparatus (Biometra, Göttingen, Germany) was used. The PVDF membrane was activated by incubation for 60 seconds in methanol, washed with water and incubated in Western blot transfer buffer for a few seconds. The SDS-gel and the activated membrane were embedded between two layers of 3 Whatman-Papers each that were soaked with transfer buffer and placed between the electrodes of the blotting apparatus. Proteins were blotted to the membrane for 90 min at 1.5 mA/cm^2 SDS-PAGE gel. The transfer efficiency was monitored by migration of the molecular weight marker. The membrane was blocked with 5 % milk powder in PBS-T overnight at 4 °C shaking to saturate unspecific protein binding sites. After washing the membrane three times for 10 min with PBS-T, the primary antibody was added in dilutions between 1:2000 and 1:6000 in 1 % milk powder in PBS-T and incubated for 60 min. After three more washing steps with PBS-T for 10 min, the membrane was incubated with the appropriate secondary

horseradish peroxidase-conjugated antibody in a 1:10,000 dilution in PBS-T for 60 min and washed again three times with PBS-T for 10 min. Antibody binding was visualized by chemiluminescence detection using the WesternBright™ ECL-Spray (Advansta) and the ImageQuant LAS 4000 system (GE Healthcare). Analysis of the chemiluminescence signal was performed with ImageQuant LAS 4000 Software (GE Healthcare) and ImageJ (Schneider et al., 2012).

Western blot transfer buffer:	Tris, pH 9.0	48 mM
	Glycine	39 mM
	Methanol	20 % (v/v)
	SDS	0.037 % (w/v)
PBS-T, pH 7.4 :	KH_2PO_4	4 mM
	Na_2HPO_4* 2 H_2O	16 mM
	NaCl	115 mM
	Tween-20	0.1 % (v/v)

3.3 Preparative methods

3.3.1 Cell disruption

E. coli cell suspension was mixed with Protease Inhibitor Mix G (Promega, Madison, USA). Cell disruption was performed in a high pressure cell disruption system BasicZ (ConstantSystems, Daventry, United Kingdom) at 1.8 kbar. Some DNaseI (PanReac AppliChem) was added to the lysate. The lysate was cleared from cell fragments and other insoluble components by centrifugation at 40,000 x g at 8 °C for 45 min in a Beckman Avanti J-26 XP centrifuge with a JA-25.50 rotor. In case of inclusion body production the lysate after cell disruption was treated as described in chapter 3.5.1.

3.3.2 Concentration of proteins

Pressure- based sample concentration of protein volumes higher than 10 ml were carried out with Amicon Stirred Ultrafiltration Cells (Millipore). Therefore ultracel ultrafiltration discs with a molecular weight cutoff of 3 kDa or 10 kDa were used. Pressure was adjusted by a constant nitrogen-flow pressing the solution through the membrane whereas the protein was retained. To avoid protein aggregation or clogging of the membrane the solution was slowly stirred. Concentration of native proteins was carried out at 4 °C whereas concentration of proteins in denaturing buffers was performed at room temperature.

For concentration of small volumes Amicon Ultra Centrifugal Filter Units with a cutoff of 3 kDa were used in a tabletop centrifuge at 3,000 x g.

3.3.3 Dialysis of proteins

To exchange the protein buffer solution, proteins were dialyzed overnight at 4 °C in large excess of target buffer. Spectral/Por dialysis tubes (Spectrumlabs) with a molecular weight cutoff of 6-8 kDa were used. For small volumes dialysis was performed with Xpress Micro Dialyzer MD300 (Scienova) according to the manufacturers' protocol.

3.4 Chromatography

All columns were cleaned with 1 M NaOH solution and ddH_2O before use.

3.4.1 Ion exchange chromatography

Ion exchange chromatography was used to separate proteins according to their charge. Therefore a chromatographic matrix with covalently bound charged residues is used as a stationary phase. The charged side chains of the proteins compete with ionic compounds in the mobile phase. Therefore, binding and elution buffer have to be adjusted according to the chemical properties of the specific target protein. The net charge of the protein depends on its isoelectric point (pI) and the pH of the buffer. In this work the cation exchange SP-Sepharose and the anion exchange Q-Sepharose and Resource Q were used. The columns were equilibrated with the appropriate loading buffer by washing with 5-10 column volumes. The cleared lysate or protein solution was loaded to the column and washed with 5 column volumes of loading buffer. Bound proteins were eluted via competitive displacement with high salt buffer using a linear salt gradient ranging from 0 M to 1 M NaCl. Fractions were analyzed using SDS-PAGE.

3.4.2 Size exclusion chromatography

Using size exclusion chromatography the proteins could be separated according to their hydrodynamic radius. The principle of this method is a column matrix with defined pores leading to a longer retention time for small proteins whereas larger proteins can permeate faster through the column matrix. In this work Superdex 75 and Superdex 200 were used for preparative size exclusion chromatography.

3.5 Expression and Purification of Proteins

3.5.1 Expression and purification of CeHsp16 proteins

Hsp16 proteins were purified under denaturing conditions. For the expression of Hsp16 proteins *E. coli* BL21 (DE3)-CodonPlus cells were transformed with the pET-21a(+) vector containing the respective Hsp16 gene. The transformed cells were directly used to inoculate a 50 ml overnight culture with LB-medium and Ampicillin (100 µg/ml) as a selection marker. The overnight culture was grown at 37 °C and 180 rpm. The next, day 2 l cultures were inoculated with the overnight pre-culture to a optical density of OD_{595}= 0.025. The cultures were further grown at 37°C and 180 rpm until OD_{595} = 0.7-0.8 was reached. Then, protein expression was induced by adding 1 mM IPTG. Protein expression was carried out overnight at 37 °C and 180 rpm. Under these expression conditions the Hsp16 proteins form insoluble inclusion bodies. Cells were harvested by centrifugation for 20 min and 6,000 rpm at 4 °C. For centrifugation a Beckman Avanti J-26 XP centrifuge with a JA-10 rotor was used. The pelleted cells were resuspended in 50 ml ice-cold IB-Buffer added with 1 ml Protease Inhibitor Mix G (Serva). Cell disruption was performed as described in section 3.3.1.

1 % Triton X-100 was added to the lysate and stirred for at least 1 h at 4 °C. Then the inclusion bodies were harvested by centrifugation at 20,000 rpm for 25 min at 8 °C in a Beckman Avanti J-26 XP centrifuge with a JA-25.50 rotor. The pellet containing the inclusion bodies was washed with IB buffer three times. The inclusion bodies were either stored at -20 °C or directly used for further purification.

Inclusion bodies were resuspended in IB-dissolving buffer and dissolved by stirring for 2 h at room temperature. Insoluble parts were separated by centrifugation for 20 min at 20,000 rpm and 25 °C in a Beckman Avanti J-26 XP centrifuge with a JA-25.50 rotor. The cleared supernatant was loaded to a Q-sepharose equilibrated in Buffer B1 and eluted using a gradient of 0-100 % Buffer B2. The collected fractions were analyzed by SDS-PAGE as described in 3.2.2. Fractions containing the protein of interest were pooled and loaded to a SP-sepharose equilibrated in Buffer B1 and were eluted using a gradient of 0-100 % Buffer B2. Again the success of purification was assessed by SDS-PAGE. Selected fractions were pooled and the volume was

reduced to 10 ml as described in 3.3.2 using a membrane with a 3 kDa cutoff. In a next step the concentrated sample was applied to a Superdex 75 26/60 equilibrated in Buffer F and, after analysis by SDS-PAGE, the fractions containing the protein of interest in high purity were pooled.

Refolding was performed using a Superdex 200 26/60 equilibrated in PBS. Fractions containing correctly folded Hsp16 protein were pooled and dialyzed overnight against 5 l of PBS at 4 °C as described in 3.3.3. Purified proteins were concentrated to the desired concentration and flash-frozen in liquid nitrogen after 5 % glycerol had been added to the protein solution. Proteins were stored at -20°C.

IB-Buffer:	50 mM Tris, pH 7.5 10 mM EDTA 50 mM NaCl
IB-dissoving Buffer:	50 mM Tris, pH 7.5 5 mM EDTA 6 M Urea 10 mM β-Mercaptoethanol
Buffer B1:	50 mM Tris, pH 7.5 5 mM EDTA 50 mM NaCl 5 mM DTT 6 M Urea
Buffer B2:	50 mM Tris, pH 7.5 5 mM EDTA 1 M NaCl 5 mM DTT 6 M Urea

Buffer F:	50 mM Tris, pH 7.5
	5 mM EDTA
	150 mM NaCl
	5 mM DTT
	4 M Guanidinhydrochloride
Phosphate-buffered saline (PBS):	8.1 mM $Na_2HPO_4*2H_2O$, pH 7.4
	1.76 mM KH_2PO_4
	137 mM NaCl
	2.7 mM KCl

3.5.2 Expression and purification of human αB- crystallin

For the production of αB-crystallin, chemically competent *E. coli* BL21 (DE3)-CodonPlus cells were transformed with the pET28b plasmid containing the αB-crystallin wildtype gene. The transformed cells were directly used to inoculate a 50 ml overnight culture with LB-medium and Kanamycin (35 µg/ml) for selection. The overnight culture was grown at 37 °C and 180 rpm. The next day 2 l cultures were inoculated with the overnight pre-culture to a optical density of OD_{595}= 0.04. The cultures were further grown at 37 °C and 180 rpm. At OD_{595} = 0.8 the cultures were cooled down on ice. Then, protein expression was induced by adding 1 mM IPTG. Protein expression was carried out overnight at 30 °C and 180 rpm. Cells were harvested by centrifugation for 20 min and 6,000 rpm at 4 °C. For centrifugation a Beckman Avanti J-26 XP centrifuge with a JA-10 rotor was used. The pelleted cells were resuspended in 50 ml ice-cold Buffer A added with 1 ml Protease Inhibitor Mix G (Serva). Cell disruption was performed as described in section 3.3.1.

The cleared supernatant was loaded to a Q-sepharose column equilibrated in Buffer A and eluted using a linear gradient of 0-50 % Buffer B. The collected fractions were analyzed by SDS-PAGE as described in 3.2.2.

Fractions containing the protein of interest were pooled, concentrated to a volume of 10 ml as described in 3.3.2 and loaded to a Superdex75 26/60 column

equilibrated in PBS. Fractions of 3 ml were collected and analyzed by SDS-PAGE. Fractions of adequate purity were pooled and dialyzed overnight at 4 °C in PBS-buffer as described in 3.3.3. Protein aliquots were frozen in liquid nitrogen and stored at -20 °C.

Buffer A:	50 mM Tris, pH 8.2 2 mM EDTA
Buffer B:	50 mM Tris, pH 8.2 2 mM EDTA 1 M NaCl
Phosphate-buffered saline (PBS):	8.1 mM Na_2HPO_4*$2H_2O$, pH 7.4 1.76 mM KH_2PO_4 137 mM NaCl 2.7 mM KCl

3.5.3 Expression and purification of ScHsp26wt and truncation mutants

Hsp26 wt and truncation mutants were either expressed in LB- medium or, if labeled protein was required, in M9 medium with the specific components which contribute to ^{13}C, ^{15}N or D_2O labelling.

For expression in LB- medium, chemically competent *E. coli* BL21 (DE3)-CodonPlus cells were transformed with the pET28b-vector containing the DNA- sequence for the respective Hsp26 construct. The transformed cells were directly used to inoculate a 50 ml overnight culture. For selection 35 µg/ml Kanamycin were added to the LB-medium. The culture was grown overnight at 37 °C and 180 rpm. The overnight culture was used to inoculate 1-2 l of LB-medium + Kanamycin (35 µg/ml)

to an OD_{595} = 0.025. The culture was incubated at 37 °C and 180 rpm. At OD_{595}= 0.6-0.8 protein expression was induced by adding 1 mM IPTG. Expression was carried out overnight at 37 °C and 180 rpm.

Proteins that were used for NMR experiments had to be incorporated either with ^{13}C, ^{15}N, D_2O or a combination of those three labels. Therefore, expression had to be performed in the defined M9 medium. First, the *E. coli* BL21 (DE3)-CodonPlus cells were transformed as described above. The transformed cells were used to inoculate two times 5 ml LB with Kanamycin (35 µg/ml) added. These precultures were grown overnight at 37 °C rotating. The precultures were spinned down and the cell pellets were used to inoculate 50 ml M9 medium with 35 µg/ml Kanamycin added. After incubation for 8 h at 37 °C and 180 rpm the cells were harvested again and used to inoculate 100 ml M9 medium with Kanamycin (35µg/ml) added. The culture was grown overnight at 37 °C and 180 rpm. The whole 100 ml culture was added to 900 ml M9 medium plus 35 µg/ml Kanamycin and incubated at 37 °C and 180 rpm until OD_{595}= 0.8 was reached. Then, the culture was cooled down on ice and 1 mM IPTG was added. Protein expression was carried out at 30 °C and 180 rpm overnight.

Cells were harvested in a Beckman Avanti J-26 XP centrifuge with a JA-10 rotor for 20 min and 6,000 rpm at 4 °C. The pelleted cells were resuspended in 25 ml ice-cold Buffer A added with 1 ml Protease Inhibitor Mix G (Serva). Cell disruption was performed as described in section 3.3.1.

The cleared supernatant was loaded to a SP-sepharose equilibrated in Buffer A and eluted using a linear gradient of 0-100 % Buffer B. The collected fractions were analyzed by SDS-PAGE as described in 3.2.2.

Fractions containing the protein of interest were pooled, concentrated to a volume of 10 ml as described in 3.3.2 and loaded to a Superdex75 26/60 equilibrated in Buffer C. Fractions of 5 ml were collected and analyzed by SDS-PAGE. If adequate purity was reached, the fractions were pooled and dialyzed overnight at 4 °C in NMR-buffer as described in 3.3.3. In case of insufficient purity, the protein was further purified using a Resource Q column.

Protein aliquots were either directly used for NMR-experiments or frozen in liquid nitrogen and stored at -20 °C.

Buffer A:	20 mM Hepes, pH 6.0 10 mM NaCl 5 mM EDTA
Buffer B:	20 mM Hepes, pH 6.0 500 mM NaCl 5 mM EDTA
Buffer C:	20 mM Hepes, pH 6.8
NMR-Buffer:	20 mM NaP, pH 6.5 50 mM NaCl

3.6 Spectroscopical methods

3.6.1 UV/VIS-Spectroscopy

UV-Vis spectroscopy can be used for the analysis of biomolecules. For proteins the absorbance of their aromatic tryptophan, tyrosine and phenylalanine residues can be observed at 280 nm, whereas the absorption of the peptide bonds can be monitored at 230 nm. Protein concentrations were determined by their specific absorbance at 280 nm. The molar extinction coefficients ε depend on the particular amino acid composition of each protein (Pace et al., 1995). To calculate the theoretical extinction coefficients the ProtParam tool (Wilkins et al., 1999) was used. When applying the Beer-Lambert law (equation 1) it is possible to calculate the molar concentration of the absorbing substance with known molar extinction coefficient (Atkins, 2013):

$$A = \varepsilon \cdot c \cdot d \qquad (1)$$

A	=	absorbance [a.u.]
ε	=	molar extinction coefficient [M^{-1} cm^{-1}]
c	=	molar protein concentration [M]
d	=	path length [cm]

The absorbance was determined in a NanoDrop1000 or Cary 50 spectrophotometer and was baseline corrected for buffer absorbance.

3.6.2 Chaperone activity assays

To assess the chaperone activity of proteins *in vitro,* chaperone activity assays were performed. The ability to suppress aggregation of thermally or chemically induced unfolding of model substrate proteins was analyzed. Aggregation was followed by measuring the increase in pseudo-absorbance at 360 nm in a Cary 50 spectrophotometer. For temperature regulation the cuvette chamber of the spectrophotometer was connected to a water bath. As substrate proteins L-Malat-Dehydrogenase (MDH) and Citrate Synthase (CS) were used.

MDH is known to aggregate at 42 °C due to thermally induced changes in the native structure (Hartman et al., 1993). As a buffer for MDH aggregation assays, filtered and degassed PBS was used. MDH concentration was adjusted to 2 µM. The concentration of the chaperones was varied between 0.25 µM and 8 µM. Measurements were carried out until saturation of the substrate aggregation was reached.

Citrate synthase (CS) is a heat sensitive protein which aggregates at 42 °C (Buchner et al., 1998). The experiments were performed in 20 mM Hepes-KOH, pH 7.5 until saturation of the substrate aggregation was reached. CS was added to a final concentration of 1 µM to the reaction whereas the concentration of chaperones was varied between 2 µM and 10 µM.

To analyze the chaperone activity at lower temperatures, chemically denatured Citrate synthase (CS) was added to the buffer which already contained varying concentrations of the sHsps. The aggregation of the model substrate was followed at 25 °C.

3.6.3 CD-Spectroscopy

Using CD spectroscopy, information about the structure of proteins can be obtained. The principle of this method is based on the fact that proteins exhibit different extinction coefficients for left and right hand circularly polarized light mainly due to chiral structure elements. This difference can be measured and is referred to as ellipticity θ.

$$\Delta A(\lambda) = A_L(\lambda) - A_R(\lambda) = [\varepsilon_L(\lambda) - \varepsilon_R(\lambda)]lc = \Delta\varepsilon lc \qquad (2)$$

A	=	absorption
λ	=	wavelength
L	=	left-handed circular polarized
R	=	right-handed circular polarized

The measured ellipticity is concentration dependent and can be converted to the mean residue ellipticity, which reflects the ellipticity in relation to the average molecular weight of the amino acids of the proteins. Herefore the following equations was used:

$$\theta_{MRW} = \frac{\theta \cdot 100 \cdot M}{d \cdot c \cdot N_{AA}} \qquad (3)$$

θ_{MRW}	=	mean residue ellipticity [deg cm^2 dmol^{-1}]
θ	=	ellipticity [deg]
d	=	path length [cm]
c	=	concentration [M]
N_{aa}	=	numbers of amino acids

The far-UV region (260-170 nm) is used to get information about the secondary structure elements of the protein. Depending on the secondary structure of the protein characteristic shapes of spectra are observed. Proteins that are rich in β-sheets exhibit one specific minimum at around 218 nm, whereas α-helical proteins

show two local minima at 222 nm and 208 nm. Random coil structures lead to a minimum at 200 nm in the spectrum.

CD-Spectra were measured in a 0.5 mm quartz cuvette (Hellma) in a Jasco J-715 Circular Dichroism (CD) spectropolarimeter. The experimental parameters were used as shown below.

Parameters of CD-spectroscopie measurements

wavelength	260 – 200 nm
data pitch	0.2 nm
scanning mode	continuous
speed	20 nm/min
response	4 s
bandwidth	1 nm
accumulations	7

3.6.4 Analytical Size Exclusion Chromatography

Analytical Size Exclusion Chromatography can be used to analyze the oligomeric state of proteins. The stationary phase of the column consists of matrix beads with defined pore size. Proteins are separated according to their size as smaller proteins diffuse into the pores while larger proteins don't fit into the pores and therefore pass the matrix faster (Porath and Flodin, 1959). The retention times of the analyzed proteins were compared to the retention times of a gel filtration standard (BioRad). The standard mixture contains the proteins γ-Globulin with a molecular mass of 158 kDa, Ovalbumin with 44 kDa, Myoglobin with 17 kDa and Vitamin B12 with 1.35 kDa. The elution times of the standard proteins were determined under the respective conditions and were plotted against the logarithm of the molecular weight. For analysis, a Shimadzu HPLC system equipped with a SPD-20A detector and a fluorescence detection system RF-10A XL was used. Detailed information on each experiment is shown in section 4.

3.6.5 Analytical Ultracentrifugation

To analyze different hydrodynamic parameters of proteins in solution without disturbing matrix interactions, analytical ultracentrifugation (AUC) can be performed. Separation is achieved by application of a centrifugal force to the protein solution. Sedimentation of the proteins is monitored in "real-time" by absorption, interference or fluorescence spectroscopy. The sedimentation process itself depends on three factors: gravitation, buoyancy and the hydrodynamic friction. These three factors are taken into account in the Svedberg equation (equation 4) (Patel et al., 2016, Lebowitz et al., 2002):

$$s = \frac{v}{\omega^2 r} = \frac{MD(1-\bar{\bar{V}}\rho)}{RT} \qquad (4)$$

s	=	sedimentation coefficient [s]
v	=	observed radial velocity [m/s]
ω	=	angular velocity of the rotor [m/s^2]
$\omega^2 r$	=	centrifugal field
M	=	molecular weight [g/mol]
$\bar{\bar{V}}$	=	partial specific volume [cm^3/g]
ρ	=	density of the solvent [g/cm^3]
D	=	diffusion coefficient [m^2/s]
R	=	gas constant [8.314472 J/K mol]
T	=	absolute temperature [K]

In this thesis, sedimentation velocity experiments were performed. Therefore a high centrifugal force is applied to an initially evenly distributed protein solution. The proteins start sedimenting whereby the protein concentration at the meniscus decreases continuously and the protein concentration at the bottom of the AUC-cell increases. The sedimentation coefficient is dependent on the size and shape of a protein. Usually large proteins sediment faster than small proteins. As every species shows its own sedimentation front this method can be used to analyze the homo- or heterogeneity of a sample containing a complex protein mixture.

For sedimentation velocity experiments 400 µl of a protein sample were centrifuged in a 2-channel cell with quartz windows of 12-mm path length using a ProteomeLab XL-I (Beckman, Krefeld, Germany) with an eight-hole Beckman-Coulter AN-50 Ti rotor. The experiments were performed at 20 °C and 30,000 rpm. Dependent of the sample concentration sedimentation was monitored at 230 or 280 nm.

Data analysis was performed using the dc/dt+ version 2.4.1 by John Philo (Philo, 2006, Stafford, 1992) or Sedfit (Schuck, 2000) with a non-model based continuous Svedberg distribution method (c(S)), with time (TI) and radial (RI) invariant noise (Schuck, 2000, Brown et al., 2011).

3.6.6 Electron Microscopy

The electron microscopy experiments in this thesis were performed in collaboration with the group of Prof. Dr. Sevil Weinkauf (Technical University of Munich, Garching). EM experiments and data analysis were conducted by Dr. Beate Roeckel. A detailed analysis of the EM method is published elsewhere (Braun et al., 2011, Peschek et al., 2009).

3.7 Mass spectrometry

3.7.1 Co-Immunoprecipitation

3.7.1.1 human

The Co-Immunoprecipitation experiments with human sHsps were carried out by Dr. Evgeny Mymrikov as described in Mymrikov *et al.*, 2017 (Mymrikov et al., 2017). HEK293 lysate with a concentration of 0.8 mg/ml was incubated with 10 µM sHsp in PBS, 1 mM DTT for 90 min at 45 °C in a water bath. The samples were chilled down on ice and incubated for 1 h with the corresponding antibodies at 4 °C with constant mixing. After that Protein G Sepharose was added and incubated for 2 h at 4 °C with constant mixing. Three to four washing steps with ice-cold PBS-T (PBS containing 0.1 % Tween 20) were applied to remove unbound proteins. Bound sHsp-substrate complexes were eluted using 0.1 M glycine buffer, pH 2.5. As a reference the total HEK293 heat-sensitive protein fraction was analyzed. Therefore 0.8 mg/ml HEK293 lysate was incubated for 90 min at 45 °C. After heat shock, soluble and insoluble fraction were separated by centrifugation for 10 min at 8,600 x g. The pellet was washed twice with ice- cold PBS and dissolved in 1-fold Laemmli buffer prior analyzing the samples by SDS-PAGE. The CoIPs were performed in triplicates in two different experiments (CoIP1 and CoIP2). For CoIP1, samples were analyzed on 15 %, for CoIP2 4-20% precasted SDS-gels (Serva Electrophoresis GmbH) followed by mass spectrometry. The Coomassie-stained gel lanes were cut into 5 pieces each and treated as individual samples. Each sample was cut into pieces of approximately 1-2 mm^2. The gel pieces were stored at -80 °C or directly used for in-gel digest and extraction.

3.7.1.2 C. elegans

Protein G Sepharose was washed three times with IP-buffer. To minimize unspecific binding of lysate components 450 µl of *C. elegans* lysate (~ 18 mg/ml protein) were preincubated with 50 µl protein G- sepharose for 4 hours at 5 °C rotating. The sepharose was removed by centrifugation and 50-75 µl (~ 1 mg protein) of lysate were incubated together with 10 µg sHsp for 45 min at 37 °C to allow binding of the sHsps to their specific substrates. In control samples, equal volumes of buffer were added to the lysate instead of sHsp. Then, 10 µl of the corresponding α-sHsp-

antibody were added and the samples were incubated for 1 hour at 5 °C rotating. After 1 hour, 50 µl protein G- sepharose, that was pre-equilibrated by washing three times in IP-buffer was added and the samples were rotated overnight at 5 °C. The samples were centrifuged and the supernatant was separated from the pellet. The sepharose pellet was washed twice for 20 min with 1 ml IP-buffer, twice for 20 min with 1 ml high salt buffer and once with 1 ml low salt buffer. The washing steps were carried out at 5 °C.

To analyze the samples via SDS-PAGE, 25 µl 1x Lämmli were added to the sepharose pellet and heated to 95 °C for 5 min.

For quantitative mass spec analysis the sepharose pellet was washed two additional times with TBS to dispose the detergent. The beads with precipitate were resuspended in 30 µl PBS and stored at -80 °C. For LC-MS/MS an on bead digest was performed and the samples were desalted by StageTipping as described in 3.7.3.

High salt buffer:	15 mM MES, pH 7.5
	15 mM MOPS
	500 mM NaCl
	0.1 % Nonidet P40
	0.05 % Na deoxycholate
Low salt buffer:	15 mM MES, pH 7.5
	15 mM MOPS
	0.1 % Nonidet P40
	0.05 % Na deoxycholate
TBS:	50 mM Tris/HCl, pH 7.5
	150 mM NaCl
	5 % glycerol

3.7.2 In-gel digest and extraction

The gel samples were thawed and washed two times with 250 µl 10 mM NH_4HCO_3 and one time with 750 µl 10 mM NH_4HCO_3:ACN (1:1) for 10 min each. The supernatant was discarded. The samples were reduced by adding 100 µl Buffer R and shaking for 30 min at 30 °C. Modification of free cysteins was achieved by further addition of 10 µl Buffer M and incubation for 15 min in the dark. After that, the supernatant was discarded. Subsequently, 1 mM β-mercaptoethanol and 100 µl 10 mM NH_4HCO_3 were added and incubated for 5 min at 25 °C shaking. The supernatant was discarded and five further washing steps for 10 min each were performed with alternating addition of 750 µl ACN:NH_4HCO_3 (1:1) or 250 µl 10 mM NH_4HCO_3. After the final washing step, the gels were dried completely in a SpeedVac™ Concentrator (Thermo Scienfitic™). To digest the samples, 30 µl trypsin solution (25 ng/µl) were added and incubated overnight at 37 °C. The peptides were extracted from the gel in 6 extraction steps, each followed by a sonication treatment in an ultrasonic bath for 15 min. In the first step, 100 µl 10 mM NH_4HCO_3 were added, second 160 µl ACN were added and, after sonication, the supernatant was collected in a new reaction tube. In the next steps 100 µl 0.1 % FA, followed by 120 µl ACN were added and the supernatant was again transferred to the new reaction tube. In the last two steps, the gels slices were squeezed out completely by two times adding 100 µl ACN and again collecting the supernatant after the sonication steps. The collected supernatant was dried completely in a SpeedVac™ Concentrator (Thermo Scienfitic™) and stored at -80°C.

Buffer R:	0.1 mM Tris/HCl, pH 8.2
	80 mM DTT
	0.5 M Gua/HCl
	0.8 mM EDTA
Buffer M:	100 mM Tris/ HCl, pH 8.2
	0.5 M Iodoacetamide (IAA)

3.7.3 On-bead digest and sample desalting for LC-MS/MS

For the on bead digest of the CoIP samples and the further sample preparation for LC-MS/MS, an adapted protocol from Keilhauer et al., 2015 (Keilhauer et al., 2015) was used. The beads with the CoIP precipitates were thawed and after addition of 25 µl Elution buffer I, incubated for 30 min at room temperature. Subsequently, 100 µl of Elution buffer II were added and overnight incubation was performed at room temperature while shaking. The elution was quenched by adding 0.5 % TFA. The beads were separated by a centrifugation step for 1 min at 16,900 x g . The samples were desalted using self-packed StageTips with a double C_{18} layer. The stage tips were equilibrated by washing once with 70 µl MeOH and three times with 70 µl 0.5 % freshly prepared FA using centrifugation steps at 1,000 g in between without letting the C_{18} material run dry. Then, up to 200 µl of sample were loaded and washed again three times with 70 µl 0.5 % FA. The elution was performed using two times 30 µl of 80 % ACN, 0.5 % FA. The samples were dried completely in a SpeedVac™ Concentrator (Thermo Scienfitic™) and stored at -80 °C.

Elution Buffer I:	50 mM Tris-HCl, pH 7.5
	5 ng/µl Trypsin
	2 M Urea
	1 mM DTT

Elution Buffer II:	50 mM Tris-HCl, pH 7.5
	2 M Urea
	5 mM IAA

3.7.4 Sample preparation for LC-MS/MS

Samples were thawed and dissolved in 24 µl 0.1 % FA by pipetting up and down and a following ultrasonication treatment for 15 min in an ultrasonic bath USC-T (VWR).

The dissolved samples were loaded to 0.22 µm centrifuge filter (Merck Millipore) and centrifuged two times at 1,377 x g for 2 min. The flow-through was transferred to Chromacol vials (Thermo Scientific) with Chromacol closures (Thermo Scientific).

3.7.5 Measurements at Orbitrap Mass Spectrometers

Two different Orbitrap LC-MS instruments were used during this work. The LTQ Orbitrap XL™ Hybrid Ion Trap-Orbitrap Mass Spectrometer (ThermoFisher Scientific) was used for samples that were already enriched by SDS-PAGE while the Orbitrap Fusion Tribrid Mass Spectrometer (ThermoFisher Scientific) was used for more complex samples.

3.7.5.1 Orbitrap XL

The filtered peptide samples were loaded onto an Acclaim PepMap RSLC C18 trap column (Trap Column, NanoViper, 75 µm × 20 mm, C18, 3 µm, 100 Å; ThermoFisher Scientific) with a flow rate of 5 µl/min and separated on a PepMap RSLC C18 column (C18, 2 µm, 100 Å, ThermoFisher Scientific) at a flow rate of 0.2 µl/min. For the human CoIP1 a separation column of 75 µm × 150 mm was used whereas for the human CoIP2 a 75 µm × 500 mm column was used. A linear gradient from 4 % (v/v) to 35 % (v/v) buffer B (acetonitrile with 0.1 % formic acid and 5 % DMSO) eluted the peptides in 80 min (CoIP1) or 135 min (CoIP2) to an LTQ Orbitrap XL™ Hybrid Ion Trap-Orbitrap Mass Spectrometer (ThermoFisher Scientific). Full scans and five dependent collision-induced dissociation MS^2 scans were recorded in each cycle.

3.7.5.2 Orbitrap Fusion

The filtered peptide samples were loaded onto an Acclaim™ PepMap™ C18 trap column (Trap Column, NanoViper, 75 µm x 20 mm, C18, 3 µm, 100 Å; ThermoFisher Scientific) with a flow rate of 5 µl/min and separated on an EASY-Spray™ C18 LC-Column (analytical column, EASY-Spray, 75 µm x 500mm, C18, 2 µm, 100 Å, ThermoFisher Scientific) at a flow rate of 0.3 µl/min. A gradient from 5 % (v/v) to 90 % (v/v) buffer B (acetonitrile with 0.1 % formic acid) eluted the peptides in 140

min to an Orbitrap Fusion Tribrid Mass Spectrometer (ThermoFisher Scientific). Full scans and HCD induced MS^2-scans were recorded.

3.7.6 Data analysis

For the analysis of the mass spectrometry data from CoIPs with human sHsps, the software Proteome Discoverer 1.4 (Thermo Scientific) was used. The evaluation was perfomed as described in Mymrikov *et al.*, 2007 (Mymrikov et al., 2017).

For the quantitative analysis of mass spectrometry data from CoIPs with the sHsps from *C. elegans,* the MaxQuant Software version 1.5.3.8 was used. All datafiles were searched against a Swissprot *C. elegans* Database downloaded from Uniprot (13.06.2017 edition). The search was limited to tryptic peptides with up to two missed cleavages and a peptide tolerance of 4.5 ppm. A label-free quantification was performed with a LFQ min. ratio count of 1. Matching of peptide spectra between different runs was performed. For peptide quantification only unique peptides were allowed. The false discovery rate (FDR) was set to 1 %. A reversed decoy database was used for evaluation. With the results from MaxQuant further evaluation of the dataset was conducted using the Perseus Software version 1.5.3.2. Contminants were excluded from further data processing. Only proteins that were identified by at least 2 different peptides were included in the hit list. For statistical analysis a Students T-Test was performed. Results were visualized by creating volcano plots with a FDR of 5% and values of S0=0.1.

3.8 *In vivo* studies in *C. elegans*

All strains were ordered from the Caenorhabditis Genetics Center (CGC) or the National Bioresource Project for the Experimental Animal "Nematode *C. elegans*". The methods were conducted according to the Stiernagle protocols (Stiernagle, 2006).

3.8.1 Maintenance of *C. elegans*

C. elegans were grown at 20 °C on Nematode Growth Medium (NGM) agar plates that were aseptically poured into 60 mm petri plates (Brenner, 1974) and seeded with an OP50 layer as food source.

Worms were transferred to new NGM plates by either "chunking" a small piece of agar from a populated plate to a new one or by picking single worms under the microscope.

NGM:
3 g NaCl
17 g Agar
2.5 g Peptone
975 ml H_2O
autoclave and cool down to 55 °C
1ml 1 M $CaCl_2$
1 ml 5mg/ml Cholesterol in Ethanol
1 ml 1 M $MgSO_4$
25 ml 1M KPO_4 buffer, pH 6.0

3.8.2 Growth in liquid culture

For the preparation of *C. elegans* lysate, large quantities of *C. elegans* were needed. Therefore the worms were grown in liquid medium. *C. elegans* of approximately 20 populated NGM plates were washed off with M9-Medium and used to inoculate 250 ml S-Medium that was supplied with OP50 harvested from a 2 liter overnight culture. The culture was incubated at 20 °C shaking vigorously in baffled flasks to ensure good oxygenation. The growth of the culture was monitored every day by checking a drop of the culture under the microscope. After 5 days the cultures were transferred to 50 ml falcon tubes and harvested by centrifugation for at least 2 min

at 1,150 x g. The worm pellets were washed once with M9-medium, frozen in liquid nitrogen and stored at -80 °C.

M9 medium:	3 g KH_2PO_4
	6 g Na_2HPO_4
	5 g NaCl
	1 ml 1M $MgSO_4$
	H_2O to 1 l
	sterilize by autoclaving
S Basal:	5.85 g NaCl
	1 g K_2HPO_4
	6 g KH_2PO_4
	1 ml cholesterol (5mg/ml in ethanol)
	H_2O to 1 l
	sterilize by autoclaving
1M Potassium citrate, pH 6.0:	20 g citric acid monohydrate
	293.5 g tri-potassium citrate monohydrate
	H_2O to 1 l
	sterilize by autoclaving
Trace metals solution:	1.86 g disodium EDTA
	0.69 g $FeSO_4*7H_2O$
	0.2 g $MnCl_2*4H_2O$
	0.29 g $ZnSO_4*7H_2O$
	0.025 g $CuSO_4*5H_2O$
	H_2O to 1l
	sterilize by autoclaving, store in the dark

S-Medium:	1 l S Basal
	10 ml 1M Potassium citrate
	10 ml Trace metals solution
	3 ml 1M $CaCl_2$
	3 ml 1 M $MgSO_4$

3.8.3 Synchronisation of worms

To synchronize *C. elegans* worms the animals were cultivated at 20 °C on NGM plates until the plates contained many gravid hermaphrodites. The worms were washed of the plates with M9-medium (see 3.8.2) and collected in a 10 ml conical tube. After the sedimentation of the worms by centrifugation for 1 min at 1,300 x g the supernatant was removed until only 3.5 ml were left. To the remaining resuspension, 1.5 ml of bleaching solution were added and incubation at room temperature was performed for 4 min with vortexing the suspension from time to time. The bleaching solution opens up the adult worms and releases the eggs. The eggs themselves are protected by their cuticula. After 4 min of incubation the eggs were pelleted by centrifugation for 1 min at 1,000 x g. Then the bleaching solution was quickly removed to avoid damaging of the eggs cuticula and the eggs were washed 4-5 times with 14 ml M9 buffer. After washing, the eggs were incubated overnight at 20 °C rotating to allow the larvae to hatch. Due to a lack of nutrients in the M9 medium all larvae remain in the L1 stadium and will then develop synchronously when transferred to NGM plates.

Bleaching Solution:	10 ml Chlorix
	5 ml 5 M NaOH

3.8.4 Preparation of *C. elegans* lysate

The preparation of *C. elegans* lysate was performed according to the protocol described in Fleckenstein et al., 2015 (Fleckenstein et al., 2015). The worm pellets were thawed on ice and resuspended in an equal volume of IP-buffer. After grinding the worms with 40 strokes in a glass mortar on ice, they were transferred to 1.5 ml Eppendorf tubes and 0.25-0.5 mm glass beads were added before they were frozen in liquid nitrogen. The pellet was thawed on ice and broken up in a bead mill at 30 Hz for 3 x 1 min with 1 min breaks on ice in between to avoid overheating of the samples. Glass beads and cell debris was separated by centrifugation for 10 min at 16,900 x g. The supernatant was transferred to a new tube and the centrifugation step was repeated to remove last traces of contaminants. The protein concentration of the supernatant was assessed using the BCA assay.

IP-buffer:	15 mM MES, pH 7.5
	15 mM MOPS
	150 mM NaCl
	1 % Nonidet P 40
	0.5 % Na deoxycholate
	0.7 µg/ml pepstatin
	1 mM PMSF
	protease inhibitor mix G (Serva)

3.8.5 Lyate Assay

C. elegans lysate was prepared as described in 3.8.4. The lysate was incubated at a concentration of 0.8 mg/ml for 90 min at 37 °C in absence or presence of different sHsp concentrations. After the heat shock, soluble and insoluble fractions were separated by centrifugation at 16,900 x g for 10 min. Both fractions were analyzed by SDS-PAGE using precasted gels (SERVAGel™ TG PRiME™ 4-20 %, 15 sample wells, Serva) and quantified with the ImageQuant TL (GE Healthcare) software and ImageJ (Schneider et al., 2012).

4. Results and Discussion

4.1 Hsp26 from *S. cerevisiae*

Concerning their structural properties, sHsps constitute an exceptional diverse species. Some sHsps form large oligomers whereas others exist in monomeric or dimeric form. Hsp26 has often been described to be a 24mer (Haslbeck et al., 1999, Franzmann et al., 2005, White et al., 2006), but also higher oligomeric species have been observed (Benesch et al., 2010). Also the structural organization of the oligomers differs a lot between sHsps. Aside of the number of subunits, also the symmetries and the arrangement of subunits in an oligomer vary. The basic building block is often described as a dimer (Kim et al., 1998, van Montfort et al., 2001, Bagneris et al., 2009, Peschek et al., 2009, Haslbeck et al., 2008, Fleckenstein et al., 2015). Crystal structures revealed that dimerization is achieved by interaction between two ACDs of two different subunits. For the dimerization, two different modes are known so far: a dimer interface via domain swapping or the interaction of two antiparallel β-strands. For Hsp26 the mode of dimerization is not known to date.

4.1.1 Structural analysis of Hsp26 truncation mutants

To gain further insight into the oligomer formation, and especially about the mode of dimerization, several truncation mutants were cloned and purified. All mutants contain the highly conserved alpha crystallin domain, ranging from amino acid position 95-194 with C- and N-terminal elongations of various length (Figure 9). The mutants 87-206 and 95-214 additionally contain the conserved IXI or IEV motif, which spans the positions 204-206 of the Hsp26 protein. Some of the truncation mutants were already used in previous studies to find out about residues contributing to the dimer formation of Hsp26 (Chen et al., 2010).

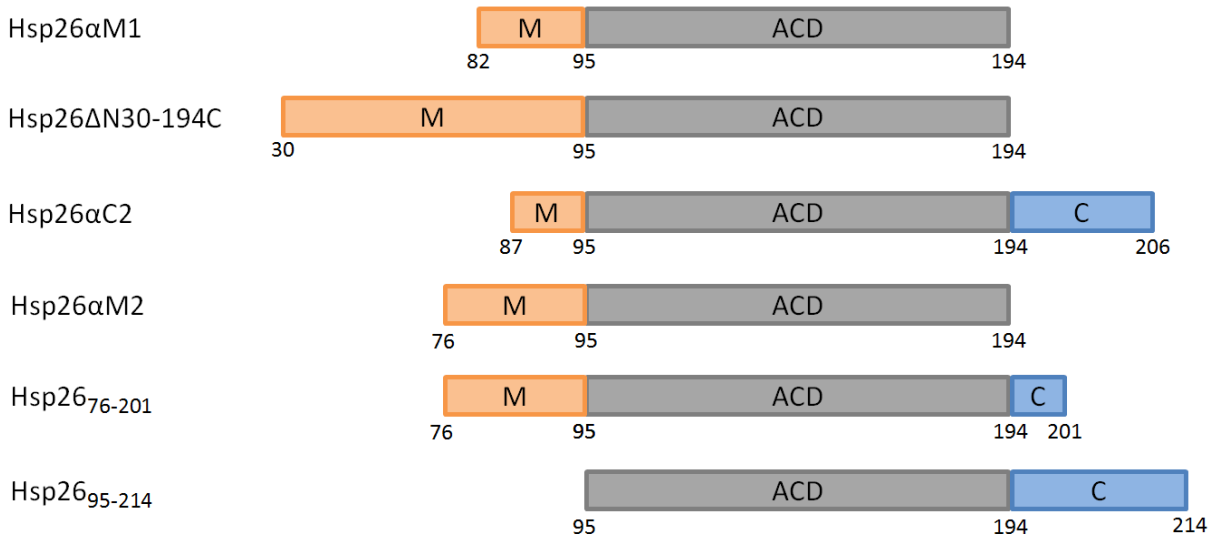

Figure 9: Schematic overview of the domain structure of the different truncation mutants of Hsp26. All mutants contain the highly conserved alpha crystallin domain (ACD) and N- and C-terminal elongations of various length.

4.1.1.1 Secondary structure analysis of Hsp26 truncation mutants

To gain information about the secondary structure of the different truncation mutants of Hsp26, far-UV CD spectroscopy was used.

The mutants were analyzed in 10 mM NaP, 150 mM NaCl, pH 6.5 at 20 °C in a wavelength range between 200 and 260 nm. The spectra of the mutants Hsp26αM1, $Hsp26_{76\text{-}201}$, Hsp26αC2 and $Hsp26_{95\text{-}214}$ looked quite comparable with a minimum between 206 nm and 209 nm (Figure 10). This is in good agreement to the already published data of Jin Chen where the spectra showed a minimum between 205 nm and 212 nm (Chen et al., 2010). The shape of the spectra indicates a high content in beta-sheet structure. This is not surprising as the alpha crystallin domain is known to form predominantly beta-sheets (MacRae, 2000, Horwitz, 2003). The spectra of the mutants Hsp26αM2 and Hsp26ΔN30-194C differ in their shape from the other mutants. The minimum for the mutant Hsp26αM2 was observed at 204 nm and for the mutant Hsp26ΔN30-194C at 207 nm (Figure 10). The shape of spectra for these mutants suggests a high content of random coil which leads to the assumption that these mutants are not correctly folded or are present in an unfolded state.

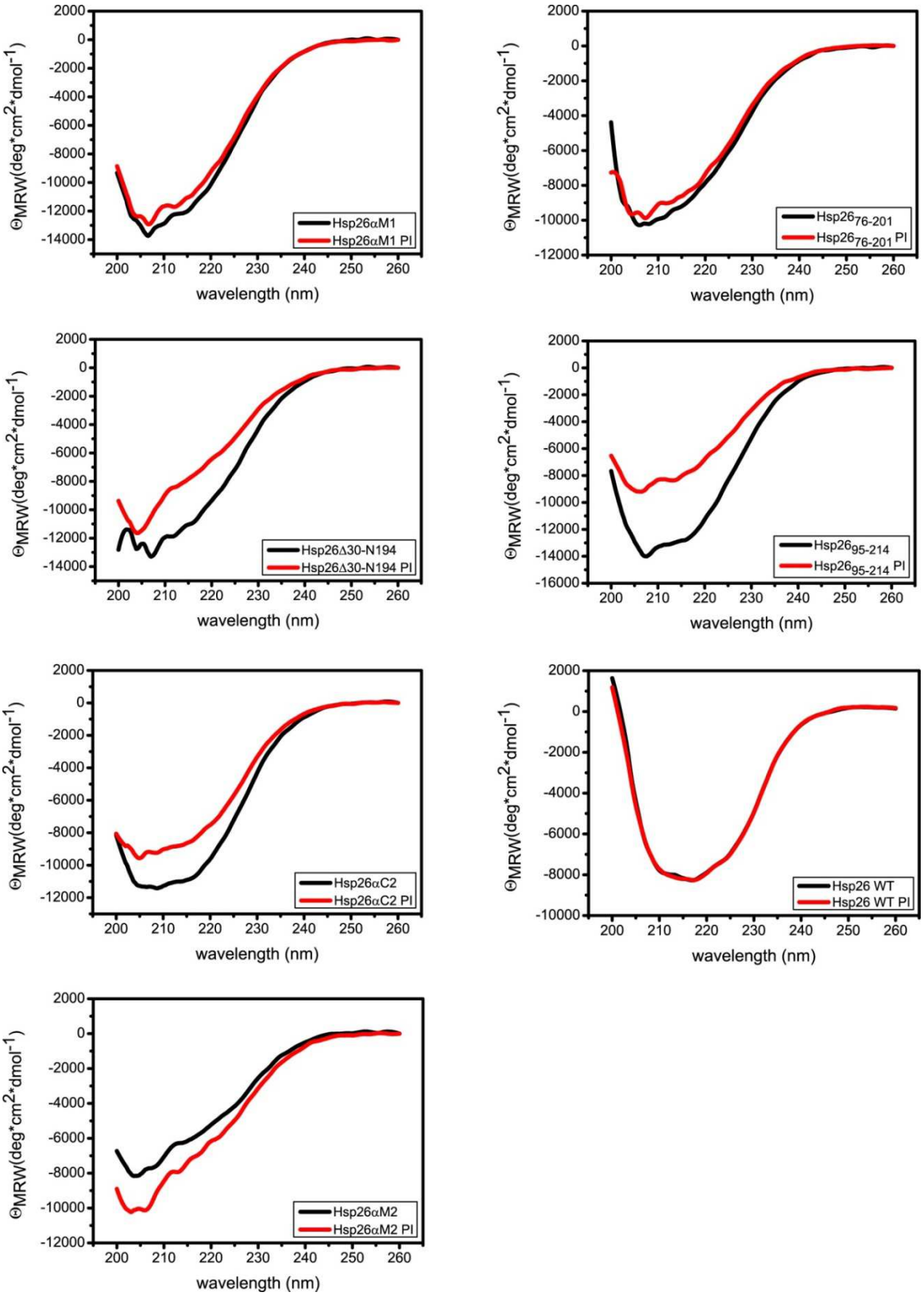

Figure 10: Far-UV CD spectra of the Hsp26 truncation mutants. The protein concentration was adjusted to 0.5 mg/ml. Measurements were performed in 10 mM NaP, 150 mM NaCl, pH 6.5 at a constant temperature of 20 °C. The mutants were either analyzed with (red) or without (black) preincubation (PI) at 37 °C.

As it has been observed in the past that Hsp26 reacts very sensitive to changes in temperature, the secondary structure was also assessed after preincubation of Hsp26 at 37 °C overnight. This mode of preincubation was described by Thomas Kriehuber to result in stable and homogenous Hsp26 oligomers (Kriehuber, 2012). In general, the shape of spectra was barely influenced by the preincubation procedure. For all mutants, the signal intensity was lower in comparison to the measurements without preincubation, though. The only exception is the mutant Hsp26αM2 where the signal intensity was found to be increased after preincubation. As a reference, the Hsp26 wildtype protein was analyzed as well. The Hsp26 wildtype protein showed a characteristic minimum at 217 nm, which indicates the presence of a high content of β-sheet in the secondary structure (Figure 10). For the wiltype protein, as well, no difference in the CD- spectrum was observed after preincubation of the protein at 37 °C.

4.1.1.2 Quaternary structure analysis of Hsp26 truncation mutants

HPLC

To find out about the quaternary structure of the truncation mutants, especially to distinguish between monomeric, dimeric and higher oligomeric states, analytical SEC-HPLC was performed. Therefore a Superdex75 10/300GL column (GE Healthcare) was used with 10 mM sodium phosphate buffer containing 150 mM NaCl at pH 6.5 as the mobile phase. The experiment was conducted at a temperature of 20 °C with a flow rate of 0.5 ml/min.

To be able to estimate the size of the truncation mutants, a standard curve was generated using a Gel Filtration Standard (Biorad). The elution times of the standard proteins were determined under the respective conditions and were plotted against the logarithm of the molecular weight (Figure 11). The standard curve consequently allows to draw conclusions on the molecular weight of the truncation mutants from the respective retention times.

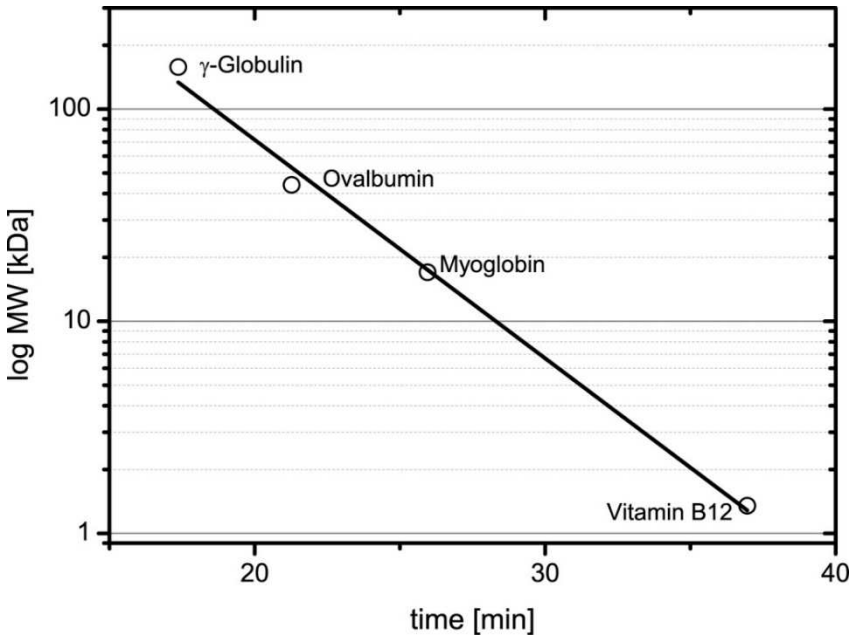

Figure 11: Standard curve for the SEC-HPLC experiment on a Superdex75 10/300GL column in 10 mM sodium phosphate, 150 mM NaCl, pH 6.5: Retention times of the standard proteins γ-Globulin (158 kDa), Ovalbumin (44 kDa), Myoglobin (17 kDa) and Vitamin B12 (1.35 kDa) were plotted against the logarithm of the molecular weight.

As for the analysis of the secondary structure, the investigation of the quaternary structure was performed with and without preincubation at 37 °C to assess the influence of temperature (Figure 12). The truncation mutant Hsp26αM1 eluted from the column with a retention time of 25.3 minutes without preincubation which would correspond to a molecular mass of about 20 kDa which does not allow to discriminate between the monomeric and dimeric state. Even after preincubation at 37 °C no shift in the retention time was observed for this mutant. For the truncation mutant Hsp26αC2 with a retention time of 23.9 minutes the molecular mass of 28 kDa was estimated indicating a dimeric form. After preincubation a slight shift towards later retention times was observed. The retention time accounted for 25 minutes with a molecular mass of 22 kDa, which would still value for the presence of a dimeric state. The truncation mutant Hsp26αM2 showed a very similar elution profile with and without preincubation. Next to a main peak at 25.7 minutes another small peak is visible at 23.1 minutes. The estimation with the help of the standard

curve lead to molecular mass values of 18 kDa and 34 kDa, which suggests the main species to be present as a monomer and the smaller amount to exist in a dimeric form. For the mutant $Hsp26_{76\text{-}201}$ again the preincubation didn't show an effect on the elution profile at all. One single peak was observed at 24.7 minutes matching a molecular weight of 23.7 kDa and therefore a dimeric form. The preincubation treatment also didn't influence the elution behavior of the mutant Hsp26ΔN30-C194. However for this mutant two peak maxima were distinguished with retention times of 25.7 and 28 minutes corresponding to a molecular mass of 18.7 kDa and 10 kDa. Yet, the calculated molecular mass of the mutant is 19.4 kDa, which presumably means that this mutant is present in a monomeric form but with a large amount of degraded protein. Already during the purification process, constantly slight degradation bands were observed on SDS gels. Probably this mutant is degraded from the N-terminal side as the N-terminal domain is supposed to be unstructured and flexible and might therefore easily be accessible to proteases. The mutant $Hsp26_{95\text{-}214}$ elutes without preincubation at 25.1 minutes corresponding a molecular mass of 21.4 kDa and therefore a dimeric form. After preincubation a slight shift towards a retention time of 24.6 kDa was observed, still suggesting a dimeric form. The analysis of the Hsp26 wildtype protein revealed a main peak with a retention time of 15.8 min. The retention time of the wildtype protein is significantly reduced compared to the truncation mutants indicating a larger molecular weight and thereby a higher oligomeric complex. An exact determination of the molecular weight and the number of subunits was not possible in this experiment due to the insufficient separation range of the used column for proteins or complexes of higher molecular masses.

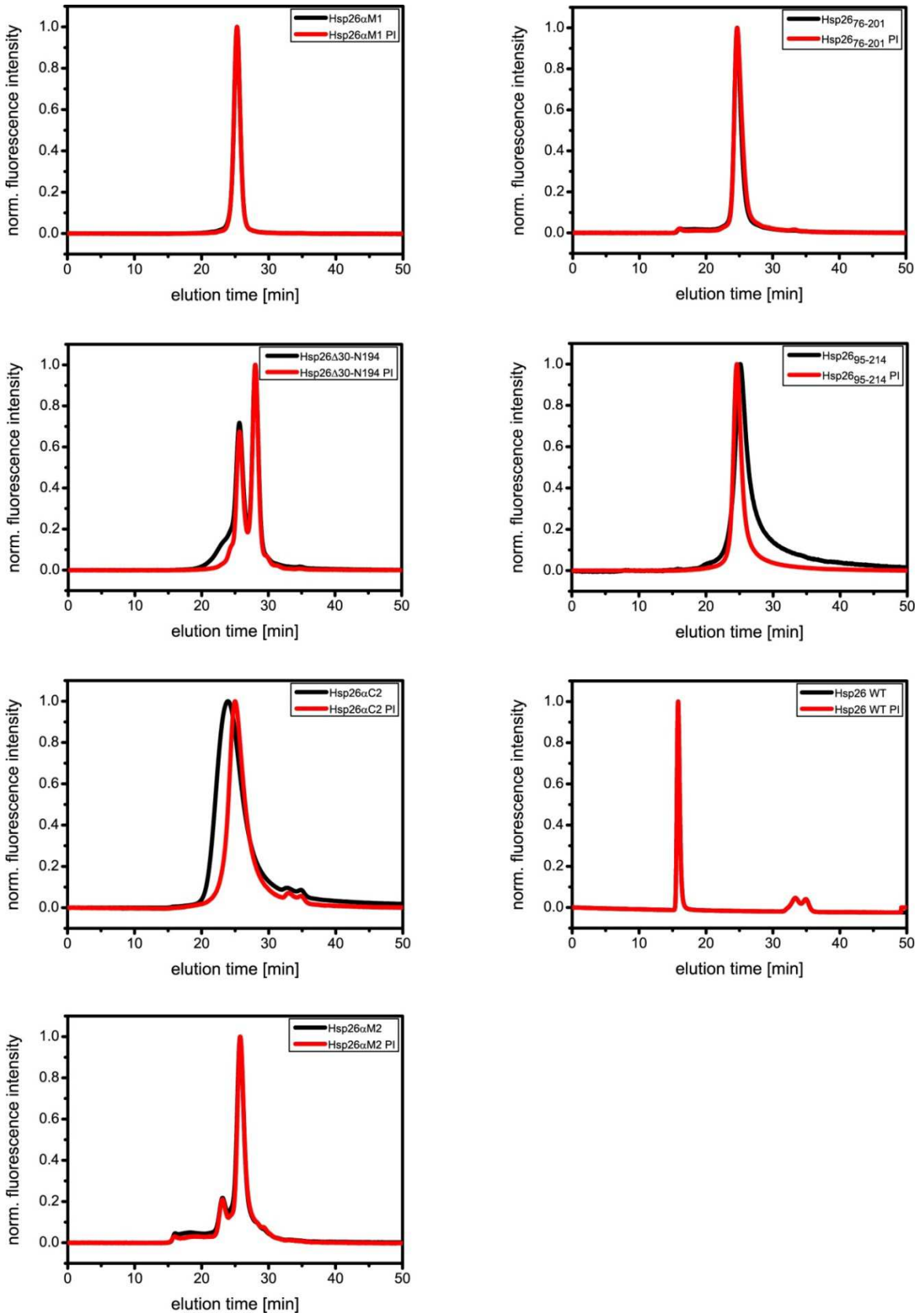

Figure 12: Analysis of the Hsp26 truncation mutants by SEC-HPLC on a Superdex75 10/300GL column in 10 mM sodium phosphate, 150 mM NaCl, pH 6.5 with a protein concentration of 0.5 mg/ml. The mutants were either analyzed with (red) or without (black) preincubation (PI) at 37 °C.

AUC

Another method to analyze the oligomerisation state is via analytical ultracentrifugation. With this method the proteins are sedimented in measuring buffer and detected by UV-spectrometry during the time of the experiment. On the basis of the sedimentation velocity a Svedberg value (S) can be calculated and also the rough estimation of the molecular weight is possible. An advantage of this method is the absence of protein- matrix interactions which might influence the native state of the protein.

The experiments were performed in 10 mM sodium phosphate buffer with 150 mM NaCl at pH 6.5 in a Beckman XL-I analytical ultracentrifuge with 30,000 rpm at a constant temperature of 20 °C. Data analysis was carried out using the Sedfit (P. Schnuck) software with a non-model based continuous Svedberg distribution c(S).

The Hsp26 wildtype protein showed a sedimentation coefficient of 25 S (Figure 13). With the Sedfit software the approximate molecular weight can be calculated. For Hsp26 WT a molecular mass of 788 kDa was determined which would correspond to a relatively large oligomer with approximately 32 subunits. Such an oligomer could not be observed for any of the truncation mutants analyzed (Figure 13). The mutant Hsp26αM1 shows a Svedberg value of 1.8 S and a molecular mass of 19.5 kDa suggesting a dimeric form which is in good agreement with the SEC-HPLC results. For Hsp26αC2 a sedimentation coefficient of 2.1 S and a molecular mass of 27.5 kDa were determined. This result indicates a dimeric form which was as well already observed in the SEC-HPLC runs. In contrast to the SEC-HPLC measurements only one species was observed for the truncation mutant Hsp26αM2 with 1.2 S and a molecular mass of 14.6 kDa pointing to a monomeric species, which has also been the predominant species in the SEC-HPLC experiments. A difference compared to the SEC-HPLC measurements was also found for the $Hsp26_{76\text{-}201}$ mutant, which showed a sedimentation coefficient of 1.4 S in the ultracentrifugation experiment and with 15.9 kDa is supposed to be present as a monomer whereas the SEC-HPLC data rather suggested a dimeric form. For the Hsp26ΔN30-C194 mutant again only one species was observed sedimenting with 1.1 S. The molecular mass of 11.1 kDa, which was calculated by the Sedfit software, again disclosed the degradation of this mutant. The

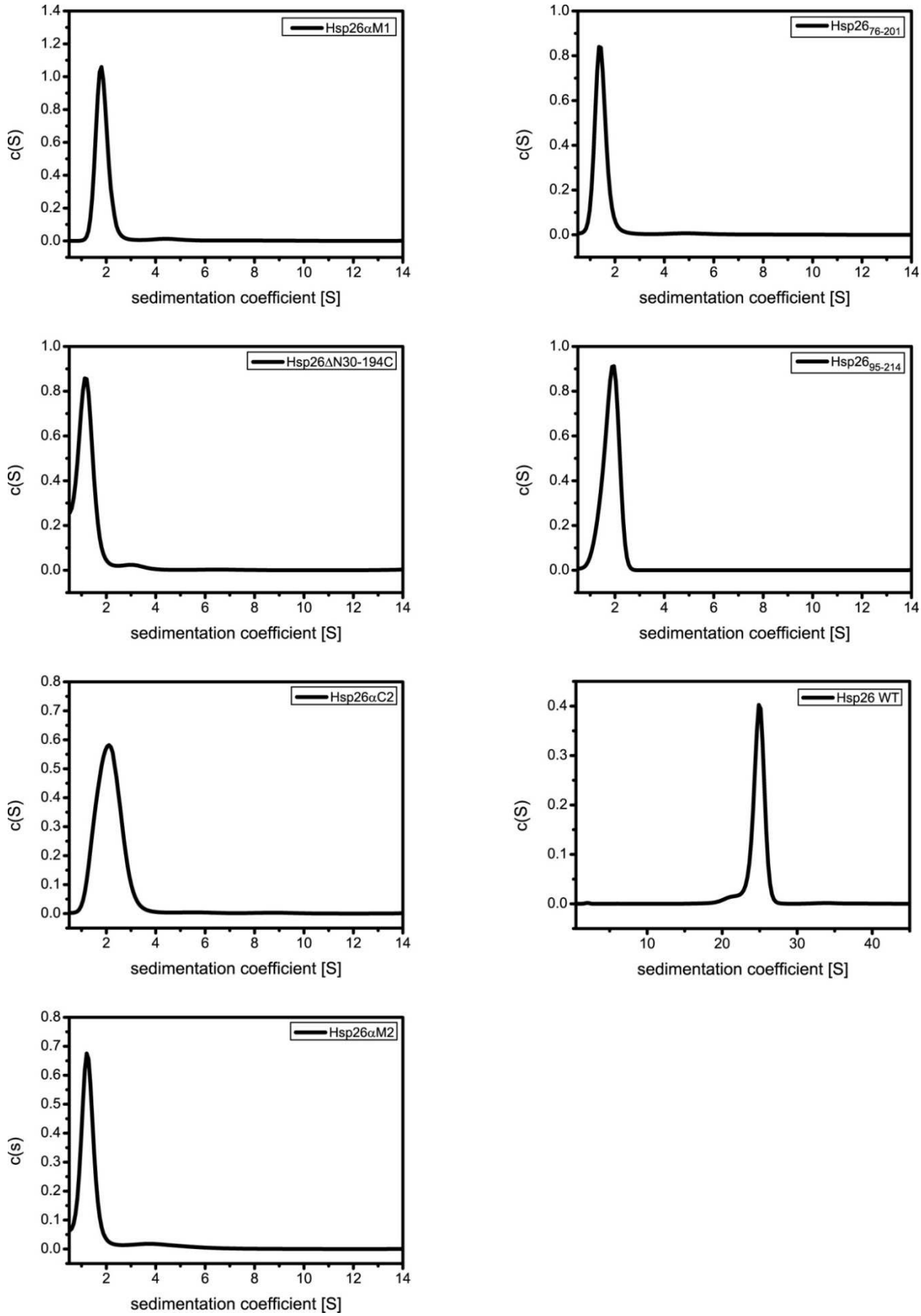

Figure 13: Analysis of the Hsp26 truncation mutants by analytical ultracentrifugation in a Backman XL-A at 30,000 rpm and 20 °C in 10 mM sodium phosphate, 150 mM NaCl, pH 6.5.

results for the mutant $Hsp26_{95-214}$ were again in good accordance to the SEC-HPLC measurements. A sedimentation coefficient of 2.0 S and a molecular weight of 21 kDa was determined confirming the dimeric form which was already suggested before.

4.1.1.3 Analysis of truncation mutants by NMR

For the determination of proteins structures several methods are applied: X-ray crystallography, Electron microscopy (EM) and Nuclear magnetic resonance spectroscopy (NMR). One advantage of NMR over X-ray crystallography and EM is the possibility to assess the protein structure in solution, which means more physiologic conditions than in X-ray crystallography, where a crystal of the protein is needed or EM, where the protein has to be applied to grids.

To determine the structure of the Hsp26 ACD-dimer some of the truncation mutants were labeled for solution-state NMR experiments either with ^{15}N only, or with ^{13}C plus ^{15}N or triple labeled mutants were generated with ^{13}C, ^{15}N and D_2O. The NMR experiments were performed by Dr. Hyun-Seo Kang at the chair for biomolecular NMR spectroscopy at the Technical University of Munich. The mutant Hsp26ΔN30-C194 had already been used before to record NMR spectra attempting to identify the Hsp26 ACD-dimer structure. However, this construct generated very crowded spectra, probably due to the fact that it forms dimers.

To start with an easier construct, the short truncation mutant Hsp26αM1 was chosen. This mutant consists only of the alpha crystallin domain and 13 residues of the middle domain of Hsp26. One dimensional ^{1}H NMR spectra in the amide region at different temperatures ranging from 278 K- 318 K were recorded. In general the signal intensity directly correlates to the sample concentrations and due to faster molecular tumbling the signal intensities are increased at higher temperatures. This could not be observed for the Hsp26αM1 mutant. In contrast, the signal intensities were decreasing at higher temperatures (Figure 14). This tempts to suggest an increase in the size of the molecule. However, for Hsp26 a decrease in oligomeric size has been reported upon heat activation (Haslbeck et al., 1999).

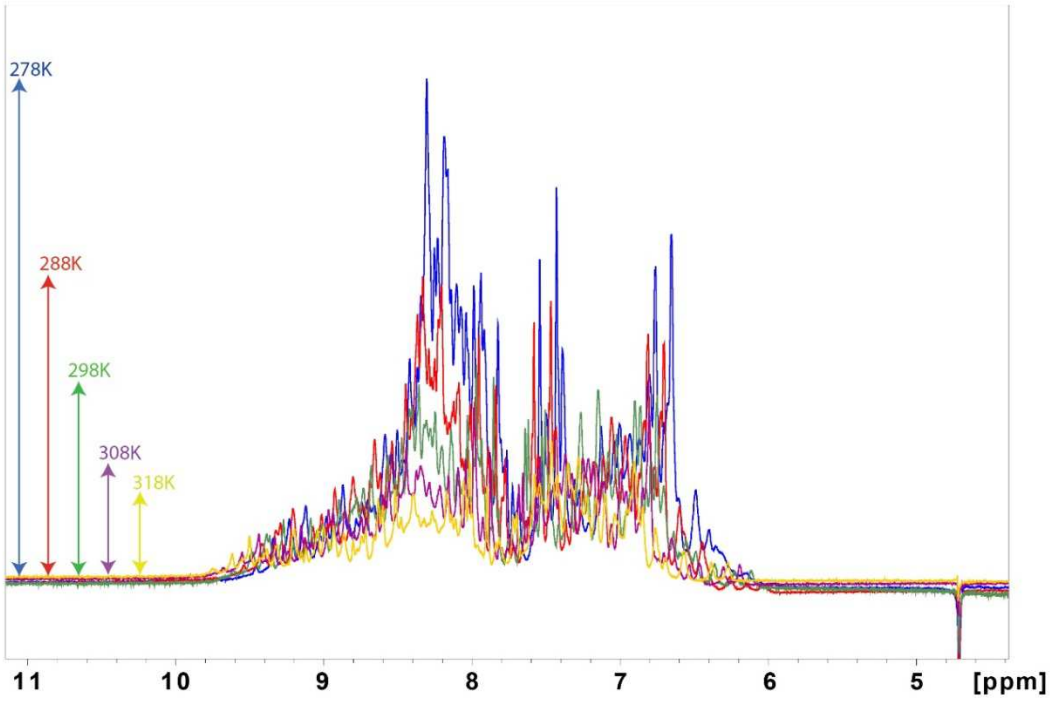

Figure 14: One dimensional ^{1}H NMR spectra of the truncation mutant Hsp26αM1 at different temperatures. A protein concentration of 0.1 mM was used. Signal intensities were decreasing with higher temperatures. Figure provided by Dr. Hyun-Seo Kang (Chair for biomolecular NMR spectroscopy, TUM).

In a next step, the triple labeled construct was used to record a HSQC spectrum at 600 MHz at 288 K, which had emerged as the optimal temperature to work with in the one dimensional ^{1}H NMR measurements. The obtained spectrum allowed the assignment of about 90 % of the residues (Figure 15). The missing residues are residues 95-99 of the ACD and furthermore mainly residues located in the middle domain. A comparison to the spectra of the Hsp26ΔN30-C194 mutant revealed that many dispersed signals are missing in the spectrum of the Hsp26αM1 construct. By lowering the contour level some more signals came up but were shifted in comparison to the Hsp26ΔN30-C194 spectrum. This might be due to a conformational exchange of a certain region in this construct leading to the question if this is real or maybe an artefact of cutting the construct too short and thereby maybe disrupting the structure.

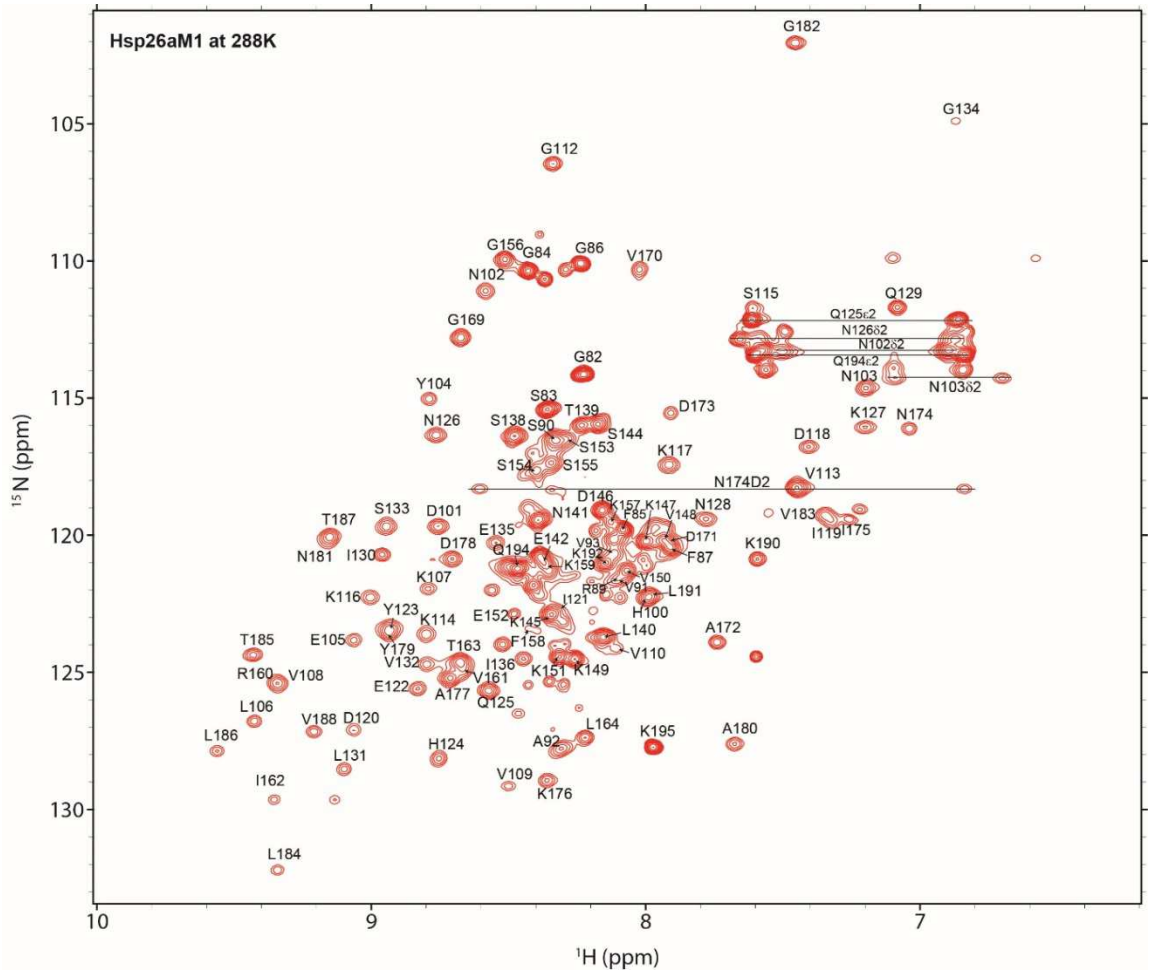

Figure 15: HSQC spectrum of the truncation mutant Hsp26αM1 at 288 K in 20 mM sodium phosphate, 50 mM NaCl, pH 6.5. A protein concentration of 0.1 mM was used. About 90 % of the residues could be assigned. Figure provided by Dr. Hyun-Seo Kang (Chair for biomolecular NMR spectroscopy, TUM).

As Hsp26 has been shown to exhibit different characteristics depending on the specific buffer system, different buffer conditions were tested. As the basic buffer 20 mM sodium phosphate was used. The pH values were varied between pH 5.5, pH 6.5 and pH 7.5. At pH 6.5 also different salt concentrations of 20 mM, 50 mM, 100 mM and 200 mM NaCl were tested. In summary, the variations in the buffer conditions didn't have an effect on the spectra of this mutant.

With the help of the assigned residues from the HSQC spectrum of the Hsp26αM1 mutant, heteronuclear NOE spectra could be recorded and interpreted. To a high extent the protein was found to be structured under the conditions used. Structured regions largely overlap with the respective structured regions in wheat Hsp16.9. A

decrease in the signal intensities in the area of the residues 135-155 (Figure 16) may hint to the presence of a flexible linker region.

Figure 16: Heteronuclear NOE spectrum of the truncation mutant Hsp26αM1. A protein concentration of 0.1 mM was used. A decrease in signal intensities is observed for the residues 135-155. Structured elements of the respective wheat Hsp16.9 residues are indicated in green. Figure provided by Dr. Hyun-Seo Kang (Chair for biomolecular NMR spectroscopy, TUM).

Summarized, the Hsp26αM1 mutant allowed for the assignment of the residues in the HSQC spectrum but does not form a stable dimer. To use a longer construct that might rather form a stable dimer-interface but not be as complex as the Hsp26ΔN30-C194 construct, the mutant $Hsp26_{76\text{-}201}$ was ^{13}C and ^{15}N labeled. SAXS measurements at high concentrations of 2 mM revealed a dimeric state of this mutant. The HSQC spectra at higher concentrations like 2 mM or 1 mM protein showed only very crowded signals (Figure 17) which were not able to be further evaluated. The spectrum at 0.1 mM protein concentration gave nicer dispersed peaks (Figure 17), however SAXS measurement showed that at this concentration the mutant was present in a monomeric state, which again could not contribute to the identification of the dimer interface.

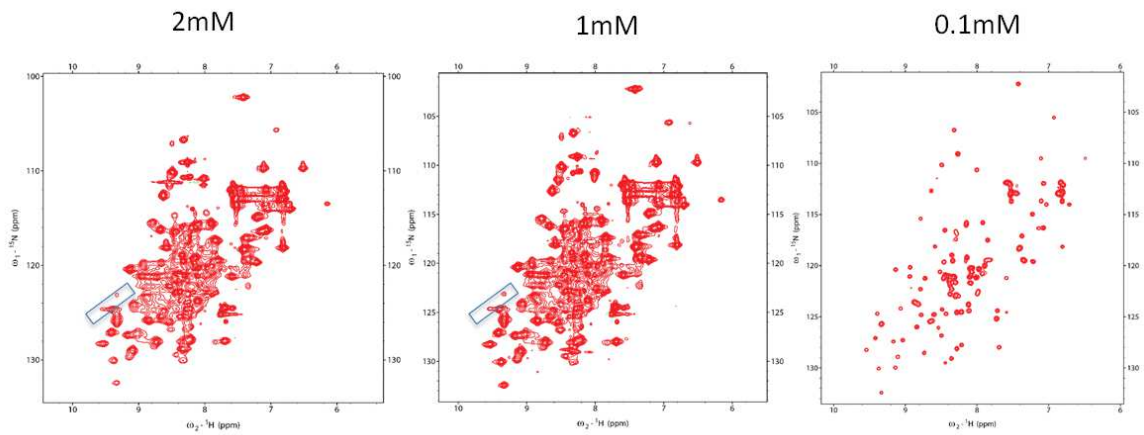

Figure 17: HSQC spectra of the truncation mutant $Hsp26_{76-201}$ at 288 K in 20 mM sodium phosphate, 50 mM NaCl, pH 6.5 at different protein concentrations. Blue boxes indicate residues which might be involved in the dimer interface. Figure provided by Dr. Hyun-Seo Kang (Chair for biomolecular NMR spectroscopy, TUM).

A further attempt to obtain NMR spectra of a stable dimer was made with the construct $Hsp26_{95-214}$ which has been shown to be present in the dimeric state by SEC-HPLC and AUC. This construct consists of the ACD and the whole C-terminal domain and lacks the residues of the N-terminal elongation. In the HSQC spectra obtained with this mutant, again no signature signals that would potentially correspond to a dimer could be observed.

4.1.1.4 Electron microscopic analysis of Hsp26

To further approach the understanding of the Hsp26 structure, also electron microscopic experiments were performed. As Hsp26 is a very heterogeneous protein, the $Hsp26_{S4C}$ mutant was used for EM studies. With the substitution of the S4 residue by a cysteine in the N-terminal region this mutant has been described to form artificial disulfide bridges between the different subunits in the oxidized form leading to a stabilization of the oligomeric complex and a complete inhibition of subunit exchange and dissociation (Franzmann et al., 2005).

To further enhance the homogeneity of the sample, SEC-HPLC runs were performed previous to electron microscopy experiments and only the middle fractions of the elution peaks were used to prepare the grids. The SEC-HPLC runs were carried out

on a TSK G4000PW column in 40 mM Hepes, 50 mM KCl, 1 mM DTTox, pH 7.4 with a flow rate of 0.5 ml/min at 20 °C and 4 drops (~120 µl) of the middle peak fractions were collected manually resulting in a protein concentration of 31 µM for fraction 28 (Figure 18 B).

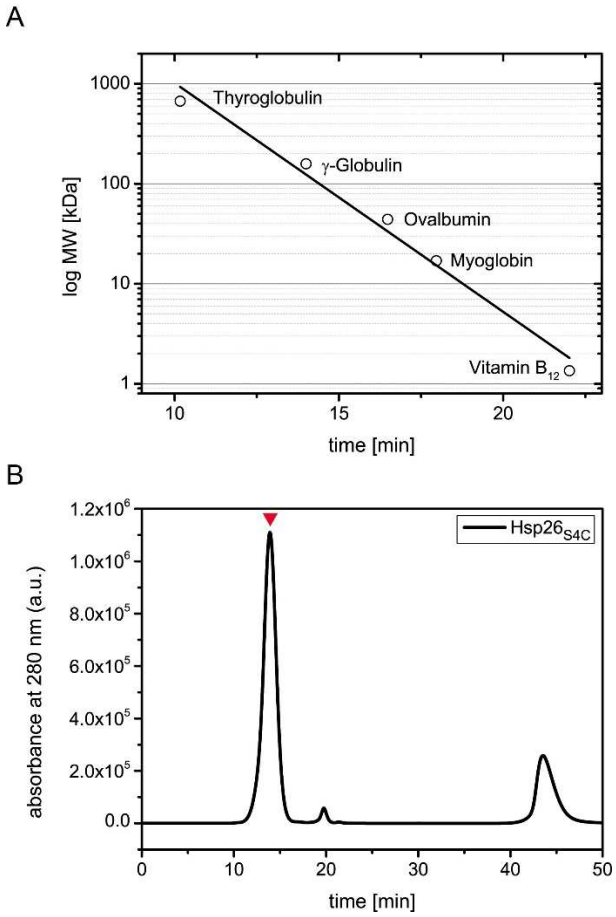

Figure 18: SEC-HPLC experiment on a TSK G4000PW column in 40 mM Hepes, 50 mM KCl, 1 mM DTT_{ox}, pH 7.4 with a flow rate of 0.5 ml/min at 20 °C. A) Retention times of the standard proteins Thyreoglobulin (670 kDa), γ-Globulin (158 kDa), Ovalbumin (44 kDa), Myoglobin (17 kDa) and Vitamin B12 (1.35 kDa) were plottet against the logarithmized molecular weight. B) SEC-HPLC run of the mutant $Hsp26_{S4C}$ with a protein concentration of 619 µM and an injection volume of 100 µl. The red arrow indicates fraction 28 which was further used for electron microscopy analysis.

The grid preparation and electron microscopy experiments were performed by Dr. Beate Rockel from the electron microscopy lab at the Technical University of Munich. A volume of 4 µl of the SEC-HPLC fraction 28 was applied on lacey carbon grids and manually plunged into liquid ethane. The micrographs were recorded at

Tecnai F20 with an Eagle camera operated at 200 kV with a nominal magnification of 50,000 resulting in a pixel size of 0.21 nm on the specimen level. The images were collected with the SerialEM program under low-dose conditions. An example of a micrograph image is shown in figure 19 A. In total 307 micrographs were recorded and 27,393 particles were selected interactively and submitted to cl2d classification runs in the Relion software. After the calculation of 2D-averages (examples shown in Figure 19 B) 12,123 particles were kept for further analysis. Based on an Hsp26 wildtype model with octahedral symmetry (Figure 19 C left model) a starting model for a preliminary 3D refinement of the 12,123 particles of the $Hsp26_{S4C}$ mutant was created. This resulted in a 3D-reconstruction with a resolution of approximately 1.5 nm (Figure 19 C, right model).

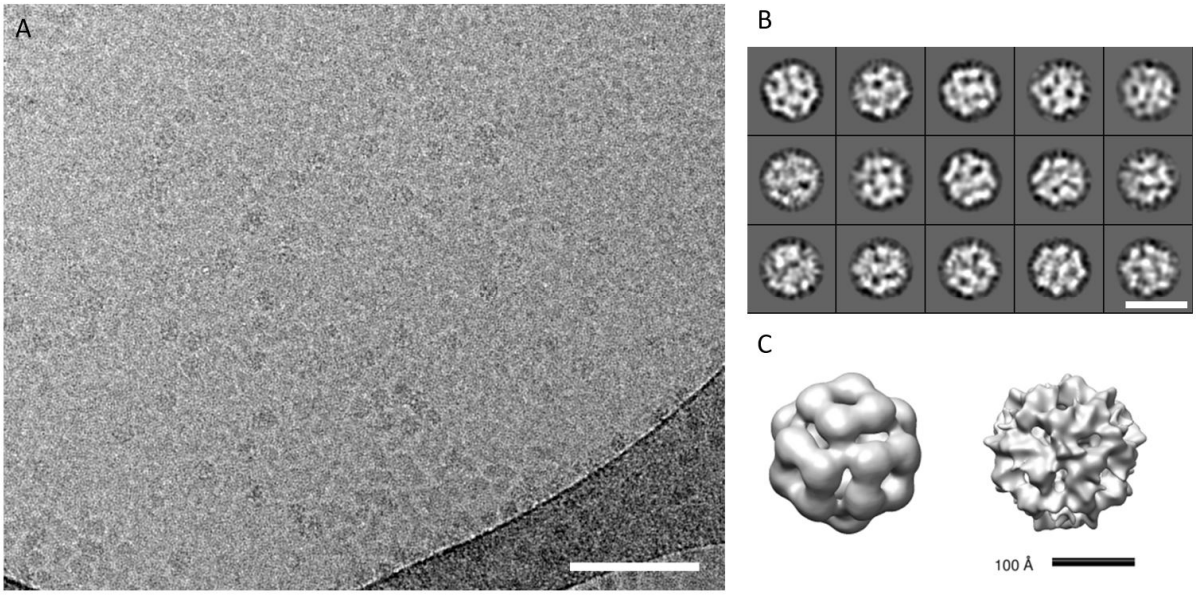

Figure 19: Electron microscopy analysis of $Hsp26_{S4C}$. A) Micrograph of $Hsp26_{S4C}$ recorded at Technai F20 with a nominal magnification of 50,000. Scale bar 100 nm. B) Examples for 2D averages calculated by with Relion software. C) An octahedrally symmetrized model of Hsp26 wildtype (left model) was used as a starting model for a preliminary 3D-refinement of the 2D-average particles resulting in a 3D-reconstruction of a resolution of ~1.5 nm (left model). Figure provided by Dr. Beate Rockel (Electron microscopy lab, TUM).

4.1.1.5 Summary on Hsp26 structure

To understand complex and heterogeneous systems such as constituted by sHsps, a versatile approach involving several different techniques is advantageous. For the small heat shock protein of the human eye lens, αB- crystallin, a triple hybrid approach was successful in developing a structural model of this protein (Braun et al., 2011). In the case of Hsp26, it is of particular interest to understand its mode of dimerization to allow for structural modelling based on the cryo-electron microscopy data.

As Hsp26 shows very heterogeneous properties, truncation mutants were produced to reduce the complexity of the system. The SEC-HPLC and AUC results of the analyzed mutants are summarized in table 2. In SEC-HPLC analysis no effect of the preincubation treatment at 37 °C could be observed on the quaternary structure of the respective mutants. For Hsp26 a temperature induced activation mechanism has been described (Haslbeck et al., 1999) leading to a conformational rearrangement of the middle domain (Franzmann et al., 2008) and to an increased chaperone activity. Furthermore the preincubation procedure at 37 °C has been described to lead to the formation of a homogenous oligomer species (Kriehuber, 2012). Except for the truncation mutant Hsp26ΔN30-C194, all other mutans only contain a few residues of the middle domain or even no N-terminal elongation at all. With the shortened sequence of the Hsp26 protein and the disruption of the middle domain such an effect was not visible in the conducted experiments.

In general the SEC-HPLC data and the AUC results nicely fit together. Discrepancies might be due to the nonideal globularity of the protein or caused by protein-matrix interactions during the SEC-HPLC runs. In comparison to the published data of the tested mutants the results were consistent. The degraded truncation mutant Hsp26ΔN30-C194 is published to form a stable dimer (Chen et al., 2010, Franzmann et al., 2008), whereas Hsp26αM1 was described to be monomeric (Chen et al., 2010). Previous studies reported the minimal alpha crystallin domain to be monomeric and stably folded, whereas the induction of dimerization was possible by elongations of the N- and C- terminus (Chen et al., 2010). For the formation of stable dimers either the presence of the complete middle domain was required, or the presence of a C-

terminal extension including the IXI motif (Chen et al., 2010). With the mutants analyzed in the present work these findings could be confirmed.

	HPLC -PI	HPLC +PI	AUC
Hsp26αM1	Monomer/Dimer	Monomer/Dimer	Dimer
Hsp26αC2	Dimer	Dimer	Dimer
Hsp26αM2	Monomer/Dimer	Monomer/Dimer	Monomer
$Hsp26_{76-201}$	Dimer	Dimer	Monomer
Hsp26ΔN30-C194	Monomer/degraded	Monomer/degraded	degraded
$Hsp26_{95-214}$	Dimer	Dimer	Dimer
Hsp26 WT	-	-	32 mer

Table 2: Overview of the results obtained by SEC-HPLC and AUC for the Hsp26 truncation mutants. Experiments were performed in 10 mM sodium phosphate, 150 mM NaCl, pH 6.5 at 20 °C. For HPLC experiments the protein sample was either preincubated at 37 °C overnight (+ PI) or analyzed without preincubation (-PI).

The truncation mutants were used for NMR experiments with the aim to elucidate the dimerization mode. With the mutant Hsp26αM1, well resolved HSQC spectra could be generated which allowed for the assignment of most of the signals. In NMR studies on αB-crystallin is has been shown that changes in pH and temperature influenced the monomer-dimer equilibrium of the protein (Jehle et al., 2009). For the Hsp26αM1 construct, no effect of buffers with different pH values or salt concentrations could be observed.

With the use of longer constructs compared to the Hsp26αM1 mutant, the spectra became more crowded, probably due to the fact that dimeric states were present. Changes in temperature or concentration improved the spectrum quality but at the same time led to the disruption of the dimers. The challenging task is to find a construct which is present as a stable homogenous dimer under the conditions used for NMR experiments. The construct Hsp26ΔN30-C194 containing the ACD and the whole middle domain might be a good choice. Even though previous NMR experiments with this mutant were too complex to work with, the latest progress with the mutant Hsp26αM1 and the assignment of most of the residues might be helpful for future investigations with more complex samples. However, in the

present work, attempts to label and purify the Hsp26ΔN30-C194 mutant for NMR resulted in degraded protein samples, probably due to the flexible N-terminal region which might be easily accessible for proteases.

Based on the present data, only speculations on the dimerization mode of Hsp26 are possible. With the help of the assigned HSQC spectrum of the truncation mutant Hsp26αM1, a flexible linker could be identified in heteronuclear NOE experiments in this mutant. The linker comprises the residues 135-155 of Hsp26. With the presence of a flexible linker in this region rather the dimerization mode via domain swapping would be supported. In an Hsp26 model of a domain swapping dimer based on the structure of *M. jannaschii* Hsp16.5 (Kim et al., 1998) this linker region is present as an isolated loop lying on one side allowing flexibility to a certain extent (Figure 20). In contrast to that, an Hsp26 model of an antiparallel dimer based on the human αB-crystallin structure (Jehle et al., 2009) shows most of the residues 135-155 to be involved in intra-domain/inter-strands interactions suggesting a more rigid environment, in which the flexibility of the linker is not allowed. Therefore, for Hsp26, the dimerization mode via domain swapping is suggested, as it has been shown for sHsps from archaea (Kim et al., 1998) and plants like Hsp16.9 from *T. aestivum*, for example (van Montfort et al., 2001).

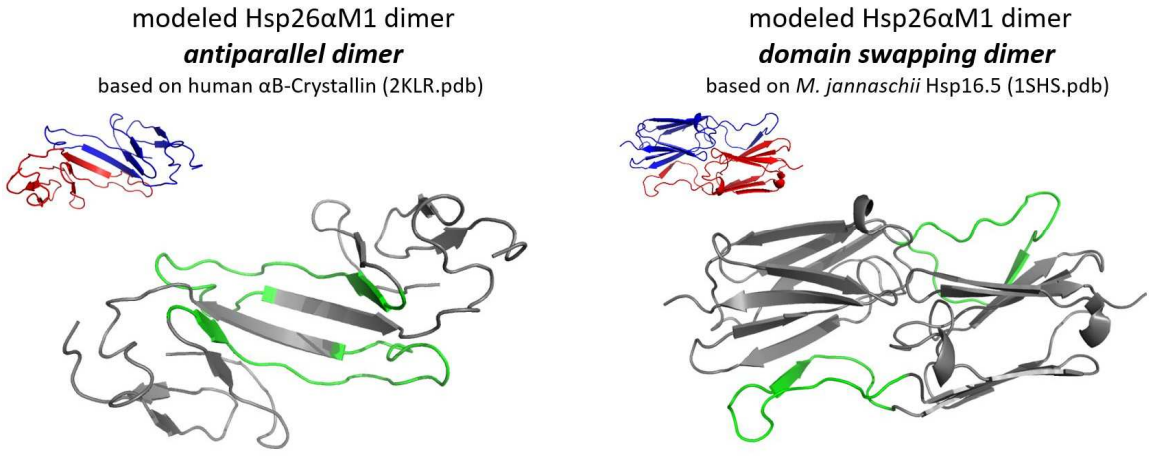

Figure 20: Homology models of Hsp26αM1 based on the antiparallel dimer of human αB-Crystallin (2KLR.pdb) or the domain swapping dimer of *M. jannaschii* Hsp16.5 (1SHS.pdb). Residues that were identified to be flexible in hetNOE experiments are highlighted in green. The template structures are shown in red and blue.

The Hsp26 dimers are supposed to be the basic building block for the formation of larger oligomers. Regarding the oligomerization state, Hsp26 has been shown to be heterogeneous and a variety of different oligomeric species have been observed. Earlier studies reported Hsp26 to assemble into a 24mer (Haslbeck et al., 1999, Franzmann et al., 2005), which was shown by cryo- electron microscopic analysis to be dynamic and exist in a compact and expanded form (White et al., 2006). Later studies applying mass spectrometry have shown oligomerization states of up to 42 subunits (Benesch et al., 2010). Furthermore, the stabilization of larger oligomerization states by higher salt concentrations has been reported and the presence of up to 48mers was shown (Kriehuber, 2012). By EM analysis of the $Hsp26_{S4C}$ mutant a 3D model of an Hsp26 oligomer could be constructed with a resolution of ~1.5 nm. Therefore, the mass of a 48mer was assumed and a octahedrally symmetry was calculated. For further refinement of the model, the collection of a larger dataset of $Hsp26_{S4C}$ on a direct detector is needed.

4.1.2 Regulation of Hsp26

For Hsp26 a regulation via heat activation accompanied by conformational changes in the middle domain is described (Franzmann et al., 2008, Haslbeck et al., 1999). Small heat shock proteins have been shown to rest in an inactive low-affinity state which can turn into a high affinity state via activation and be then able to bind substrates and prevent their aggregation (Haslbeck and Vierling, 2015). A common mechanism in proteins in general is the regulation via posttranslational modification like phosphorylation, acetylation and methylation for example (Karve and Cheema, 2011, Prabakaran et al., 2012). For Hsp26 some phosphorylation sites are already known (Table 3).

Position	BioGRID	ppt1	Hsp90
T42	P	P	P
S47	P	P_1	
T48		P_1	
S90	P	P	P
S144		P	
T163	P	P	
S207	P		
S208	P	P_2	P_2
S211	P	P_2	P_2

Table 3: Overview on the identified phosphorylation sites of Hsp26. Indices show the presence of diphosphopeptides that have been observed. Data provided by the BioGRID database (https://thebiogrid.org/) originates from proteomewide phosphostudies in *S. cerevisiae* (Ficarro et al., 2002, Smolka et al., 2007, Albuquerque et al., 2008, Bodenmiller et al., 2010, Helbig et al., 2010, Holt et al., 2009). Additional phospho-sites were identified by investigations on the Ser/Thr phosphatase ppt1 (Schreiber et al., 2012) and in Hsp90 pull-down experiments (Soroka et al., 2012).

Already annotated phosphosites that can be found in databases like BioGRID (https://thebiogrid.org/), for example, originate from proteomewide phosphostudies in *S. cerevisiae* (Ficarro et al., 2002, Smolka et al., 2007, Albuquerque et al., 2008, Bodenmiller et al., 2010, Helbig et al., 2010, Holt et al., 2009). Investigations on the phosphoproteome regulation by the Ser/Thr phosphatase ppt1 revealed an additional phosphorylation site on position S144. In addition to the single phosphosites also peptides containing two phosphorylations were identified in this attempt. In this connection, peptides with phosphorylation sites on positions S47/T48 and S208/S211 were identified (Schreiber et al., 2012). The presence of the twofold phosphorylated Hsp26 peptide S208/S211 was confirmed by pull-down experiments with Hsp90 as well (Soroka et al., 2012).

Interestingly, none of the phosphorylation sites known so far is located in the N-terminal domain of Hsp26 but they are distributed over the middle domain, alpha crystallin domain and C-terminal domain (Figure 21). This is of particular interest, as it has been shown before that deletion of the N-terminal domain has almost no effect on the oligomerization or chaperone activity of Hsp26 (Haslbeck et al., 2004b).

Figure 21: Position of the nine phospho-sites in Hsp26. The phosphosites (P) are distributed over the middle domain (M), alpha crystallin domain (ACD) and C-terminal domain (C). No phosphosites have been identified in the N-terminal domain (N) so far.

4.1.2.1 Analysis of phosphomimetic Hsp26 mutants

To analyze the effect of phosphorylation in proteins, a common approach is to introduce negative charges by substitution of the specific amino acid by the negatively charged glutamic acid (Ahmad et al., 2008, Ito et al., 2001, Koteiche and McHaourab, 2003, Shashidharamurthy et al., 2005). Dr. Thomas Kriehuber already started with the cloning, purification and investigation of phosphomimetic mutants of Hsp26 and was able to show that the mutants were more active in chaperone assays with chemically denatured citrate synthase compared to the wildtype protein (Kriehuber, 2012).

In the present work, the mutants were further investigated. Therefore chaperone assays with chemically denatured citrate synthase were performed under varying conditions. Four different phosphometic mutants, the single mutants $Hsp26_{T163E}$ and $Hsp26_{S144E}$ and the double mutants $Hsp26_{S47E/T48E}$ and $Hsp26_{S208E/S211E}$, were characterized for their ability to suppress the aggregation of citrate synthase compared to the Hsp26 wildtype protein (Figure 22). The experiments were performed either with or without a heat activation step of the sHsps for 10 min at 43 °C. After addition of the substrate, a rapid increase of the relative turbidity at 360 nm could be observed implying a strong induction of aggregation. In general, the phosphomimetic mutants showed a higher chaperone activity than the wildtype Hsp26 protein. Heat activation did not increase their chaperone activity. The mutant $Hsp26_{S144E}$ seems to become instable after heat activation in buffer with low ionic strength and seems to co-aggregate with the substrate (Figure 22 C). The mutant $Hsp26_{S208E/S211E}$ shows a very noticeable signal which slowly and continuously

increases during the time of the experiment. This characteristic has already been observed by Dr. Thomas Kriehuber and could point to the inability of this mutant to stably bind the substrate. It suggests that the substrate is continuously released which leads to a delayed aggregation (Kriehuber, 2012).

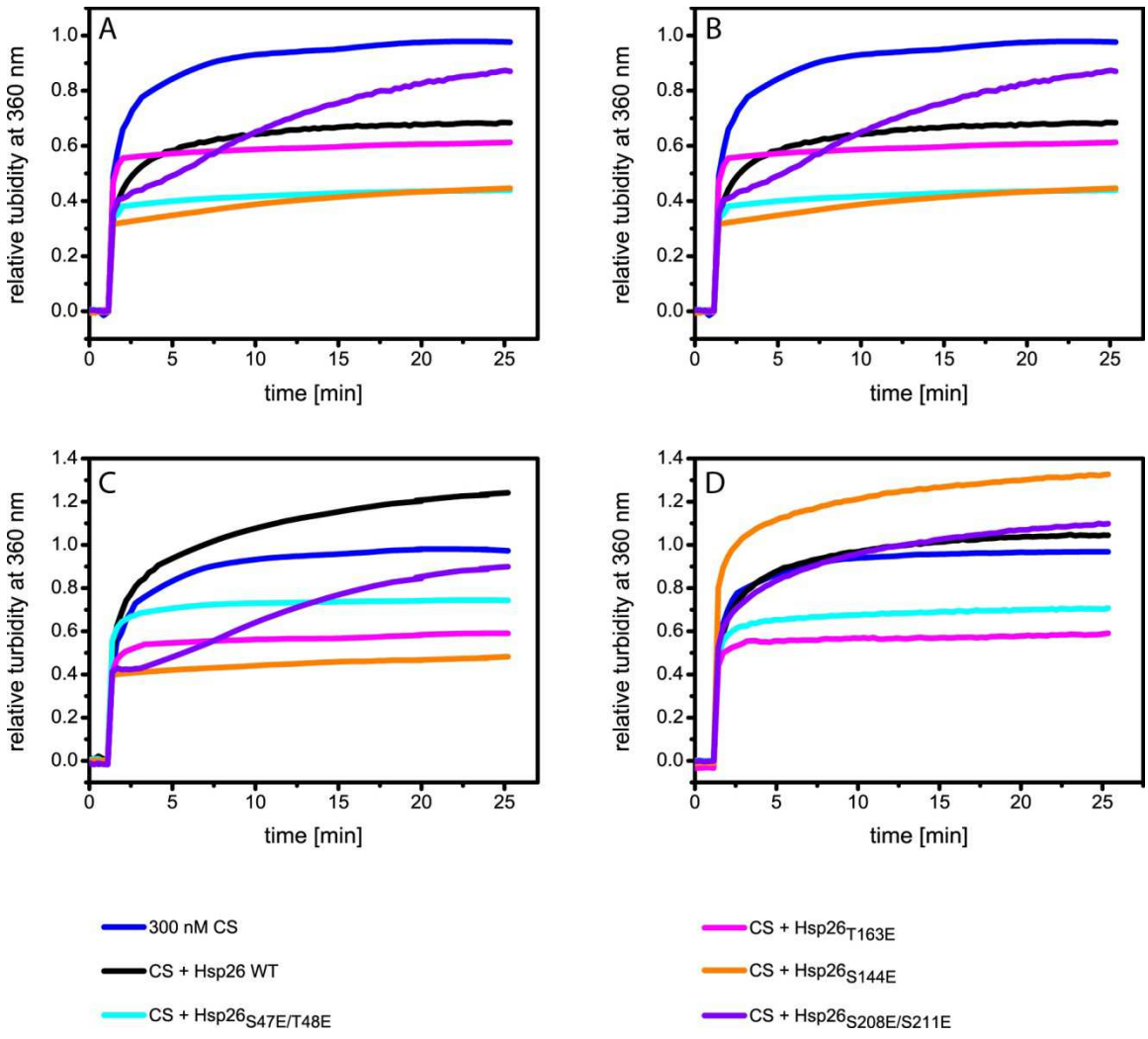

Figure 22: Chaperone activity assays of the phosphomimetic mutants (600 nM) and denatured citrate synthase (300 nM) as a model substrate. Measurements were performed at 25 °C in 40 mM Hepes, 50 mM NaCl, pH 7.4 (A+B) or 40 mM Hepes, pH 7.4 (C+D), either without heat activated sHsps (A+C) or after heat activation for 10 min at 43 °C (B+D).

To further analyze the interaction of Hsp26 and the respective phosphomimetic mutants with substrate, the size of the formed sHsp-substrate complexes was assessed by analytical SEC-HPLC. Therefore the sHsp-substrate complexes were

loaded onto a YMC-Pack Diol 300 column (YMC) and separated in 40 mM Hepes, pH 7.4 with a flow rate of 0.6 ml/min. Without a previous heat activation step, the Hsp26 wildtype protein shows a retention time of 6.6 minutes (Figure 23 A). The retention time of the main peak of the sHsp-substrate complexes with Hsp26 WT is slightly shifted to 5.9 minutes, which roughly corresponds to a size of 400 kDa. The analyzed phosphomimetic mutants alone all clearly show a broader peak than the wildtype with a retention time between 5.7-20 minutes. In sHsp-substrate complexes of citrate synthase and the double mutants $Hsp26_{S47E/T48E}$ or $Hsp26_{S208E/S211E}$ a considerable shift towards smaller species is visible. The main peaks show retention times of about 17 minutes (Figure 23 C/D). For the mutant $Hsp26_{T163E}$ the effect is not that prominent. The main species shows a retention time of 5.8 minutes, however further species elute until 18 minutes (Figure 23 B).

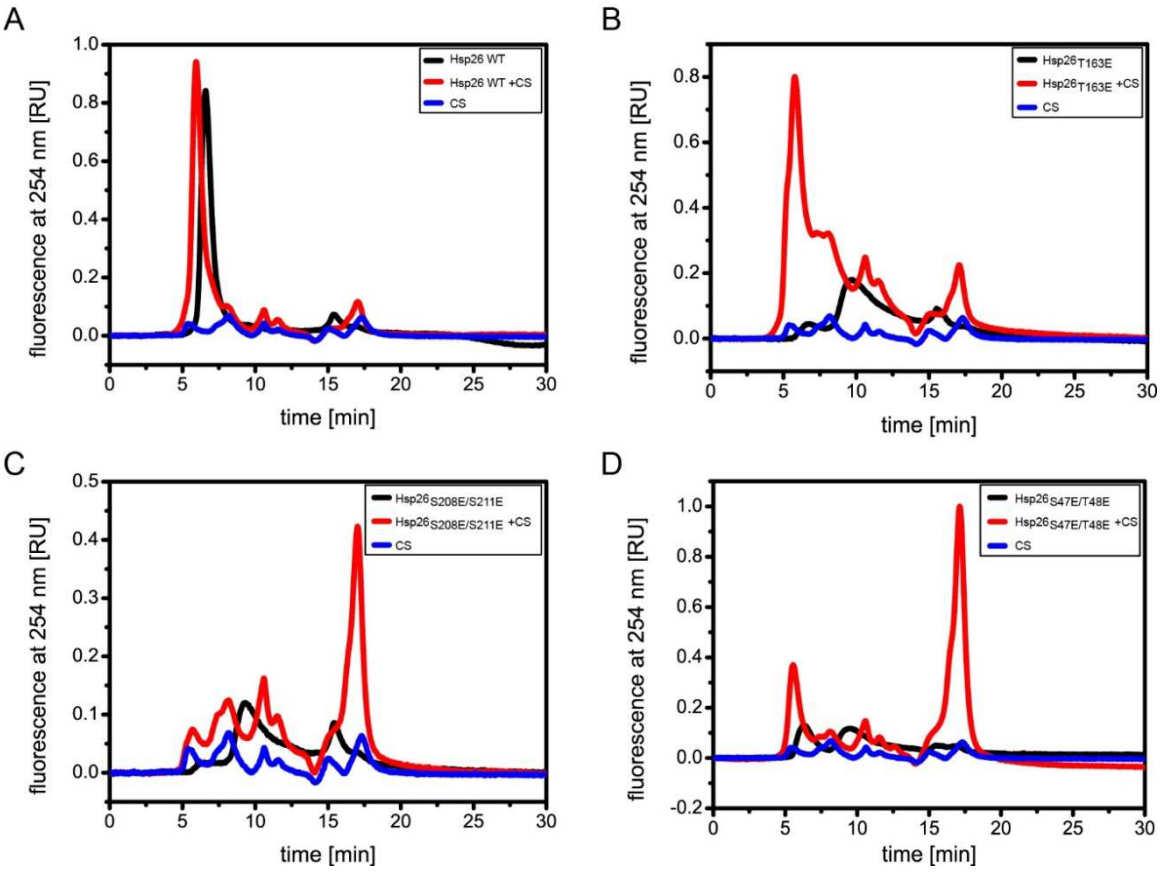

Figure 23: Analysis of the Hsp26 phosphomimetic mutants by SEC-HPLC on a YMC-Pack Diol 300 column in 40 mM Hepes, pH 7.4 with a flow rate of 0.6 ml/min. The mutants were either analyzed alone (black) or after a chaperone assay with citrate synthase (red) without prior heat activation.

In comparison, the sHsp-substrate complexes were also analyzed after pretreatment of the sHsp for 10 min at 43 °C. For the Hsp26 wildtype protein, a peak at a retention time of 6.0 minutes was observed similar to the measurements without heat activation, but, in addition, a second peak appeared at a retention time of 17.2 minutes (Figure 24 A). This means that after heat activation, the Hsp26 WT is able to form smaller sHsp-substrate complexes with citrate synthase. With the $Hsp26_{T163E}$ mutant as well, a shift towards smaller sHsp-substrate complexes could be generated upon heat activation (Figure 24 B). Here, the main peak shows a retention time of 17 minutes. For the $Hsp26_{S47E/T48E}$ mutant, no further shift towards smaller species could be obtained by heat activation (Figure 24 D). The $Hsp26_{S208E/S211E}$ mutant even showed the tendency to form larger sHsp-substrate complexes after the heat pretreatment (Figure 24 C).

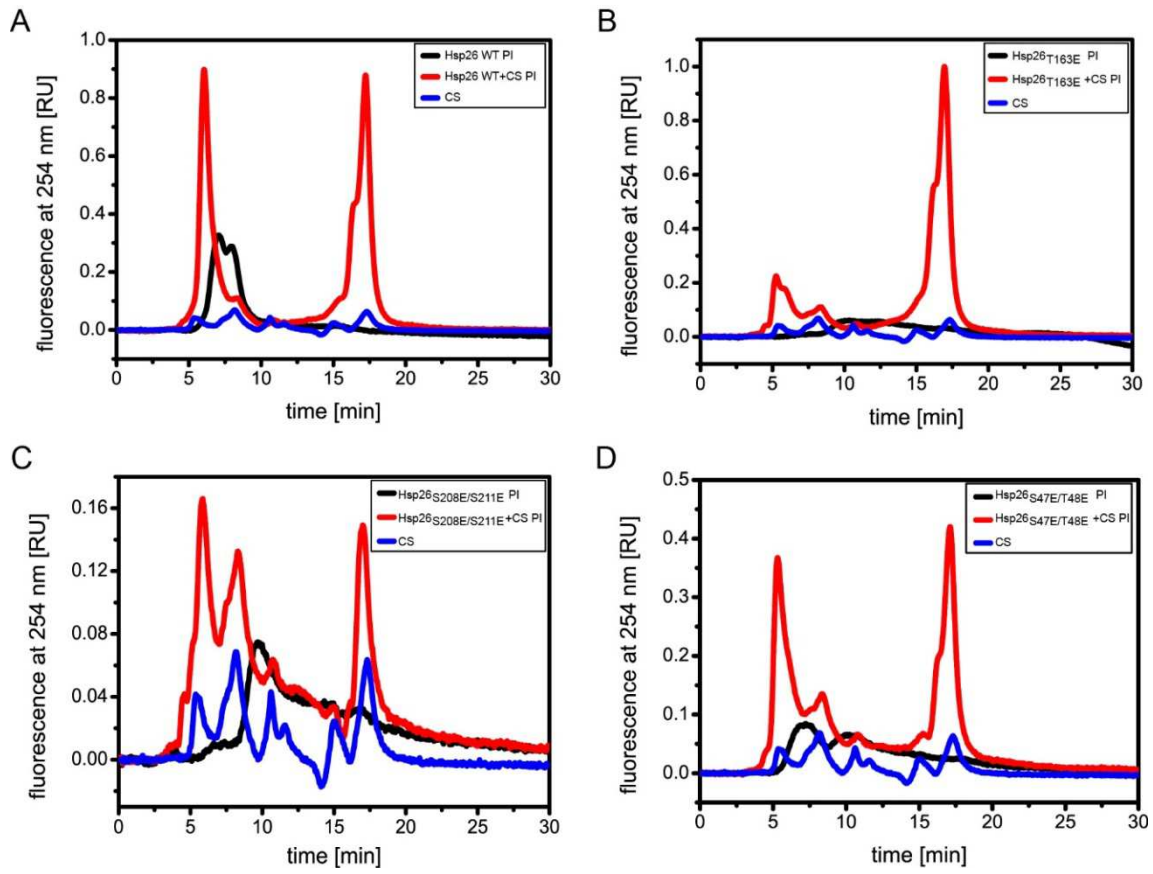

Figure 24: Analysis of the Hsp26 phosphomimetic mutants by SEC-HPLC on a YMC-Pack Diol 300 column in 40 mM Hepes, pH 7.4 with a flow rate of 0.6 ml/min. The mutants were either analyzed alone (black) or subsequent to a chaperone assay with citrate synthase (red) after a heat activation treatment for 10 min at 43 °C.

4.1.2.2 Summary on the regulation of Hsp26

As a possible activation mechanism for Hsp26, heat activation has been proposed so far. Heat activation of Hsp26 was shown to come along with the dissociation of the oligomer and an increase in chaperone activity (Haslbeck et al., 1999, Stromer et al., 2004). The SEC-HPLC analysis revealed that without heat shock the phosphomimetic mutants already exist in smaller oligomeric species compared to the wildtype protein. These results are in line with previous studies on the mutants $Hsp26_{S47E/T48E}$, $Hsp26_{S144E}$ and $Hsp26_{S208E/S211E}$ that showed smaller oligomers by AUC and EM analysis (Kriehuber, 2012). Moreover the phosphomimetic mutants have been shown to form sHsp-substrate complexes of a small size which is observed for the wildtype protein only after heat shock treatment (Figure 25).

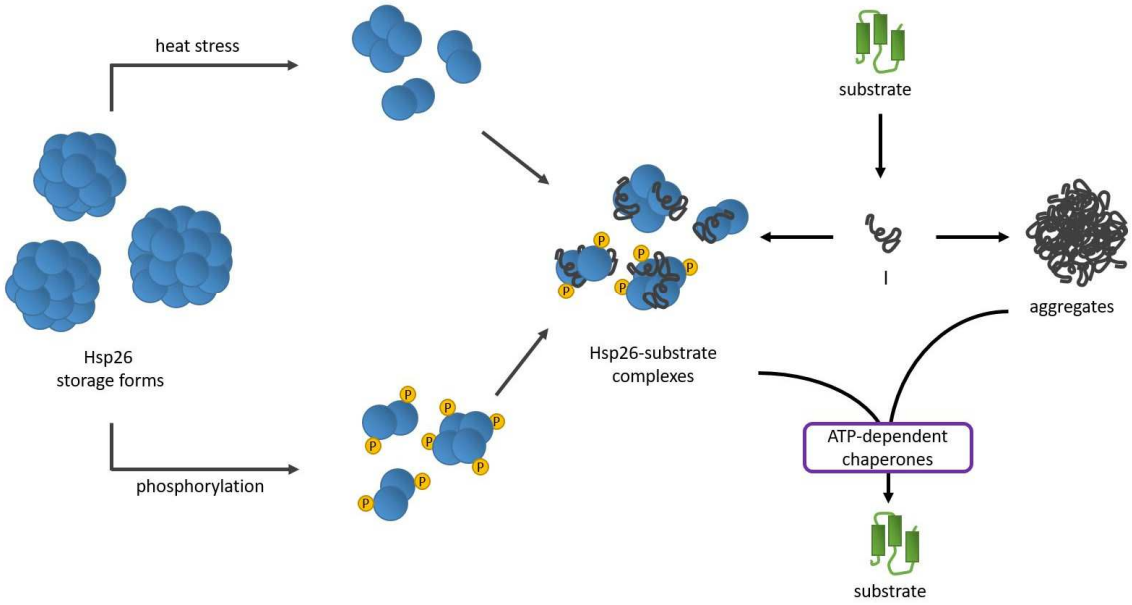

Figure 25: Model of the two possible activation mechanisms for Hsp26. Hsp26 is present in large oligomeric storage forms. The dissociation of the oligomers and formation of smaller Hsp26-substrate complexes can either be induced by heat activation or by phosphorylation of Hsp26. By the formation of soluble sHsp-substrate complexes, Hsp26 prevents unfolding substrates from aggregation and keeps them in a refolding- competent state.

Phosphorylation sites have been investigated for a number of other sHsp already. It has been shown that phosphorylation can be induced by a variety of different stimuli like heat stress, H_2O_2, arsenite, sorbitol or NaCl for example (Ito et al., 2001). As a general effect of phorphorylation, the dissociation of large oligomers can be

mentioned, probably due to the introduction of negative charges and the consequent charge repulsion which then leads to the destabilization of the oligomeric structure (Bakthisaran et al., 2015). As observed for the analyzed Hsp26 phosphomimetic mutants, *in vitro* experiments with phosphomimicking mutants of Hsp27 from Chinese hamster and human αB- crystallin have shown a decrease in oligomeric size compared to the wildtype proteins (Theriault et al., 2004, Peschek et al., 2013). Along with that, a higher rate of subunit exchange has been observed for the αB-crystallin mutant (Peschek et al., 2013, Ahmad et al., 2008). Subunit exchange and a dynamic oligomeric structure of sHsps are thought to be important prerequisites for the regulation of substrate binding in sHsps, making the interaction surfaces more accessible to the target proteins (Cheng et al., 2008, Jaya et al., 2009, Bakthisaran et al., 2015).

Regarding the chaperone activity of the phosphomimicking mutants, differential observations were made. The chaperone activity of phosphomimicking αB-crystallin mutants was shown to be target dependent. With substrates like T4 lysozyme (Koteiche and McHaourab, 2003), insulin and alcohol dehydrogenase (ADH) (Ecroyd et al., 2007), as well as MDH and p53 (Peschek et al., 2013) the mutants showed higher chaperone activity compared to the wildtype αB- crystallin, whereas for lactate dehydrogenase (LDH), for example, the activity was decreased (Ito et al., 2001). Under the conditions tested, the Hsp26 phosphomimetic mutants mostly revealed a higher chaperone activity in *in vitro* aggregation assays than the wildtype Hsp26. However further analysis with different substrates is needed to draw general conclusions. Besides, differential investigations regarding the various phosphorylation sites in Hsp26 are of special interest. For Hsp26, nine possible phosphorylation sites have been identified, suggesting the possibility of differential regulation by specific phosphorylation of respective residues or patterns of residues. For Hsp27, the discrimination between its targets has been shown to be regulated via phosphorylation of the different phosphorylation sites (Paul et al., 2010, Gibert et al., 2012, Arrigo and Gibert, 2012, Arrigo and Gibert, 2013). Furthermore it was shown that for the dissociation of the oligomer, phosphorylation of residue S90 was sufficient whereas its thermoprotective function needed the phosphorylation of S90 and S15 in combination (Rogalla et al., 1999). A recent study on optic nerve injury in

rat retina even revealed a cell-type specific phosphorylation pattern of HspB1 and HspB5 (Schmidt et al., 2016). In summary, regulation of sHsps via phosphorylation opens a wide field of possibilities which surely is profitable to gain further insight in. Results in the present work support the idea that aside of thermal activation phosphorylation might be a further regulation mechanism for Hsp26.

4.2 Substrate spectra of human small heat shock proteins

Some higher eukaryotes contain a large number of sHsps. This raises the question if the sHsps in those organisms fulfill redundant functions or if they are specialized on specific substrates or mechanisms. In the human genome, in total 10 different sHsps are found, which are named HspB1- HspB10. They were shown to have different expression patterns and different biochemical properties (Bakthisaran et al., 2015). Furthermore they exhibit different oligomeric states ranging from monomers, as shown for HspB8 (Mymrikov et al., 2010, Kasakov et al., 2007), to large oligomeric species like HspB5 (Braun et al., 2011), for example. Such differences may hint to the presence of different substrate spectra for sHsps and different functions *in vivo*. In the present work, the substrate spectra of the human sHsps were analyzed by a mass spectrometric approach.

4.2.1 Identification of interactors of human sHsps

For the analysis of substrate spectra of the different human sHsps, co-immunoprecipitation experiments were performed under heat-shock conditions (90 min at 45 °C) with cell lysates of HEK293 cells and the respective recombinantly purified sHsp. Specificity was ensured by the use of the respective anti-sHsp-antibody. Samples with the isolated sHsp-substrate complexes were analyzed via SDS-PAGE (Figure 26). The co-immunoprecipitation experiments were carried out by Dr. Evgeny Mymrokov for the proteins HspB1-HspB8. Under the experimental conditions used, HspB8 was instable and degraded during the experimental procedure. Therefore HspB8 had to be excluded from the analysis. Analysis of the samples by SDS-PAGE revealed that most interactors were bound by HspB1, HspB3 and HspB5, whereas for HspB2, HspB4, HspB6 and HspB7 substrate proteins on the gels were less intense (Figure 26). The co-immunoprecipitation experiments were performed in triplicates in two distinct experiments, CoIP1 and CoIP2, with slight modifications in the experimental procedure (for details see section 3.7.1 and 3.7.5). As a reference, the heat-sensitive fraction of HEK293 cell lysate was determined. Therefore the lysate was incubated for 90 min at 45 °C followed by a centrifugation step to separate the soluble from the insoluble protein fraction. The insoluble

fraction was as well analyzed by SDS-PAGE and is referred to as heat-sensitive fraction (HS).

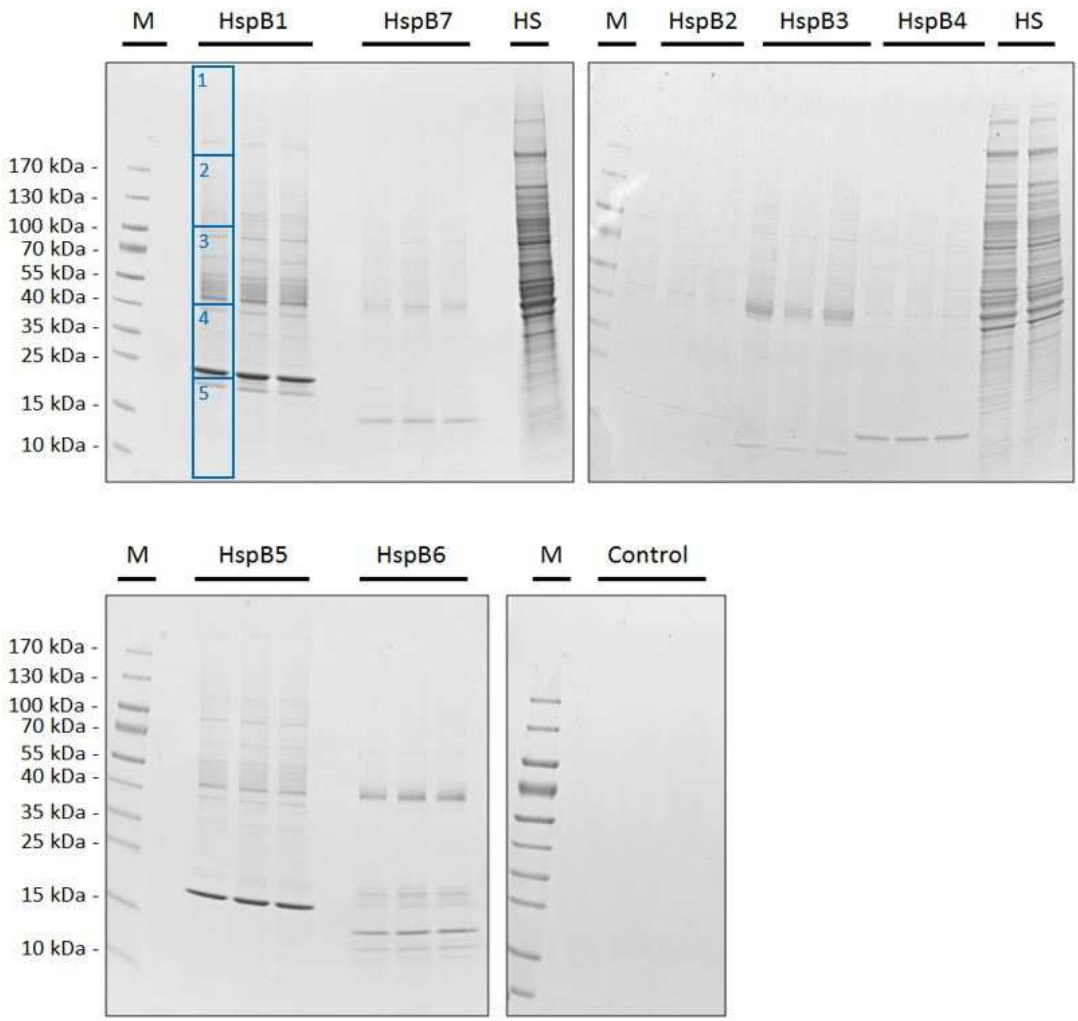

Figure 26: SDS-PAGE of the co-immunoprecipitation with 10 µM of the indicated human sHsps and 0.8 mg/ml HEK293 lysate under heat shock conditions (90 min at 45 °C). Each gel lane was cut into 5 pieces as indicated in blue for HspB1.

To further analyze the substrate spectra of human sHsps each gel lane was cut into 5 pieces (Figure 26) and treated as an individual sample. The proteins were reduced, alkylated and in-gel digested with trypsin overnight. After extraction of the peptides they were analyzed by liquid chromatrography- mass spectrometry on a LTQ Orbitrap XL (ThermoFisher Scientific) instrument. Full scans and 5 collision-induced dissociation MS^2 scans were recorded in each cycle.

Data evaluation was performed using the "Proteome Discoverer 1.4" software (ThermoFisher Scientific) with the implemented search algorithm Sequest HT. The data were searched against the Swiss-Prot *Homo sapiens* database (15.02.2016 edition). A maximum of two missed cleavage sites was allowed and the peptide tolerance was set to 10 ppm for precursors and 0.6 Da for fragment masses. For the false discovery rate, a threshold of < 1% of false positive hits was set according to the decoy search. Only proteins with at least two distinct peptides found were counted as hits. Proteins that were found in the control samples were excluded from further evaluation due to unspecific interactions with the protein G- sepharose beads. Keratin hits had to be excluded as well due to the inability to distinguish "real" hits like interactors from the human cell lysates from contaminations. In a last step, the results of both individual experiments, CoIP1 and CoIP2, were combined. Only hits that appeared in both datasets were accepted for further analysis. Furthermore the hits had to be observed in at least two replicates in both datasets. All other hits were excluded.

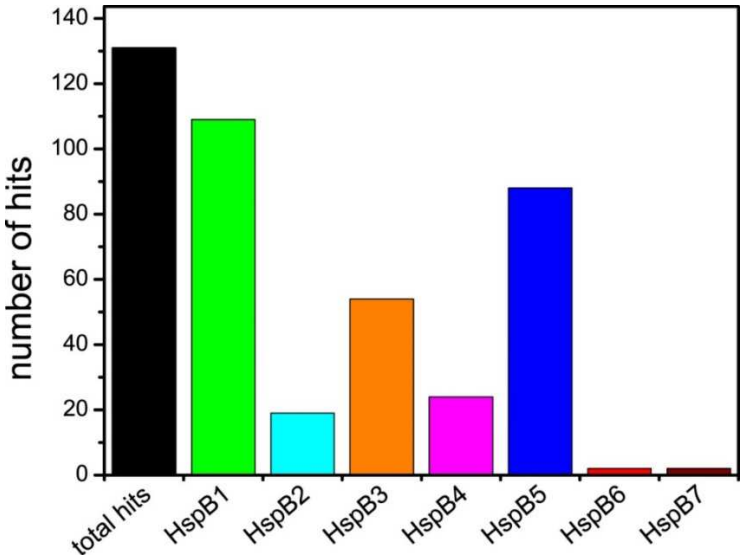

Figure 27: Number of protein interactors for HspB1-HspB7 detected in co-immunoprecipitation experiments and mass spectrometric analysis. The black bar represents the number of total unique hits.

Applying such strict selection criteria, in total 130 unique protein hits were detected as potential sHsp substrates. Compared to the heat-sensitive fraction, which revealed about 1100 different proteins by mass spectrometric analysis, the sHsps interactors found by pulldown experiments constitute about 12 %. Notably the number of hits varied a lot among the different human sHsps (Figure 27). For HspB1 the highest number of putative substrates was found with 109 different hits. HspB5 and HspB3 showed 88 and 54 hits, whereas the number of hits clearly decreased with 24 hits for HspB4 and 19 hits for HspB2. For HspB6 and HspB7 only 3 and 2 hits could be detected. The number of detected protein hits confirms the first quantitative estimation assessed by SDS-PAGE. A detailed list of the identified protein hits is attached in the appendix.

To analyze if the human sHsps share some common substrates, a pairwise comparison of the substrate hits of the different sHsps was conducted (Table 4). To illustrate the results in proportional Venn-diagrams the "Venn diagram plotter" by the Pacific Northwest National Laboratory (https://omics.pnl.gov/software/venn-diagram-plotter) was used.

sHsp 1	total hits sHsp 1	hits sHsp1 only	overlapping hits	hits sHsp2 only	total hits sHsp 2	sHsp 2
HspB1	109	93	16	3	19	HspB2
HspB1	109	62	47	7	54	HspB3
HspB1	109	86	23	1	24	HspB4
HspB1	109	34	75	13	88	HspB5
HspB1	109	107	2	1	3	HspB6
HspB1	109	107	2	0	2	HspB7
HspB2	19	2	17	37	54	HspB3
HspB2	19	7	12	12	24	HspB4
HspB2	19	5	14	74	88	HspB5
HspB2	19	18	1	2	3	HspB6
HspB2	19	17	2	0	2	HspB7
HspB3	54	34	20	4	24	HspB4
HspB3	54	11	43	45	88	HspB5
HspB3	54	52	2	1	3	HspB6
HspB3	54	52	2	0	2	HspB7
HspB4	24	1	23	65	88	HspB5
HspB4	24	22	2	1	3	HspB6
HspB4	24	22	2	0	2	HspB7
HspB5	88	86	2	1	3	HspB6
HspB5	88	86	2	0	2	HspB7
HspB6	3	2	1	1	2	HspB7

Table 4: Pairwise comparison of the identified protein hits for the different sHsps. The numbers of overlapping hits for the two partners sHsp 1 and sHsp 2 are shown.

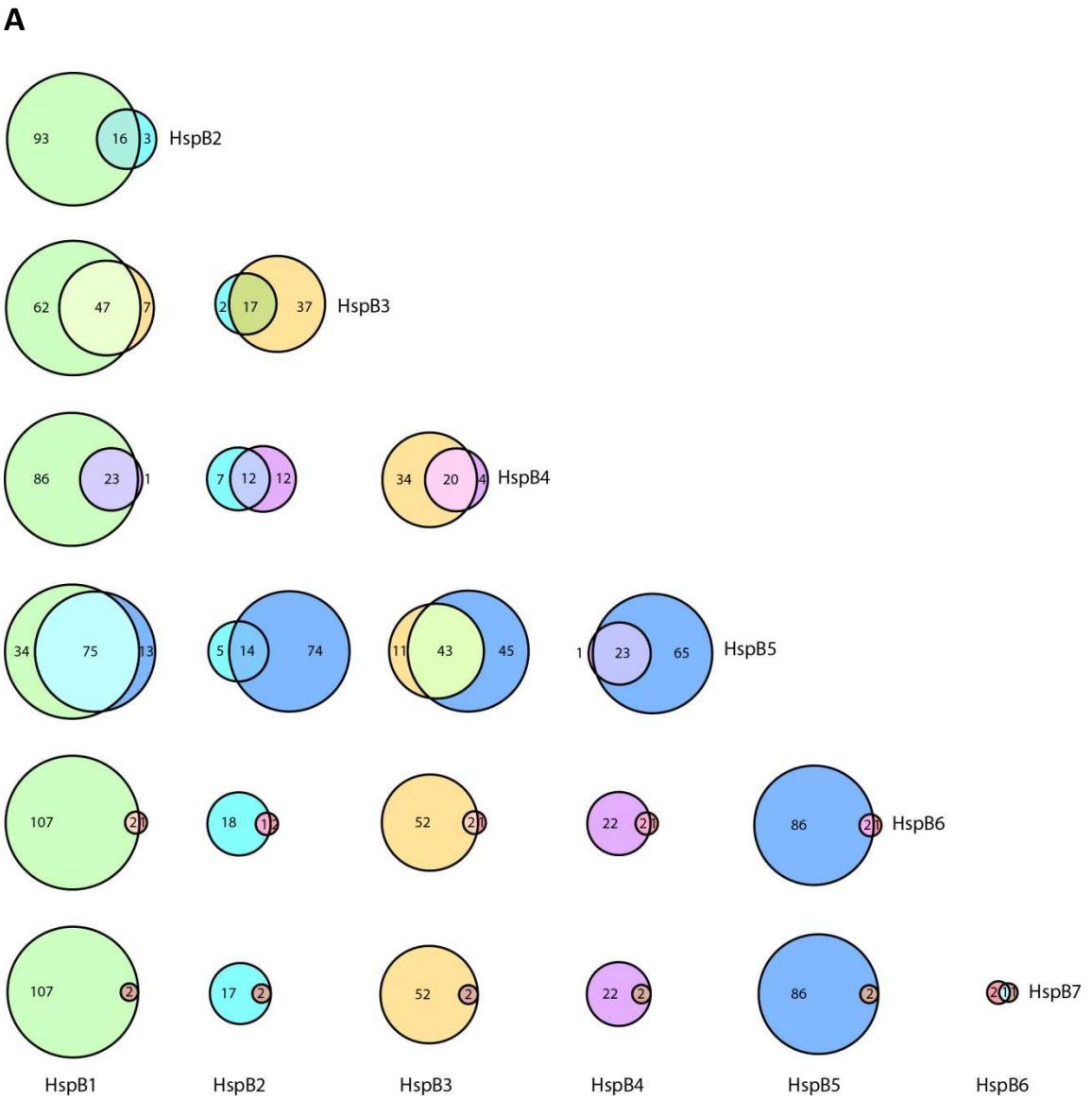

Figure 28: Numbers of overlapping interactors. Color code for the different sHsps: HspB1 (green), HspB2 (cyan), HspB3 (orange), HspB4 (magenta), HspB5 (blue), HspB6 (red), HspB7 (brown). A) Proportional representation of common interactors in pairwise comparison. B) Overlapping interactors for HspB1, HspB3 and HspB5.

In general, all sHsps analyzed show overlapping substrates with any other sHsp (Figure 28 A). There's no sHsp with a specific unique set of substrates. One interactor which was found in pulldowns with all sHsps tested is CCT8, a subunit of the TRiC/CCT complex. A further subunit of this complex, CCT3, was found for six out of the seven sHsps analyzed. All interactors that were found for HspB4 were also identified for HspB1 and HspB5, except DnaJB1 as the only exception. The identification of DnaJB1 as a unique hit for HspB4 is astonishing as DnaJB1 is the most ubiquitous member of the Hsp40 protein family.

The highest number of overlapping protein hits was found for HspB1, HspB3 and HspB5, which were also the sHsps with the highest number of identified interactors in total. HspB1 and HspB5 share 75 protein hits, whereas HspB1 and HspB3 have 47 interactors in common. HspB3 and HspB5 show an overlap of 43 potential substrates. In total HspB1, HspB3 and HspB5 were found to have 41 common proteins hits (Figure 28 B).

4.2.2 Biochemical properties of human sHsps substrate proteins

To get insight into the common features of the potential sHsp substrates, they were compared for biochemical properties (Figure 29). As for HspB6 and HspB7 only very few hits were detected, they were excluded from statistical analysis.

Regarding the monomeric molecular masses, the first quartile for substrates of HspB1 and HspB5 lies at 48 kDa with a median at 59 kDa and 60 kDa respectively. For HspB3 and HspB4 the values for the first quartile are shifted towards higher monomeric molecular masses of 56 kDa and 58 kDa, with the median at 76 kDa for both samples. HspB2 showed a more narrow range, probably due to the lower number of identified substrates, with the first quartile at 50 and the median at 59 kDa. As a comparison, the heat-sensitive fraction and the whole human proteome were analyzed as well. Most of the hits for the heat-sensitive fraction lie in the range of 31-93 kDa for their monomeric molecular mass with a median at 50 kDa. With this, the heat-sensitive fraction shows a broader distribution compared to the whole human proteome, with a slight shift towards proteins of higher monomeric molecular masses. Compared to the whole human proteome and to the heat-

sensitive fraction as well, the distributions of the sHsp substrates are significantly shifted towards higher monomeric molecular masses. Also the range for sHsps substrates is more narrow compared to the heat-sensitive fraction. The present results indicate a preferred binding of the analyzed sHsps to larger, aggregation-prone substrate proteins in the range between 50-100 kDa.

In a next step, the pI distribution of the sHsp substrates was analyzed. As a reference again the heat-sensitive fraction and the whole human proteome was assessed. The pI distribution in the whole human proteome ranges from 2.8 to 13.3. The extremely broad distribution shows a median at about 7. Compared to that, the heat-sensitive fraction shows a lower median at 6.5 with a more narrow distribution. Here about 50 % of the protein hits lie between pI values of 5.6 and 7.7 in the neutral region. In contrast to that, the sHsp substrates show a narrower distribution with a shift towards lower pI values. Most of the hits showed pI values ranging from 5.4 to 6.8. There was no sHsp substrate detected with a pI <4.3 and only two substrates of HspB1 showed a pI above 9.0. In summary, human sHsps seem to preferentially bind to moderately negatively charged proteins.

As it is suggested that sHsps bind to their substrates via hydrophobic patches that become surface exposed upon unfolding (Basha et al., 2012, Patel et al., 2014), the hydrophobicity of the substrate proteins was analyzed. A value which can be easily compared is the GRAVY index (Kyte and Doolittle, 1982) which is a hydrophobicity score calculated based on the amino acid composition. Proteins with a positive GRAVY index show a high percentage of hydrophobic residues, whereas a negative GRAVY index indicates a low amount of hydrophobic residues. For the whole human proteome, the calculations of the GRAVY index resulted in a median of –0.37. For the heat sensitive fraction a median of -0.4 was observed with most of the proteins ranging between values from -0.6 to -0.2. In general only minor shifts in the distribution of the GRAVY index were seen for the sHsp substrates. It is important to note that no shift towards positive values could be detected. The whole human proteome only showed a slightly broader range compared to the heat-sensitive fraction and the human sHsp substrates.

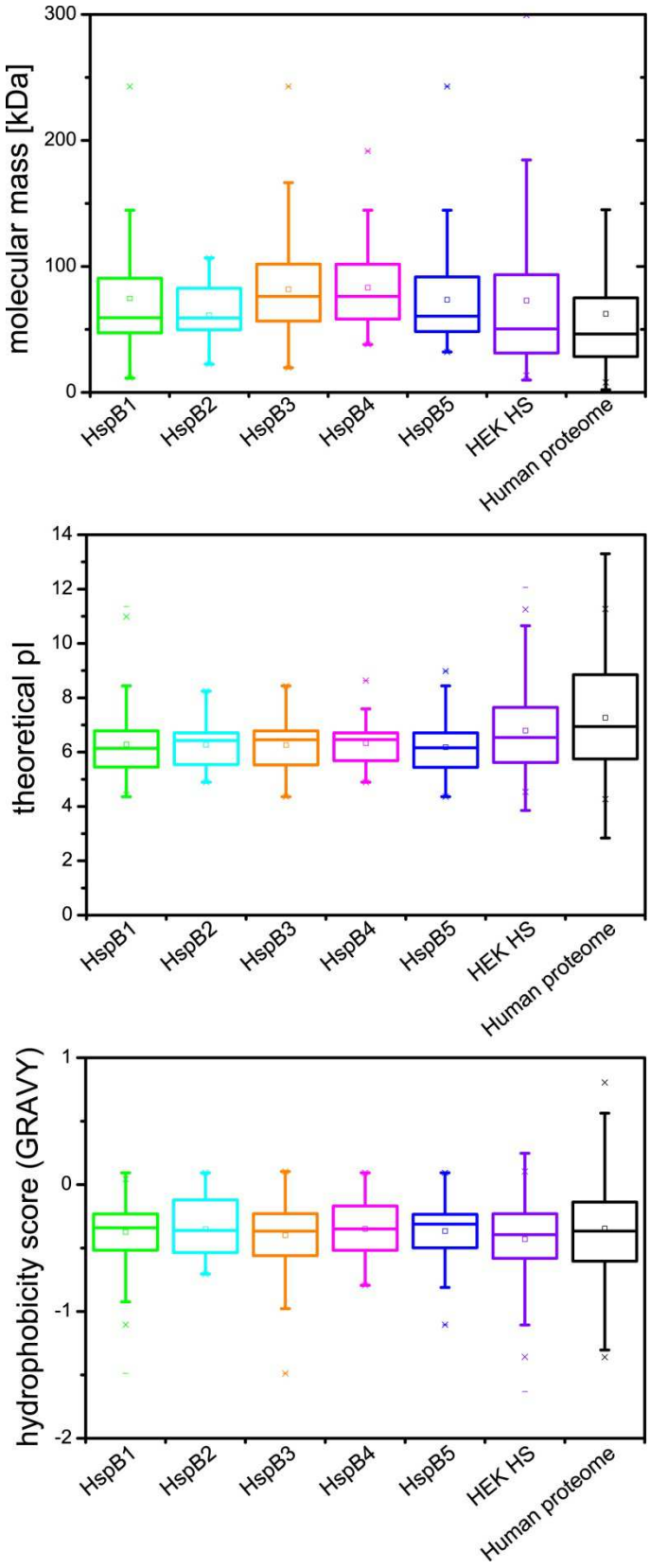

Figure 29: Statistical analysis of molecular mass, pI and hydrophobicity (GRAVY index) distributions for the human sHsps interactors in comparison to the heat-sensitive fraction of HEK293 lysate (HEK HS) and the complete human proteome.

4.2.3 Functional analysis of human sHsps substrate proteins

To elucidate if the human sHsps preferentially bind to substrate proteins with certain functions or involved in specific pathways, the Gene Ontologies were analyzed as well. Therefore the PANTHER online tool (Mi et al., 2016) was used to perform statistical overrepresentation tests with the complete human proteome containing 20,814 unique hits as a reference.

An overrepresentation test with default settings for the "GO biological functions" showed that a high amount of the potential substrates is involved in DNA-, RNA- and protein- "metabolic processes" (Figure 30). The sHsp substrate spectra are also enriched in proteins involved in translation as shown by the GO-terms "regulation of translation", "translation" and "tRNA metabolic processes". Also protein turnover was noticeable with the classes "protein folding", "protein complex assembly" and "protein complex biogenesis" that showed up to 30 fold enrichment for HspB2 for example. The class "tRNA metabolic process" is the class which is overall mostly enriched for the five sHsp substrate spectra analyzed. In this class mainly aminoacyl-tRNA ligases were found, again indicating that human sHsps preferentially bind to proteins involved in the regulation and functioning of the translation machinery. Among all hits in the substrate spectra of the human sHsps also several chaperones were identified, for example the aforementioned subunits of the TRiC/CCT complex CCT3 and CCT8, as well as HSPA4/Hsp70RY/APG2 and DNAJB1/Hsp40. Probably those chaperones are not direct substrates of the human sHsps but are involved in chaperone activities during the elevated temperatures and therefore bind to the same substrates as the sHsps and might so be pulled out in the experimental approach as well.

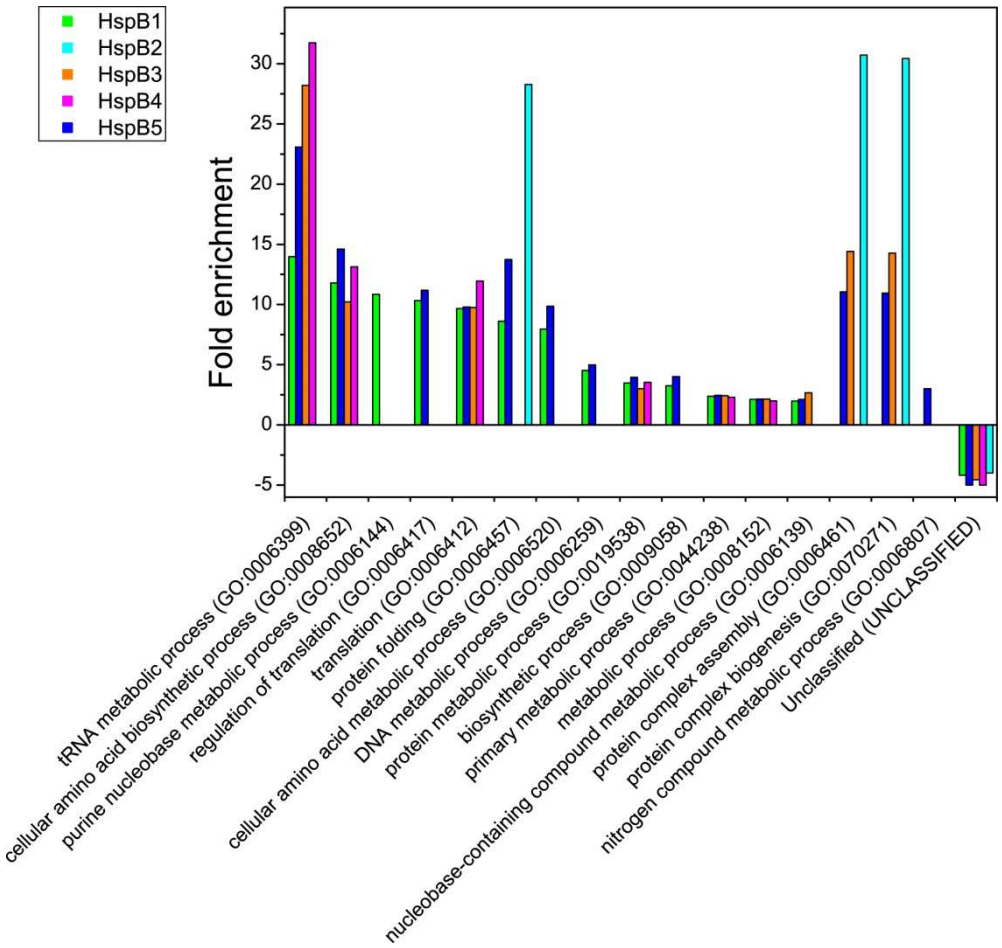

Figure 30: Statistical overrepresentation analysis of the GO categories in "biological processes" for HspB1-HspB5 interactors with the total human proteome as a reference. The analysis was carried out using the PANTHER online tool with default settings considering only classes with $p<0.05$.

4.2.4 Abundance distribution of human sHsps substrate proteins

To analyze the abundancy of the detected substrate proteins and the heat-sensitive fraction, the PaxDb database (Wang et al., 2012) containing the protein abundances for HEK293 was used. Compared to the entries in the PaxDb low abundant proteins with abundancies of <0.1 ppm are under-represented in the heat-sensitive fraction (Figure 31). An explanation for this observation might be detection limits in the mass spectrometry system. In general, proteins which are annotated with abundancies between 0.1 and 10,000 ppm in HEK293 cells could be detected. Nevertheless some very low abundant proteins were detected in the heat-sensitive fraction as for example the dual specifity mitogen-activated protein kinase kinase 2 with an abundancy of 0.003 ppm, the integrator complex subunit 3 with 0.056 ppm and the EH domain-binding protein 1 with 0.074 ppm.

About 18 % of the protein hits in the heat-sensitive fraction were not included in the PaxDb with the total HEK293 proteome. Therefore their abundances could not be analyzed. In general rather highly abundant proteins were detected as substrates for the human sHsps compared to the total HEK293 proteome and the heat-sensitive fraction. However some highly abundant proteins that were found in the heat-sensitive fraction were not found to be human sHsp substrates like for example the heterogeneous nuclear ribonucleoproteins A2/B1 and peroxiredoxin-1.

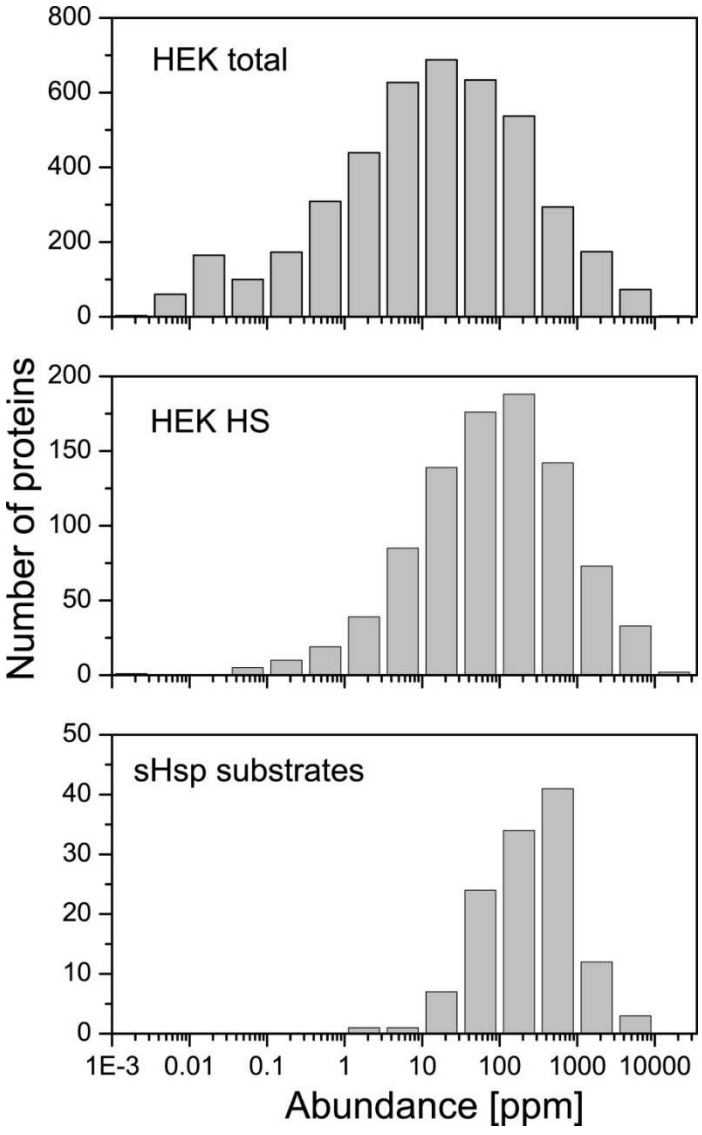

Figure 31: Abundance distributions for all detected human sHsps interactors compared to the heat-sensitive fraction of HEK293 lysate (HEK HS) and the proteins of the HEK293 cell line. Abundance information was taken from the PaxDb database.

4.2.5 Summary on the substrate spectra of human sHsps

sHsps constitute a protein family with diverse biochemical and structural properties and variable expression patterns. The presence of a large numbers of sHsps in higher eukaryotes leads to the question if they fulfill specific functions or if they redundantly are involved in the same processes. To illuminate the substrate spectra of the different human sHsps, co-immunoprecipitation experiments were performed for HspB1-HspB7 under heat shock conditions and analyzed by liquid chromatography-mass spectrometry. In comparison, the heat-sensitive fraction of HEK293 cell lysate was determined. HspB1 and HspB5 showed the highest number of substrate proteins. These two sHsps are the most ubiquitously expressed sHsps in human with a high upregulation upon heat stress (Mymrikov et al., 2011) and have also been shown to have the highest chaperone activity in aggregation assays (Mymrikov et al., 2017). HspB3 showed a lower number of substrate proteins and has also been reported to be less active in aggregation assays (Mymrikov et al., 2017). For HspB1, HspB3 and HspB5 a high number of overlapping substrates has been observed. HspB4, which is mainly expressed in the human eye lens only showed 24 hits in the substrate spectrum. Probably this sHsp shows a higher specificity to its substrates due to the adaption to the environment in the eye lens. For HspB6 and HspB7 only a few substrate proteins were detected. As HspB6 was shown to suppress aggregation of reduced proteins and cell lysates (Mymrikov et al., 2017), an explanation for the low number of detected substrate proteins might be that this sHsp doesn't form stable sHsp-substrate complexes but instead recognizes substrates promiscuously and binds them only transiently. Similar interaction modes have been described for Hsp17.7 from *Deinococcus radiodurans* (Bepperling et al., 2012). Also HspB1 and HspB5 recently have been shown to prevent amyloid-like aggregation of alpha-synuclein via transient interactions (Cox et al., 2016).

Regarding the biochemical properties of the identified substrate proteins they showed a larger monomeric molecular mass of 50-100 kDa and lower pI values from 5.4 to 6.8 compared to the heat-sensitive fraction of HEK293 cell lysate. Taking into account that many of the detected proteins like aminoacyl-tRNA ligases of class II and D-3-phosphoglycerate dehydrogenase form different oligomeric species (Grant et al., 2004, Cusack et al., 1991, Dey et al., 2008) the actual average size of

interactors is even higher. For Hsp20.2 from *D. radiodurans* and Sip1 from *C. elegans* also preffered binding to substrates with slightly acidic pI values has been reported (Fleckenstein et al., 2015, Fu et al., 2014). Regarding the molecular mass distributions, it has been shown for Sip1, Hsp20.2 and IbpB from *E. coli* that ≥ 60 % of the identified interactors were below 50 kDa (Fleckenstein et al., 2015, Fu et al., 2014). Compared to that, human sHsps seem to bind larger substrates. Surprisingly the substrate spectra were not enriched in hydrophobic proteins, which could be expected as sHsps are thought to bind hydrophobic patches in unfolding substrate proteins.

A functional overrepresentation test showed that the substrate spectra of human sHsps are enriched in proteins that are involved in tRNA metabolism, the translation machinery and amino acid and nucleic acid metabolism. Interaction of sHsps with those proteins may be important for the maintenance of translation processes under stress conditions. Additionally, among all hits in the substrate spectra also several molecular chaperones were detected. Those chaperones might not be direct substrates of the human sHsps but might rather bind to the same substrates and are therefore pulled out as well in the experimental approach. For some human sHsps like HspB1, HspB5 and HspB6 it is known that they bind to cytoskeletal proteins like actin or keratin (Tessier et al., 2003, Kayser et al., 2013). As proteins like alpha-tubulin, alpha-centractin, dynein1, kinesin1 and keratins also occurred in the control samples those proteins had to be excluded from the final substrate list.

4.3 The Hsp16 protein core family from *C. elegans*

In *C. elegans*, a total number of 16 sHsps has been identified. Thereof, 7 members belong to the Hsp16 protein family. Among the Hsp16 protein family there is the Hsp16 core family consisting of the two subfamilies Hsp16.11/Hsp16.2 and Hsp16.41/Hsp16.48. The proteins within a subfamily share 93 % sequence identity, whereas the two subfamilies show 70 % identity between their sequences (Candido, 2002). A sequence alignment which was conducted with the four members of the Hsp16 core family, the well-studied embryo specific protein Sip1 and the two less characterized proteins F08H9.3 and F08H9.4 shows the domain organization of the Hsp16 protein family (Figure 32) (Fleckenstein, 2014). In addition to the members of the Hsp16 protein family also Hsp16.0 from *Schizosaccharomyces pombe* as an example for non-metazoan sHsp structures with the β6 and β7 strand divided by a short linker region and human αB-crystallin featuring the long β(6+7) strand typical for mammalian sHsps were included in the sequence alignment providing further insight into possible structural properties.

Like for all sHsps, the highest sequence identity is found in the conserved alpha crystallin domain, which is flanked by a longer N-terminal elongation and a shorter C-terminal domain. In contrast to SpHsp16.0 the members of the Hsp16 core family do not show a short linker region between β6 and β7 strand, but rather show an elongated β(6+7)-strand as already reported for Sip1 and αB-crystallin (Fleckenstein et al., 2015, Jehle et al., 2009).

Going along with the high sequence similarity, the proteins of the Hsp16 core family do not show significant differences in their biochemical properties. Compared to Sip1 they are slightly smaller with a monomeric size of 16.3 kDa and show a lower pI with values ranging from 5.3 for Hsp16.2, 5.4 for Hsp16.11 and 5.5 for Hsp16.48 to 5.9 for Hsp16.41. The proteins Hsp16.11 and Hsp16.2 exhibit one cysteine on position 33 in the N-terminal elongation each whereas the proteins of the subfamily Hsp16.41/Hsp16.48 do not contain any cysteines.

RNAi experiments with a ΔHsf1-strain revealed a reduced thermotolerance by specific knock down of either one of the two Hsp16 subfamilies (Weinfurtner, 2008). This leads to the assumption that each subfamily fulfills specific roles that are

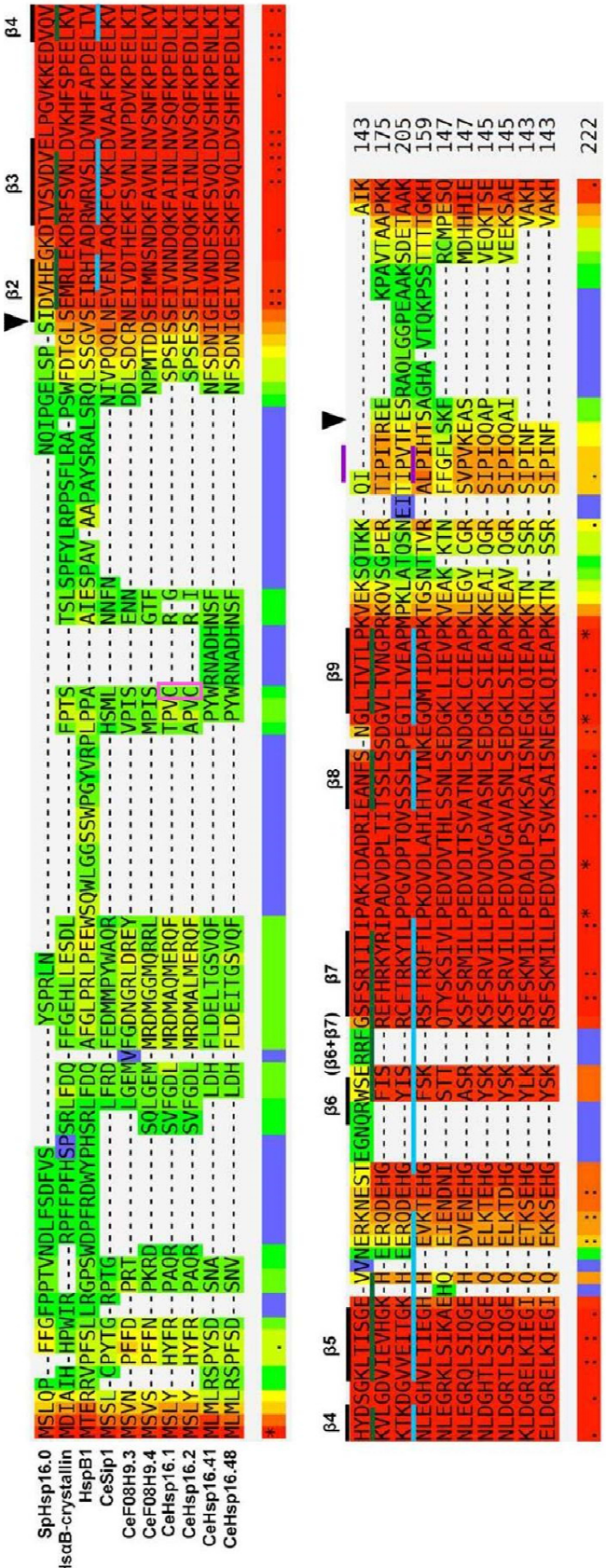

Figure 32: Alignment of the CeHsp16 proteins, revealing the archetypical sHsp domain organisation. Highest sequence identity (shown in red) is found in the middle domain, the α-crystallin domain, which is typically highly conserved and consists of an immunoglobulin-like, β-sheet-rich fold. It is flanked by a poorly conserved N-terminal region (NTR) and a short C-terminal extension which contains the conserved IXI motif (over-lined in purple). Sequence homology within the core subfamilies is 93 %, between Hsp16.11/2 and Hsp16.41/48 identity is 70 % (Candido, 2002). Sip1 differs from its closest relatives' sequences, especially in its NTR and by an additional 10 aa stretch in its CTR, which contributes to its overall larger size. A comparison of the residues that form β-strands in the crystal structure is facilitated by including *Schizosaccharomyces pombe* Hsp16.0 and human αB-crystallin in the alignment. One main difference between these representatives of the non-mammalian and mammalian sHsp dimer architecture is the separate β6- and β7-strands in SpHsp16.0 vs. the extended β6+7-strand in CRYAB and Sip1. The β-strands are over-lined in black, green and blue, respectively. The Cystein residues in Hsp16.11 and Hsp16.2 are highlighted in pink. sHsp sequences were aligned using T-COFFEE web server at default parameters.

Adapted from Fleckenstein, 2014 (Fleckenstein, 2014)

essential for the survival of the nematode under heat stress conditions and cannot be substituted by the members of the other subfamily.

To further elucidate the difference between the four members of the Hsp16 protein core family the proteins were assessed regarding their structural and functional properties and analyzed for their respective substrate spectra.

4.3.1 Purification of the Hsp16 core family proteins

As various attempts to purify the Hsp16 proteins natively failed due to protein precipitation during the purification procedure, the gene sequences of Hsp16.11, Hsp16.2, Hsp16.41 and Hsp16.48 were cloned into a pET-SUMO vector. The production of fusion proteins with an N-terminal small ubiquitin-like modifier (SUMO) protein has been shown to be advantageous to increase the protein solubility during protein expression and purification (Panavas et al., 2009). Expression of the Hsp16-SUMO fusion proteins and purification via the additional His_6-tag worked well and led to a high yield of the respective Hsp16 fusion protein. However, upon cleavage of the SUMO-tag with a SUMO protease the Hsp16 protein almost completely precipitated.

Therefore a purification strategy was used in which the proteins were purified under denaturing conditions based on a protocol by Daniel Weinfurtner (Weinfurtner, 2008). After purification, the proteins were refolded on a Superdex 200 column in PBS. The yield was approximately 4-7 mg of >95 % pure protein per 1 l LB culture. A flow scheme of the purification process is depicted in figure 33. For further details see chapter 3.5.1.

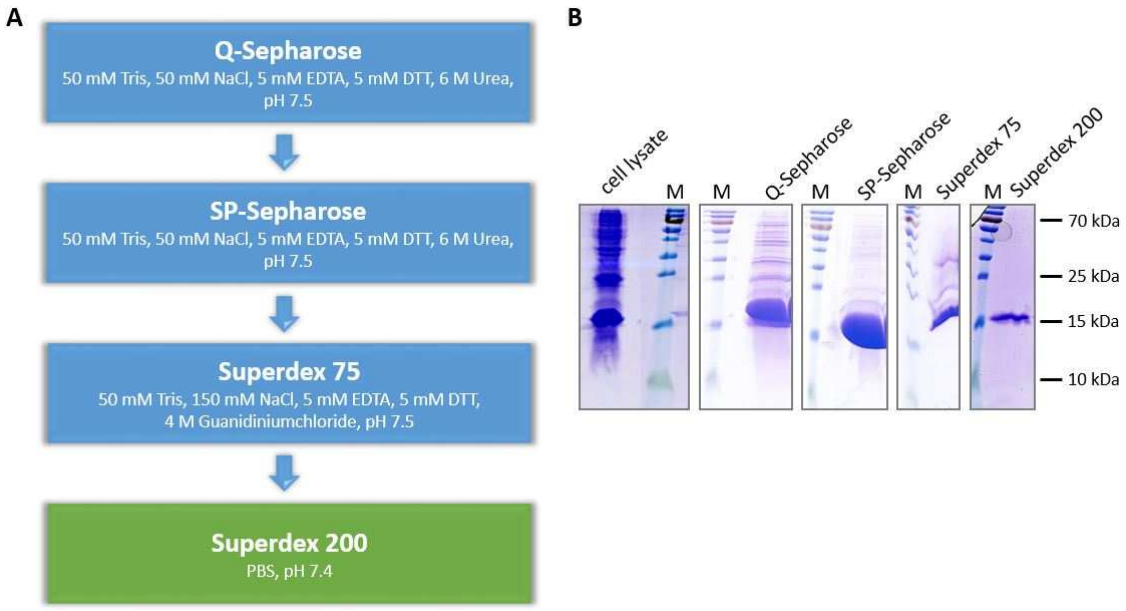

Figure 33: Overview on the purification procedure for Hsp16.11, Hsp16.2, Hsp16.41 and Hsp16.48. A) Schematic overview on the different purification steps. B) Exemplary pictures of the SDS-PAGE gels from the indicated purification steps of Hsp16.41.

4.3.2 Structural analysis of the Hsp16 protein core family

To assess the correct folding and to compare the secondary structure features of Hsp16.11, Hsp16.2, Hsp16.41 and Hsp16.48, far-UV CD spectra were recorded. The measurements were conducted at a constant temperature of 20 °C in 10 mM sodium phosphate buffer, pH 7, in a wavelength range from 200 – 260 nm and corrected for the buffer spectrum. The shape of spectra for all four Hsp16 proteins is comparable (Figure 34). For Hsp16.11 and Hsp16.48 minima were observed at 217 nm. The minima for Hsp16.2 and Hsp16.41 lie at 216 nm. All four show characteristic features of what is expected for sHsps. A minimum at 216/217 nm in general hints to the existence of a predominantly beta-sheet structure (Kelly et al., 2005). This might be caused by the conserved alpha-crystallin domain, which has been shown before to adopt beta-sheet structure (MacRae, 2000, Horwitz, 2003). Also the minimum values of θ_{MRW} between -4000 and -6000 are characteristic for sHsps with their high content of beta-sheet structure (Caspers et al., 1995, Bepperling et al.,

2012, Stromer et al., 2004). The results are in line with previous CD analysis of the four Hsp16 proteins (Weinfurtner, 2008). The correct folding of the four Hsp16 proteins after purification is therefore confirmed.

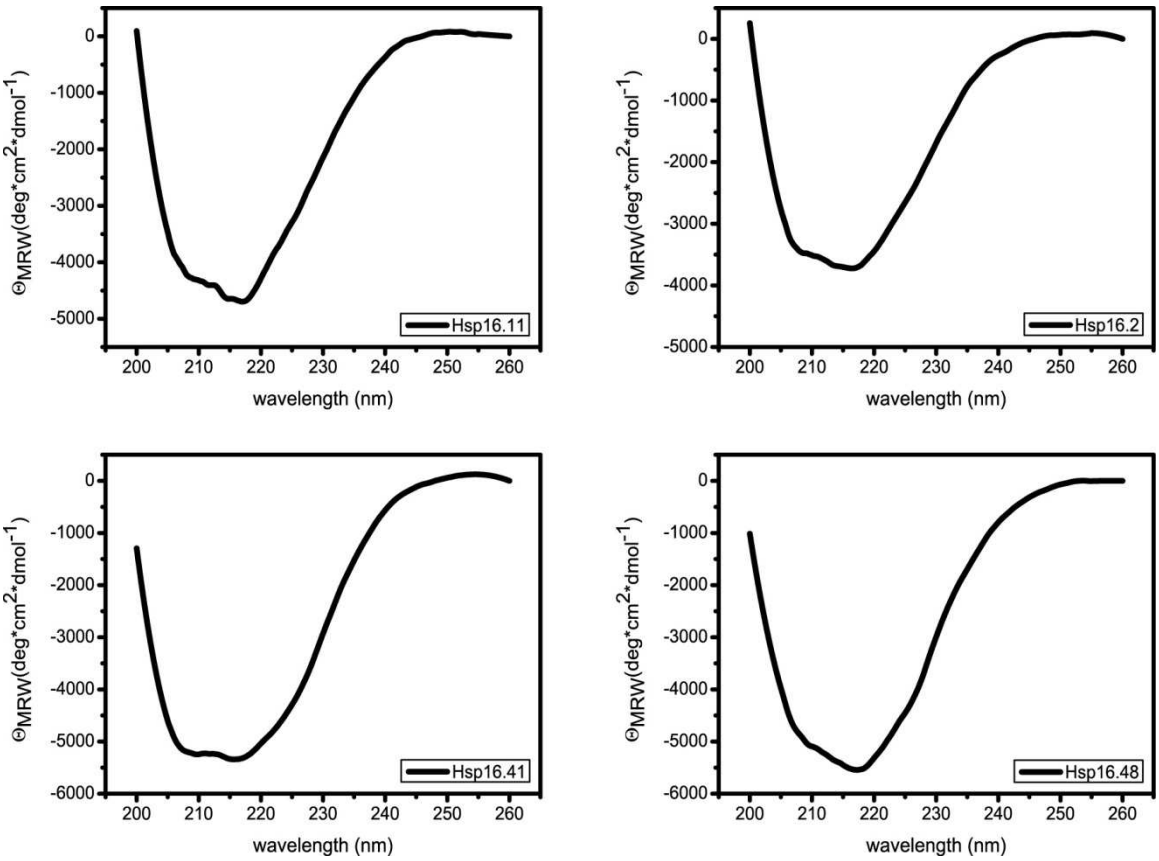

Figure 34: Far-UV CD spectra of 0.5 mg/ml Hsp16.11, Hsp16.2, Hsp16.41 and Hsp16.48 in 10 mM sodium phosphate, pH 7.0 at 20 °C.

To get further insight into the secondary structure, a quantitative analysis of secondary structure elements using the program CDNN (Bohm et al., 1992) was conducted. Therefore a reference set of 33 protein spectra of proteins with known structure was used to assess the amount of secondary structure elements in the Hsp16 proteins. As already assumed from the assessment of the CD spectra, the four Hsp16 core proteins share comparable amounts of secondary structure elements (Figure 35). The main element of secondary structure is constituted by antiparallel and parallel beta-sheet and beta-turn structures with approximately 55 % in total. About 35 % of the secondary structure elements is represented by random coil and

around 12 % are helical structures. Only very slight variations between the four Hsp16 core family proteins are observed. Hsp16.2 for example contains 2 % more antiparallel beta-sheets compared to the other three proteins but is slightly reduced in helical content. Due to the high sequence similarity of the four Hsp16 proteins, the comparable secondary structure distribution is not surprising. Previous investigations on the secondary structure elements of the four Hsp16 proteins where the CD spectra were analyzed with the CDSSTR algorithm on the webserver DichroWeb (Whitmore and Wallace, 2004) revealed similar amounts of beta sheets, random coil and helical content (Weinfurtner, 2008).

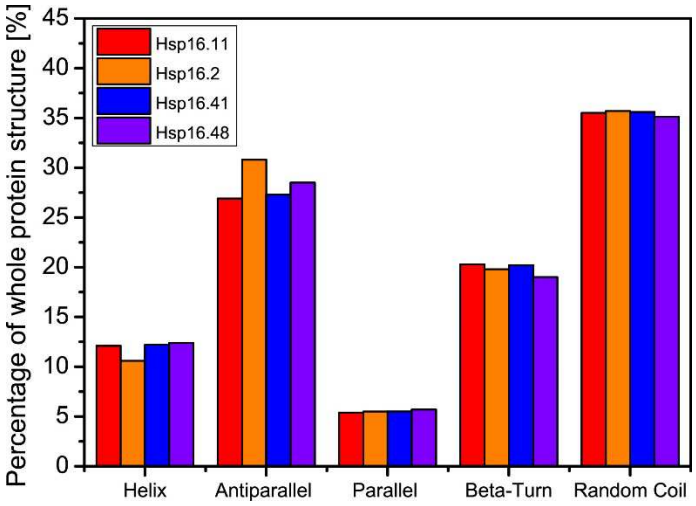

Figure 35: CDNN analysis of the far-UV CD spectra of Hsp16.11, Hsp16.2, Hsp16.41 and Hsp16.48

In a next step, the quaternary structure of Hsp16.11, Hsp16.2, Hsp16.41 and Hsp16.48 was analyzed in sedimentation velocity experiments by analytical ultracentrifugation. The measurements were performed by Dr. Christine John in PBS in a Beckman XL-A centrifuge at 20 °C and 30,000 rpm. For the evaluation the Sedfit software (Schuck, 2000) was used. In general two main peaks were detected for each of the four Hsp16 proteins (Figure 36). For Hsp16.11 one species sedimented with an S-value of 1.5 Svedberg and another species sedimented with 11.7 Svedberg. According to the Sedfit calculations this would correspond to approximately 22.4 kDa and 320 kDa, respectively. The four Hsp16 proteins from the core family all show a molecular mass of 16.3 kDa. With such a molecular mass, for Hsp16.11 this

would suggest a monomer-dimer distribution for the first species and furthermore an oligomeric species of about 20 subunits. For Hsp16.2, S-values of 1.4 S and 12.4 S were determined. These two species with an estimated molecular mass of 14 kDa and 326 kDa would correspond to a monomer and a 20mer. The experiment with Hsp16.41 revealed S-values of 1.6 S and 12.4 S from which the molecular mass of 34.8 kDa and 348 kDa were calculated. This would hint to a dimeric species and as well an oligomeric species with 21 subunits. The highest S-values were found for Hsp16.48 with 2.2 and 12.2 corresponding to 44 kDa and 358 kDa which would equal a dimer-trimer distribution and a 22mer. It has to be mentioned, that the calculation of molecular masses by the Sedfit software should rather be used as a rough estimation than as absolute values. Nevertheless it can be stated that for all four Hsp16 proteins the formation of large oligomeric species were observed. This is in good accordance with previous studies on the quaternary structure of Hsp16 proteins where large oligomers of 20-24 subunits were observed by analytical ultracentrifugation experiments (Weinfurtner, 2008).

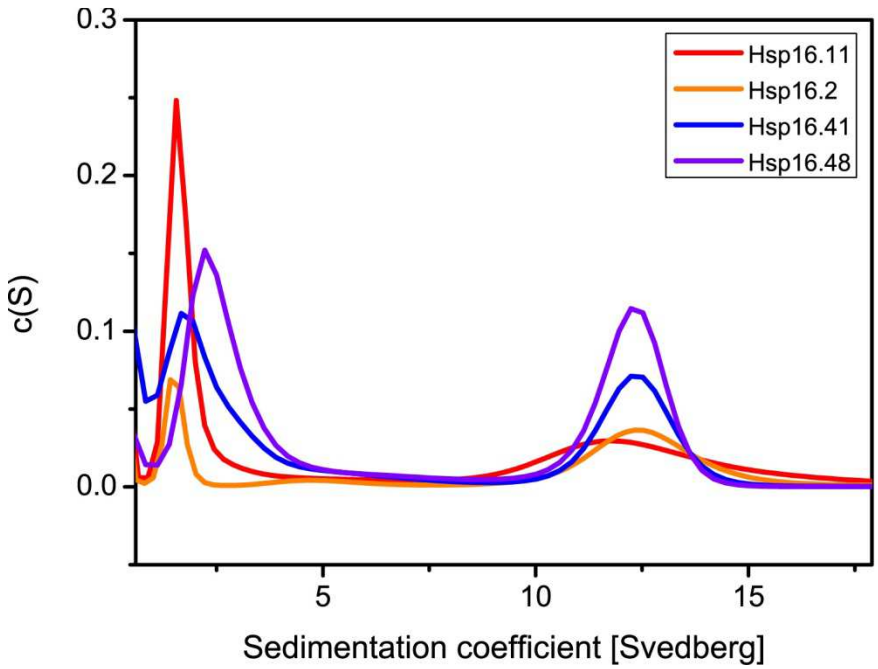

Figure 36: Normalized c(S) distributions obtained from AUC data analyzed with Sedfit (P. Schuck). AUC experiments were performed in PBS at 20 °C and 30,000 rpm.

4.3.3 Functional analysis of the Hsp16 protein core family

As the four recombinantly expressed and purified Hsp16 proteins were shown to be correctly folded and able to form large oligomeric species, another characteristic feature of sHsps, the chaperone activity, was assessed. Therefore aggregation assays with model substrates were conducted *in vitro*.

In a first attempt the suppression of aggregation was analyzed with thermally destabilized citrate synthase (CS) at 42 °C in 20 mM Hepes, pH 7.5 in a Cary 50 at 360 nm. CS is a homo-dimer originating from porcine heart composed of two identical subunits of 49 kDa in size. For the analysis of chaperone activity, the sHsps were added in 2-10 fold molar excess compared to CS (1µM). After normalization the aggregation levels were plottet against the sHsp concentration. Furthermore the IC_{50} values were determined representing the sHsp/substrate ratio which is needed for half- maxium suppression of aggregation.

The highest chaperone activity under these conditions was observed for Hsp16.2 with an IC_{50} value of 3.5 (Figure 37). With the addition of 6 fold molar excess of Hsp16.2 over CS almost complete suppression of aggregation was achieved. A concentration- dependent effect of chaperone activity was also observed for Hsp16.11. However, a complete suppression of aggregation could not be reached. With the highest concentration tested corresponding to a 10fold excess of sHsp over CS, the aggregation could be suppressed to values of 0.2. The IC_{50} value was 5.9. In contrast to that, the effects of Hsp16.41 and Hsp16.48 were much weaker. Determination of IC_{50} values were not possible for these two proteins, as a halfmaximal suppression of aggregation could not be reached in these experiments. Only weak effects can be observed in a concentration dependent manner. With 10fold excess of Hsp16.41 the aggregation of CS was reduced to 0.7, with Hsp16.48 to 0.8.

As the chaperone activity has been shown to be dependent on the substrate used (Mymrikov et al., 2017), malate dehydrogenase (MDH) was chosen as an additional substrate for further *in vitro* studies. Again temperature- induced aggregation of the model substrate was assessed by the increased turbidity at 360nm (Figure 38).

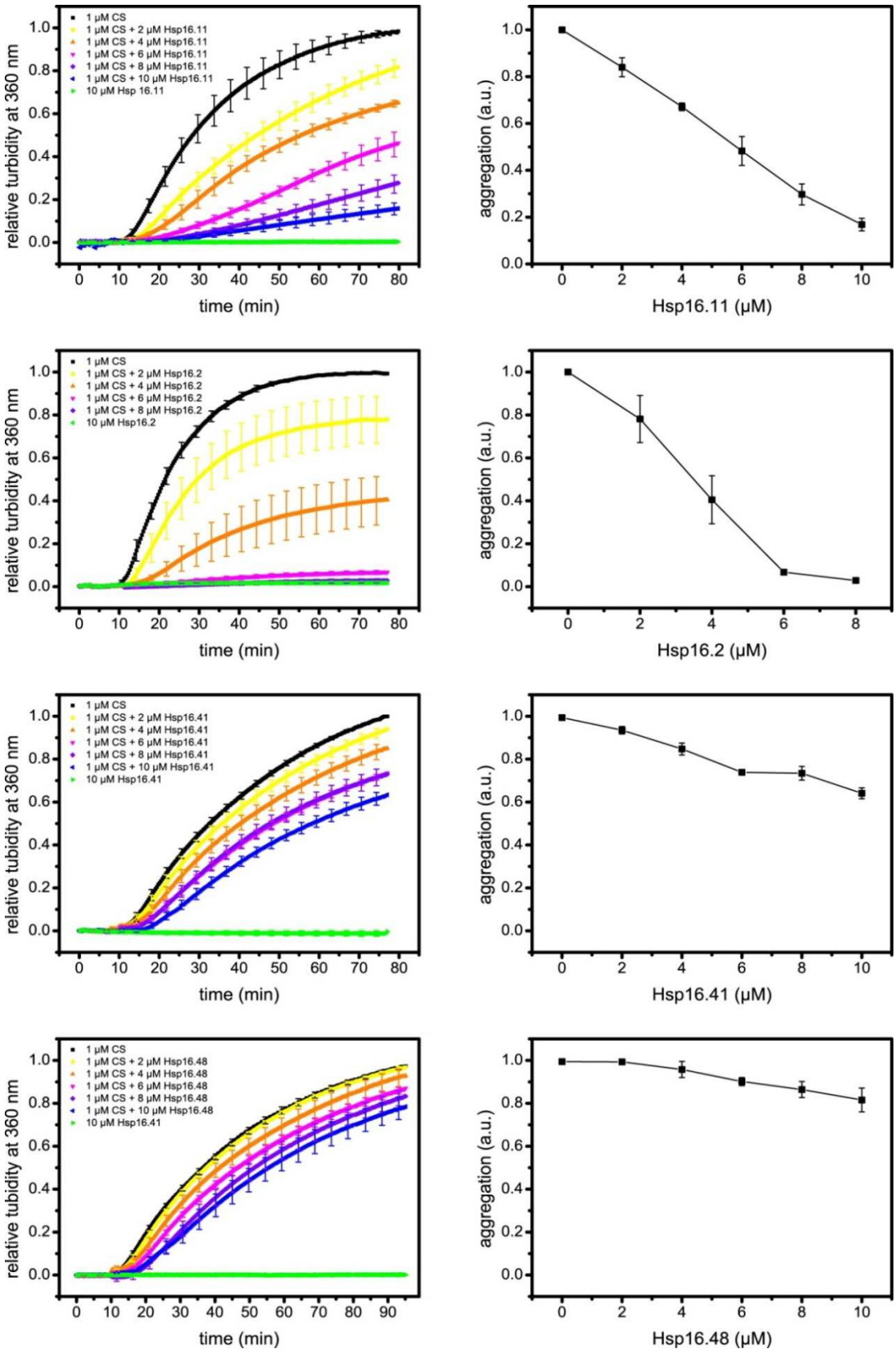

Figure 37: Chaperone assay of Hsp16.11, Hsp16.2, Hsp16.41 and Hsp16.48 in 20 mM Hepes, pH 7.5. Thermally induced aggregation of heat sensitive CS (1 µM) was monitored in a Cary 50 spectrophotometer at 42 °C in the presence of varying concentrations of sHsps. Measurements were performed in triplicates.

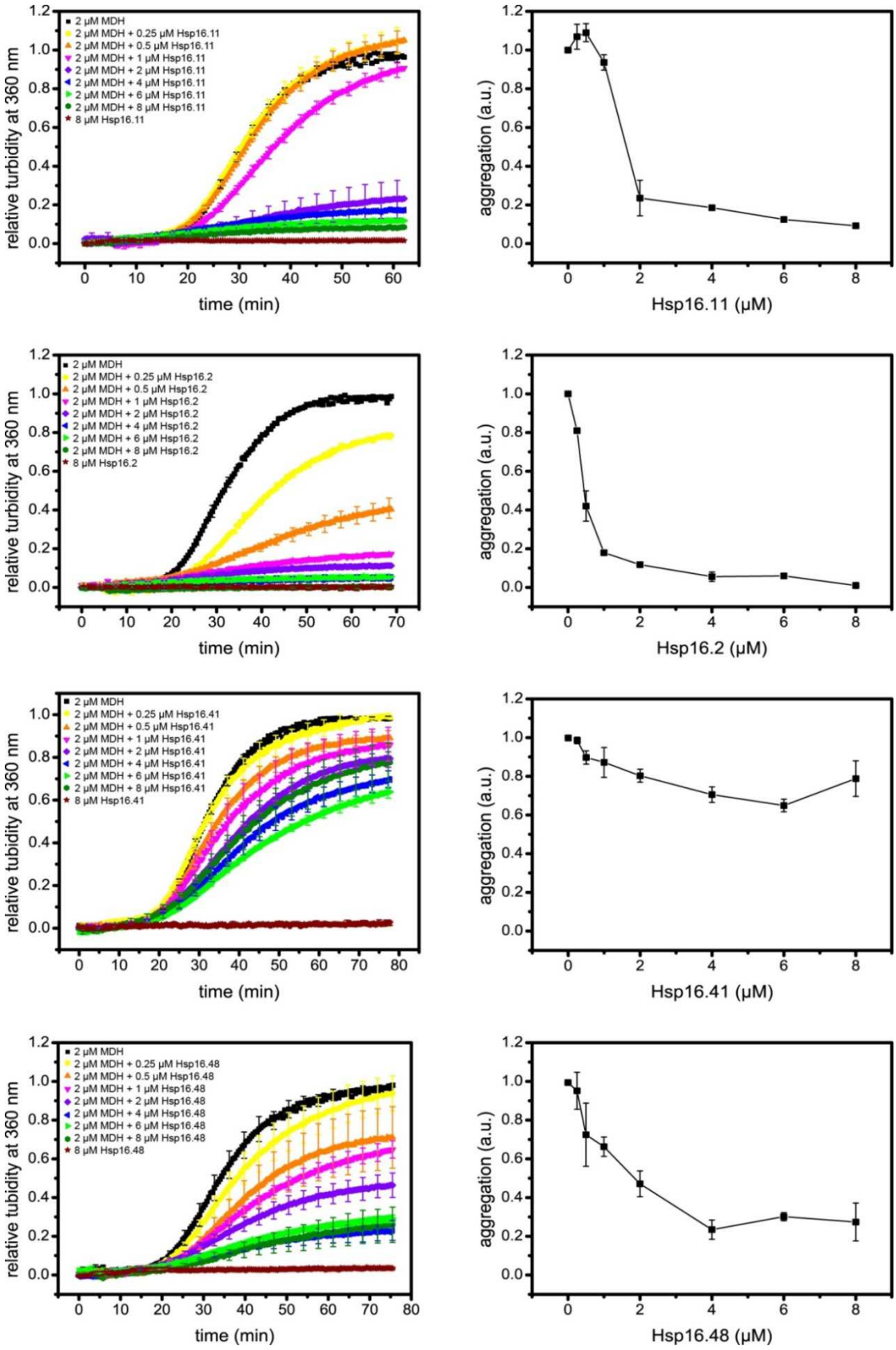

Figure 38: Chaperone assay of Hsp16.11, Hsp16.2, Hsp16.41 and Hsp16.48 in PBS. Thermally induced aggregation of heat sensitive MDH (2 µM) was monitored in a Cary 50 spectrophotometer at 42 °C in presence of varying concentrations of sHsps. Measurements were performed in triplicates.

The concentration of MDH was set to 2 µM and sHsps were added in defined steps between 0.25 µM – 8 µM. In these assays the highest chaperone activity was again observed for Hsp16.2. The IC_{50} value in this experiment was determined to be 0.2. A twofold excess of Hsp16.2 was sufficient for complete suppression of aggregation. Also Hsp16.11 was highly active in aggregation assays with MDH as a model substrate. The IC_{50} value was 0.8. The same is true for Hsp16.48 with an IC_{50} value of 0.9. A twofold molar excess of Hsp16.48 decreased the aggregation of MDH to values of about 0.2. In contrast to that, Hsp16.41 showed only weak chaperone activity. Halfmaximal suppression of aggregation could not be reached and only slight concentration dependent effects were observed. At higher concentrations of 8 µM Hsp16.41, aggregation levels even started to increase again, probably due to co-aggregation of the sHsp with the model substrate.

In general the subfamily of Hsp16.11/Hsp16.2 exhibits higher chaperone activity with both model substrates, CS and MDH, under the conditions tested compared to the subfamily Hsp16.41/Hsp16.48. Overall the activities were higher with MDH as a model substrate. This was especially noticeable for Hsp16.48 which showed almost no activity in assays with CS but was highly active in the prevention of MDH aggregation.

As the chaperone activity is dependent on the model substrates used, lysate assays were conducted to assess the ability for the suppression of aggregation with more "native" substrates in a biologically complex environment. Analysis of chaperon activity with cell lysates and monitoring by light scattering was already described before (Jovcevski et al., 2015, Peschek et al., 2013). Recently SDS-PAGE was described as a better approach to follow the aggregation of proteins in the lysate (Mymrikov et al., 2017).

For the experiment, fresh lysate was prepared from mixed N2 *C. elegans* populations. Different concentrations of sHsps were added to the lysate and heat shocked for 90 min at 37 °C. Then, aggregated proteins were separated from the soluble fraction by centrifugation. The pellet fraction (P) and soluble fraction (S) were analyzed by SDS-PAGE and each gel lane was quantified by densitometry with

ImageJ (Figure 39). The values were normalized to the control sample (without sHsp) which was set to a value of 1 meaning 100 % aggregation in the pellet fraction.

The highest chaperone activity in this assay was observed for Hsp16.11 with a decrease in aggregation of approximately 40 % after addition of 16 µM sHsp. Hsp16.2 was able to suppress the aggregation to values of 0.7, meaning 30 % suppression of aggregation. For Hsp16.41 and Hsp16.48 no chaperone activity could be observed in this assay. As control proteins, human HspB5 and Sip1 from *C. elegans* were used. For HspB5 high chaperone activity in lysate assays with HEK293 cell lysate was reported with up to 60 % reduction of aggregation (Mymrikov et al., 2017). In the experiments with *C. elegans* N2 lysate, HspB5 was able to suppress aggregation for about 30 %. An explanation for the minor activity could be the nonnative substrates in *C. elegans* lysate and the modification in the heat shock protocol, which was adjusted for *C. elegans* to 37 °C instead of 45 °C which was used for human cell lysates. Sip1, a member of the extended Hsp16 protein family in *C. elegans*, was also assessed for chaperone activity in the lysate assay. However, no chaperone activity could be observed. In *C. elegans*, Sip1 is exclusively expressed in oocytes and embryos, suggesting a more specialized substrate spectrum and probably unfavorable conditions in the lysate of the mixed N2 polulation. Furthermore a preference of Sip1 chaperone activity for lower pH values of about pH 6.3 has been shown before in accordance with the lowered pH present in nematode eggs (Fleckenstein et al., 2015).

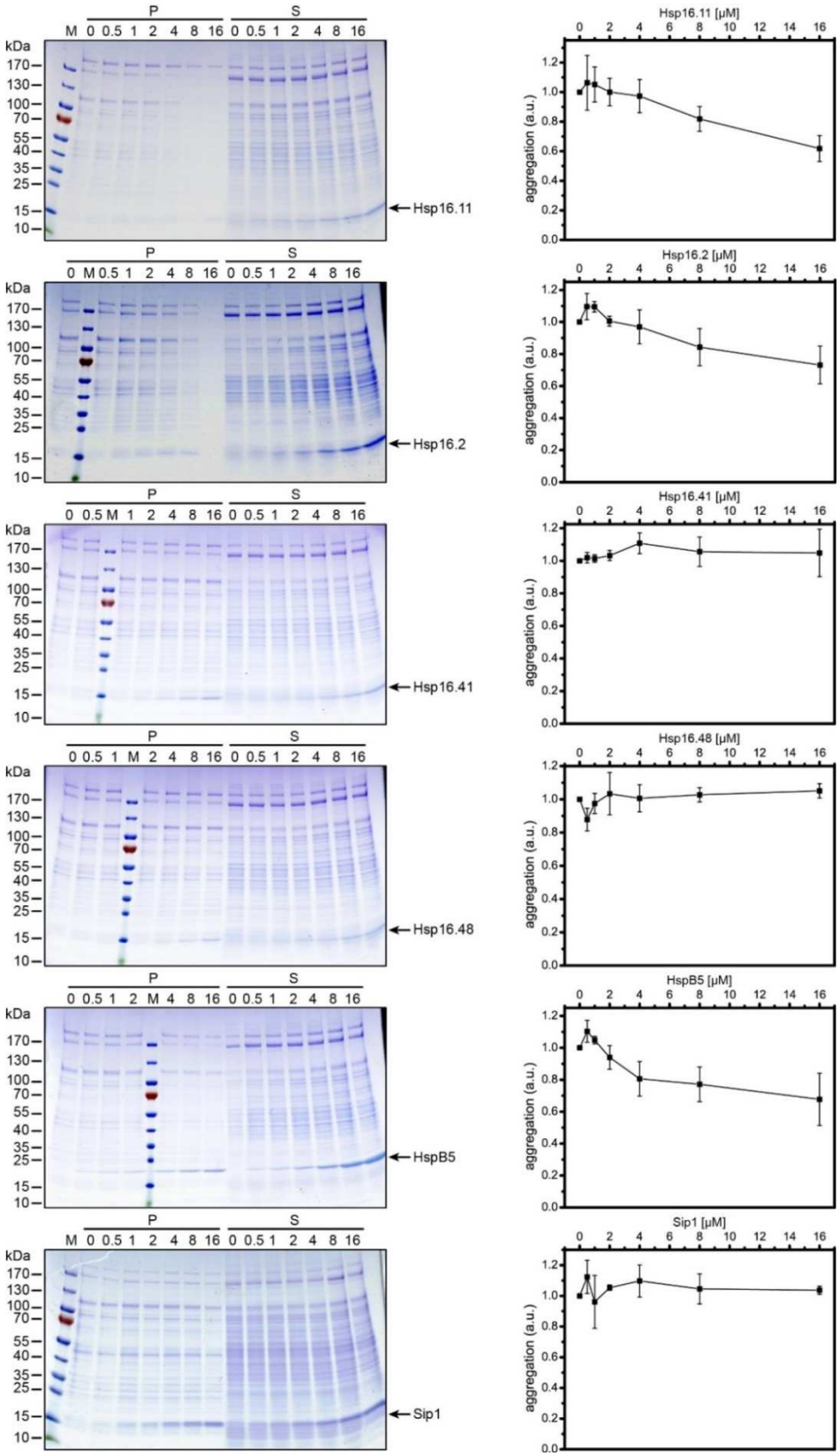

Figure 39: Lysate assay for Hsp16.11, Hsp16.2, Hsp16.41, Hsp16.48, HspB5 and Sip1. 0.8 mg/ml lysate of mixed N2 populations were heat shocked for 90 min at 37 °C in the presence of varying sHsp concentrations (0-16 µM). Insoluble fraction (P) and soluble fraction (S) were separated and analyzed by SDS-PAGE and quantified by densitometry. Quantification for the insoluble fraction is shown on the right.

4.3.4 Identification of Hsp16 interactors

To further investigate the substrate specificity of Hsp16.11, Hsp16.2, Hsp16.41 and Hsp16.48, co-immunoprecipitation experiments with *C. elegans* lysate of mixed N2 populations were performed. The respective Hsp16 protein was incubated with *C. elegans* lysate for 90 min at 37 °C. The use of a specific anti-Hsp16-antibody allowed the pull down of the deployed sHsp and the bound interactors with the help of protein G sepharose beads. To identify the interactors an on-bead digest with trypsin was performed followed by mass spectrometry analysis on an Orbitrap Fusion Tribrid Mass Spectrometer (ThermoFisher Scientific) and a label-free quantification (LFQ) approach. Data processing was conducted using the MaxQuant software version 1.5.3.8 and a search against a Swissprot *C. elegans* database (edition 16.6.2017) was performed. For the distinct identification, only protein hits identified by at least two peptides were allowed and unique peptides were set as a prerequisite.

Statistical analysis was carried out using Perseus version 1.5.3.1. Known contaminants and hits identified by a decoy search were removed from the hit lists. The experiment was performed in triplicates for each sHsp and a control without addition of sHsp was performed in triplicates as well. To identify the significant hits a students-t-test was performed pair wisely comparing the triplicates of the different sHsps to the control samples. A false discovery rate (FDR) of 0.05 meaning 5 % of false positive hits compared to the decoy database was allowed and the S0 value was set to 0.1 (Tusher et al., 2001). Results are presented as volcano plots (Figure 40 A-D).

Based on these results, protein hits that were overrepresented in comparison to the control sample were selected for further analysis. In total, 257 unique significant protein hits were identified constituting approximately 7 % of the used Swissprot *C. elegans* database. The largest number of significant interactors was found for Hsp16.11 with 228 protein hits (Figure 40 E) which is in good agreement with the high chaperone activity in the lysate assay. For Hsp16.2, which showed the highest chaperone activity in aggregation assays with the model substrates CS and MDH,

only 147 hits were identified. Surprisingly a relatively high number of interactors was found for Hsp16.41 with 159 hits and for Hsp16.48 with 193 protein hits.

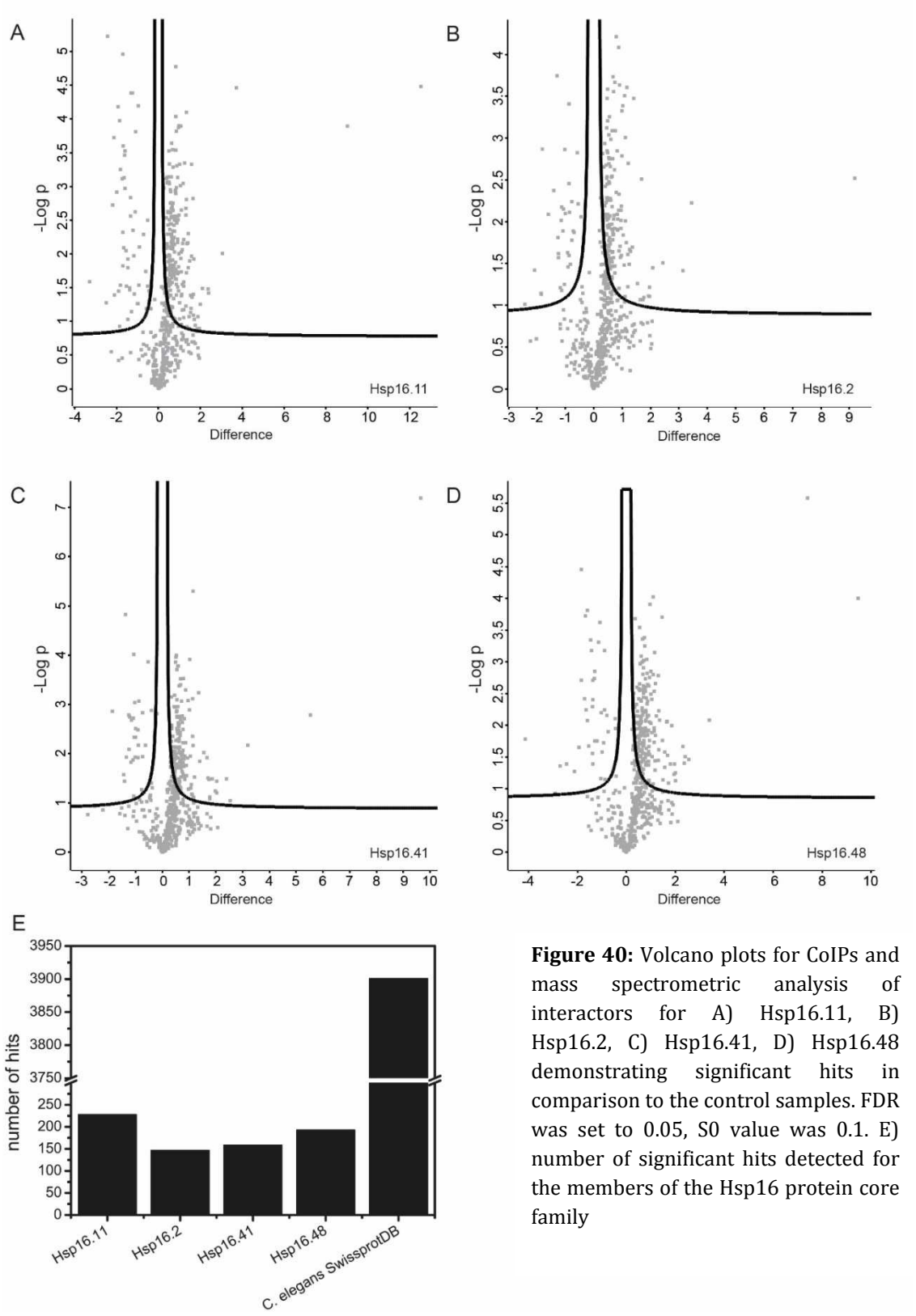

Figure 40: Volcano plots for CoIPs and mass spectrometric analysis of interactors for A) Hsp16.11, B) Hsp16.2, C) Hsp16.41, D) Hsp16.48 demonstrating significant hits in comparison to the control samples. FDR was set to 0.05, S0 value was 0.1. E) number of significant hits detected for the members of the Hsp16 protein core family

To analyze if the proteins of the Hsp16 core family share common substrates or if the single proteins are specialized on specific substrates, overlapping hits were determined and depicted in a Venn diagramm (Figure 41). Out of the 257 protein hits identified in total, 102 interactors were found for all four Hsp16 proteins. Amongst them, with high significance, the acetlytransferase cbp-1, which is a worm orthologue of the human p300/CBP, and seems to play a role in the prevention of DNA-damage induced apoptosis (Yang et al., 2009). A further example for an interactor that showed up for all four Hsp16 proteins with high significance is asparagin- tRNA ligase. In total 11 different tRNA ligases were identified as Hsp16 substrates suggesting proteins involved in protein synthesis as an important substrate group for the Hsp16 core protein family.

Regarding the two subfamilies of the Hsp16 core protein family, no significant differences or exclusive substrate spectra could be observed. A number of 12 proteins was identified specifically for the Hsp16.11/Hsp16.2 subfamily, whereas for the subfamily Hsp16.41/Hsp16.48 only 4 unique hits were found. As an interactor for Hsp16.11/Hsp16.2, the subunit CCT6 of the TRiC/CCT complex was identified, whereas the subunit CCT4 was identified for the other subfamily Hsp16.41/Hsp16.48 only.

As it had already been observed for the human sHsp substrate spectra (chapter 4.2.1 and 4.2.3), several other chaperones like Hsp90, Hsp70 or Hsp110 were found among the Hsp16 interacting proteins. In those cases, the identified proteins might not necessarily be direct substrates of the analyzed sHsps but rather interact with the same substrates and are therefore be pulled down as well. *In vitro* studies with Luciferase as a model substrate had shown show an interplay between the Hsp70/Hsp40 chaperone system and Hsp16.2 or Hsp16.11 in the refolding activity of denatured substrate (Weinfurtner, 2008).

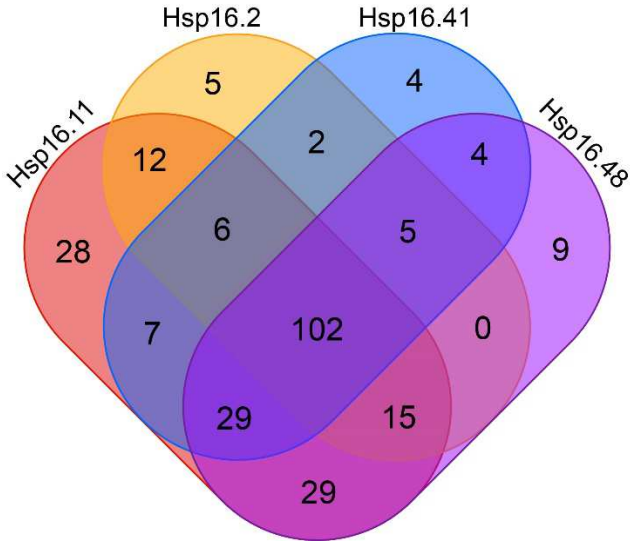

Figure 41: Venn diagram displaying the overlap of the interactors of Hsp16.11, Hsp16.2, Hsp16.41 and Hsp16.48 identified by CoIP and mass spectrometric analysis.

4.3.5 Biochemical properties of Hsp16 substrate proteins

The substrate spectra of the four different Hsp16 proteins were further compared according to their biochemical properties like molecular mass, pI and hydrophobicity (Figure 42). As a reference, the Swissprot *C. elegans* database (edition 16.6.2017) was used.

Regarding the monomeric molecular mass of the identified substrate proteins of the Hsp16 core protein family, only neglectable differences could be observed. For the Hsp16.11 interactors, the first quartile was found to lie at 28 kDa with a median at 44 kDa. For Hsp16.2, the first quartile was observed at 29 kDa and the median at 46 kDa. Hsp16.41 and Hsp16.48 showed the first quartile of their interactors' molecular mass at 31 kDa and 30 kDa with a median at 46 kDa and 42 kDa, respectively. The distribution of the Swissprot *C. elegans* database was shown to lie in the same range with the first quartile at 28 kDa and a median at 45 kDa. In total, the proteins of the Hsp16 core family do not exhibit a preference for a certain size of their interactors at least regarding the monomeric molecular mass.

Also concerning the pI of their interactors, the Hsp16 proteins revealed similar characteristics. The median of all four distributions was found to be at pI 6.3 with the first quartile lying at 5.6 for Hsp16.11 and Hsp16.2 or 5.7 for Hsp16.41 and Hsp16.48. The distribution of the Swissprot *C. elegans* database was found to be slightly broader with a median at pI 6.6. Throughout all the interactors identified, the lowest pI was at 4.34 whereas the highest pI of an interactor found was 11.64, demonstrating a broad range of possible interactors regarding their pI.

As sHsps are thought to bind hydrophobic patches in their substrate molecules the hydrophobicity of the identified interactors was assessed using the GRAVY index (Kyte and Doolittle, 1982), which is calculated based on the amino acid composition of the respective proteins. Hereby positive values indicate a high percentage of hydrophobic amino acids. The values found for the Hsp16 interactors mainly lie in the negative range. For Hsp16.11, the first quartile starts at –0.48 with a median at -0.35, for Hsp16.2 a slight shift towards even lower values with the first quartile at -0.57 and a median at -0.38 were observed. For Hsp16.41 and Hsp16.48, the first quartiles were found to be at -0.55 and -0.47 with median values at -0.36 and -0.35 respectively. Compared to the whole *C. elegans* Swissprot database with the first quartile at -0.60 and a median at -0.40, the values for the Hsp16 interactors are slightly shifted towards higher values. However, in total only 18 protein hits with positive GRAVY indices were found among all 257 identified Hsp16 interactors.

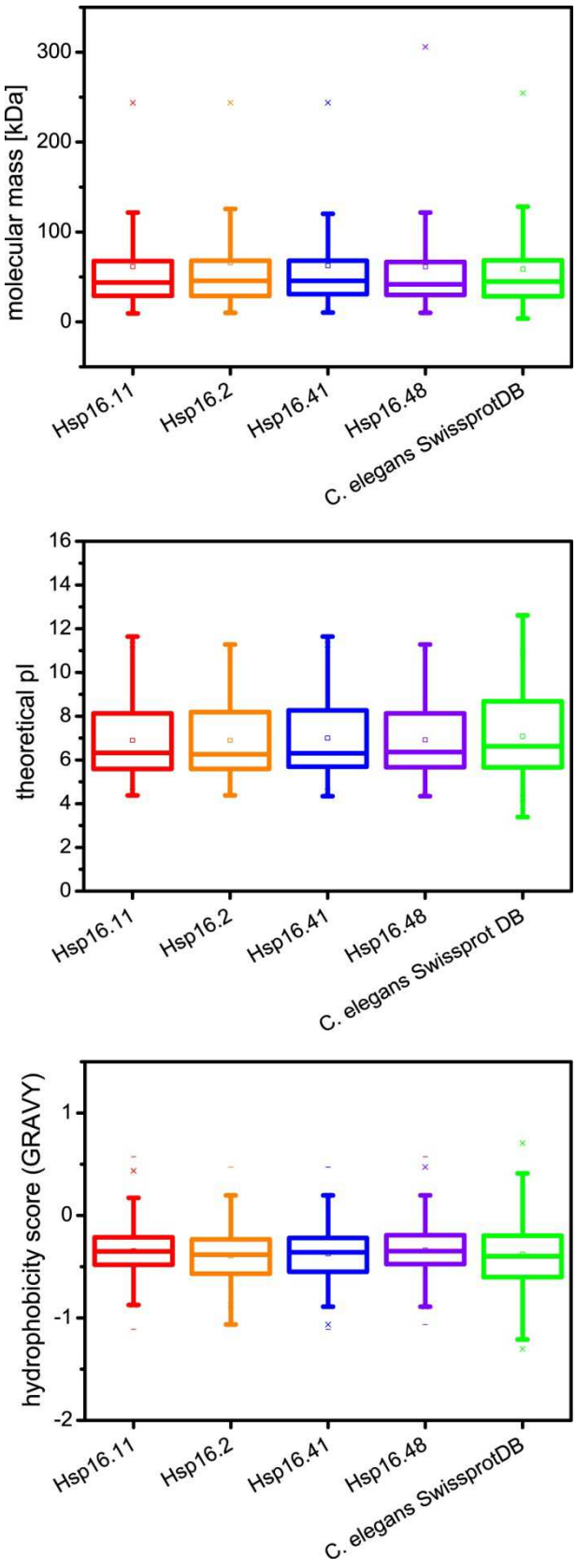

Figure 42: Statistical analysis of molecular mass, pI and hydrophobicity (GRAVY index) distributions for the Hsp16 core family interactors in comparison to the complete *C. elegans* Swissprot database.

4.3.6 Functional analysis of Hsp16 substrate proteins

To further classify the identified protein interactors, a statistical overrepresentation analysis was performed using the PANTHER online tool (Mi et al., 2016) with default settings. The overrepresentation test was performed with a *C. elegans* protein database containing 20,078 entries as a reference. Only classes with $p<0.05$ were considered for further analysis.

Regarding the GO term "protein class" (Figure 43), a dramatic overrepresentation is found for all four Hsp16 core family interactomes in the GOs "chaperonin" and "chaperone" with an enrichment of more than 60-fold compared to the reference list. A more detailed look reveals that this dramatic overrepresentation mainly results from the presence of the different T- complex protein 1 subunits (TRiC/CCT1) among the identified protein hits. Additionally, Hsp90, STI1 and Daf-41 belong to these classes as well. As already mentioned before, the presence of chaperones in the interactomes of the different Hsp16 core family proteins might not necessarily depict them as direct Hsp16 substrates but rather suggests them to be involved in chaperoning activities on the same substrates.

Further protein classes that were found to be overrepresented in Hsp16.11, Hsp16.2, Hsp16.41 and Hsp16.48 are the classes "actin binding motor protein" with the protein hits Myosin 1 to Myosin 4, but also the Dynein light chain. Interactions of sHsps with cytoskeletal proteins like actin or keratin have been reported before (Tessier et al., 2003, Kayser et al., 2013). Therefore the appearance of motor proteins interacting with parts of the cytoskeleton is not surprising in the interactomes of the Hsp16s. Furthermore, in the overrepresentation tests, protein classes like "translation factor", "ribosomal proteins" with different representatives of the 40S and 60S subunits, "RNA binding proteins" and diverse types of "dehydrogenases" and "nucleic acid binding" proteins were found to be enriched in all four interactomes.

The determination of distinct substrate spectra between the two subfamilies Hsp16.11/Hsp16.2 and Hsp16.41/Hsp16.48 was not possible. The protein class "RNA helicase" was the only class that could uniquely be identified as overrepresented for the subfamily Hsp16.41/Hsp16.48. For the Hsp16.41/Hsp16.48

subfamily in total 6 hits out of 56 possible proteins assigned to this protein class for the whole *C. elegans* database have been found. But otherwise, no subfamily-specific protein classes have been found.

For Hsp16.2, substrate spectra have already been published showing an overrepresentation of protein classes like “chaperone”, “cytoskeletal protein” and “nucleic acid binding protein” (Fleckenstein et al., 2015). Even though the experiment was performed under different conditions (co-Immunoprecipitation at 15°C without heat shock), the results confirm the tendency of Hsp16 proteins to interact with proteins of the cytoskeleton or proteins involved in transcriptional and translational processes.

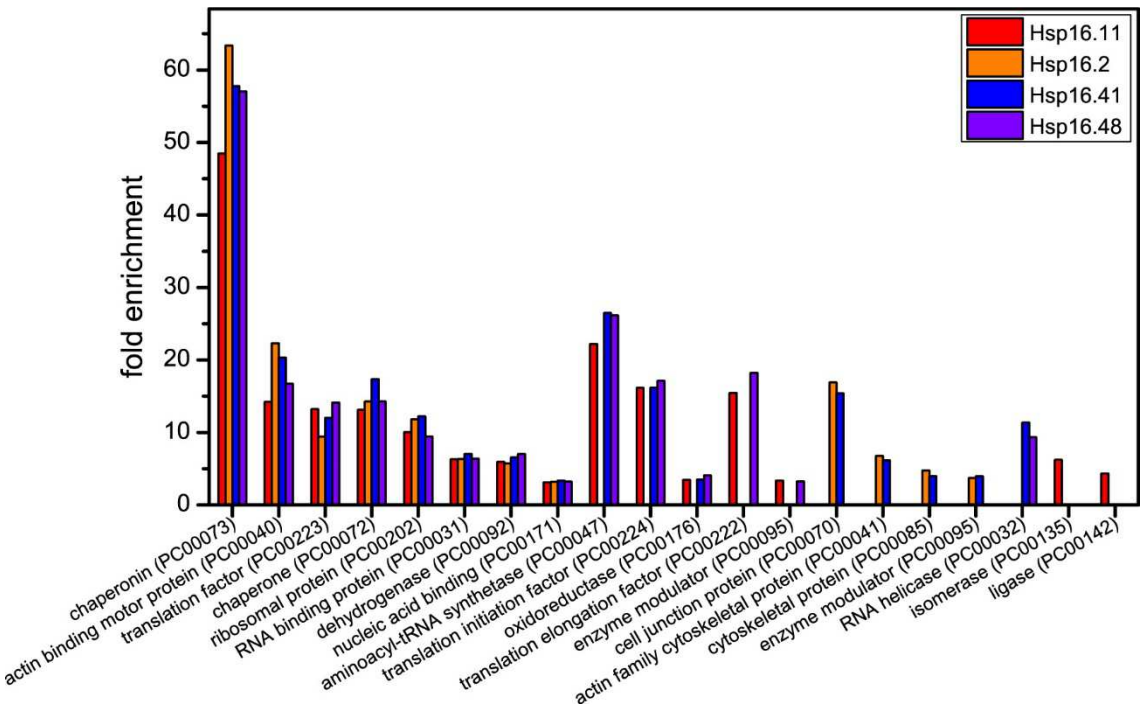

Figure 43: Statistical overrepresentation analysis of the GO categories in “protein class” for Hsp16.11, Hsp16.2, Hsp16.41 and Hsp16.48 interactors with the total *C. elegans* proteome as a reference. The analysis was carried out using the PANTHER online tool with default settings considering only classes with $p<0.05$.

In contrast to what was published before (Fleckenstein et al., 2015), the egg yolk precursor proteins vitellogenins were also found to be interactors of the Hsp16 core family and not exclusive substrates of Sip1. It has to be mendtioned that the previous analysis of Hsp16.2 substrate spectra was performed under non-heat shock conditions at 15 °C (Fleckenstein et al., 2015) constituting the only difference to the analysis in the present thesis. In the present analysis, Vitellogenin-6 was found for all four Hsp16 core family proteins, whereas Vitellogenin-5 and Vitellogenin-2 were only detected in Hsp16.11 and Hsp16.2 substrate spectra. Vitellogenin-6, a homologue of the mammalian apolipoprotein B, was suggested to have a function in thermotolerance (Fischer et al., 2014) already indicating a more general role aside of the transport of cholesterol from food sources to oocytes providing energy supply for developing embryos (Grant and Hirsh, 1999).

4.3.7 Abundance of identified Hsp16 core family interactors

To assess how abundant the identified Hsp16 interactors in *C. elegans* are, data from the PaxDb database (Wang et al., 2012) was used. Therefore the integrated *C. elegans* database for the whole organism was chosen, covering 61 % of the nematode proteome with 12,418 protein entries. The database provides a good coverage as only 2 hits identified in the Hsp16 substrate spectra were not found to be annotated, constituting less than 0.8 % of hits that were missing in the analysis. Compared to all entries in the database, rather highly abundant proteins were detected as Hsp16 interactors (Figure 44). With entries reaching from 0.001 ppm to 10,000 ppm for the total *C. elegans* database, for Hsp16 interactors only proteins in the range between 6 ppm to 10,000 ppm were found. The proteins with the lowest abundance detected in the co-immunoprecipitation experiments were the Peptide transporter family 1 with 6.76 ppm and protein cbp-1 with 25.5 ppm. However, those low abundant proteins were identified for all four proteins of the Hsp16 core family. Furthermore, many high abundant proteins were only detected in interactomes of one or two Hsp16 proteins (for a detailed table of the identified interactors of the Hsp16 core family see appendix).

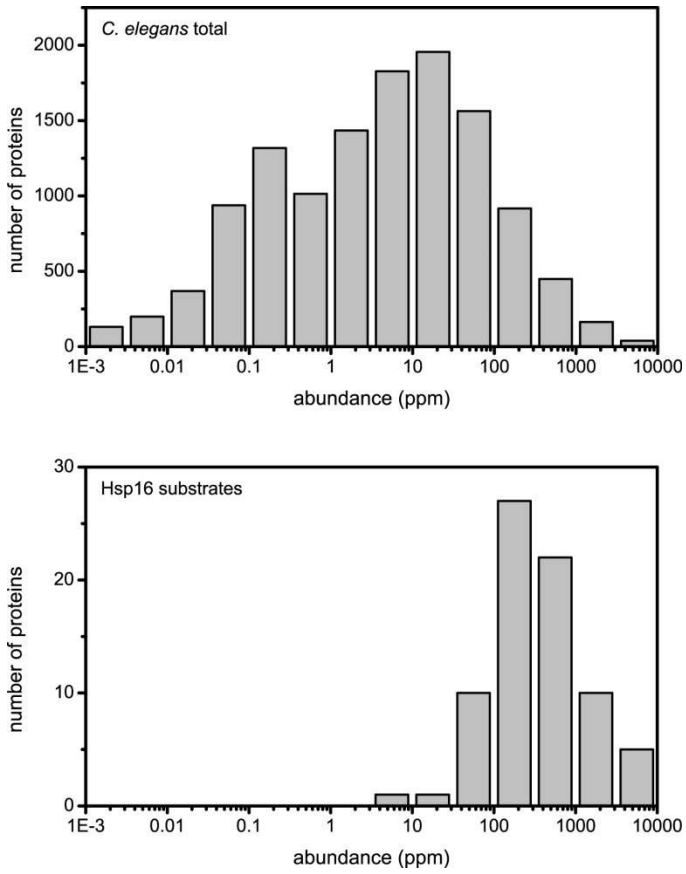

Figure 44: Abundance distributions for all detected Hsp16 core family interactors compared to the integrated *C. elegans* database for the whole organism. Abundance information was taken from the PaxDb database.

4.3.8 Summary on the Hsp16 protein core family and their interaction with substrate proteins

The proteins Hsp16.11, Hsp16.2, Hsp16.41 and Hsp16.48 were purified under denaturing conditions and refolded on a Superdex 200 column in PBS. The correct folding of the proteins was confirmed by far-UV CD spectroscopy. Analysis of secondary structure elements were in good agreement with previous investigations on the Hsp16 protein core family (Weinfurtner, 2008) and exhibited mainly beta-sheet like structure as expected for sHsps with their conserved alpha-crystallin domain (MacRae, 2000, Horwitz, 2003). The content in antiparallel and parallel beta-sheets and beta-turn structures accounted for approximately 55 % for the Hsp16 core family proteins. In comparison to that 46-49 % beta-sheet and beta-turn content was determined for Sip1, a member of the extended Hsp16 protein family,

depending of the pH (Fleckenstein, 2014). The Hsp12 protein family in *C. elegans* however showed a lower amount of beta-sheet and bets-turn elements in their structures (30-34 %) with a high content of up to 44 % in disordered structures (Krause, 2013).

Analysis of the quaternary structure of the Hsp16 protein core family by analytical ultracentrifugation revealed the presence of large oligomeric species of approximately 20-22 subunits. These results are in line with the investigations by Dr. Daniel Weinfurtner, who characterized the Hsp16 core family proteins to form oligomeric species of 20-22 subunits by analytical ultracentrifugation as well (Table 5) (Weinfurtner, 2008). In analytical SEC-HPLC experiments even larger oligomers were observed with a size of up to 550 kDa corresponding to 32 mers (Weinfurtner, 2008). For Sip1, as one of the closest relatives of the Hsp16 protein core family, a pH dependent oligomer formation has been reported ranging from a 24mer at pH 6.3 to a 32mer at pH 8.2 (Fleckenstein et al., 2015).

			Data from Weinfurtner (2008)			
Protein	**AUC**	**AUC SU**	**AUC**	**AUC SU**	**SEC-HPLC**	**SEC-HPLC SU**
Hsp16.11	320 kDa	20	-	-	500 ± 50 kDa	27-32
Hsp16.2	326 kDa	20	360 kDa	22	500 ± 50 kDa	27-32
Hsp16.41	348 kDa	21	361 kDa	22	400 ± 50 kDa	22-27
Hsp16.48	358 kDa	22	325 kDa	20	415 ± 50 kDa	23-29

Table 5: Quaternary structure data of Hsp16.11, Hsp16.2, Hsp16.41 and Hsp16.48 compared to data from Weinfurtner (2008). Molecular masses determined by analytical ultracentrifugation (AUC) and size-exclusion-chromatography-HPLC (SEC-HPLC) and the calculated number of subunits (SU) based on the determined molecular masses.

A crystal structure with a resolution of 3.6 Å of a full-length Sip1 complex revealed a hollow sphere composed of two identical hemispheres containing 16 subunits each (Fleckenstein et al., 2015). The basic building block was shown to be an antiparallel homodimer formed by the β6/β7 strands of the respective alpha-crystallin domains (Fleckenstein et al., 2015). Preliminary analysis of the Hsp16 core family proteins by electron microscopy suggested a 12 nm hollow spherical architecture with

tetrahedral symmetry. Class averages revealed a 24 mer composed out of dimers as a major species (Kastenmüller, 2011).

Regarding the chaperone function, the highest chaperone activity in *in vitro* assays with the model substrates CS and MDH was observed for Hsp16.2 followed by Hsp16.11. With CS as a substrate, the subfamily Hsp16.41 and Hsp16.48 showed almost no activity, whereas the suppression of MDH aggregation could be achieved by Hsp16.48 in a concentration- dependent manner. In *in vitro* assays it had already been shown before, that the chaperone activity of the subfamily Hsp16.41/Hsp16.48 was remarkably decreased compared to Hsp16.11/Hsp16.2 (Weinfurtner, 2008, Fleckenstein, 2014). For Sip1, the chaperone activity was shown to be pH dependent with the highest activity at pH 6.3 (Fleckenstein et al., 2015). But also for members of the Hsp16 protein core family a slight influence of the pH on the chaperone activity was reported in *in vitro* assays with MDH with an optimum at pH 7.5 for Hsp16.11 and pH 8.2 for Hsp16.2 (Fleckenstein, 2014). The pH dependency might be the reason why Sip1 was not able to prevent the aggregation of *C. elegans* lysate in the lysate assay. The lysate assay was perfomed at pH 7.5 under optimal conditions for the Hsp16 protein core family. Again Hsp16.11 and Hsp16.2 showed chaperone activity in a concentration- dependent manner and were able to suppress the aggregation of lysate proteins by 40 % and 30 %, respectively. However, Hsp16.41 and Hsp16.48 did not show activity in the lysate assay.

Having the low chaperone activity of Hsp16.41 and Hsp16.48 in mind, it seems surprising that a high number of 159 potential interactors were identified for Hsp16.48 by co-immunoprecipitation and mass spectrometric analysis, whereas for the highly active Hsp16.2 only 147 potential substrates were identified. A preference of Hsp16.41/Hsp16.48 towards low-abundant proteins lying below the detection limit of SDS-PAGE analysis can be excluded as all four proteins were found to bind to proteins present with comparable abundances in *C. elegans* by the highly sensitive mass spectrometric analysis. In general, as already observed for the human sHsp substrate spectra (chapter 4.2.4), rather highly abundant proteins were detected as possible Hsp16 interactors. However, with average abundances of the interactors of 700-800 ppm, no differences between the four Hsp16 proteins could be observed. A possible explanation for the contradicting observations in chaperone and lysate

assays and the co-immunoprecipitation experiments could be provided by the different modes of interactions between sHsps and their substrates. sHsps have been shown to either interact with their substrates by forming stable sHsp-substrate complexes with high affinity or via weak transient interactions with high dissociation constants (Kulig and Ecroyd, 2012). The stringent washing procedure during the CoIP protocol favors the identification of strong binders, whereas transient interactions are lost by this approach (Vasilescu et al., 2004). It has to be mentioned that the stability of the sHsp-substrate complex does not necessarily correlate to the degree of aggregation prevention. For example, high chaperone activity has been observed for Hsp17.7 from *Deinococcus radiodurans*, which was shown to only transiently interact with its substrates (Bepperling et al., 2012). Also for human HspB1 and HspB5 the prevention of amyloid-like aggregation of α-synuclein via transient interactions has been shown (Cox et al., 2016). In polyglutamin-induced neurodegeneration HspB5 has been shown to play a role in the suppression by inhibiting aggregation via transient interactions with monomeric Josephin (Robertson et al., 2010). The comparatively low amount of identified interactors for Hsp16.11 and Hsp16.2 compared to Hsp16.41 and Hsp16.48 might be due to a stronger contribution of transient interactions to the chaperone activity of the subfamily Hsp16.11/Hsp16.2, which are missing in the mass spec approach due to extensive washing steps. This problem could be circumvented by *in vivo* crosslinking approaches followed by mass spectrometric analysis which allow to "freeze" also transient protein-protein interactions by covalent bonds (Vasilescu et al., 2004, Kaake et al., 2014, Yang et al., 2012).

Concerning the identified interactors, no preferences of the four different Hsp16 proteins regarding the monomeric molecular mass, pI or hydrophobicity of their substrates could be observed. About 57 % of the interactors were found to have a monomeric molecular mass below 50 kDa. A similar size distribution was already reported for the substrates of Sip1 from *C. elegans*, IbpB from *E. coli* and Hsp20.2 from *Deinococcus radiodurans* (Fleckenstein et al., 2015, Bepperling et al., 2012, Fu et al., 2014). The hydrophobicity of the substrates, assessed by the GRAVY index, showed a slight shift towards higher values compared to the total *C. elegans* Swissprot database, meaning a slightly increased hydrophobicity.

Functional analysis via statistical overrepresentation tests using the PANTHER online tool revealed an enrichment of interactors involved in transcriptional and translational processes and cytoskeletal proteins. Similar protein classes have already been found to be enriched for Sip1 substrates (Fleckenstein et al., 2015). In contrast to previous findings, the egg yolk precursor proteins vitellogenins are not exclusive substrates of Sip1, but were also found to be Hsp16 substrates. It has to be mentioned that the experimental conditions between the two approaches for identifying substrate proteins of Sip1 and the Hsp16 proteins varied, as the published interactors of Hsp16.2 for example were pulled down under non-heat shock conditions at 15 °C (Fleckenstein et al., 2015) whereas the interactors of the four different Hsp16 core family proteins were pulled down at 37 °C. The temperature of 37 °C was recommended as heat shock condition in experiments with *C. elegans* (Zevian and Yanowitz, 2014). Proteins involved in transcriptional and translational processes have also been found to be a major component in aggregation profiling experiments of thermally sensitive proteins in *S. cerevisiae* (Wallace et al., 2015). Especially proteins like eukaryotic initiation factors (eIFs) and RNA helicases have been identified (Wallace et al., 2015), which have also been shown to be important interactors of the Hsp16 core family. A regulatory feedback loop, starting with the reduction of the translation of non-stress relevant mRNAs by stress-induced aggregation of initiation and unwinding factors and a subsequent restoration of those factors by molecular chaperones, was suggested (Wallace et al., 2015). Further analysis of the Hsp16 interactomes under varying conditions might lead to a better understanding of their specific functions in the cell.

5. Summary

Small heat shock proteins (sHsps) constitute a diverse family of molecular chaperones binding to unfolding substrates and thereby preventing their aggregation. They are characterized by a small monomeric molecular mass, a tendency to form large oligomers and the presence of a conserved alpha-crystallin domain. sHsps are found in all domains of life and especially in higher eukaryotes a large number of sHsps is present leading to the question whether they fulfill redundant functions or possibly are specialized for specific substrates. Therefore, aside of the structural and functional characterization of diverse sHsps, a special focus in this thesis was set on the elucidation of the substrate spectra of the sHsps.

As the chaperone function was shown to be dependent on the structure of sHsps, several truncation mutants of Hsp26 from *S. cerevisiae* were structurally characterized by far-UV CD spectroscopy, AUC and SEC-HPLC and analyzed by NMR with the aim to identify the mode of dimerization. The analysis of a dimeric structure by NMR was not successful as no truncation mutant could be found which forms a stable dimer under the conditions used in NMR experiments. However, a HSQC spectrum of the mutant Hsp26αM1 led to the assignment of about 90 % of the residues creating an important basis for further analysis. Heteronuclear NOE spectra of Hsp26αM1 allowed the identification of a flexible linker region in the area of the residues 135-155, supporting a dimerization mode via domain swapping. Furthermore, phosphomimetic mutants were analyzed to assess the regulation of Hsp26. In aggregation assays, the mutants were shown to be more active compared to the Hsp26 wildtype. For the Hsp26 wildtype, the size of the sHsp-substrate complexes decreases upon heat activation. However, the mutants formed smaller sHsp-substrate complexes, even without the need of heat activation. Therefore, phosphorylation seems to be a possible mode of regulation for Hsp26 aside of the already known heat activation.

In human, 10 sHsps have been identified exhibiting diverse biochemical properties and expression patterns. In a comparative approach using co-immunoprecipitation with HEK293 lysate under heat shock conditions followed by mass spectrometry, the substrate spectra of the human sHsps HspB1- HspB7 were analyzed. In total 130

unique protein hits were identified as interactors of human sHsps. Additionally, the heat sensitive fraction of HEK293 lysate (HEK HS) was determined resulting in approximately 1100 hits. A large overlap in common substrates was found for HspB1, HspB3 and HspB5, which were at the same time the sHsps with the largest number of interactors identified. Compared to the HEK HS fraction and the whole HEK293 proteome, the interactors of the human sHsps were shown to have higher monomeric molecular masses and lower pI values. A favoured binding of human sHsps to hydrophobic substrates could not be observed. Functional classification revealed that human sHsps preferentially bind to substrates involved in DNA-, RNA-, and protein metabolic processes.

As a third project, the four members Hsp16.11, Hsp16.2, Hsp16.41 and Hsp16.48 of the *C. elegans* Hsp16 core family were investigated. Their high sequence identity of up to 93 % gives reason to wonder why there is a need for all four of them. Structural analysis revealed a typical beta-sheet rich secondary structure and the presence of large oligomers consisting of about 22 subunits. In *in vitro* aggregation assays with the model substrates CS and MDH, as well as in aggregation assays with *C. elegans* lysate under heat shock conditions, Hsp16.11 and Hsp16.2 were shown to be more active compared to Hsp16.41 and Hsp16.48. Nevertheless, a comparable number of interactors was found for all four of them in co-immunoprecipitation experiments and mass spectrometric analysis using a label free quantification approach. Regarding the identified interactors, no differences could be detected between the four sHsps. In contrast, they were shown to share a high number of 102 common substrates. Among the interactors of the Hsp16 protein core family mainly proteins involved in transcriptional and translational processes as well as proteins of the cytoskeleton were overrepresented.

Taken together, this thesis provides new insights into the substrate spectra of human sHsps and the *C. elegans* Hsp16 protein core family. Additionally an important basis for future structural investigations on Hsp26 and its regulation via phosphorylation was made.

6. References

WormBase 2017. *WormBase: Nematode Information Resource* [Online]. http://www.wormbase.org/#012-34-5. [Accessed 2017].

ACUNZO, J., KATSOGIANNOU, M. & ROCCHI, P. 2012. Small heat shock proteins HSP27 (HspB1), alphaB-crystallin (HspB5) and HSP22 (HspB8) as regulators of cell death. *Int J Biochem Cell Biol,* 44**,** 1622-31.

AHMAD, M. F., RAMAN, B., RAMAKRISHNA, T. & RAO CH, M. 2008. Effect of phosphorylation on alpha B-crystallin: differences in stability, subunit exchange and chaperone activity of homo and mixed oligomers of alpha B-crystallin and its phosphorylation-mimicking mutant. *J Mol Biol,* 375**,** 1040-51.

AHRMAN, E., LAMBERT, W., AQUILINA, J. A., ROBINSON, C. V. & EMANUELSSON, C. S. 2007. Chemical cross-linking of the chloroplast localized small heat-shock protein, Hsp21, and the model substrate citrate synthase. *Protein Sci,* 16**,** 1464-78.

AL REFAII, A. & ALIX, J. H. 2009. Ribosome biogenesis is temperature-dependent and delayed in Escherichia coli lacking the chaperones DnaK or DnaJ. *Mol Microbiol,* 71**,** 748-62.

ALBUQUERQUE, C. P., SMOLKA, M. B., PAYNE, S. H., BAFNA, V., ENG, J. & ZHOU, H. 2008. A multidimensional chromatography technology for in-depth phosphoproteome analysis. *Mol Cell Proteomics,* 7**,** 1389-96.

ANDRIEU, C., TAIEB, D., BAYLOT, V., ETTINGER, S., SOUBEYRAN, P., DE-THONEL, A., NELSON, C., GARRIDO, C., SO, A., FAZLI, L., BLADOU, F., GLEAVE, M., IOVANNA, J. L. & ROCCHI, P. 2010. Heat shock protein 27 confers resistance to androgen ablation and chemotherapy in prostate cancer cells through eIF4E. *Oncogene,* 29**,** 1883-96.

ANFINSEN, C. B. 1973. Principles that govern the folding of protein chains. *Science,* 181**,** 223-30.

ANFINSEN, C. B., HABER, E., SELA, M. & WHITE, F. H., JR. 1961. The kinetics of formation of native ribonuclease during oxidation of the reduced polypeptide chain. *Proc Natl Acad Sci U S A,* 47**,** 1309-14.

ARRIGO, A. P. & GIBERT, B. 2012. HspB1 dynamic phospho-oligomeric structure dependent interactome as cancer therapeutic target. *Curr Mol Med,* 12**,** 1151-63.

ARRIGO, A. P. & GIBERT, B. 2013. Protein interactomes of three stress inducible small heat shock proteins: HspB1, HspB5 and HspB8. *Int J Hyperthermia,* 29**,** 409-22.

ATKINS, P. W. 2013. *Physikalische Chemie,* Weinheim, Wiley-VCH.

BAGNERIS, C., BATEMAN, O. A., NAYLOR, C. E., CRONIN, N., BOELENS, W. C., KEEP, N. H. & SLINGSBY, C. 2009. Crystal structures of alpha-crystallin domain dimers of alphaB-crystallin and Hsp20. *J Mol Biol,* 392**,** 1242-52.

BAKTHISARAN, R., TANGIRALA, R. & RAO CH, M. 2015. Small heat shock proteins: Role in cellular functions and pathology. *Biochim Biophys Acta,* 1854**,** 291-319.

BALCH, W. E., MORIMOTO, R. I., DILLIN, A. & KELLY, J. W. 2008. Adapting proteostasis for disease intervention. *Science,* 319**,** 916-9.

BALDWIN, R. L. 1996. Why is protein folding so fast? *Proc Natl Acad Sci U S A,* 93**,** 2627-8.

BASHA, E., JONES, C., BLACKWELL, A. E., CHENG, G., WATERS, E. R., SAMSEL, K. A., SIDDIQUE, M., PETT, V., WYSOCKI, V. & VIERLING, E. 2013. An unusual dimeric small heat shock protein provides insight into the mechanism of this class of chaperones. *J Mol Biol,* 425**,** 1683-96.

BASHA, E., JONES, C., WYSOCKI, V. & VIERLING, E. 2010. Mechanistic differences between two conserved classes of small heat shock proteins found in the plant cytosol. *J Biol Chem,* 285**,** 11489-97.

BASHA, E., O'NEILL, H. & VIERLING, E. 2012. Small heat shock proteins and alpha-crystallins: dynamic proteins with flexible functions. *Trends Biochem Sci,* 37**,** 106-17.

BENESCH, J. L., AQUILINA, J. A., BALDWIN, A. J., REKAS, A., STENGEL, F., LINDNER, R. A., BASHA, E., DEVLIN, G. L., HORWITZ, J., VIERLING, E., CARVER, J. A. & ROBINSON, C. V. 2010. The quaternary organization and dynamics of the molecular chaperone HSP26 are thermally regulated. *Chem Biol,* 17**,** 1008-17.

BENTLEY, N. J., FITCH, I. T. & TUITE, M. F. 1992. The small heat-shock protein Hsp26 of Saccharomyces cerevisiae assembles into a high molecular weight aggregate. *Yeast,* 8**,** 95-106.

BEPPERLING, A., ALTE, F., KRIEHUBER, T., BRAUN, N., WEINKAUF, S., GROLL, M., HASLBECK, M. & BUCHNER, J. 2012. Alternative bacterial two-component small heat shock protein systems. *Proc Natl Acad Sci U S A,* 109**,** 20407-12.

BODENMILLER, B., WANKA, S., KRAFT, C., URBAN, J., CAMPBELL, D., PEDRIOLI, P. G., GERRITS, B., PICOTTI, P., LAM, H., VITEK, O., BRUSNIAK, M. Y., ROSCHITZKI, B., ZHANG, C., SHOKAT, K. M., SCHLAPBACH, R., COLMAN-LERNER, A., NOLAN, G. P., NESVIZHSKII, A. I., PETER, M., LOEWITH, R., VON MERING, C. & AEBERSOLD, R. 2010. Phosphoproteomic analysis reveals interconnected system-wide responses to perturbations of kinases and phosphatases in yeast. *Sci Signal,* 3**,** rs4.

BOELENS, W. C., CROES, Y. & DE JONG, W. W. 2001. Interaction between alphaB-crystallin and the human 20S proteasomal subunit C8/alpha7. *Biochim Biophys Acta,* 1544**,** 311-9.

BOHM, G., MUHR, R. & JAENICKE, R. 1992. Quantitative analysis of protein far UV circular dichroism spectra by neural networks. *Protein Eng,* 5**,** 191-5.

BOVA, M. P., DING, L. L., HORWITZ, J. & FUNG, B. K. 1997. Subunit exchange of alphaA-crystallin. *J Biol Chem,* 272**,** 29511-7.

BOVA, M. P., MCHAOURAB, H. S., HAN, Y. & FUNG, B. K. 2000. Subunit exchange of small heat shock proteins. Analysis of oligomer formation of alphaA-crystallin and Hsp27 by fluorescence resonance energy transfer and site-directed truncations. *J Biol Chem,* 275**,** 1035-42.

BRADFORD, M. M. 1976. A rapid and sensitive method for the quantitation of microgram quantities of protein utilizing the principle of protein-dye binding. *Anal Biochem,* 72**,** 248-54.

BRAUN, N., ZACHARIAS, M., PESCHEK, J., KASTENMULLER, A., ZOU, J., HANZLIK, M., HASLBECK, M., RAPPSILBER, J., BUCHNER, J. & WEINKAUF, S. 2011. Multiple molecular architectures of the eye lens chaperone alphaB-crystallin elucidated by a triple hybrid approach. *Proc Natl Acad Sci U S A,* 108**,** 20491-6.

BRENNER, S. 1974. The genetics of Caenorhabditis elegans. *Genetics,* 77**,** 71-94.

BROWN, P. H., BALBO, A., ZHAO, H., EBEL, C. & SCHUCK, P. 2011. Density contrast sedimentation velocity for the determination of protein partial-specific volumes. *PLoS One,* 6**,** e26221.

BRYCHZY, A., REIN, T., WINKLHOFER, K. F., HARTL, F. U., YOUNG, J. C. & OBERMANN, W. M. 2003. Cofactor Tpr2 combines two TPR domains and a J domain to regulate the Hsp70/Hsp90 chaperone system. *EMBO J,* 22**,** 3613-23.

BUCHAN, J. R. & PARKER, R. 2009. Eukaryotic stress granules: the ins and outs of translation. *Mol Cell,* 36**,** 932-41.

BUCHNER, J. 1996. Supervising the fold: functional principles of molecular chaperones. *FASEB J,* 10**,** 10-9.

BUCHNER, J. 1999. Hsp90 & Co. - a holding for folding. *Trends Biochem Sci,* 24**,** 136-41.

BUCHNER, J., GRALLERT, H. & JAKOB, U. 1998. Analysis of chaperone function using citrate synthase as nonnative substrate protein. *Methods Enzymol,* 290**,** 323-38.

BUGL, H., FAUMAN, E. B., STAKER, B. L., ZHENG, F., KUSHNER, S. R., SAPER, M. A., BARDWELL, J. C. & JAKOB, U. 2000. RNA methylation under heat shock control. *Mol Cell,* 6**,** 349-60.

BUKAU, B. & HORWICH, A. L. 1998. The Hsp70 and Hsp60 chaperone machines. *Cell,* 92**,** 351-66.

CANDIDO, E. P. 2002. The small heat shock proteins of the nematode Caenorhabditis elegans: structure, regulation and biology. *Prog Mol Subcell Biol,* 28**,** 61-78.

CASPERS, G. J., LEUNISSEN, J. A. & DE JONG, W. W. 1995. The expanding small heat-shock protein family, and structure predictions of the conserved "alpha-crystallin domain". *J Mol Evol,* 40**,** 238-48.

CATELLI, M. G., BINART, N., JUNG-TESTAS, I., RENOIR, J. M., BAULIEU, E. E., FERAMISCO, J. R. & WELCH, W. J. 1985. The common 90-kd protein component of non-transformed '8S' steroid receptors is a heat-shock protein. *EMBO J,* 4**,** 3131-5.

CHEN, J., FEIGE, M. J., FRANZMANN, T. M., BEPPERLING, A. & BUCHNER, J. 2010. Regions outside the alpha-crystallin domain of the small heat shock protein Hsp26 are required for its dimerization. *J Mol Biol,* 398**,** 122-31.

CHENG, G., BASHA, E., WYSOCKI, V. H. & VIERLING, E. 2008. Insights into small heat shock protein and substrate structure during chaperone action derived from hydrogen/deuterium exchange and mass spectrometry. *J Biol Chem,* 283**,** 26634-42.

COX, D., SELIG, E., GRIFFIN, M. D., CARVER, J. A. & ECROYD, H. 2016. Small Heat-shock Proteins Prevent alpha-Synuclein Aggregation via Transient Interactions and Their Efficacy Is Affected by the Rate of Aggregation. *J Biol Chem,* 291**,** 22618-22629.

CREIGHTON, T. E. 1988. Toward a better understanding of protein folding pathways. *Proc Natl Acad Sci U S A,* 85**,** 5082-6.

CUSACK, S., HARTLEIN, M. & LEBERMAN, R. 1991. Sequence, structural and evolutionary relationships between class 2 aminoacyl-tRNA synthetases. *Nucleic Acids Res,* 19**,** 3489-98.

DE JONG, W. W., CASPERS, G. J. & LEUNISSEN, J. A. 1998. Genealogy of the alpha-crystallin--small heat-shock protein superfamily. *Int J Biol Macromol,* 22**,** 151-62.

DEN ENGELSMAN, J., BOROS, S., DANKERS, P. Y., KAMPS, B., VREE EGBERTS, W. T., BODE, C. S., LANE, L. A., AQUILINA, J. A., BENESCH, J. L., ROBINSON, C. V., DE JONG, W. W. & BOELENS, W. C. 2009. The small heat-shock proteins HSPB2 and HSPB3 form well-defined heterooligomers in a unique 3 to 1 subunit ratio. *J Mol Biol,* 393**,** 1022-32.

DEN ENGELSMAN, J., KEIJSERS, V., DE JONG, W. W. & BOELENS, W. C. 2003. The small heat-shock protein alpha B-crystallin promotes FBX4-dependent ubiquitination. *J Biol Chem,* 278**,** 4699-704.

DEY, S., BURTON, R. L., GRANT, G. A. & SACCHETTINI, J. C. 2008. Structural analysis of substrate and effector binding in Mycobacterium tuberculosis D-3-phosphoglycerate dehydrogenase. *Biochemistry,* 47**,** 8271-82.

DILL, K. A., BROMBERG, S., YUE, K., FIEBIG, K. M., YEE, D. P., THOMAS, P. D. & CHAN, H. S. 1995. Principles of protein folding--a perspective from simple exact models. *Protein Sci,* 4**,** 561-602.

DING, L. & CANDIDO, E. P. 2000a. Association of several small heat-shock proteins with reproductive tissues in the nematode Caenorhabditis elegans. *Biochem J,* 351**,** 13-7.

DING, L. & CANDIDO, E. P. 2000b. HSP25, a small heat shock protein associated with dense bodies and M-lines of body wall muscle in Caenorhabditis elegans. *J Biol Chem,* 275**,** 9510-7.

DING, L. & CANDIDO, E. P. 2000c. HSP43, a small heat-shock protein localized to specific cells of the vulva and spermatheca in the nematode Caenorhabditis elegans. *Biochem J,* 349**,** 409-12.

DINNER, A. R., SALI, A., SMITH, L. J., DOBSON, C. M. & KARPLUS, M. 2000. Understanding protein folding via free-energy surfaces from theory and experiment. *Trends Biochem Sci,* 25**,** 331-9.

DOBSON, C. M. & KARPLUS, M. 1999. The fundamentals of protein folding: bringing together theory and experiment. *Curr Opin Struct Biol,* 9**,** 92-101.

DOBSON, C. M., SALI, A. & KARPLUS, M. 1998. Protein Folding: A Perspective from Theory and Experiment. *Angewandte Chemie International Edition,* 37**,** 868-893.

ECROYD, H., MEEHAN, S., HORWITZ, J., AQUILINA, J. A., BENESCH, J. L., ROBINSON, C. V., MACPHEE, C. E. & CARVER, J. A. 2007. Mimicking phosphorylation of alphaB-crystallin affects its chaperone activity. *Biochem J,* 401**,** 129-41.

EHRNSPERGER, M., GRABER, S., GAESTEL, M. & BUCHNER, J. 1997. Binding of non-native protein to Hsp25 during heat shock creates a reservoir of folding intermediates for reactivation. *EMBO J,* 16**,** 221-9.

ELLIS, R. J. 2001. Macromolecular crowding: an important but neglected aspect of the intracellular environment. *Curr Opin Struct Biol,* 11**,** 114-9.

ELLIS, R. J. & HARTL, F. U. 1999. Principles of protein folding in the cellular environment. *Curr Opin Struct Biol,* 9**,** 102-10.

ELLIS, R. J., VAN DER VIES, S. M. & HEMMINGSEN, S. M. 1989. The molecular chaperone concept. *Biochem Soc Symp,* 55**,** 145-53.

ESCUSA-TORET, S., VONK, W. I. & FRYDMAN, J. 2013. Spatial sequestration of misfolded proteins by a dynamic chaperone pathway enhances cellular fitness during stress. *Nat Cell Biol,* 15**,** 1231-43.

EYLES, S. J. & GIERASCH, L. M. 2010. Nature's molecular sponges: small heat shock proteins grow into their chaperone roles. *Proc Natl Acad Sci U S A,* 107**,** 2727-8.

FAIRBANKS, G., STECK, T. L. & WALLACH, D. F. 1971. Electrophoretic analysis of the major polypeptides of the human erythrocyte membrane. *Biochemistry,* 10**,** 2606-17.

FICARRO, S. B., MCCLELAND, M. L., STUKENBERG, P. T., BURKE, D. J., ROSS, M. M., SHABANOWITZ, J., HUNT, D. F. & WHITE, F. M. 2002. Phosphoproteome analysis by mass spectrometry and its application to Saccharomyces cerevisiae. *Nat Biotechnol,* 20**,** 301-5.

FISCHER, M., FITZENBERGER, E., KULL, R., BOLL, M. & WENZEL, U. 2014. The zinc matrix metalloproteinase ZMP-2 increases survival of Caenorhabditis elegans through interference with lipoprotein absorption. *Genes Nutr,* 9**,** 414.

FLECKENSTEIN, T. 2014. *Sip1, a unique small heat shock protein of the nematode Caenorhabditis elegans.* Doctoral Thesis, Technische Universität München.

FLECKENSTEIN, T., KASTENMULLER, A., STEIN, M. L., PETERS, C., DAAKE, M., KRAUSE, M., WEINFURTNER, D., HASLBECK, M., WEINKAUF, S., GROLL, M. & BUCHNER, J. 2015. The Chaperone Activity of the Developmental Small Heat Shock Protein Sip1 Is Regulated by pH-Dependent Conformational Changes. *Mol Cell,* 58**,** 1067-78.

FONTE, V., KIPP, D. R., YERG, J., 3RD, MERIN, D., FORRESTAL, M., WAGNER, E., ROBERTS, C. M. & LINK, C. D. 2008. Suppression of in vivo beta-amyloid peptide toxicity by overexpression of the HSP-16.2 small chaperone protein. *J Biol Chem,* 283**,** 784-91.

FRANZMANN, T. M., MENHORN, P., WALTER, S. & BUCHNER, J. 2008. Activation of the chaperone Hsp26 is controlled by the rearrangement of its thermosensor domain. *Mol Cell,* 29**,** 207-16.

FRANZMANN, T. M., WUHR, M., RICHTER, K., WALTER, S. & BUCHNER, J. 2005. The activation mechanism of Hsp26 does not require dissociation of the oligomer. *J Mol Biol,* 350**,** 1083-93.

FU, X., CHANG, Z., SHI, X., BU, D. & WANG, C. 2014. Multilevel structural characteristics for the natural substrate proteins of bacterial small heat shock proteins. *Protein Sci,* 23**,** 229-37.

FULDA, S., GORMAN, A. M., HORI, O. & SAMALI, A. 2010. Cellular Stress Responses: Cell Survival and Cell Death. *International Journal of Cell Biology,* 2010**,** 23.

GARRIDO, C., BRUNET, M., DIDELOT, C., ZERMATI, Y., SCHMITT, E. & KROEMER, G. 2006. Heat shock proteins 27 and 70: anti-apoptotic proteins with tumorigenic properties. *Cell Cycle,* 5**,** 2592-601.

GARRIDO, C., PAUL, C., SEIGNEURIC, R. & KAMPINGA, H. H. 2012. The small heat shock proteins family: the long forgotten chaperones. *Int J Biochem Cell Biol,* 44**,** 1588-92.

GASTMANN, O., BURFEIND, P., GUNTHER, E., HAMEISTER, H., SZPIRER, C. & HOYER-FENDER, S. 1993. Sequence, expression, and chromosomal assignment of a human sperm outer dense fiber gene. *Mol Reprod Dev,* 36**,** 407-18.

GHOSH, J. G., SHENOY, A. K., JR. & CLARK, J. I. 2007. Interactions between important regulatory proteins and human alphaB crystallin. *Biochemistry,* 46**,** 6308-17.

GIBERT, B., ECKEL, B., FASQUELLE, L., MOULIN, M., BOUHALLIER, F., GONIN, V., MELLIER, G., SIMON, S., KRETZ-REMY, C., ARRIGO, A. P. & DIAZ-LATOUD, C. 2012. Knock down of heat shock protein 27 (HspB1) induces degradation of several putative client proteins. *PLoS One,* 7**,** e29719.

GLOVER, J. R. & LINDQUIST, S. 1998. Hsp104, Hsp70, and Hsp40: a novel chaperone system that rescues previously aggregated proteins. *Cell,* 94**,** 73-82.

GOLOUBINOFF, P., MOGK, A., ZVI, A. P., TOMOYASU, T. & BUKAU, B. 1999. Sequential mechanism of solubilization and refolding of stable protein aggregates by a bichaperone network. *Proc Natl Acad Sci U S A,* 96**,** 13732-7.

GRALLERT, H. & BUCHNER, J. 2001. Review: a structural view of the GroE chaperone cycle. *J Struct Biol,* 135**,** 95-103.

GRANT, B. & HIRSH, D. 1999. Receptor-mediated endocytosis in the Caenorhabditis elegans oocyte. *Mol Biol Cell,* 10**,** 4311-26.

GRANT, G. A., XU, X. L. & HU, Z. 2004. Quantitative relationships of site to site interaction in Escherichia coli D-3-phosphoglycerate dehydrogenase revealed by asymmetric hybrid tetramers. *J Biol Chem,* 279**,** 13452-60.

HALEY, D. A., BOVA, M. P., HUANG, Q. L., MCHAOURAB, H. S. & STEWART, P. L. 2000. Small heat-shock protein structures reveal a continuum from symmetric to variable assemblies. *J Mol Biol,* 298**,** 261-72.

HANSON, P. I. & WHITEHEART, S. W. 2005. AAA+ proteins: have engine, will work. *Nat Rev Mol Cell Biol,* 6**,** 519-29.

HARRIS, S. F., SHIAU, A. K. & AGARD, D. A. 2004. The crystal structure of the carboxy-terminal dimerization domain of htpG, the Escherichia coli Hsp90, reveals a potential substrate binding site. *Structure,* 12**,** 1087-97.

HARTL, F. U., BRACHER, A. & HAYER-HARTL, M. 2011. Molecular chaperones in protein folding and proteostasis. *Nature,* 475**,** 324-32.

HARTL, F. U. & HAYER-HARTL, M. 2002. Molecular chaperones in the cytosol: from nascent chain to folded protein. *Science,* 295**,** 1852-8.

HARTMAN, D. J., SURIN, B. P., DIXON, N. E., HOOGENRAAD, N. J. & HOJ, P. B. 1993. Substoichiometric amounts of the molecular chaperones GroEL and GroES prevent thermal denaturation and aggregation of mammalian mitochondrial malate dehydrogenase in vitro. *Proc Natl Acad Sci U S A,* 90**,** 2276-80.

HASLBECK, M., BRAUN, N., STROMER, T., RICHTER, B., MODEL, N., WEINKAUF, S. & BUCHNER, J. 2004a. Hsp42 is the general small heat shock protein in the cytosol of Saccharomyces cerevisiae. *EMBO J,* 23**,** 638-49.

HASLBECK, M. & BUCHNER, J. 2015. Assays to characterize molecular chaperone function in vitro. *Methods in Molecular Biology,* 1292**,** 39-51.

HASLBECK, M., FRANZMANN, T., WEINFURTNER, D. & BUCHNER, J. 2005a. Some like it hot: the structure and function of small heat-shock proteins. *Nat Struct Mol Biol,* 12**,** 842-6.

HASLBECK, M., IGNATIOU, A., SAIBIL, H., HELMICH, S., FRENZL, E., STROMER, T. & BUCHNER, J. 2004b. A domain in the N-terminal part of Hsp26 is essential for chaperone function and oligomerization. *J Mol Biol,* 343**,** 445-55.

HASLBECK, M., KASTENMULLER, A., BUCHNER, J., WEINKAUF, S. & BRAUN, N. 2008. Structural dynamics of archaeal small heat shock proteins. *J Mol Biol,* 378**,** 362-74.

HASLBECK, M., MIESS, A., STROMER, T., WALTER, S. & BUCHNER, J. 2005b. Disassembling protein aggregates in the yeast cytosol. The cooperation of Hsp26 with Ssa1 and Hsp104. *J Biol Chem,* 280**,** 23861-8.

HASLBECK, M. & VIERLING, E. 2015. A first line of stress defense: small heat shock proteins and their function in protein homeostasis. *J Mol Biol,* 427**,** 1537-48.

HASLBECK, M., WALKE, S., STROMER, T., EHRNSPERGER, M., WHITE, H. E., CHEN, S., SAIBIL, H. R. & BUCHNER, J. 1999. Hsp26: a temperature-regulated chaperone. *EMBO J,* 18**,** 6744-51.

HELBIG, A. O., ROSATI, S., PIJNAPPEL, P. W., VAN BREUKELEN, B., TIMMERS, M. H., MOHAMMED, S., SLIJPER, M. & HECK, A. J. 2010. Perturbation of the yeast N-acetyltransferase NatB induces elevation of protein phosphorylation levels. *BMC Genomics,* 11**,** 685.

HILTON, G. R., LIOE, H., STENGEL, F., BALDWIN, A. J. & BENESCH, J. L. 2013. Small heat-shock proteins: paramedics of the cell. *Top Curr Chem,* 328**,** 69-98.

HOCKERTZ, M. K., CLARK-LEWIS, I. & CANDIDO, E. P. 1991. Studies of the small heat shock proteins of Caenorhabditis elegans using anti-peptide antibodies. *FEBS Lett,* 280**,** 375-8.

HOLT, L. J., TUCH, B. B., VILLEN, J., JOHNSON, A. D., GYGI, S. P. & MORGAN, D. O. 2009. Global analysis of Cdk1 substrate phosphorylation sites provides insights into evolution. *Science,* 325**,** 1682-6.

HORWICH, A. L., FARR, G. W. & FENTON, W. A. 2006. GroEL-GroES-mediated protein folding. *Chem Rev,* 106**,** 1917-30.

HORWITZ, J. 1992. Alpha-crystallin can function as a molecular chaperone. *Proc Natl Acad Sci U S A,* 89**,** 10449-53.

HORWITZ, J. 2003. Alpha-crystallin. *Exp Eye Res,* 76**,** 145-53.

ITO, H., KAMEI, K., IWAMOTO, I., INAGUMA, Y., NOHARA, D. & KATO, K. 2001. Phosphorylation-induced change of the oligomerization state of alpha B-crystallin. *J Biol Chem,* 276**,** 5346-52.

JAKOB, U., GAESTEL, M., ENGEL, K. & BUCHNER, J. 1993. Small heat shock proteins are molecular chaperones. *J Biol Chem,* 268**,** 1517-20.

JANTSCHITSCH, C. & TRAUTINGER, F. 2003. Heat shock and UV-B-induced DNA damage and mutagenesis in skin. *Photochem Photobiol Sci,* 2**,** 899-903.

JAYA, N., GARCIA, V. & VIERLING, E. 2009. Substrate binding site flexibility of the small heat shock protein molecular chaperones. *Proc Natl Acad Sci U S A,* 106**,** 15604-9.

JEHLE, S., VAN ROSSUM, B., STOUT, J. R., NOGUCHI, S. M., FALBER, K., REHBEIN, K., OSCHKINAT, H., KLEVIT, R. E. & RAJAGOPAL, P. 2009. alphaB-crystallin: a hybrid solid-state/solution-state NMR investigation reveals structural aspects of the heterogeneous oligomer. *J Mol Biol,* 385**,** 1481-97.

JONES, D. & CANDIDO, E. P. 1999. Feeding is inhibited by sublethal concentrations of toxicants and by heat stress in the nematode Caenorhabditis elegans: relationship to the cellular stress response. *J Exp Zool,* 284**,** 147-57.

JONES, D., RUSSNAK, R. H., KAY, R. J. & CANDIDO, E. P. 1986. Structure, expression, and evolution of a heat shock gene locus in Caenorhabditis elegans that is flanked by repetitive elements. *J Biol Chem,* 261**,** 12006-15.

JONES, D., STRINGHAM, E. G., BABICH, S. L. & CANDIDO, E. P. 1996. Transgenic strains of the nematode C. elegans in biomonitoring and toxicology: effects of captan and related compounds on the stress response. *Toxicology,* 109**,** 119-27.

JOVCEVSKI, B., KELLY, M. A., ROTE, A. P., BERG, T., GASTALL, H. Y., BENESCH, J. L., AQUILINA, J. A. & ECROYD, H. 2015. Phosphomimics destabilize Hsp27 oligomeric assemblies and enhance chaperone activity. *Chem Biol,* 22**,** 186-95.

KAAKE, R. M., WANG, X., BURKE, A., YU, C., KANDUR, W., YANG, Y., NOVTISKY, E. J., SECOND, T., DUAN, J., KAO, A., GUAN, S., VELLUCCI, D., RYCHNOVSKY, S. D. & HUANG, L. 2014. A new in vivo cross-linking mass spectrometry platform to define protein-protein interactions in living cells. *Mol Cell Proteomics,* 13**,** 3533-43.

KAMPINGA, H. H. & CRAIG, E. A. 2010. The HSP70 chaperone machinery: J proteins as drivers of functional specificity. *Nat Rev Mol Cell Biol,* 11**,** 579-92.

KAPPE, G., BOELENS, W. C. & DE JONG, W. W. 2010. Why proteins without an alpha-crystallin domain should not be included in the human small heat shock protein family HSPB. *Cell Stress Chaperones,* 15**,** 457-61.

KAPPE, G., FRANCK, E., VERSCHUURE, P., BOELENS, W. C., LEUNISSEN, J. A. & DE JONG, W. W. 2003. The human genome encodes 10 alpha-crystallin-related small heat shock proteins: HspB1-10. *Cell Stress Chaperones,* 8**,** 53-61.

KAPPE, G., LEUNISSEN, J. A. & DE JONG, W. W. 2002. Evolution and diversity of prokaryotic small heat shock proteins. *Prog Mol Subcell Biol,* 28**,** 1-17.

KAPPE, G., VERSCHUURE, P., PHILIPSEN, R. L., STAALDUINEN, A. A., VAN DE BOOGAART, P., BOELENS, W. C. & DE JONG, W. W. 2001. Characterization of two novel human small heat shock proteins: protein kinase-related HspB8 and testis-specific HspB9. *Biochim Biophys Acta,* 1520**,** 1-6.

KARVE, T. M. & CHEEMA, A. K. 2011. Small changes huge impact: the role of protein posttranslational modifications in cellular homeostasis and disease. *J Amino Acids,* 2011**,** 207691.

KASAKOV, A. S., BUKACH, O. V., SEIT-NEBI, A. S., MARSTON, S. B. & GUSEV, N. B. 2007. Effect of mutations in the beta5-beta7 loop on the structure and properties of human small heat shock protein HSP22 (HspB8, H11). *FEBS J,* 274**,** 5628-42.

KASTENMÜLLER, A. 2011. *Elektronenmikroskopische Untersuchungen zur Assemblierung und Struktur von kleinen Hitzeschockproteinen.* Docotral Thesis, Technische Universität München.

KAYSER, J., HASLBECK, M., DEMPFLE, L., KRAUSE, M., GRASHOFF, C., BUCHNER, J., HERRMANN, H. & BAUSCH, A. R. 2013. The small heat shock protein Hsp27 affects assembly dynamics and structure of keratin intermediate filament networks. *Biophys J,* 105**,** 1778-85.

KEILHAUER, E. C., HEIN, M. Y. & MANN, M. 2015. Accurate protein complex retrieval by affinity enrichment mass spectrometry (AE-MS) rather than affinity purification mass spectrometry (AP-MS). *Mol Cell Proteomics,* 14**,** 120-35.

KELLY, S. M., JESS, T. J. & PRICE, N. C. 2005. How to study proteins by circular dichroism. *Biochim Biophys Acta,* 1751**,** 119-39.

KIM, K. K., KIM, R. & KIM, S. H. 1998. Crystal structure of a small heat-shock protein. *Nature,* 394**,** 595-9.

KOHARA, Y. 2005. *The Nematode Expression Pattern DataBase* [Online]. http://nematode.lab.nic.ac.jp/. [Accessed 2005].

KOKKE, B. P., BOELENS, W. C. & DE JONG, W. W. 2001. The lack of chaperonelike activity of Caenorhabditis elegans Hsp12.2 cannot be restored by domain swapping with human alphaB-crystallin. *Cell Stress Chaperones,* 6**,** 360-7.

KOKKE, B. P., LEROUX, M. R., CANDIDO, E. P., BOELENS, W. C. & DE JONG, W. W. 1998. Caenorhabditis elegans small heat-shock proteins Hsp12.2 and Hsp12.3 form tetramers and have no chaperone-like activity. *FEBS Lett,* 433**,** 228-32.

KOTEICHE, H. A. & MCHAOURAB, H. S. 2003. Mechanism of chaperone function in small heat-shock proteins. Phosphorylation-induced activation of two-mode binding in alphaB-crystallin. *J Biol Chem,* 278**,** 10361-7.

KOULOV, A. V., LAPOINTE, P., LU, B., RAZVI, A., COPPINGER, J., DONG, M. Q., MATTESON, J., LAISTER, R., ARROWSMITH, C., YATES, J. R., 3RD & BALCH, W. E. 2010. Biological and structural basis for Aha1 regulation of Hsp90 ATPase activity in maintaining proteostasis in the human disease cystic fibrosis. *Mol Biol Cell,* 21**,** 871-84.

KRAUSE, M. 2013. *Structural and functional characterization of small Heat shock proteins of the nematode Caenorhabditis elegans.* Doctoral Thesis, Technische Universtät München.

KRIEHUBER, T. 2012. *Strukturelle Organisation von kleinen Hitzeschockproteinen.* Doctoral Thesis, Technische Universität München.

KRIEHUBER, T., RATTEI, T., WEINMAIER, T., BEPPERLING, A., HASLBECK, M. & BUCHNER, J. 2010. Independent evolution of the core domain and its flanking sequences in small heat shock proteins. *FASEB J,* 24**,** 3633-42.

KRUUV, J., GLOFCHESKI, D., CHENG, K. H., CAMPBELL, S. D., AL-QYSI, H. M., NOLAN, W. T. & LEPOCK, J. R. 1983. Factors influencing survival and growth of mammalian cells exposed to hypothermia. I. Effects of temperature and membrane lipid perturbers. *J Cell Physiol,* 115**,** 179-85.

KULIG, M. & ECROYD, H. 2012. The small heat-shock protein alphaB-crystallin uses different mechanisms of chaperone action to prevent the amorphous versus fibrillar aggregation of alpha-lactalbumin. *Biochem J,* 448**,** 343-52.

KYTE, J. & DOOLITTLE, R. F. 1982. A simple method for displaying the hydropathic character of a protein. *J Mol Biol,* 157**,** 105-32.

LAEMMLI, U. K. 1970. Cleavage of structural proteins during the assembly of the head of bacteriophage T4. *Nature,* 227**,** 680-5.

LAGANOWSKY, A., BENESCH, J. L., LANDAU, M., DING, L., SAWAYA, M. R., CASCIO, D., HUANG, Q., ROBINSON, C. V., HORWITZ, J. & EISENBERG, D. 2010. Crystal structures of truncated alphaA and alphaB crystallins reveal structural mechanisms of polydispersity important for eye lens function. *Protein Sci,* 19**,** 1031-43.

LAMBOWITZ, A. M., KOBAYASHI, G. S., PAINTER, A. & MEDOFF, G. 1983. Possible relationship of morphogenesis in pathogenic fungus, Histoplasma capsulatum, to heat shock response. *Nature,* 303**,** 806-8.

LANNEAU, D., WETTSTEIN, G., BONNIAUD, P. & GARRIDO, C. 2010. Heat shock proteins: cell protection through protein triage. *ScientificWorldJournal,* 10**,** 1543-52.

LEBOWITZ, J., LEWIS, M. S. & SCHUCK, P. 2002. Modern analytical ultracentrifugation in protein science: a tutorial review. *Protein Sci,* 11**,** 2067-79.

LEE, G. J., ROSEMAN, A. M., SAIBIL, H. R. & VIERLING, E. 1997. A small heat shock protein stably binds heat-denatured model substrates and can maintain a substrate in a folding-competent state. *EMBO J,* 16**,** 659-71.

LEE, G. J. & VIERLING, E. 2000. A small heat shock protein cooperates with heat shock protein 70 systems to reactivate a heat-denatured protein. *Plant Physiol,* 122**,** 189-98.

LEROUX, M. R., MA, B. J., BATELIER, G., MELKI, R. & CANDIDO, E. P. 1997a. Unique structural features of a novel class of small heat shock proteins. *J Biol Chem,* 272**,** 12847-53.

LEROUX, M. R., MELKI, R., GORDON, B., BATELIER, G. & CANDIDO, E. P. 1997b. Structure-function studies on small heat shock protein oligomeric assembly and interaction with unfolded polypeptides. *J Biol Chem,* 272**,** 24646-56.

LEVIN, M., HASHIMSHONY, T., WAGNER, F. & YANAI, I. 2012. Developmental milestones punctuate gene expression in the Caenorhabditis embryo. *Dev Cell,* 22**,** 1101-8.

LEVINTHAL, C. 1968. Are there pathways for protein folding? *Journal De Chimie Physique Et De Physico-Chimie Biologique,* 65**,** 44.

LEVINTHAL, C. 1969. How to fold graciously. *Mössbauer Spectroscopy in Biological Systems Proceedings,* 67**,** 22-24.

LI, J., SOROKA, J. & BUCHNER, J. 2012. The Hsp90 chaperone machinery: conformational dynamics and regulation by co-chaperones. *Biochim Biophys Acta,* 1823**,** 624-35.

LINDER, B., JIN, Z., FREEDMAN, J. H. & RUBIN, C. S. 1996. Molecular characterization of a novel, developmentally regulated small embryonic chaperone from Caenorhabditis elegans. *J Biol Chem,* 271**,** 30158-66.

LINDQUIST, S. 1980. Varying patterns of protein synthesis in Drosophila during heat shock: implications for regulation. *Dev Biol,* 77**,** 463-79.

MACRAE, T. H. 2000. Structure and function of small heat shock/alpha-crystallin proteins: established concepts and emerging ideas. *Cell Mol Life Sci,* 57**,** 899-913.

MALMENDAL, A., OVERGAARD, J., BUNDY, J. G., SORENSEN, J. G., NIELSEN, N. C., LOESCHCKE, V. & HOLMSTRUP, M. 2006. Metabolomic profiling of heat stress: hardening and recovery of homeostasis in Drosophila. *Am J Physiol Regul Integr Comp Physiol,* 291**,** R205-12.

MAYER, M. P. 2010. Gymnastics of molecular chaperones. *Mol Cell,* 39**,** 321-31.

MAYER, M. P. & BUKAU, B. 2005. Hsp70 chaperones: cellular functions and molecular mechanism. *Cell Mol Life Sci,* 62**,** 670-84.

MCHAOURAB, H. S., GODAR, J. A. & STEWART, P. L. 2009. Structure and mechanism of protein stability sensors: chaperone activity of small heat shock proteins. *Biochemistry,* 48**,** 3828-37.

MEYER, P., PRODROMOU, C., HU, B., VAUGHAN, C., ROE, S. M., PANARETOU, B., PIPER, P. W. & PEARL, L. H. 2003. Structural and functional analysis of the middle segment of hsp90: implications for ATP hydrolysis and client protein and cochaperone interactions. *Mol Cell,* 11**,** 647-58.

MI, H., POUDEL, S., MURUGANUJAN, A., CASAGRANDE, J. T. & THOMAS, P. D. 2016. PANTHER version 10: expanded protein families and functions, and analysis tools. *Nucleic Acids Res,* 44**,** D336-42.

MIOT, M., REIDY, M., DOYLE, S. M., HOSKINS, J. R., JOHNSTON, D. M., GENEST, O., VITERY, M. C., MASISON, D. C. & WICKNER, S. 2011. Species-specific collaboration of heat shock proteins (Hsp) 70 and 100 in thermotolerance and protein disaggregation. *Proc Natl Acad Sci U S A,* 108**,** 6915-20.

MOGK, A. & BUKAU, B. 2004. Molecular chaperones: structure of a protein disaggregase. *Curr Biol,* 14**,** R78-80.

MOGK, A. & BUKAU, B. 2017. Role of sHsps in organizing cytosolic protein aggregation and disaggregation. *Cell Stress Chaperones,* 22**,** 493-502.

MORIMOTO, R. I. 2008. Proteotoxic stress and inducible chaperone networks in neurodegenerative disease and aging. *Genes Dev,* 22**,** 1427-38.

MYMRIKOV, E. V., BUKACH, O. V., SEIT-NEBI, A. S. & GUSEV, N. B. 2010. The pivotal role of the beta 7 strand in the intersubunit contacts of different human small heat shock proteins. *Cell Stress Chaperones,* 15**,** 365-77.

MYMRIKOV, E. V., DAAKE, M., RICHTER, B., HASLBECK, M. & BUCHNER, J. 2017. The Chaperone Activity and Substrate Spectrum of Human Small Heat Shock Proteins. *J Biol Chem,* 292**,** 672-684.

MYMRIKOV, E. V., SEIT-NEBI, A. S. & GUSEV, N. B. 2011. Large potentials of small heat shock proteins. *Physiol Rev,* 91**,** 1123-59.

NAGARAJ, R. H., OYA-ITO, T., PADAYATTI, P. S., KUMAR, R., MEHTA, S., WEST, K., LEVISON, B., SUN, J., CRABB, J. W. & PADIVAL, A. K. 2003. Enhancement of chaperone function of alpha-crystallin by methylglyoxal modification. *Biochemistry,* 42**,** 10746-55.

NARBERHAUS, F. 2002. Alpha-crystallin-type heat shock proteins: socializing minichaperones in the context of a multichaperone network. *Microbiol Mol Biol Rev,* 66**,** 64-93; table of contents.

NEUWALD, A. F., ARAVIND, L., SPOUGE, J. L. & KOONIN, E. V. 1999. AAA+: A class of chaperone-like ATPases associated with the assembly, operation, and disassembly of protein complexes. *Genome Res,* 9**,** 27-43.

NICHOLL, I. D. & QUINLAN, R. A. 1994. Chaperone activity of alpha-crystallins modulates intermediate filament assembly. *EMBO J,* 13**,** 945-53.

NOVER, L., SCHARF, K. D. & NEUMANN, D. 1989. Cytoplasmic heat shock granules are formed from precursor particles and are associated with a specific set of mRNAs. *Mol Cell Biol,* 9**,** 1298-308.

OYA-ITO, T., LIU, B. F. & NAGARAJ, R. H. 2006. Effect of methylglyoxal modification and phosphorylation on the chaperone and anti-apoptotic properties of heat shock protein 27. *J Cell Biochem,* 99**,** 279-91.

PACE, C. N., VAJDOS, F., FEE, L., GRIMSLEY, G. & GRAY, T. 1995. How to measure and predict the molar absorption coefficient of a protein. *Protein Sci,* 4**,** 2411-23.

PANAVAS, T., SANDERS, C. & BUTT, T. R. 2009. SUMO fusion technology for enhanced protein production in prokaryotic and eukaryotic expression systems. *Methods Mol Biol,* 497**,** 303-17.

PATEL, S., VIERLING, E. & TAMA, F. 2014. Replica exchange molecular dynamics simulations provide insight into substrate recognition by small heat shock proteins. *Biophys J,* 106**,** 2644-55.

PATEL, T. R., WINZOR, D. J. & SCOTT, D. J. 2016. Analytical ultracentrifugation: A versatile tool for the characterisation of macromolecular complexes in solution. *Methods,* 95**,** 55-61.

PATRIARCA, E. J. & MARESCA, B. 1990. Acquired thermotolerance following heat shock protein synthesis prevents impairment of mitochondrial ATPase activity at elevated temperatures in Saccharomyces cerevisiae. *Exp Cell Res,* 190**,** 57-64.

PAUL, C., SIMON, S., GIBERT, B., VIROT, S., MANERO, F. & ARRIGO, A. P. 2010. Dynamic processes that reflect anti-apoptotic strategies set up by HspB1 (Hsp27). *Exp Cell Res,* 316**,** 1535-52.

PEARL, L. H. & PRODROMOU, C. 2006. Structure and mechanism of the Hsp90 molecular chaperone machinery. *Annu Rev Biochem,* 75**,** 271-94.

PERNG, M. D., CAIRNS, L., VAN DEN, I. P., PRESCOTT, A., HUTCHESON, A. M. & QUINLAN, R. A. 1999. Intermediate filament interactions can be altered by HSP27 and alphaB-crystallin. *J Cell Sci,* 112 (Pt 13)**,** 2099-112.

PESCHEK, J., BRAUN, N., FRANZMANN, T. M., GEORGALIS, Y., HASLBECK, M., WEINKAUF, S. & BUCHNER, J. 2009. The eye lens chaperone alpha-crystallin forms defined globular assemblies. *Proc Natl Acad Sci U S A,* 106**,** 13272-7.

PESCHEK, J., BRAUN, N., ROHRBERG, J., BACK, K. C., KRIEHUBER, T., KASTENMULLER, A., WEINKAUF, S. & BUCHNER, J. 2013. Regulated structural transitions unleash the chaperone activity of alphaB-crystallin. *Proc Natl Acad Sci U S A,* 110**,** E3780-9.

PHILO, J. S. 2006. Improved methods for fitting sedimentation coefficient distributions derived by time-derivative techniques. *Anal Biochem,* 354**,** 238-46.

PIPER, P. W., MILLSON, S. H., MOLLAPOUR, M., PANARETOU, B., SILIGARDI, G., PEARL, L. H. & PRODROMOU, C. 2003. Sensitivity to Hsp90-targeting drugs can arise with mutation to the Hsp90 chaperone, cochaperones and plasma membrane ATP binding cassette transporters of yeast. *Eur J Biochem,* 270**,** 4689-95.

PORATH, J. & FLODIN, P. 1959. Gel filtration: a method for desalting and group separation. *Nature,* 183**,** 1657-9.

POULAIN, P., GELLY, J. C. & FLATTERS, D. 2010. Detection and architecture of small heat shock protein monomers. *PLoS One,* 5**,** e9990.

POWERS, E. T., MORIMOTO, R. I., DILLIN, A., KELLY, J. W. & BALCH, W. E. 2009. Biological and chemical approaches to diseases of proteostasis deficiency. *Annu Rev Biochem,* 78**,** 959-91.

PRABAKARAN, S., LIPPENS, G., STEEN, H. & GUNAWARDENA, J. 2012. Post-translational modification: nature's escape from genetic imprisonment and the basis for dynamic information encoding. *Wiley Interdiscip Rev Syst Biol Med,* 4**,** 565-83.

PRATT, W. B., MORISHIMA, Y., MURPHY, M. & HARRELL, M. 2006. Chaperoning of glucocorticoid receptors. *Handb Exp Pharmacol***,** 111-38.

QIU, X. B., SHAO, Y. M., MIAO, S. & WANG, L. 2006. The diversity of the DnaJ/Hsp40 family, the crucial partners for Hsp70 chaperones. *Cell Mol Life Sci,* 63**,** 2560-70.

QUINLAN, R. A. 2015. DRUG DISCOVERY. A new dawn for cataracts. *Science,* 350**,** 636-7.

RENKAWEK, K., BOSMAN, G. J. & DE JONG, W. W. 1994. Expression of small heat-shock protein hsp 27 in reactive gliosis in Alzheimer disease and other types of dementia. *Acta Neuropathol,* 87**,** 511-9.

RETZLAFF, M., HAGN, F., MITSCHKE, L., HESSLING, M., GUGEL, F., KESSLER, H., RICHTER, K. & BUCHNER, J. 2010. Asymmetric activation of the hsp90 dimer by its cochaperone aha1. *Mol Cell,* 37**,** 344-54.

RICHTER, K., HASLBECK, M. & BUCHNER, J. 2010. The heat shock response: life on the verge of death. *Mol Cell,* 40**,** 253-66.

RITOSSA, F. 1996. Discovery of the heat shock response. *Cell, Stress & Chaperones,* 1**,** 97-98.

ROBERTSON, A. L., HEADEY, S. J., SAUNDERS, H. M., ECROYD, H., SCANLON, M. J., CARVER, J. A. & BOTTOMLEY, S. P. 2010. Small heat-shock proteins interact with a flanking domain to suppress polyglutamine aggregation. *Proc Natl Acad Sci U S A,* 107**,** 10424-9.

ROGALLA, T., EHRNSPERGER, M., PREVILLE, X., KOTLYAROV, A., LUTSCH, G., DUCASSE, C., PAUL, C., WIESKE, M., ARRIGO, A. P., BUCHNER, J. & GAESTEL, M. 1999. Regulation of

Hsp27 oligomerization, chaperone function, and protective activity against oxidative stress/tumor necrosis factor alpha by phosphorylation. *J Biol Chem,* 274**,** 18947-56.

ROHL, A., WENGLER, D., MADL, T., LAGLEDER, S., TIPPEL, F., HERRMANN, M., HENDRIX, J., RICHTER, K., HACK, G., SCHMID, A. B., KESSLER, H., LAMB, D. C. & BUCHNER, J. 2015. Hsp90 regulates the dynamics of its cochaperone Sti1 and the transfer of Hsp70 between modules. *Nat Commun,* 6**,** 6655.

RUSSNAK, R. H. & CANDIDO, E. P. 1985. Locus encoding a family of small heat shock genes in Caenorhabditis elegans: two genes duplicated to form a 3.8-kilobase inverted repeat. *Mol Cell Biol,* 5**,** 1268-78.

RUSSNAK, R. H., JONES, D. & CANDIDO, E. P. 1983. Cloning and analysis of cDNA sequences coding for two 16 kilodalton heat shock proteins (hsps) in Caenorhabditis elegans: homology with the small hsps of Drosophila. *Nucleic Acids Res,* 11**,** 3187-205.

SAIBIL, H. 2013. Chaperone machines for protein folding, unfolding and disaggregation. *Nat Rev Mol Cell Biol,* 14**,** 630-42.

SCHMIDT, T., FISCHER, D., ANDREADAKI, A., BARTELT-KIRBACH, B. & GOLENHOFEN, N. 2016. Induction and phosphorylation of the small heat shock proteins HspB1/Hsp25 and HspB5/alphaB-crystallin in the rat retina upon optic nerve injury. *Cell Stress Chaperones,* 21**,** 167-78.

SCHNEIDER, C. A., RASBAND, W. S. & ELICEIRI, K. W. 2012. NIH Image to ImageJ: 25 years of image analysis. *Nat Methods,* 9**,** 671-5.

SCHOPF, F. H., BIEBL, M. M. & BUCHNER, J. 2017. The HSP90 chaperone machinery. *Nat Rev Mol Cell Biol,* 18**,** 345-360.

SCHREIBER, T. B., MAUSBACHER, N., SOROKA, J., WANDINGER, S. K., BUCHNER, J. & DAUB, H. 2012. Global analysis of phosphoproteome regulation by the Ser/Thr phosphatase Ppt1 in Saccharomyces cerevisiae. *J Proteome Res,* 11**,** 2397-408.

SCHUCK, P. 2000. Size-distribution analysis of macromolecules by sedimentation velocity ultracentrifugation and lamm equation modeling. *Biophys J,* 78**,** 1606-19.

SCHUMANN, W. 2006. Dynamics of the Bacterial Chromosome:Structure and Function. WILEY-VCH Verlag GmBh & Co. KGaA.

SEAL, R. L., GORDON, S. M., LUSH, M. J., WRIGHT, M. W. & BRUFORD, E. A. 2011. genenames.org: the HGNC resources in 2011. *Nucleic Acids Res,* 39**,** D514-9.

SHASHIDHARAMURTHY, R., KOTEICHE, H. A., DONG, J. & MCHAOURAB, H. S. 2005. Mechanism of chaperone function in small heat shock proteins: dissociation of the HSP27 oligomer is required for recognition and binding of destabilized T4 lysozyme. *J Biol Chem,* 280**,** 5281-9.

SHIM, J., IM, S. H. & LEE, J. 2003. Tissue-specific expression, heat inducibility, and biological roles of two hsp16 genes in Caenorhabditis elegans. *FEBS Lett,* 537**,** 139-45.

SHIN, H., LEE, H., FEJES, A. P., BAILLIE, D. L., KOO, H. S. & JONES, S. J. 2011. Gene expression profiling of oxidative stress response of C. elegans aging defective AMPK mutants using massively parallel transcriptome sequencing. *BMC Res Notes,* 4**,** 34.

SHINOHARA, H., INAGUMA, Y., GOTO, S., INAGAKI, T. & KATO, K. 1993. Alpha B crystallin and HSP28 are enhanced in the cerebral cortex of patients with Alzheimer's disease. *J Neurol Sci,* 119**,** 203-8.

SMOLKA, M. B., ALBUQUERQUE, C. P., CHEN, S. H. & ZHOU, H. 2007. Proteome-wide identification of in vivo targets of DNA damage checkpoint kinases. *Proc Natl Acad Sci U S A,* 104**,** 10364-9.

SONG, S., HANSON, M. J., LIU, B. F., CHYLACK, L. T. & LIANG, J. J. 2008. Protein-protein interactions between lens vimentin and alphaB-crystallin using FRET acceptor photobleaching. *Mol Vis,* 14**,** 1282-7.

SOROKA, J., WANDINGER, S. K., MAUSBACHER, N., SCHREIBER, T., RICHTER, K., DAUB, H. & BUCHNER, J. 2012. Conformational switching of the molecular chaperone Hsp90 via regulated phosphorylation. *Mol Cell,* 45**,** 517-28.

SPECHT, S., MILLER, S. B., MOGK, A. & BUKAU, B. 2011. Hsp42 is required for sequestration of protein aggregates into deposition sites in Saccharomyces cerevisiae. *J Cell Biol,* 195**,** 617-29.

STAFFORD, W. F., 3RD 1992. Boundary analysis in sedimentation transport experiments: a procedure for obtaining sedimentation coefficient distributions using the time derivative of the concentration profile. *Anal Biochem,* 203**,** 295-301.

STENGEL, F., BALDWIN, A. J., PAINTER, A. J., JAYA, N., BASHA, E., KAY, L. E., VIERLING, E., ROBINSON, C. V. & BENESCH, J. L. 2010. Quaternary dynamics and plasticity underlie small heat shock protein chaperone function. *Proc Natl Acad Sci U S A,* 107**,** 2007-12.

STIERNAGLE, T. 2006. Maintenance of C. elegans. *WormBook***,** 1-11.

STRINGHAM, E. G. & CANDIDO, P. M. 1994. Transgenic hsp16-lacZ strains of Caenorhabditis elegans as biological monitors of environmental stress. *Environmental Toxicology and Chemistry,* 13**,** 1211-1220.

STRINGHAM, E. G., DIXON, D. K., JONES, D. & CANDIDO, E. P. 1992. Temporal and spatial expression patterns of the small heat shock (hsp16) genes in transgenic Caenorhabditis elegans. *Mol Biol Cell,* 3**,** 221-33.

STROMER, T., EHRNSPERGER, M., GAESTEL, M. & BUCHNER, J. 2003. Analysis of the interaction of small heat shock proteins with unfolding proteins. *J Biol Chem,* 278**,** 18015-21.

STROMER, T., FISCHER, E., RICHTER, K., HASLBECK, M. & BUCHNER, J. 2004. Analysis of the regulation of the molecular chaperone Hsp26 by temperature-induced dissociation: the N-terminal domail is important for oligomer assembly and the binding of unfolding proteins. *J Biol Chem,* 279**,** 11222-8.

SUGIYAMA, Y., SUZUKI, A., KISHIKAWA, M., AKUTSU, R., HIROSE, T., WAYE, M. M., TSUI, S. K., YOSHIDA, S. & OHNO, S. 2000. Muscle develops a specific form of small heat shock protein complex composed of MKBP/HSPB2 and HSPB3 during myogenic differentiation. *J Biol Chem,* 275**,** 1095-104.

SUN, Y. & MACRAE, T. H. 2005. The small heat shock proteins and their role in human disease. *FEBS J,* 272**,** 2613-27.

SWAMY, M. S. & ABRAHAM, E. C. 1991. Reverse-phase HPLC analysis of human alpha crystallin. *Curr Eye Res,* 10**,** 213-20.

SZALAY, M. S., KOVACS, I. A., KORCSMAROS, T., BODE, C. & CSERMELY, P. 2007. Stress-induced rearrangements of cellular networks: Consequences for protection and drug design. *FEBS Lett,* 581**,** 3675-80.

TABUSE, Y., NABETANI, T. & TSUGITA, A. 2005. Proteomic analysis of protein expression profiles during Caenorhabditis elegans development using two-dimensional difference gel electrophoresis. *Proteomics,* 5**,** 2876-91.

TAYLOR, R. P. & BENJAMIN, I. J. 2005. Small heat shock proteins: a new classification scheme in mammals. *J Mol Cell Cardiol,* 38**,** 433-44.

TESSIER, D. J., KOMALAVILAS, P., PANITCH, A., JOSHI, L. & BROPHY, C. M. 2003. The small heat shock protein (HSP) 20 is dynamically associated with the actin cross-linking protein actinin. *J Surg Res,* 111**,** 152-7.

THERIAULT, J. R., LAMBERT, H., CHAVEZ-ZOBEL, A. T., CHAREST, G., LAVIGNE, P. & LANDRY, J. 2004. Essential role of the NH2-terminal WD/EPF motif in the phosphorylation-activated protective function of mammalian Hsp27. *J Biol Chem,* 279**,** 23463-71.

TILLY, K., MCKITTRICK, N., ZYLICZ, M. & GEORGOPOULOS, C. 1983. The dnaK protein modulates the heat-shock response of Escherichia coli. *Cell,* 34**,** 641-6.

TISSIERES, A., MITCHELL, H. K. & TRACY, U. M. 1974. Protein synthesis in salivary glands of Drosophila melanogaster: relation to chromosome puffs. *J Mol Biol,* 84**,** 389-98.

TODD, M. J., VIITANEN, P. V. & LORIMER, G. H. 1994. Dynamics of the chaperonin ATPase cycle: implications for facilitated protein folding. *Science,* 265**,** 659-66.

TOIVOLA, D. M., STRNAD, P., HABTEZION, A. & OMARY, M. B. 2010. Intermediate filaments take the heat as stress proteins. *Trends Cell Biol,* 20**,** 79-91.

TUSHER, V. G., TIBSHIRANI, R. & CHU, G. 2001. Significance analysis of microarrays applied to the ionizing radiation response. *Proc Natl Acad Sci U S A,* 98**,** 5116-21.

UDGAONKAR, J. B. 2008. Multiple routes and structural heterogeneity in protein folding. *Annu Rev Biophys,* 37**,** 489-510.

UNGELENK, S., MOAYED, F., HO, C. T., GROUSL, T., SCHARF, A., MASHAGHI, A., TANS, S., MAYER, M. P., MOGK, A. & BUKAU, B. 2016. Small heat shock proteins sequester misfolding proteins in near-native conformation for cellular protection and efficient refolding. *Nat Commun,* 7**,** 13673.

VAN MONTFORT, R. L., BASHA, E., FRIEDRICH, K. L., SLINGSBY, C. & VIERLING, E. 2001. Crystal structure and assembly of a eukaryotic small heat shock protein. *Nat Struct Biol,* 8**,** 1025-30.

VASILESCU, J., GUO, X. & KAST, J. 2004. Identification of protein-protein interactions using in vivo cross-linking and mass spectrometry. *Proteomics,* 4**,** 3845-54.

VEINGER, L., DIAMANT, S., BUCHNER, J. & GOLOUBINOFF, P. 1998. The small heat-shock protein IbpB from Escherichia coli stabilizes stress-denatured proteins for subsequent refolding by a multichaperone network. *J Biol Chem,* 273**,** 11032-7.

VIGH, L., NAKAMOTO, H., LANDRY, J., GOMEZ-MUNOZ, A., HARWOOD, J. L. & HORVATH, I. 2007. Membrane regulation of the stress response from prokaryotic models to mammalian cells. *Ann N Y Acad Sci,* 1113**,** 40-51.

VOGEL, J. L., PARSELL, D. A. & LINDQUIST, S. 1995. Heat-shock proteins Hsp104 and Hsp70 reactivate mRNA splicing after heat inactivation. *Curr Biol,* 5**,** 306-17.

VOIT, E. O. & RADIVOYEVITCH, T. 2000. Biochemical systems analysis of genome-wide expression data. *Bioinformatics,* 16**,** 1023-37.

WADSWORTH, W. G. & RIDDLE, D. L. 1988. Acidic intracellular pH shift during Caenorhabditis elegans larval development. *Proc Natl Acad Sci U S A,* 85**,** 8435-8.

WALLACE, E. W., KEAR-SCOTT, J. L., PILIPENKO, E. V., SCHWARTZ, M. H., LASKOWSKI, P. R., ROJEK, A. E., KATANSKI, C. D., RIBACK, J. A., DION, M. F., FRANKS, A. M., AIROLDI, E. M., PAN, T., BUDNIK, B. A. & DRUMMOND, D. A. 2015. Reversible, Specific, Active Aggregates of Endogenous Proteins Assemble upon Heat Stress. *Cell,* 162**,** 1286-98.

WALTER, S. & BUCHNER, J. 2002. Molecular chaperones--cellular machines for protein folding. *Angew Chem Int Ed Engl,* 41**,** 1098-113.

WANG, M., WEISS, M., SIMONOVIC, M., HAERTINGER, G., SCHRIMPF, S. P., HENGARTNER, M. O. & VON MERING, C. 2012. PaxDb, a database of protein abundance averages across all three domains of life. *Mol Cell Proteomics,* 11**,** 492-500.

WATERS, E. R. 1995. The molecular evolution of the small heat-shock proteins in plants. *Genetics,* 141**,** 785-95.

WEINFURTNER, D. 2008. *Strukturelle und funktionelle Charakterisierung einer Familie kleiner Hitzeschockproteine.* Doctoral Thesis, Technische Universität München.

WELCH, W. J. & SUHAN, J. P. 1985. Morphological study of the mammalian stress response: characterization of changes in cytoplasmic organelles, cytoskeleton, and nucleoli, and appearance of intranuclear actin filaments in rat fibroblasts after heat-shock treatment. *J Cell Biol,* 101**,** 1198-211.

WELCH, W. J. & SUHAN, J. P. 1986. Cellular and biochemical events in mammalian cells during and after recovery from physiological stress. *J Cell Biol,* 103**,** 2035-52.

WELKER, S., RUDOLPH, B., FRENZEL, E., HAGN, F., LIEBISCH, G., SCHMITZ, G., SCHEURING, J., KERTH, A., BLUME, A., WEINKAUF, S., HASLBECK, M., KESSLER, H. & BUCHNER, J. 2010. Hsp12 is an intrinsically unstructured stress protein that folds upon membrane association and modulates membrane function. *Mol Cell,* 39**,** 507-20.

WHITE, H. E., ORLOVA, E. V., CHEN, S., WANG, L., IGNATIOU, A., GOWEN, B., STROMER, T., FRANZMANN, T. M., HASLBECK, M., BUCHNER, J. & SAIBIL, H. R. 2006. Multiple distinct assemblies reveal conformational flexibility in the small heat shock protein Hsp26. *Structure,* 14**,** 1197-204.

WHITMORE, L. & WALLACE, B. A. 2004. DICHROWEB, an online server for protein secondary structure analyses from circular dichroism spectroscopic data. *Nucleic Acids Res,* 32**,** W668-73.

WIEGANT, F. A., DE POOT, S. A., BOERS-TRILLES, V. E. & SCHREIJ, A. M. 2012. Hormesis and Cellular Quality Control: A Possible Explanation for the Molecular Mechanisms that Underlie the Benefits of Mild Stress. *Dose Response,* 11**,** 413-30.

WILKINS, M. R., GASTEIGER, E., BAIROCH, A., SANCHEZ, J. C., WILLIAMS, K. L., APPEL, R. D. & HOCHSTRASSER, D. F. 1999. Protein identification and analysis tools in the ExPASy server. *Methods Mol Biol,* 112**,** 531-52.

YANG, B., WU, Y. J., ZHU, M., FAN, S. B., LIN, J., ZHANG, K., LI, S., CHI, H., LI, Y. X., CHEN, H. F., LUO, S. K., DING, Y. H., WANG, L. H., HAO, Z., XIU, L. Y., CHEN, S., YE, K., HE, S. M. & DONG, M. Q. 2012. Identification of cross-linked peptides from complex samples. *Nat Methods,* 9**,** 904-6.

YANG, M., SUN, J., SUN, X., SHEN, Q., GAO, Z. & YANG, C. 2009. Caenorhabditis elegans protein arginine methyltransferase PRMT-5 negatively regulates DNA damage-induced apoptosis. *PLoS Genet,* 5**,** e1000514.

YOST, H. J. & LINDQUIST, S. 1986. RNA splicing is interrupted by heat shock and is rescued by heat shock protein synthesis. *Cell,* 45**,** 185-93.

ZEVIAN, S. C. & YANOWITZ, J. L. 2014. Methodological considerations for heat shock of the nematode Caenorhabditis elegans. *Methods,* 68**,** 450-7.

ZHU, X., ZHAO, X., BURKHOLDER, W. F., GRAGEROV, A., OGATA, C. M., GOTTESMAN, M. E. & HENDRICKSON, W. A. 1996. Structural analysis of substrate binding by the molecular chaperone DnaK. *Science,* 272**,** 1606-14.

ZOU, J., GUO, Y., GUETTOUCHE, T., SMITH, D. F. & VOELLMY, R. 1998. Repression of heat shock transcription factor HSF1 activation by HSP90 (HSP90 complex) that forms a stress-sensitive complex with HSF1. *Cell,* 94**,** 471-80.

Appendix

Abbreviations

ACN	acetonitril
ADP	Adenosin diphosphate
ATP	Adenosin triphosphate
AUC	analytical ultracentrifugation
bp	base pairs
CD	circular dichroism
CoIP	co-immunoprecipitation
CS	citrate synthase
CTD	carboxy terminal domain
Da	Dalton
DNA	Deoxiribonucleic acid
EM	electron microscopy
EM	electron microscopy
ER	endoplasmic reticulum
FDR	false discovery rate
HPLC	high performance iquid chromatography
Hsp	heat shock protein
HSQC	heteronuclear single quantum coherence spectroscopy
IP	immunoprecipitation
IPTG	isopropyl-β-D-thiogalactopyranoside
LB	lysogeny broth
LC	liquid chromatography
LFQ	label free quantification
MDH	malat dehydrogenase
MS	mass spectrometry
n.d.	not determined
NGM	nematode growth medium
NMR	nuclear magnetic resonance
NOE	nuclear Overhauser effect

NTD	amino terminal domain
PBS	phosphate buffered saline
PCR	polymerase chain reaction
PI	preincubation
RNA	Ribonucleic acid
rt	room temperature
SAXS	small-angle X-ray scattering
SDS-PAGE	sodium dodecylsulfate-polyacrylamide gel electrophoresis
SEC	size exclusion chromatography
sHsp	small heat shock protein
SU	subunit
UV	ultra violet
wt	wildtype
X-link	crosslink
θ MRW	mean residue ellipticity

Table of amino acids

Amino acid	3-Letter Code	1-Letter Code
Alanine	Ala	A
Arginine	Arg	R
Asparagine	Asn	N
Aspartate	Asp	D
Cysteine	Cys	C
Glutamate	Glu	E
Glutamine	Gln	Q
Histidine	His	H
Isoleucine	Ile	I
Leucine	Leu	L
Lysine	Lys	K
Methionine	Met	M
Phenylalanine	Phe	F
Proline	Pro	P
Serine	Ser	S
Threonine	Thr	T
Tryptophan	Trp	W
Tyrosine	Tyr	Y
Valine	Val	V

Identified interactors of human sHsps

UniProtID	HspB1	HspB2	HspB3	HspB4	HspB5	HspB6	HspB7	MW [kDa]	calc. pI	GRAVY index	STRING ID	abundance
P50990	x	x	x	x	x	x	x	59.6	5.60	-0.07	9606.ENSP00000286788	1314
O43175	x	x	x	x	x	x		56.6	6.71	0.09	9606.ENSP00000358417	387
P49368	x	x	x	x	x		x	60.5	6.49	-0.25	9606.ENSP00000295688	1747
P11586	x	x	x	x	x			101.5	7.30	-0.09	9606.ENSP00000450560	568
P12956	x	x	x	x	x			69.8	6.64	-0.54	9606.ENSP00000352257	20.3
P13010	x	x	x	x	x			82.7	5.81	-0.34	9606.ENSP00000375977	438
P31939	x	x	x	x	x			64.6	6.71	-0.11	9606.ENSP00000236959	177
P49591	x	x	x	x	x			58.7	6.43	-0.50	9606.ENSP00000234677	70.6
P54577	x	x	x	x	x			59.1	7.05	-0.36	9606.ENSP00000362576	474
P68371	x	x	x	x	x			49.8	4.89	-0.36	9606.ENSP00000341289	1765
Q13263	x	x	x	x	x			88.5	5.77	-0.39	9606.ENSP00000253024	1626
Q9UQ80	x	x	x	x	x			43.8	6.55	-0.50	9606.ENSP00000302886	948
P34932	x	x	x		x			94.3	5.19	-0.58	9606.ENSP00000302961	748
P49588	x	x	x		x			106.7	5.53	-0.30	9606.ENSP00000261772	395
P61978	x	x	x					50.9	5.54	-0.70	9606.ENSP00000365439	2167
P62826	x	x	x					24.4	7.49	-0.27	9606.ENSP00000376176	3886
P22102	x		x	x	x			107.7	6.70	0.04	9606.ENSP00000371236	43.8
P26639	x		x	x	x			83.4	6.67	-0.58	9606.ENSP00000265112	397
P26640	x		x	x	x			140.4	7.59	-0.27	9606.ENSP00000364815	43.7
P52292	x		x	x	x			57.8	5.40	-0.14	9606.ENSP00000332455	160
P55884	x		x	x	x			92.4	5.00	-0.63	9606.ENSP00000354125	603
Q15459	x		x	x	x			88.8	5.22	-0.74	9606.ENSP00000215793	587
Q7KZF4	x		x	x	x			101.9	7.17	-0.43	9606.ENSP00000346762	527
Q99613	x		x	x	x			105.3	5.68	-0.79	9606.ENSP00000332604	93.7
O15355	x		x		x			59.2	4.36	-0.81	9606.ENSP00000264714	13.9
O43242	x		x		x			60.9	8.44	-0.53	9606.ENSP00000264639	165
P08133	x		x		x			75.8	5.60	-0.45	9606.ENSP00000346550	362
P27695	x		x		x			35.5	8.12	-0.58	9606.ENSP00000216714	1090
P27708	x		x		x			242.8	6.46	-0.08	9606.ENSP00000264705	144
P31153	x		x		x			43.6	6.48	-0.28	9606.ENSP00000303147	139
P33991	x		x		x			96.5	6.74	-0.41	9606.ENSP00000262105	127
P33993	x		x		x			81.3	6.46	-0.37	9606.ENSP00000307288	204
P37837	x		x		x			37.5	6.81	-0.25	9606.ENSP00000321259	44
P49736	x		x		x			101.8	5.52	-0.50	9606.ENSP00000265056	576
P49915	x		x		x			76.7	6.87	-0.16	9606.ENSP00000419851	43.5
P54136	x		x		x			75.3	6.68	-0.28	9606.ENSP00000231572	95.5
P68363	x		x		x			50.1	5.06	-0.23	9606.ENSP00000336799	n.d.
Q04637	x		x		x			175.4	5.33	-0.65	9606.ENSP00000338020	375
Q09028	x		x		x			47.6	4.89	-0.56	9606.ENSP00000362592	655
Q15393	x		x		x			135.5	5.26	-0.17	9606.ENSP00000305790	152
Q92598	x		x		x			96.8	5.39	-0.57	9606.ENSP00000318687	698
Q99460	x		x		x			105.8	5.39	-0.23	9606.ENSP00000309474	203
Q9P2J5	x		x		x			134.4	7.30	-0.40	9606.ENSP00000377954	164
P06733	x		x					47.1	7.39	-0.22	9606.ENSP00000234590	726
Q00839	x		x					90.5	6.00	-0.98	9606.ENSP00000283179	765
Q14152	x		x					166.5	6.79	-1.49	9606.ENSP00000358140	233
Q15046	x		x					68.0	6.35	-0.45	9606.ENSP00000325448	379
O15067	x			x	x			144.6	5.76	-0.20	9606.ENSP00000313490	38.8
Q00610	x			x	x			191.5	5.69	-0.24	9606.ENSP00000269122	697
Q9Y265	x			x	x			50.2	6.42	-0.25	9606.ENSP00000318297	595
O00303	x				x			37.5	5.45	0.04	9606.ENSP00000310040	498
P00491	x				x			32.1	6.95	-0.17	9606.ENSP00000354532	161
P06493	x				x			34.1	8.40	-0.28	9606.ENSP00000378699	25.5
P08243	x				x			64.3	6.86	-0.26	9606.ENSP00000175506	200
P10809	x				x			61.0	5.87	-0.08	9606.ENSP00000340019	4295
P12081	x				x			57.4	5.88	-0.25	9606.ENSP00000425634	62.7
P17980	x				x			49.2	5.24	-0.40	9606.ENSP00000298852	38.5
P19623	x				x			33.8	5.49	-0.20	9606.ENSP00000366156	149
P25205	x				x			90.9	5.77	-0.56	9606.ENSP00000229854	171
P27797	x				x			48.1	4.44	-1.10	9606.ENSP00000320866	2337
P35520	x				x			60.5	6.65	-0.28	9606.ENSP00000344460	279
P35998	x				x			48.6	5.95	-0.42	9606.ENSP00000292644	557
P38919	x				x			46.8	6.73	-0.26	9606.ENSP00000269349	722
P41250	x				x			83.1	7.03	-0.30	9606.ENSP00000373918	193
P43686	x				x			47.3	5.21	-0.35	9606.ENSP00000157812	615
P56192	x				x			101.1	6.16	-0.24	9606.ENSP00000262027	122
P60228	x				x			52.2	6.04	-0.33	9606.ENSP00000220849	26.4
P61163	x				x			42.6	6.64	-0.28	9606.ENSP00000358921	282
P62191	x				x			49.2	6.21	-0.54	9606.ENSP00000261303	276
P62195	x				x			45.6	7.55	-0.32	9606.ENSP00000310572	478

P62333	x				x			44.1	7.49	-0.44	9606.ENSP00000401802	542
Q12874	x				x			58.8	5.38	-0.92	9606.ENSP00000362110	360
Q14166	x				x			74.4	5.53	-0.39	9606.ENSP00000216129	85.8
Q14566	x				x			92.8	5.41	-0.38	9606.ENSP00000264156	245
Q15785	x				x			34.5	8.98	-0.61	9606.ENSP00000361900	n.d.
Q99873	x				x			41.5	5.43	-0.22	9606.ENSP00000406162	1442
Q9NUU7	x				x			53.9	6.58	-0.38	9606.ENSP00000306117	14.5
Q9Y230	x				x			51.1	5.64	-0.23	9606.ENSP00000473172	135
Q9Y262	x				x			66.7	6.34	-0.47	9606.ENSP00000416892	166
Q9Y3F4	x				x			38.4	5.12	-0.32	9606.ENSP00000392270	96.5
Q9Y4L1	x				x			111.3	5.22	-0.55	9606.ENSP00000384144	24.8
O14744	x							72.6	6.29	-0.33	9606.ENSP00000319169	519
O14929	x							49.5	5.69	-0.45	9606.ENSP00000264108	n.d.
O60749	x							58.4	5.12	-0.53	9606.ENSP00000368831	55.5
O75794	x							39.1	4.81	-0.53	9606.ENSP00000281141	18.7
P05387	x							11.7	4.54	-0.24	9606.ENSP00000322419	7297
P05388	x							34.3	5.97	0.04	9606.ENSP00000339027	49.3
P11413	x							59.2	6.84	-0.37	9606.ENSP00000377192	103
P18754	x							44.9	7.52	-0.26		n.d.
P23526	x							47.7	6.34	-0.10	9606.ENSP00000217426	987
P23921	x							90.0	7.15	-0.36	9606.ENSP00000300738	66
P34949	x							46.6	5.95	-0.04	9606.ENSP00000318318	n.d.
P49189	x							53.8	5.87	-0.04	9606.ENSP00000346827	7.22
P49411	x							49.5	7.61	-0.12	9606.ENSP00000322439	1277
P51570	x							42.2	6.46	-0.08	9606.ENSP00000225614	n.d.
P55786	x							103.2	5.72	-0.19	9606.ENSP00000320324	117
P62269	x							17.7	10.99	-0.71	9606.ENSP00000393241	802
P62805	x							11.4	11.36	-0.52	9606.ENSP00000367034	2043
Q01581	x							57.3	5.41	-0.28	9606.ENSP00000322706	51.9
Q12904	x							34.3	8.43	-0.52	9606.ENSP00000378191	137
Q13347	x							36.5	5.64	-0.42	9606.ENSP00000362688	741
Q13564	x							60.2	5.40	-0.33	9606.ENSP00000290810	87.8
Q14203	x							141.6	5.81	-0.56	9606.ENSP00000354791	31.9
Q14204	x							532.1	6.40	-0.34	9606.ENSP00000348965	95.5
Q14697	x							106.8	6.14	-0.36	9606.ENSP00000340466	316
Q16576	x							47.8	5.05	-0.53	9606.ENSP00000369424	755
Q9NSD9	x							66.1	6.84	-0.12	9606.ENSP00000281828	71.7
Q9UBT2	x							71.2	5.29	-0.44	9606.ENSP00000246548	540
Q9Y3I0	x							55.2	7.23	-0.23	9606.ENSP00000216038	507
P09211		x	x					23.3	5.64	-0.12	9606.ENSP00000381607	460
P37802		x						22.4	8.25	-0.61	9606.ENSP00000357075	240
Q02790		x						51.8	5.43	-0.64	9606.ENSP00000001008	1279
P17812			x		x			66.6	6.46	-0.31	9606.ENSP00000361699	635
P41252			x		x			144.4	6.15	-0.24	9606.ENSP00000364794	95.9
P00374			x					21.4	7.42	-0.46	9606.ENSP00000396308	n.d.
P07741			x					19.6	6.02	0.10	9606.ENSP00000367615	716
P33176			x					109.6	6.51	-0.81	9606.ENSP00000307078	193
P46459			x					82.5	6.95	-0.22	9606.ENSP00000381293	118
P25685				x				38.0	8.63	-0.72	9606.ENSP00000254322	1.42
O00148					x			49.1	5.68	-0.30	9606.ENSP00000242776	301
O00231					x			47.4	6.48	-0.18	9606.ENSP00000261712	48.7
P14314					x			59.4	4.41	-0.91	9606.ENSP00000252455	441
P30101					x			56.7	6.35	-0.51	9606.ENSP00000300289	612
P30520					x			50.1	6.55	-0.18	9606.ENSP00000355493	57
P47897					x			87.7	7.15	-0.31	9606.ENSP00000307567	222
P63244					x			35.1	7.69	-0.25	9606.ENSP00000426909	1644
Q01813					x			85.5	7.55	-0.15	9606.ENSP00000370517	226
Q9H4A4					x			72.5	5.74	-0.21	9606.ENSP00000295640	154
Q9UBE0					x			38.4	5.30	-0.30	9606.ENSP00000270225	469
Q9UNE7					x			34.8	5.87	-0.81	9606.ENSP00000219548	46.4

HEK293 HS Fraction

Swissprot ID	Protein name	MW [kDa]	calc. pI	GRAVY index	STRING ID	Abundance
A0AVT1	Ubiquitin-like modifier-activating enzyme 6	117.9	6.14	-0.23	9606.ENSP00000313454	28.1
A5YKK6	CCR4-NOT transcription complex subunit 1	266.8	7.11	-0.16	9606.ENSP00000320949	18.1
A6NDG6	Phosphoglycolate phosphatase	34	6.14	0.02	9606.ENSP00000330918	55.9
A6NIH7	Protein unc-119 homolog B	28.1	5.68	-0.46	9606.ENSP00000344942	n.a.
O00148	ATP-dependent RNA helicase DDX39A	49.1	5.68	-0.30	9606.ENSP00000242776	301
O00154	Cytosolic acyl coenzyme A thioester hydrolase	41.8	8.54	-0.30	9606.ENSP00000367086	286
O00170	AH receptor-interacting protein	37.6	6.29	-0.49	9606.ENSP00000279146	21.4
O00178	GTP-binding protein 1	72.4	8.34	-0.31	9606.ENSP00000216044	2.4
O00203	AP-3 complex subunit beta-1	121.2	6.04	-0.38	9606.ENSP00000255194	124
O00231	26S proteasome non-ATPase regulatory subunit 11	47.4	6.48	-0.18	9606.ENSP00000261712	48.7
O00232	26S proteasome non-ATPase regulatory subunit 12	52.9	7.65	-0.38	9606.ENSP00000348442	262
O00264	Membrane-associated progesterone receptor component 1	21.7	4.7	-0.56	9606.ENSP00000217971	1663
O00267	Transcription elongation factor SPT5	120.9	5.06	-0.74	9606.ENSP00000404029	42.7
O00299	Chloride intracellular channel protein 1	26.9	5.17	-0.28	9606.ENSP00000364934	332
O00303	Eukaryotic translation initiation factor 3 subunit F	37.5	5.45	0.04	9606.ENSP00000310040	498
O00410	Importin-5	123.5	4.94	-0.13	9606.ENSP00000261574	280
O00429	Dynamin-1-like protein	81.8	6.81	-0.26	9606.ENSP00000450399	19.6
O00487	26S proteasome non-ATPase regulatory subunit 14	34.6	6.52	-0.17	9606.ENSP00000386541	1210
O00571	ATP-dependent RNA helicase DDX3X	73.2	7.18	-0.63	9606.ENSP00000382840	254
O00762	Ubiquitin-conjugating enzyme E2 C	19.6	7.37	-0.39	9606.ENSP00000348838	n.a.
O00764	Pyridoxal kinase	35.1	6.13	-0.21	9606.ENSP00000291565	10.4
O14497	AT-rich interactive domain-containing protein 1A	241.9	6.7	-0.78	9606.ENSP00000320485	14.2
O14654	Insulin receptor substrate 4	133.7	8.44	-0.66	9606.ENSP00000361202	8.6
O14744	Protein arginine N-methyltransferase 5	72.6	6.29	-0.33	9606.ENSP00000319169	519
O14776	Transcription elongation regulator 1	123.8	8.65	-0.87	9606.ENSP00000296702	148
O14802	DNA-directed RNA polymerase III subunit RPC1	155.5	8.48	-0.25	9606.ENSP00000361446	0.107
O14818	Proteasome subunit alpha type-7	27.9	8.46	-0.43	9606.ENSP00000359910	1094
O14908	PDZ domain-containing protein GIPC1	36	6.28	-0.33	9606.ENSP00000340698	1.3
O14929	Histone acetyltransferase type B catalytic subunit	49.5	5.69	-0.45	9606.ENSP00000264108	n.a.
O14976	Cyclin-G-associated kinase	143.1	5.73	-0.42	9606.ENSP00000314499	n.a.
O14980	Exportin-1	123.3	6.06	-0.09	9606.ENSP00000384863	122
O14981	TATA-binding protein-associated factor 172	206.8	6.52	-0.17	9606.ENSP00000265990	2.14
O15027	Protein transport protein Sec16A	233.4	5.63	-0.61	9606.ENSP00000325827	3.19
O15042	U2 snRNP-associated SURP motif-containing protein	118.2	8.47	-1.14	9606.ENSP00000322376	1.72
O15067	Phosphoribosylformylglycinamidine synthase	144.6	5.76	-0.20	9606.ENSP00000313490	38.8
O15111	Inhibitor of nuclear factor kappa-B kinase subunit alpha	84.6	6.73	-0.30	9606.ENSP00000359424	5.43
O15143	Actin-related protein 2/3 complex subunit 1B	40.9	8.35	-0.20	9606.ENSP00000252725	35.7
O15144	Actin-related protein 2/3 complex subunit 2	34.3	7.36	-0.44	9606.ENSP00000295685	278
O15145	Actin-related protein 2/3 complex subunit 3	20.5	8.59	-0.61	9606.ENSP00000228825	n.a.
O15160	DNA-directed RNA polymerases I and III subunit RPAC1	39.2	5.5	-0.28	9606.ENSP00000361465	51
O15212	Prefoldin subunit 6	14.6	8.88	-0.72	9606.ENSP00000363734	n.a.
O15294	UDP-N-acetylglucosamine--peptide N-acetylglucosaminyltransferase 110 kDa subunit	116.8	6.7	-0.24	9606.ENSP00000362824	23
O15305	Phosphomannomutase 2	28.1	6.77	-0.43	9606.ENSP00000268261	6.18
O15355	Protein phosphatase 1G	59.2	4.36	-0.81	9606.ENSP00000264714	13.9
O15371	Eukaryotic translation initiation factor 3 subunit D	63.9	6.05	-0.84	9606.ENSP00000216190	1515
O15372	Eukaryotic translation initiation factor 3 subunit H	39.9	6.54	-0.55	9606.ENSP00000429931	97.6
O15397	Importin-8	119.9	5.16	-0.17	9606.ENSP00000256079	0.124
O15511	Actin-related protein 2/3 complex subunit 5	16.3	5.67	-0.40	9606.ENSP00000352918	44
O43143	Pre-mRNA-splicing factor ATP-dependent RNA helicase DHX15	90.9	7.46	-0.51	9606.ENSP00000336741	307
O43172	U4/U6 small nuclear ribonucleoprotein Prp4	58.4	7.42	-0.49	9606.ENSP00000363313	17.8
O43175	D-3-phosphoglycerate dehydrogenase	56.6	6.71	0.09	9606.ENSP00000358417	387
O43237	Cytoplasmic dynein 1 light intermediate chain 2	54.1	6.38	-0.50	9606.ENSP00000258198	15.9
O43242	26S proteasome non-ATPase regulatory subunit 3	60.9	8.44	-0.53	9606.ENSP00000264639	165
O43252	Bifunctional 3'-phosphoadenosine 5'-phosphosulfate synthase 1	70.8	6.86	-0.41	9606.ENSP00000265174	7.5
O43264	Centromere/kinetochore protein zw10 homolog	88.8	6.27	-0.26	9606.ENSP00000200135	25.2
O43324	Eukaryotic translation elongation factor 1 epsilon-1	19.8	8.54	-0.29	9606.ENSP00000369038	n.a.
O43396	Thioredoxin-like protein 1	32.2	4.96	-0.46	9606.ENSP00000217515	69.1
O43432	Eukaryotic translation initiation factor 4 gamma 3	176.5	5.38	-0.61	9606.ENSP00000364073	55.3
O43447	Peptidyl-prolyl cis-trans isomerase H	19.2	8.07	-0.06	9606.ENSP00000306614	677
O43488	Aflatoxin B1 aldehyde reductase member 2	39.6	7.17	-0.28	9606.ENSP00000235835	158
O43592	Exportin-T	109.9	5.39	-0.02	9606.ENSP00000327821	n.a.
O43617	Trafficking protein particle complex subunit 3	20.3	4.96	-0.23	9606.ENSP00000362261	n.a.
O43681	ATPase ASNA1	38.8	4.91	-0.11	9606.ENSP00000349887	n.a.
O43684	Mitotic checkpoint protein BUB3	37.1	6.84	-0.51	9606.ENSP00000357858	279
O43719	HIV Tat-specific factor 1	85.8	4.4	-1.35	9606.ENSP00000218364	151
O43747	AP-1 complex subunit gamma-1	91.3	6.8	-0.11	9606.ENSP00000377148	51.2
O43776	Asparagine--tRNA ligase, cytoplasmic	62.9	6.25	-0.49	9606.ENSP00000256854	211
O43809	Cleavage and polyadenylation specificity factor subunit 5	26.2	8.82	-0.40	9606.ENSP00000300291	3.85
O43847	Nardilysin	131.5	5	-0.45	9606.ENSP00000346890	14.3

O43865	Adenosylhomocysteinase 2	58.9	6.89	-0.27	9606.ENSP00000358814	100
O60271	C-Jun-amino-terminal kinase-interacting protein 4	146.1	5.15	-0.60	9606.ENSP00000262013	31.6
O60333	Kinesin-like protein KIF1B	204.3	5.6	-0.49	9606.ENSP00000263934	0.764
O60341	Lysine-specific histone demethylase 1A	92.8	6.52	-0.37	9606.ENSP00000383042	46.4
O60493	Sorting nexin-3	18.8	8.66	-0.63	9606.ENSP00000230085	38
O60502	Protein O-GlcNAcase	102.8	4.91	-0.34	9606.ENSP00000354850	69.8
O60573	Eukaryotic translation initiation factor 4E type 2	28.3	8.88	-0.87	9606.ENSP00000258416	126
O60610	Protein diaphanous homolog 1	141.3	5.41	-0.54	9606.ENSP00000381565	19.1
O60678	Protein arginine N-methyltransferase 3	59.8	5.35	-0.26	9606.ENSP00000331879	21.6
O60701	UDP-glucose 6-dehydrogenase	55	7.12	-0.22	9606.ENSP00000319501	97.9
O60716	Catenin delta-1	108.1	6.23	-0.73	9606.ENSP00000382004	16
O60749	Sorting nexin-2	58.4	5.12	-0.53	9606.ENSP00000368831	55.5
O60763	General vesicular transport factor p115	107.8	4.91	-0.39		n.a.
O60814	Histone H2B type 1-K	13.9	10.32	-0.72	9606.ENSP00000349430	4021
O60826	Coiled-coil domain-containing protein 22	70.7	6.74	-0.50	9606.ENSP00000365401	n.a.
O60841	Eukaryotic translation initiation factor 5B	138.7	5.49	-1.05	9606.ENSP00000289371	244
O60884	DnaJ homolog subfamily A member 2	45.7	6.48	-0.70	9606.ENSP00000314030	238
O60885	Bromodomain-containing protein 4	152.1	9.19	-1.08	9606.ENSP00000263377	4.57
O75083	WD repeat-containing protein 1	66.2	6.65	-0.24	9606.ENSP00000427687	406
O75131	Copine-3	60.1	5.85	-0.25	9606.ENSP00000198765	278
O75150	E3 ubiquitin-protein ligase BRE1B	113.6	6.23	-0.87	9606.ENSP00000325677	n.a.
O75153	Clustered mitochondria protein homolog	146.6	6.13	-0.35	9606.ENSP00000388872	17.7
O75179	Ankyrin repeat domain-containing protein 17	274.1	6.52	-0.39	9606.ENSP00000351416	7.13
O75190	DnaJ homolog subfamily B member 6	36.1	9.16	-0.95	9606.ENSP00000262177	3.56
O75340	Programmed cell death protein 6	21.9	5.4	-0.40	9606.ENSP00000264933	159
O75351	Vacuolar protein sorting-associated protein 4B	49.3	7.23	-0.55	9606.ENSP00000238497	n.a.
O75369	Filamin-B	278	5.73	-0.29	9606.ENSP00000420213	231
O75390	Citrate synthase, mitochondrial	51.7	8.32	-0.16	9606.ENSP00000342056	17.2
O75400	Pre-mRNA-processing factor 40 homolog A	108.7	7.56	-1.05	9606.ENSP00000386458	162
O75533	Splicing factor 3B subunit 1	145.7	7.09	-0.39	9606.ENSP00000335321	281
O75534	Cold shock domain-containing protein E1	88.8	6.25	-0.44	9606.ENSP00000407724	369
O75643	U5 small nuclear ribonucleoprotein 200 kDa helicase	244.4	6.06	-0.33	9606.ENSP00000317123	52.4
O75694	Nuclear pore complex protein Nup155	155.1	6.16	-0.13	9606.ENSP00000231498	21.6
O75717	WD repeat and HMG-box DNA-binding protein 1	125.9	5.62	-0.56	9606.ENSP00000353793	12.4
O75792	Ribonuclease H2 subunit A	33.4	5.25	-0.30	9606.ENSP00000221486	67
O75794	Cell division cycle protein 123 homolog	39.1	4.81	-0.53	9606.ENSP00000281141	18.7
O75821	Eukaryotic translation initiation factor 3 subunit G	35.6	6.13	-0.81	9606.ENSP00000253108	4.63
O75822	Eukaryotic translation initiation factor 3 subunit J	29	4.83	-1.01	9606.ENSP00000261868	316
O75832	26S proteasome non-ATPase regulatory subunit 10	24.4	6.1	-0.24	9606.ENSP00000217958	61.1
O75874	Isocitrate dehydrogenase [NADP] cytoplasmic	46.6	7.01	-0.39	9606.ENSP00000260985	198
O75934	Pre-mRNA-splicing factor SPF27	26.1	5.66	-0.70	9606.ENSP00000358554	n.a.
O75935	Dynactin subunit 3	21.1	5.47	-0.21	9606.ENSP00000259632	n.a.
O76003	Glutaredoxin-3	37.4	5.39	-0.26	9606.ENSP00000330836	91.9
O76094	Signal recognition particle subunit SRP72	74.6	9.26	-0.64	9606.ENSP00000342181	13.3
O94760	N(G),N(G)-dimethylarginine dimethylaminohydrolase 1	31.1	5.81	-0.13	9606.ENSP00000284031	9.6
O94776	Metastasis-associated protein MTA2	75	9.66	-0.53	9606.ENSP00000278823	3.38
O94903	Proline synthase co-transcribed bacterial homolog protein	30.3	7.5	-0.30	9606.ENSP00000333551	1.97
O94906	Pre-mRNA-processing factor 6	106.9	8.25	-0.64	9606.ENSP00000266079	40.8
O94979	Protein transport protein Sec31A	132.9	6.89	-0.40	9606.ENSP00000347329	40.5
O95071	E3 ubiquitin-protein ligase UBR5	309.2	5.85	-0.46	9606.ENSP00000429084	n.a.
O95104	Splicing factor, arginine/serine-rich 15	125.8	9.55	-0.86	9606.ENSP00000286835	4
O95155	Ubiquitin conjugation factor E4 B	146.1	6.55	-0.33	9606.ENSP00000343001	2.01
O95163	Elongator complex protein 1	150.2	5.94	-0.26	9606.ENSP00000363779	9.55
O95229	ZW10 interactor	31.3	5.15	-0.72	9606.ENSP00000363055	n.a.
O95295	SNARE-associated protein Snapin	14.9	9.31	-0.36	9606.ENSP00000357674	n.a.
O95347	Structural maintenance of chromosomes protein 2	135.6	8.43	-0.67	9606.ENSP00000286398	20.4
O95373	Importin-7	119.4	4.82	-0.25	9606.ENSP00000369042	8.67
O95394	Phosphoacetylglucosamine mutase	59.8	6.25	-0.28	9606.ENSP00000425809	117
O95433	Activator of 90 kDa heat shock protein ATPase homolog 1	38.3	5.53	-0.55	9606.ENSP00000216479	380
O95602	DNA-directed RNA polymerase I subunit RPA1	194.7	7.03	-0.41	9606.ENSP00000263857	31.9
O95747	Serine/threonine-protein kinase OSR1	58	6.43	-0.36	9606.ENSP00000311713	12.9
O95749	Geranylgeranyl pyrophosphate synthase	34.8	6.14	-0.43	9606.ENSP00000282841	49.7
O95757	Heat shock 70 kDa protein 4L	94.5	5.88	-0.53	9606.ENSP00000296464	97.7
O95801	Tetratricopeptide repeat protein 4	44.7	5.6	-0.67	9606.ENSP00000360329	112
O95816	BAG family molecular chaperone regulator 2	23.8	6.7	-0.59	9606.ENSP00000359727	30.2
O95861	3'(2'),5'-bisphosphate nucleotidase 1	33.4	5.69	-0.02	9606.ENSP00000318852	137
O95865	N(G),N(G)-dimethylarginine dimethylaminohydrolase 2	29.6	6.01	0.01	9606.ENSP00000364943	3.5
O95905	Protein ecdysoneless homolog	72.7	4.87	-0.47	9606.ENSP00000401566	n.a.
O95983	Methyl-CpG-binding domain protein 3	32.8	5.34	-0.79	9606.ENSP00000156825	n.a.
P00338	L-lactate dehydrogenase A chain	36.7	8.27	-0.01	9606.ENSP00000445175	8.47
P00374	Dihydrofolate reductase	21.4	7.42	-0.46	9606.ENSP00000396308	n.a.
P00390	Glutathione reductase, mitochondrial	56.2	8.5	-0.05	9606.ENSP00000221130	308
P00491	Purine nucleoside phosphorylase	32.1	6.95	-0.17	9606.ENSP00000354532	161
P00505	Aspartate aminotransferase, mitochondrial	47.5	9.01	-0.21	9606.ENSP00000245206	358
P00558	Phosphoglycerate kinase 1	44.6	8.1	-0.08	9606.ENSP00000362413	778
P00568	Adenylate kinase isoenzyme 1	21.6	8.63	-0.48	9606.ENSP00000362249	0.227
P00918	Carbonic anhydrase 2	29.2	7.4	-0.58	9606.ENSP00000285379	954

P00966	Argininosuccinate synthase	46.5	8.02	-0.37	9606.ENSP00000253004	21.2
P01111	GTPase NRas	21.2	5.17	-0.32	9606.ENSP00000358548	202
P02768	Serum albumin	69.3	6.28	-0.35	9606.ENSP00000295897	n.a.
P02794	Ferritin heavy chain	21.2	5.55	-0.77	9606.ENSP00000273550	5.22
P04075	Fructose-bisphosphate aldolase A	39.4	8.09	-0.26	9606.ENSP00000336927	812
P04181	Ornithine aminotransferase, mitochondrial	48.5	7.03	-0.09	9606.ENSP00000357838	273
P04183	Thymidine kinase, cytosolic	25.5	8.51	-0.03	9606.ENSP00000301634	9.96
P04350	Tubulin beta-4A chain	49.6	4.88	-0.32	9606.ENSP00000264071	776
P04406	Glyceraldehyde-3-phosphate dehydrogenase	36	8.46	-0.11	9606.ENSP00000229239	n.a.
P04792	Heat shock protein beta-1	22.8	6.4	-0.57	9606.ENSP00000248553	0.836
P04818	Thymidylate synthase	35.7	7.01	-0.41	9606.ENSP00000315644	186
P05198	Eukaryotic translation initiation factor 2 subunit 1	36.1	5.08	-0.45	9606.ENSP00000256383	127
P05387	60S acidic ribosomal protein P2	11.7	4.54	-0.24	9606.ENSP00000322419	7297
P05388	60S acidic ribosomal protein P0	34.3	5.97	0.04	9606.ENSP00000339027	49.3
P06280	Alpha-galactosidase A	48.7	5.6	-0.25	9606.ENSP00000218516	n.a.
P06493	Cyclin-dependent kinase 1	34.1	8.4	-0.28	9606.ENSP00000378699	25.5
P06576	ATP synthase subunit beta, mitochondrial	56.5	5.4	0.02	9606.ENSP00000262030	1615
P06730	Eukaryotic translation initiation factor 4E	25.1	6.15	-0.70		n.a.
P06733	Alpha-enolase	47.1	7.39	-0.22	9606.ENSP00000234590	726
P06737	Glycogen phosphorylase, liver form	97.1	7.17	-0.32	9606.ENSP00000216392	28.3
P06744	Glucose-6-phosphate isomerase	63.1	8.32	-0.34		n.a.
P06748	Nucleophosmin	32.6	4.78	-0.97	9606.ENSP00000296930	136
P06899	Histone H2B type 1-J	13.9	10.32	-0.72	9606.ENSP00000342886	4191
P07195	L-lactate dehydrogenase B chain	36.6	6.05	0.06	9606.ENSP00000229319	4923
P07339	Cathepsin D	44.5	6.54	0.02	9606.ENSP00000236671	141
P07437	Tubulin beta chain	49.6	4.89	-0.35	9606.ENSP00000339001	3389
P07737	Profilin-1	15	8.27	-0.12	9606.ENSP00000225655	4174
P07741	Adenine phosphoribosyltransferase	19.6	6.02	0.10	9606.ENSP00000367615	716
P07814	Bifunctional glutamate/proline--tRNA ligase	170.5	7.33	-0.52	9606.ENSP00000355890	457
P07910	Heterogeneous nuclear ribonucleoproteins C1/C2	33.6	5.08	-0.98	9606.ENSP00000319690	1256
P07954	Fumarate hydratase, mitochondrial	54.6	8.76	-0.07	9606.ENSP00000355518	209
P08133	Annexin A6	75.8	5.6	-0.45	9606.ENSP00000346550	362
P08237	ATP-dependent 6-phosphofructokinase, muscle type	85.1	7.99	-0.17	9606.ENSP00000345771	168
P08238	Heat shock protein HSP 90-beta	83.2	5.03	-0.68	9606.ENSP00000325875	1142
P08243	Asparagine synthetase [glutamine-hydrolyzing]	64.3	6.86	-0.26	9606.ENSP00000175506	200
P08670	Vimentin	53.6	5.12	-0.82	9606.ENSP00000224237	430
P08708	40S ribosomal protein S17	15.5	9.85	-0.58	9606.ENSP00000346046	2587
P08758	Annexin A5	35.9	5.05	-0.33	9606.ENSP00000296511	653
P08865	40S ribosomal protein SA	32.8	4.87	-0.31	9606.ENSP00000346067	2855
P09211	Glutathione S-transferase P	23.3	5.64	-0.12	9606.ENSP00000381607	460
P09417	Dihydropteridine reductase	25.8	7.37	0.00	9606.ENSP00000281243	4.86
P09429	High mobility group protein B1	24.9	5.74	-1.61	9606.ENSP00000343040	3592
P09651	Heterogeneous nuclear ribonucleoprotein A1	38.7	9.13	-0.89	9606.ENSP00000341826	4351
P09661	U2 small nuclear ribonucleoprotein A'	28.4	8.62	-0.50	9606.ENSP00000254193	12
P09874	Poly [ADP-ribose] polymerase 1	113	8.88	-0.54	9606.ENSP00000355759	2415
P09884	DNA polymerase alpha catalytic subunit	165.8	5.85	-0.46	9606.ENSP00000368349	5.51
P09936	Ubiquitin carboxyl-terminal hydrolase isozyme L1	24.8	5.48	-0.30	9606.ENSP00000284440	1920
P09960	Leukotriene A-4 hydrolase	69.2	6.18	-0.26	9606.ENSP00000228740	78
P0C0S5	Histone H2A.Z	13.5	10.58	-0.31	9606.ENSP00000296417	589
P0CG48	Polyubiquitin-C	77	7.66	-0.48	9606.ENSP00000344818	4.86
P10155	60 kDa SS-A/Ro ribonucleoprotein	60.6	8.03	-0.19	9606.ENSP00000356411	26.7
P10768	S-formylglutathione hydrolase	31.4	7.02	-0.30	9606.ENSP00000367992	n.a.
P10809	60 kDa heat shock protein, mitochondrial	61	5.87	-0.08	9606.ENSP00000340019	4295
P11172	Uridine 5'-monophosphate synthase	52.2	7.24	0.08	9606.ENSP00000232607	7.2
P11177	Pyruvate dehydrogenase E1 component subunit beta, mitochondrial	39.2	6.65	0.00	9606.ENSP00000307241	564
P11216	Glycogen phosphorylase, brain form	96.6	6.86	-0.33	9606.ENSP00000216962	15.8
P11413	Glucose-6-phosphate 1-dehydrogenase	59.2	6.84	-0.37	9606.ENSP00000377192	103
P11441	Ubiquitin-like protein 4A	17.8	8.66	-0.41	9606.ENSP00000358674	n.a.
P11586	C-1-tetrahydrofolate synthase, cytoplasmic	101.5	7.3	-0.09	9606.ENSP00000450560	568
P11766	Alcohol dehydrogenase class-3	39.7	7.49	0.16	9606.ENSP00000296412	193
P11802	Cyclin-dependent kinase 4	33.7	7.01	-0.17	9606.ENSP00000257904	33.6
P11908	Ribose-phosphate pyrophosphokinase 2	34.7	6.61	0.06	9606.ENSP00000381504	137
P11940	Polyadenylate-binding protein 1	70.6	9.5	-0.51	9606.ENSP00000313007	602
P12004	Proliferating cell nuclear antigen	28.8	4.69	-0.09	9606.ENSP00000368438	351
P12081	Histidine--tRNA ligase, cytoplasmic	57.4	5.88	-0.25	9606.ENSP00000425634	62.7
P12268	Inosine-5'-monophosphate dehydrogenase 2	55.8	6.9	-0.11	9606.ENSP00000321584	1098
P12270	Nucleoprotein TPR	267.1	5.02	-0.97	9606.ENSP00000356448	84.8
P12277	Creatine kinase B-type	42.6	5.59	-0.42	9606.ENSP00000299198	1136
P12956	X-ray repair cross-complementing protein 6	69.8	6.64	-0.54	9606.ENSP00000352257	20.3
P13010	X-ray repair cross-complementing protein 5	82.7	5.81	-0.34	9606.ENSP00000375977	438
P13051	Uracil-DNA glycosylase	34.6	9.32	-0.49	9606.ENSP00000242576	21.1
P13639	Elongation factor 2	95.3	6.83	-0.21	9606.ENSP00000307940	5537
P13693	Translationally-controlled tumor protein	19.6	4.93	-0.43	9606.ENSP00000431872	n.a.
P13804	Electron transfer flavoprotein subunit alpha, mitochondrial	35.1	8.38	0.15	9606.ENSP00000452762	525
P13861	cAMP-dependent protein kinase type II-alpha regulatory subunit	45.5	5.07	-0.50	9606.ENSP00000265563	2.77
P13984	General transcription factor IIF subunit 2	28.4	9.23	-0.74	9606.ENSP00000340823	21.8

P14314	Glucosidase 2 subunit beta	59.4	4.41	-0.91	9606.ENSP00000252455	441
P14324	Farnesyl pyrophosphate synthase	48.2	6.15	-0.24	9606.ENSP00000349078	132
P14550	Alcohol dehydrogenase [NADP(+)]	36.5	6.79	-0.27	9606.ENSP00000312606	275
P14618	Pyruvate kinase PKM	57.9	7.84	-0.13	9606.ENSP00000320171	2184
P14625	Endoplasmin	92.4	4.84	-0.71	9606.ENSP00000299767	1089
P14635	G2/mitotic-specific cyclin-B1	48.3	7.47	-0.24	9606.ENSP00000256442	n.a.
P14678	Small nuclear ribonucleoprotein-associated proteins B and B'	24.6	11.19	-0.37	9606.ENSP00000412566	n.a.
P14735	Insulin-degrading enzyme	117.9	6.61	-0.40	9606.ENSP00000265986	49.7
P14868	Aspartate--tRNA ligase, cytoplasmic	57.1	6.55	-0.42	9606.ENSP00000264161	318
P15531	Nucleoside diphosphate kinase A	17.1	6.19	-0.19	9606.ENSP00000013034	3751
P15880	40S ribosomal protein S2	31.3	10.24	-0.23	9606.ENSP00000341885	1526
P15924	Desmoplakin	331.6	6.81	-0.82	9606.ENSP00000369129	24.3
P15927	Replication protein A 32 kDa subunit	29.2	6.15	-0.31	9606.ENSP00000363021	279
P16152	Carbonyl reductase [NADPH] 1	30.4	8.32	-0.21	9606.ENSP00000290349	149
P17174	Aspartate aminotransferase, cytoplasmic	46.2	7.01	-0.28	9606.ENSP00000359539	333
P17812	CTP synthase 1	66.6	6.46	-0.31	9606.ENSP00000361699	635
P17844	Probable ATP-dependent RNA helicase DDX5	69.1	8.92	-0.64	9606.ENSP00000225792	983
P17858	ATP-dependent 6-phosphofructokinase, liver type	85	7.5	-0.08	9606.ENSP00000269848	175
P17980	26S protease regulatory subunit 6A	49.2	5.24	-0.40	9606.ENSP00000298852	38.5
P17987	T-complex protein 1 subunit alpha	60.3	6.11	-0.04	9606.ENSP00000317334	1142
P18085	ADP-ribosylation factor 4	20.5	7.14	-0.09	9606.ENSP00000306010	96.9
P18124	60S ribosomal protein L7	29.2	10.65	-0.62	9606.ENSP00000339795	3172
P18621	60S ribosomal protein L17	21.4	10.17	-0.90	9606.ENSP00000462023	672
P18669	Phosphoglycerate mutase 1	28.8	7.18	-0.50	9606.ENSP00000359991	1306
P18754	Regulator of chromosome condensation	44.9	7.52	-0.26		n.a.
P18858	DNA ligase 1	101.7	5.62	-0.62	9606.ENSP00000263274	n.a.
P19105	Myosin regulatory light chain 12A	19.8	4.81	-0.83	9606.ENSP00000217652	350
P19174	1-phosphatidylinositol 4,5-bisphosphate phosphodiesterase gamma-1	148.4	6.05	-0.55	9606.ENSP00000244007	5.43
P19367	Hexokinase-1	102.4	6.8	-0.21	9606.ENSP00000384774	5.03
P19387	DNA-directed RNA polymerase II subunit RPB3	31.4	4.92	-0.55	9606.ENSP00000219252	23.3
P19388	DNA-directed RNA polymerases I, II, and III subunit RPABC1	24.5	5.95	-0.54	9606.ENSP00000215587	70.6
P19623	Spermidine synthase	33.8	5.49	-0.20	9606.ENSP00000366156	149
P19784	Casein kinase II subunit alpha'	41.2	8.56	-0.54	9606.ENSP00000262506	154
P20248	Cyclin-A2	48.5	6.54	-0.37	9606.ENSP00000274026	n.a.
P20290	Transcription factor BTF3	22.2	9.38	-0.74	9606.ENSP00000369965	246
P20339	Ras-related protein Rab-5A	23.6	8.15	-0.43	9606.ENSP00000273047	131
P20340	Ras-related protein Rab-6A	23.6	5.54	-0.42	9606.ENSP00000311449	0.78
P20618	Proteasome subunit beta type-1	26.5	8.13	-0.12	9606.ENSP00000262193	739
P21127	Cyclin-dependent kinase 11B	92.7	5.57	-1.28	9606.ENSP00000384442	5.21
P21266	Glutathione S-transferase Mu 3	26.5	5.54	-0.41	9606.ENSP00000256594	294
P21281	V-type proton ATPase subunit B, brain isoform	56.5	5.81	-0.16	9606.ENSP00000276390	166
P21333	Filamin-A	280.6	6.06	-0.32	9606.ENSP00000358866	915
P21399	Cytoplasmic aconitate hydratase	98.3	6.68	-0.14	9606.ENSP00000309477	3.96
P22061	Protein-L-isoaspartate(D-aspartate) O-methyltransferase	24.6	7.21	-0.17	9606.ENSP00000356348	n.a.
P22102	Trifunctional purine biosynthetic protein adenosine-3	107.7	6.7	0.04	9606.ENSP00000371236	43.8
P22314	Ubiquitin-like modifier-activating enzyme 1	117.8	5.76	-0.27	9606.ENSP00000338413	146
P22626	Heterogeneous nuclear ribonucleoproteins A2/B1	37.4	8.95	-0.93	9606.ENSP00000346694	13913
P23258	Tubulin gamma-1 chain	51.1	6.14	-0.37	9606.ENSP00000251413	109
P23284	Peptidyl-prolyl cis-trans isomerase B	23.7	9.41	-0.20	9606.ENSP00000300026	4554
P23396	40S ribosomal protein S3	26.7	9.66	-0.15	9606.ENSP00000433821	637
P23526	Adenosylhomocysteinase	47.7	6.34	-0.10	9606.ENSP00000217426	987
P23528	Cofilin-1	18.5	8.09	-0.36	9606.ENSP00000309629	0.486
P23919	Thymidylate kinase	23.8	8.27	-0.30	9606.ENSP00000304802	75.8
P23921	Ribonucleoside-diphosphate reductase large subunit	90	7.15	-0.36	9606.ENSP00000300738	66
P24534	Elongation factor 1-beta	24.7	4.67	-0.49	9606.ENSP00000236957	172
P24666	Low molecular weight phosphotyrosine protein phosphatase	18	6.74	-0.49	9606.ENSP00000272065	913
P24752	Acetyl-CoA acetyltransferase, mitochondrial	45.2	8.85	0.09	9606.ENSP00000265838	255
P24928	DNA-directed RNA polymerase II subunit RPB1	217	7.37	-0.53	9606.ENSP00000314949	23.2
P24941	Cyclin-dependent kinase 2	33.9	8.68	-0.08	9606.ENSP00000266970	n.a.
P25205	DNA replication licensing factor MCM3	90.9	5.77	-0.56	9606.ENSP00000229854	171
P25325	3-mercaptopyruvate sulfurtransferase	33.2	6.6	-0.43	9606.ENSP00000380318	176
P25398	40S ribosomal protein S12	14.5	7.21	-0.19	9606.ENSP00000230050	203
P25685	DnaJ homolog subfamily B member 1	38	8.63	-0.72	9606.ENSP00000254322	1.42
P25786	Proteasome subunit alpha type-1	29.5	6.61	-0.43	9606.ENSP00000414359	594
P25787	Proteasome subunit alpha type-2	25.9	7.43	-0.19	9606.ENSP00000455744	n.a.
P25789	Proteasome subunit alpha type-4	29.5	7.72	-0.46	9606.ENSP00000044462	92.1
P26196	Probable ATP-dependent RNA helicase DDX6	54.4	8.66	-0.32	9606.ENSP00000264018	49.1
P26368	Splicing factor U2AF 65 kDa subunit	53.5	9.09	-0.59	9606.ENSP00000307863	3086
P26373	60S ribosomal protein L13	24.2	11.65	-0.85	9606.ENSP00000307889	801
P26599	Polypyrimidine tract-binding protein 1	57.2	9.17	-0.15	9606.ENSP00000349428	360
P26639	Threonine--tRNA ligase, cytoplasmic	83.4	6.67	-0.58	9606.ENSP00000265112	397
P26640	Valine--tRNA ligase	140.4	7.59	-0.27	9606.ENSP00000364815	43.7
P26641	Elongation factor 1-gamma	50.1	6.67	-0.48	9606.ENSP00000331901	522
P27348	14-3-3 protein theta	27.7	4.78	-0.51	9606.ENSP00000238081	1914
P27361	Mitogen-activated protein kinase 3	43.1	6.74	-0.31	9606.ENSP00000263025	153
P27635	60S ribosomal protein L10	24.6	10.08	-0.55	9606.ENSP00000341730	2617

P27694	Replication protein A 70 kDa DNA-binding subunit	68.1	7.21	-0.36	9606.ENSP00000254719	153
P27695	DNA-(apurinic or apyrimidinic site) lyase	35.5	8.12	-0.58	9606.ENSP00000216714	1090
P27707	Deoxycytidine kinase	30.5	5.21	-0.54	9606.ENSP00000286648	n.a.
P27708	CAD protein	242.8	6.46	-0.08	9606.ENSP00000264705	144
P27797	Calreticulin	48.1	4.44	-1.10	9606.ENSP00000320866	2337
P27816	Microtubule-associated protein 4	120.9	5.43	-0.54	9606.ENSP00000353375	66.2
P28066	Proteasome subunit alpha type-5	26.4	4.79	-0.11	9606.ENSP00000271308	104
P28161	Glutathione S-transferase Mu 2	25.7	6.37	-0.46	9606.ENSP00000241337	5.13
P28340	DNA polymerase delta catalytic subunit	123.6	7.03	-0.26	9606.ENSP00000406046	9.98
P28482	Mitogen-activated protein kinase 1	41.4	6.98	-0.29	9606.ENSP00000215832	286
P28838	Cytosol aminopeptidase	56.1	7.93	-0.17	9606.ENSP00000226299	126
P29144	Tripeptidyl-peptidase 2	138.3	6.32	-0.34	9606.ENSP00000365233	38.5
P29401	Transketolase	67.8	7.66	-0.17	9606.ENSP00000405455	1315
P29692	Elongation factor 1-delta	31.1	5.01	-0.59	9606.ENSP00000391944	642
P30040	Endoplasmic reticulum resident protein 29	29	7.31	-0.30	9606.ENSP00000261735	6.32
P30041	Peroxiredoxin-6	25	6.38	-0.21	9606.ENSP00000342026	1093
P30043	Flavin reductase (NADPH)	22.1	7.65	-0.06	9606.ENSP00000263368	n.a.
P30050	60S ribosomal protein L12	17.8	9.42	-0.35	9606.ENSP00000354739	4486
P30084	Enoyl-CoA hydratase, mitochondrial	31.4	8.07	-0.06	9606.ENSP00000357535	n.a.
P30085	UMP-CMP kinase	22.2	5.57	-0.57	9606.ENSP00000360939	15.3
P30101	Protein disulfide-isomerase A3	56.7	6.35	-0.51	9606.ENSP00000300289	612
P30153	Serine/threonine-protein phosphatase 2A 65 kDa regulatory subunit A alpha isoform	65.3	5.11	0.07	9606.ENSP00000324804	54
P30154	Serine/threonine-protein phosphatase 2A 65 kDa regulatory subunit A beta isoform	66.2	4.94	0.08	9606.ENSP00000311344	n.a.
P30419	Glycylpeptide N-tetradecanoyltransferase 1	56.8	7.8	-0.53	9606.ENSP00000258960	n.a.
P30520	Adenylosuccinate synthetase isozyme 2	50.1	6.55	-0.18	9606.ENSP00000355493	57
P30876	DNA-directed RNA polymerase II subunit RPB2	133.8	6.87	-0.37	9606.ENSP00000312735	19.7
P31150	Rab GDP dissociation inhibitor alpha	50.6	5.14	-0.30	9606.ENSP00000394071	416
P31153	S-adenosylmethionine synthase isoform type-2	43.6	6.48	-0.28	9606.ENSP00000303147	139
P31350	Ribonucleoside-diphosphate reductase subunit M2	44.8	5.38	-0.19	9606.ENSP00000353770	5.93
P31689	DnaJ homolog subfamily A member 1	44.8	7.08	-0.73	9606.ENSP00000369127	793
P31939	Bifunctional purine biosynthesis protein PURH	64.6	6.71	-0.11	9606.ENSP00000236959	177
P31942	Heterogeneous nuclear ribonucleoprotein H3	36.9	6.87	-0.73	9606.ENSP00000265866	866
P31943	Heterogeneous nuclear ribonucleoprotein H	49.2	6.3	-0.60	9606.ENSP00000349168	2909
P31948	Stress-induced-phosphoprotein 1	62.6	6.8	-0.94	9606.ENSP00000305958	1018
P32119	Peroxiredoxin-2	21.9	5.97	-0.20	9606.ENSP00000301522	201
P32969	60S ribosomal protein L9	21.8	9.95	-0.35	9606.ENSP00000346022	1056
P33176	Kinesin-1 heavy chain	109.6	6.51	-0.81	9606.ENSP00000307078	193
P33316	Deoxyuridine 5'-triphosphate nucleotidohydrolase, mitochondrial	26.5	9.36	-0.30	9606.ENSP00000370376	124
P33552	Cyclin-dependent kinases regulatory subunit 2	9.9	8.46	-1.02	9606.ENSP00000364976	765
P33991	DNA replication licensing factor MCM4	96.5	6.74	-0.41	9606.ENSP00000262105	127
P33992	DNA replication licensing factor MCM5	82.2	8.37	-0.35	9606.ENSP00000216122	99
P33993	DNA replication licensing factor MCM7	81.3	6.46	-0.37	9606.ENSP00000307288	204
P34897	Serine hydroxymethyltransferase, mitochondrial	56	8.53	-0.27	9606.ENSP00000333667	484
P34932	Heat shock 70 kDa protein 4	94.3	5.19	-0.58	9606.ENSP00000302961	748
P34949	Mannose-6-phosphate isomerase	46.6	5.95	-0.04	9606.ENSP00000318318	n.a.
P35244	Replication protein A 14 kDa subunit	13.6	5.08	0.02	9606.ENSP00000223129	n.a.
P35249	Replication factor C subunit 4	39.7	8.02	-0.20	9606.ENSP00000296273	0.838
P35250	Replication factor C subunit 2	39.1	6.44	-0.10	9606.ENSP00000055077	n.a.
P35270	Sepiapterin reductase	28	8.05	0.00	9606.ENSP00000234454	100
P35520	Cystathionine beta-synthase	60.5	6.65	-0.28	9606.ENSP00000344460	279
P35573	Glycogen debranching enzyme	174.7	6.76	-0.33	9606.ENSP00000294724	17.1
P35579	Myosin-9	226.4	5.6	-0.85	9606.ENSP00000216181	77.1
P35580	Myosin-10	228.9	5.54	-0.86	9606.ENSP00000269243	58.8
P35606	Coatomer subunit beta'	102.4	5.27	-0.31	9606.ENSP00000329419	130
P35612	Beta-adducin	80.8	5.92	-0.66	9606.ENSP00000264436	3.78
P35658	Nuclear pore complex protein Nup214	213.5	7.47	-0.21	9606.ENSP00000352400	22.9
P35998	26S protease regulatory subunit 7	48.6	5.95	-0.42	9606.ENSP00000292644	557
P36404	ADP-ribosylation factor-like protein 2	20.9	6.34	-0.23	9606.ENSP00000246747	n.a.
P36507	Dual specificity mitogen-activated protein kinase kinase 2	44.4	6.55	-0.32	9606.ENSP00000262948	0.003
P36543	V-type proton ATPase subunit E 1	26.1	8	-0.53	9606.ENSP00000253413	27.1
P36578	60S ribosomal protein L4	47.7	11.06	-0.61	9606.ENSP00000311430	1321
P36871	Phosphoglucomutase-1	61.4	6.76	-0.13		n.a.
P37108	Signal recognition particle 14 kDa protein	14.6	10.04	-0.44	9606.ENSP00000267884	215
P37802	Transgelin-2	22.4	8.25	-0.61	9606.ENSP00000357075	240
P37837	Transaldolase	37.5	6.81	-0.25	9606.ENSP00000321259	44
P38117	Electron transfer flavoprotein subunit beta	27.8	8.1	-0.12	9606.ENSP00000346173	549
P38606	V-type proton ATPase catalytic subunit A	68.3	5.52	-0.19	9606.ENSP00000273398	30
P38919	Eukaryotic initiation factor 4A-III	46.8	6.73	-0.26	9606.ENSP00000269349	722
P39019	40S ribosomal protein S19	16.1	10.32	-0.61	9606.ENSP00000470004	4420
P39023	60S ribosomal protein L3	46.1	10.18	-0.65	9606.ENSP00000346001	3317
P39748	Flap endonuclease 1	42.6	8.62	-0.53	9606.ENSP00000305480	n.a.
P40123	Adenylyl cyclase-associated protein 2	52.8	6.37	-0.43	9606.ENSP00000229922	21.8
P40222	Alpha-taxilin	61.9	6.52	-1.23	9606.ENSP00000362711	31.9
P40227	T-complex protein 1 subunit zeta	58	6.68	-0.10	9606.ENSP00000275603	375
P40429	60S ribosomal protein L13a	23.6	10.93	-0.48	9606.ENSP00000375730	994
P40616	ADP-ribosylation factor-like protein 1	20.4	5.72	-0.08	9606.ENSP00000261636	n.a.

P40763	Signal transducer and activator of transcription 3	88	6.3	-0.40	9606.ENSP00000264657	n.a.
P40818	Ubiquitin carboxyl-terminal hydrolase 8	127.4	8.51	-0.88	9606.ENSP00000302239	10.1
P40925	Malate dehydrogenase, cytoplasmic	36.4	7.36	-0.04	9606.ENSP00000438144	2435
P40926	Malate dehydrogenase, mitochondrial	35.5	8.68	0.14	9606.ENSP00000327070	1176
P40939	Trifunctional enzyme subunit alpha, mitochondrial	82.9	9.04	-0.08	9606.ENSP00000370023	184
P41091	Eukaryotic translation initiation factor 2 subunit 3	51.1	8.4	-0.01	9606.ENSP00000253039	786
P41214	Eukaryotic translation initiation factor 2D	64.7	7.65	-0.34	9606.ENSP00000271764	28
P41227	N-alpha-acetyltransferase 10	26.4	5.64	-0.76	9606.ENSP00000417763	83.4
P41229	Lysine-specific demethylase 5C	175.6	5.58	-0.49	9606.ENSP00000364550	0.151
P41240	Tyrosine-protein kinase CSK	50.7	7.06	-0.27	9606.ENSP00000220003	19.7
P41250	Glycine--tRNA ligase	83.1	7.03	-0.30	9606.ENSP00000373918	193
P41252	Isoleucine--tRNA ligase, cytoplasmic	144.4	6.15	-0.24	9606.ENSP00000364794	95.9
P42166	Lamina-associated polypeptide 2, isoform alpha	75.4	7.66	-0.55	9606.ENSP00000266732	477
P42224	Signal transducer and activator of transcription 1-alpha/beta	87.3	6.05	-0.52	9606.ENSP00000354394	34.6
P42285	Superkiller viralicidic activity 2-like 2	117.7	6.52	-0.32	9606.ENSP00000230640	41.7
P42695	Condensin-2 complex subunit D3	168.8	7.5	-0.20	9606.ENSP00000433681	n.a.
P42704	Leucine-rich PPR motif-containing protein, mitochondrial	157.8	6.13	-0.21	9606.ENSP00000260665	31.7
P42771	Cyclin-dependent kinase inhibitor 2A	16.5	5.81	-0.23	9606.ENSP00000394932	n.a.
P42858	Huntingtin	347.4	6.2	-0.07	9606.ENSP00000347184	0.173
P43243	Matrin-3	94.6	6.25	-0.93	9606.ENSP00000354346	1009
P43246	DNA mismatch repair protein Msh2	104.7	5.77	-0.24	9606.ENSP00000233146	136
P43487	Ran-specific GTPase-activating protein	23.3	5.29	-1.10	9606.ENSP00000327583	n.a.
P43490	Nicotinamide phosphoribosyltransferase	55.5	7.15	-0.43	9606.ENSP00000222553	231
P43686	26S protease regulatory subunit 6B	47.3	5.21	-0.35	9606.ENSP00000157812	615
P45974	Ubiquitin carboxyl-terminal hydrolase 5	95.7	5.03	-0.44	9606.ENSP00000229268	266
P45985	Dual specificity mitogen-activated protein kinase kinase 4	44.3	8.07	-0.38	9606.ENSP00000262445	n.a.
P46060	Ran GTPase-activating protein 1	63.5	4.68	-0.24	9606.ENSP00000348577	49.4
P46379	Large proline-rich protein BAG6	119.3	5.6	-0.37	9606.ENSP00000365131	7.05
P46459	Vesicle-fusing ATPase	82.5	6.95	-0.22	9606.ENSP00000381293	118
P46734	Dual specificity mitogen-activated protein kinase kinase 3	39.3	7.43	-0.34	9606.ENSP00000345083	1.87
P46776	60S ribosomal protein L27a	16.6	11	-0.65	9606.ENSP00000346015	5024
P46777	60S ribosomal protein L5	34.3	9.72	-0.74	9606.ENSP00000359345	5619
P46778	60S ribosomal protein L21	18.6	10.49	-0.89	9606.ENSP00000346027	2698
P46781	40S ribosomal protein S9	22.6	10.65	-0.64	9606.ENSP00000302896	1451
P46783	40S ribosomal protein S10	18.9	10.15	-0.85	9606.ENSP00000347271	675
P46821	Microtubule-associated protein 1B	270.5	4.81	-0.84	9606.ENSP00000296755	74.6
P46926	Glucosamine-6-phosphate isomerase 1	32.6	6.92	-0.25	9606.ENSP00000311876	165
P46940	Ras GTPase-activating-like protein IQGAP1	189.1	6.48	-0.49	9606.ENSP00000268182	115
P47756	F-actin-capping protein subunit beta	31.3	5.59	-0.56	9606.ENSP00000264202	163
P47897	Glutamine--tRNA ligase	87.7	7.15	-0.31	9606.ENSP00000307567	222
P48147	Prolyl endopeptidase	80.6	5.86	-0.33	9606.ENSP00000358106	107
P48444	Coatomer subunit delta	57.2	6.21	-0.39	9606.ENSP00000264028	342
P48556	26S proteasome non-ATPase regulatory subunit 8	39.6	9.7	-0.33	9606.ENSP00000215071	n.a.
P48643	T-complex protein 1 subunit epsilon	59.6	5.66	-0.19	9606.ENSP00000280326	815
P49005	DNA polymerase delta subunit 2	51.3	5.58	-0.11	9606.ENSP00000386105	124
P49189	4-trimethylaminobutyraldehyde dehydrogenase	53.8	5.87	-0.04	9606.ENSP00000346827	7.22
P49327	Fatty acid synthase	273.3	6.44	-0.07	9606.ENSP00000304592	417
P49368	T-complex protein 1 subunit gamma	60.5	6.49	-0.25	9606.ENSP00000295688	1747
P49411	Elongation factor Tu, mitochondrial	49.5	7.61	-0.12	9606.ENSP00000322439	1277
P49419	Alpha-aminoadipic semialdehyde dehydrogenase	58.5	7.99	-0.06	9606.ENSP00000387123	356
P49427	Ubiquitin-conjugating enzyme E2 R1	26.7	4.54	-0.61	9606.ENSP00000215574	n.a.
P49588	Alanine--tRNA ligase, cytoplasmic	106.7	5.53	-0.30	9606.ENSP00000261772	395
P49589	Cysteine--tRNA ligase, cytoplasmic	85.4	6.76	-0.58	9606.ENSP00000369897	28.2
P49591	Serine--tRNA ligase, cytoplasmic	58.7	6.43	-0.50	9606.ENSP00000234677	70.6
P49593	Protein phosphatase 1F	49.8	5.1	-0.43	9606.ENSP00000263212	18.2
P49643	DNA primase large subunit	58.8	7.91	-0.59		n.a.
P49720	Proteasome subunit beta type-3	22.9	6.55	0.03	9606.ENSP00000225426	447
P49721	Proteasome subunit beta type-2	22.8	7.02	-0.17	9606.ENSP00000362334	970
P49736	DNA replication licensing factor MCM2	101.8	5.52	-0.50	9606.ENSP00000265056	576
P49770	Translation initiation factor eIF-2B subunit beta	39	6.16	-0.14	9606.ENSP00000266126	n.a.
P49815	Tuberin	200.5	7.31	-0.18	9606.ENSP00000219476	n.a.
P49840	Glycogen synthase kinase-3 alpha	50.9	8.75	-0.22	9606.ENSP00000222330	n.a.
P49841	Glycogen synthase kinase-3 beta	46.7	8.78	-0.32	9606.ENSP00000324806	5.23
P49914	5-formyltetrahydrofolate cyclo-ligase	23.2	7.88	-0.51	9606.ENSP00000258874	0.081
P49915	GMP synthase [glutamine-hydrolyzing]	76.7	6.87	-0.16	9606.ENSP00000419851	43.5
P49959	Double-strand break repair protein MRE11A	80.5	5.9	-0.67	9606.ENSP00000325863	40.5
P50225	Sulfotransferase 1A1	34.1	6.62	-0.36	9606.ENSP00000321988	0.924
P50454	Serpin H1	46.4	8.69	-0.22	9606.ENSP00000350894	5.62
P50502	Hsc70-interacting protein	41.3	5.27	-0.86	9606.ENSP00000216218	503
P50570	Dynamin-2	98	7.44	-0.43	9606.ENSP00000347890	43.8
P50851	Lipopolysaccharide-responsive and beige-like anchor protein	318.9	5.6	-0.20	9606.ENSP00000349629	5.6
P50990	T-complex protein 1 subunit theta	59.6	5.6	-0.07	9606.ENSP00000286788	1314
P50991	T-complex protein 1 subunit delta	57.9	7.83	0.03	9606.ENSP00000377958	997
P50995	Annexin A11	54.4	7.65	-0.52	9606.ENSP00000265447	n.a.
P51149	Ras-related protein Rab-7a	23.5	6.7	-0.38	9606.ENSP00000265062	499
P51151	Ras-related protein Rab-9A	22.8	5.47	-0.43	9606.ENSP00000420127	48.5
P51532	Transcription activator BRG1	184.5	7.88	-0.84	9606.ENSP00000350720	15.9

P51570	Galactokinase	42.2	6.46	-0.08	9606.ENSP00000225614	n.a.
P51610	Host cell factor 1	208.6	7.46	-0.09	9606.ENSP00000309555	77.4
P51665	26S proteasome non-ATPase regulatory subunit 7	37	6.77	-0.52	9606.ENSP00000219313	n.a.
P51784	Ubiquitin carboxyl-terminal hydrolase 11	109.7	5.45	-0.52	9606.ENSP00000218348	18.9
P51812	Ribosomal protein S6 kinase alpha-3	83.7	6.89	-0.34	9606.ENSP00000368884	49.2
P52209	6-phosphogluconate dehydrogenase, decarboxylating	53.1	7.23	-0.15	9606.ENSP00000270776	1164
P52272	Heterogeneous nuclear ribonucleoprotein M	77.5	8.7	-0.34	9606.ENSP00000325376	1362
P52292	Importin subunit alpha-1	57.8	5.4	-0.14	9606.ENSP00000332455	160
P52564	Dual specificity mitogen-activated protein kinase kinase 6	37.5	7.39	-0.28	9606.ENSP00000468348	n.a.
P52565	Rho GDP-dissociation inhibitor 1	23.2	5.11	-0.69	9606.ENSP00000269321	1773
P52701	DNA mismatch repair protein Msh6	152.7	6.9	-0.50	9606.ENSP00000234420	45
P52732	Kinesin-like protein KIF11	119.1	5.64	-0.54	9606.ENSP00000260731	1.3
P52789	Hexokinase-2	102.3	6.05	-0.19	9606.ENSP00000290573	21.6
P52888	Thimet oligopeptidase	78.8	6.05	-0.47	9606.ENSP00000304467	43.5
P52907	F-actin-capping protein subunit alpha-1	32.9	5.69	-0.67	9606.ENSP00000263168	1757
P53004	Biliverdin reductase A	33.4	6.44	-0.22	9606.ENSP00000265523	9.55
P53367	Arfaptin-1	41.7	6.7	-0.53	9606.ENSP00000296557	49.5
P53384	Cytosolic Fe-S cluster assembly factor NUBP1	34.5	5.33	-0.16	9606.ENSP00000283027	4.3
P53396	ATP-citrate synthase	120.8	7.33	-0.11	9606.ENSP00000253792	451
P53602	Diphosphomevalonate decarboxylase	43.4	7.23	-0.10	9606.ENSP00000301012	n.a.
P53618	Coatomer subunit beta	107.1	6.05	-0.09	9606.ENSP00000249923	62.8
P53621	Coatomer subunit alpha	138.3	7.66	-0.29	9606.ENSP00000357048	203
P53992	Protein transport protein Sec24C	118.2	7.06	-0.23	9606.ENSP00000321845	38.6
P53999	Activated RNA polymerase II transcriptional coactivator p15	14.4	9.6	-1.09	9606.ENSP00000265073	4011
P54136	Arginine--tRNA ligase, cytoplasmic	75.3	6.68	-0.28	9606.ENSP00000231572	95.5
P54577	Tyrosine--tRNA ligase, cytoplasmic	59.1	7.05	-0.36	9606.ENSP00000362576	474
P54687	Branched-chain-amino-acid aminotransferase, cytosolic	42.9	5.3	-0.17	9606.ENSP00000443459	n.a.
P55036	26S proteasome non-ATPase regulatory subunit 4	40.7	4.79	-0.46	9606.ENSP00000357879	640
P55039	Developmentally-regulated GTP-binding protein 2	40.7	8.88	-0.14	9606.ENSP00000225729	24.5
P55060	Exportin-2	110.3	5.77	-0.03	9606.ENSP00000262982	432
P55072	Transitional endoplasmic reticulum ATPase	89.3	5.26	-0.35	9606.ENSP00000351777	662
P55209	Nucleosome assembly protein 1-like 1	45.3	4.46	-0.95	9606.ENSP00000261182	n.a.
P55210	Caspase-7	34.3	6.07	-0.51	9606.ENSP00000358327	108
P55263	Adenosine kinase	40.5	6.7	-0.32	9606.ENSP00000286621	39.4
P55786	Puromycin-sensitive aminopeptidase	103.2	5.72	-0.19	9606.ENSP00000320324	117
P55795	Heterogeneous nuclear ribonucleoprotein H2	49.2	6.3	-0.60	9606.ENSP00000361927	1610
P55884	Eukaryotic translation initiation factor 3 subunit B	92.4	5	-0.63	9606.ENSP00000354125	603
P56192	Methionine--tRNA ligase, cytoplasmic	101.1	6.16	-0.24	9606.ENSP00000262027	122
P56537	Eukaryotic translation initiation factor 6	26.6	4.68	0.09	9606.ENSP00000363559	420
P56545	C-terminal-binding protein 2	48.9	6.95	-0.22	9606.ENSP00000311825	3.27
P57076	UPF0769 protein C21orf59	33.2	7.44	-0.69	9606.ENSP00000290155	n.a.
P57737	Coronin-7	100.5	5.8	-0.25	9606.ENSP00000460885	n.a.
P59998	Actin-related protein 2/3 complex subunit 4	19.7	8.43	-0.13	9606.ENSP00000388169	21.6
P60174	Triosephosphate isomerase	30.8	5.92	-0.17	9606.ENSP00000229270	7501
P60228	Eukaryotic translation initiation factor 3 subunit E	52.2	6.04	-0.33	9606.ENSP00000220849	26.4
P60510	Serine/threonine-protein phosphatase 4 catalytic subunit	35.1	5.06	-0.17	9606.ENSP00000279387	7.51
P60660	Myosin light polypeptide 6	16.9	4.65	-0.39	9606.ENSP00000446714	110
P60709	Actin, cytoplasmic 1	41.7	5.48	-0.20	9606.ENSP00000349960	2.11
P60842	Eukaryotic initiation factor 4A-I	46.1	5.48	-0.26	9606.ENSP00000293831	2641
P60866	40S ribosomal protein S20	13.4	9.94	-0.40	9606.ENSP00000429374	5983
P60900	Proteasome subunit alpha type-6	27.4	6.76	-0.18	9606.ENSP00000261479	772
P61006	Ras-related protein Rab-8A	23.7	9.07	-0.38	9606.ENSP00000300935	43.8
P61011	Signal recognition particle 54 kDa protein	55.7	8.75	-0.24	9606.ENSP00000216774	163
P61019	Ras-related protein Rab-2A	23.5	6.54	-0.35	9606.ENSP00000262646	242
P61026	Ras-related protein Rab-10	22.5	8.38	-0.33	9606.ENSP00000264710	330
P61081	NEDD8-conjugating enzyme Ubc12	20.9	7.69	-0.52	9606.ENSP00000253023	416
P61088	Ubiquitin-conjugating enzyme E2 N	17.1	6.57	-0.27	9606.ENSP00000316176	2821
P61158	Actin-related protein 3	47.3	5.88	-0.27	9606.ENSP00000263238	158
P61160	Actin-related protein 2	44.7	6.74	-0.18	9606.ENSP00000367220	291
P61163	Alpha-centractin	42.6	6.64	-0.28	9606.ENSP00000358921	282
P61204	ADP-ribosylation factor 3	20.6	7.43	-0.25	9606.ENSP00000256682	414
P61221	ATP-binding cassette sub-family E member 1	67.3	8.34	-0.19	9606.ENSP00000296577	37.4
P61247	40S ribosomal protein S3a	29.9	9.73	-0.62	9606.ENSP00000346050	2304
P61254	60S ribosomal protein L26	17.2	10.55	-1.11	9606.ENSP00000293842	5124
P61289	Proteasome activator complex subunit 3	29.5	5.95	-0.37	9606.ENSP00000293362	150
P61313	60S ribosomal protein L15	24.1	11.62	-0.93	9606.ENSP00000309334	3695
P61353	60S ribosomal protein L27	15.8	10.56	-0.64	9606.ENSP00000253788	10.1
P61586	Transforming protein RhoA	21.8	6.1	-0.37	9606.ENSP00000400175	92
P61758	Prefoldin subunit 3	22.6	7.11	-0.71	9606.ENSP00000286428	n.a.
P61923	Coatomer subunit zeta-1	20.2	4.81	-0.05	9606.ENSP00000262061	n.a.
P61978	Heterogeneous nuclear ribonucleoprotein K	50.9	5.54	-0.70	9606.ENSP00000365439	2167
P62081	40S ribosomal protein S7	22.1	10.1	-0.46	9606.ENSP00000339095	3377
P62136	Serine/threonine-protein phosphatase PP1-alpha catalytic subunit	37.5	6.33	-0.30	9606.ENSP00000326031	284
P62140	Serine/threonine-protein phosphatase PP1-beta catalytic subunit	37.2	6.19	-0.24	9606.ENSP00000296122	389
P62158	Calmodulin	16.8	4.22	-0.65	9606.ENSP00000349467	456
P62191	26S protease regulatory subunit 4	49.2	6.21	-0.54	9606.ENSP00000261303	276
P62195	26S protease regulatory subunit 8	45.6	7.55	-0.32	9606.ENSP00000310572	478

P62241	40S ribosomal protein S8	24.2	10.32	-1.02	9606.ENSP00000379888	n.a.
P62249	40S ribosomal protein S16	16.4	10.21	-0.44	9606.ENSP00000251453	2919
P62258	14-3-3 protein epsilon	29.2	4.74	-0.54	9606.ENSP00000264335	460
P62263	40S ribosomal protein S14	16.3	10.05	-0.50	9606.ENSP00000311028	2224
P62269	40S ribosomal protein S18	17.7	10.99	-0.71	9606.ENSP00000393241	802
P62280	40S ribosomal protein S11	18.4	10.3	-0.61	9606.ENSP00000270625	2544
P62304	Small nuclear ribonucleoprotein E	10.8	9.44	-0.35	9606.ENSP00000400591	n.a.
P62316	Small nuclear ribonucleoprotein Sm D2	13.5	9.91	-0.71	9606.ENSP00000342374	706
P62318	Small nuclear ribonucleoprotein Sm D3	13.9	10.32	-0.43	9606.ENSP00000215829	n.a.
P62333	26S protease regulatory subunit 10B	44.1	7.49	-0.44	9606.ENSP00000401802	542
P62424	60S ribosomal protein L7a	30	10.61	-0.55	9606.ENSP00000361076	969
P62701	40S ribosomal protein S4, X isoform	29.6	10.15	-0.33	9606.ENSP00000362744	5852
P62753	40S ribosomal protein S6	28.7	10.84	-0.95	9606.ENSP00000369757	159
P62805	Histone H4	11.4	11.36	-0.52	9606.ENSP00000367034	2043
P62826	GTP-binding nuclear protein Ran	24.4	7.49	-0.27	9606.ENSP00000376176	3886
P62829	60S ribosomal protein L23	14.9	10.51	-0.19	9606.ENSP00000377865	190
P62847	40S ribosomal protein S24	15.4	10.78	-0.99	9606.ENSP00000414321	548
P62851	40S ribosomal protein S25	13.7	10.11	-0.86	9606.ENSP00000435096	298
P62913	60S ribosomal protein L11	20.2	9.6	-0.53	9606.ENSP00000363676	1047
P62937	Peptidyl-prolyl cis-trans isomerase A	18	7.81	-0.32	9606.ENSP00000419425	8785
P63104	14-3-3 protein zeta/delta	27.7	4.79	-0.62	9606.ENSP00000309503	2334
P63172	Dynein light chain Tctex-type 1	12.4	5.08	-0.09	9606.ENSP00000356056	101
P63208	S-phase kinase-associated protein 1	18.6	4.54	-0.72	9606.ENSP00000231487	394
P63241	Eukaryotic translation initiation factor 5A-1	16.8	5.24	-0.26	9606.ENSP00000336702	4775
P63244	Guanine nucleotide-binding protein subunit beta-2-like 1	35.1	7.69	-0.25	9606.ENSP00000426909	1644
P67775	Serine/threonine-protein phosphatase 2A catalytic subunit alpha isoform	35.6	5.54	-0.43	9606.ENSP00000418447	119
P67870	Casein kinase II subunit beta	24.9	5.55	-0.46	9606.ENSP00000365025	20.2
P68032	Actin, alpha cardiac muscle 1	42	5.39	-0.23	9606.ENSP00000290378	1030
P68104	Elongation factor 1-alpha 1	50.1	9.01	-0.26	9606.ENSP00000330054	5587
P68363	Tubulin alpha-1B chain	50.1	5.06	-0.23	9606.ENSP00000336799	n.a.
P68371	Tubulin beta-4B chain	49.8	4.89	-0.36	9606.ENSP00000341289	1765
P68400	Casein kinase II subunit alpha	45.1	7.74	-0.48	9606.ENSP00000217244	437
P68402	Platelet-activating factor acetylhydrolase IB subunit beta	25.6	5.92	-0.30	9606.ENSP00000435289	146
P78344	Eukaryotic translation initiation factor 4 gamma 2	102.3	7.14	-0.47	9606.ENSP00000340281	9.03
P78347	General transcription factor II-I	112.3	6.39	-0.53	9606.ENSP00000322542	93
P78371	T-complex protein 1 subunit beta	57.5	6.46	-0.01	9606.ENSP00000299300	41.3
P78406	mRNA export factor	40.9	7.83	-0.48	9606.ENSP00000360286	220
P78417	Glutathione S-transferase omega-1	27.5	6.6	-0.38	9606.ENSP00000358727	242
P78527	DNA-dependent protein kinase catalytic subunit	468.8	7.12	-0.20	9606.ENSP00000313420	65.4
P83731	60S ribosomal protein L24	17.8	11.25	-0.93	9606.ENSP00000377640	180
P84085	ADP-ribosylation factor 5	20.5	6.79	-0.20	9606.ENSP00000000233	161
P84095	Rho-related GTP-binding protein RhoG	21.3	8.12	-0.21	9606.ENSP00000339467	72.5
P84103	Serine/arginine-rich splicing factor 3	19.3	11.65	-1.52	9606.ENSP00000362820	3037
P85037	Forkhead box protein K1	75.4	9.32	-0.17	9606.ENSP00000328720	n.a.
Q00341	Vigilin	141.4	6.87	-0.50	9606.ENSP00000312042	100
Q00403	Transcription initiation factor IIB	34.8	8.35	-0.27	9606.ENSP00000359531	34.8
Q00535	Cyclin-dependent-like kinase 5	33.3	7.66	-0.31	9606.ENSP00000419782	n.a.
Q00610	Clathrin heavy chain 1	191.5	5.69	-0.24	9606.ENSP00000269122	697
Q00839	Heterogeneous nuclear ribonucleoprotein U	90.5	6	-0.98	9606.ENSP00000283179	765
Q01130	Serine/arginine-rich splicing factor 2	25.5	11.85	-1.62	9606.ENSP00000353089	314
Q01433	AMP deaminase 2	100.6	6.93	-0.48	9606.ENSP00000256578	n.a.
Q01518	Adenylyl cyclase-associated protein 1	51.9	8.06	-0.35	9606.ENSP00000361878	263
Q01581	Hydroxymethylglutaryl-CoA synthase, cytoplasmic	57.3	5.41	-0.28	9606.ENSP00000322706	51.9
Q01813	ATP-dependent 6-phosphofructokinase, platelet type	85.5	7.55	-0.15	9606.ENSP00000370517	226
Q02790	Peptidyl-prolyl cis-trans isomerase FKBP4	51.8	5.43	-0.64	9606.ENSP00000001008	1279
Q02878	60S ribosomal protein L6	32.7	10.58	-0.73	9606.ENSP00000202773	4190
Q04637	Eukaryotic translation initiation factor 4 gamma 1	175.4	5.33	-0.65	9606.ENSP00000338020	375
Q04726	Transducin-like enhancer protein 3	83.4	7.2	-0.49	9606.ENSP00000452871	11.9
Q04760	Lactoylglutathione lyase	20.8	5.31	-0.52	9606.ENSP00000362463	2650
Q06203	Amidophosphoribosyltransferase	57.4	6.76	-0.17	9606.ENSP00000264220	43.6
Q06210	Glutamine--fructose-6-phosphate aminotransferase [isomerizing] 1	78.8	7.11	-0.28	9606.ENSP00000354347	237
Q06830	Peroxiredoxin-1	22.1	8.13	-0.26	9606.ENSP00000262746	16246
Q07020	60S ribosomal protein L18	21.6	11.72	-0.72	9606.ENSP00000447001	661
Q07021	Complement component 1 Q subcomponent-binding protein, mitochondrial	31.3	4.84	-0.46	9606.ENSP00000225698	1795
Q07666	KH domain-containing, RNA-binding, signal transduction-associated protein 1	48.2	8.66	-0.81	9606.ENSP00000313829	1236
Q07864	DNA polymerase epsilon catalytic subunit A	261.4	6.39	-0.35	9606.ENSP00000322570	n.a.
Q07866	Kinesin light chain 1	65.3	6.2	-0.88	9606.ENSP00000414982	38.2
Q07955	Serine/arginine-rich splicing factor 1	27.7	10.36	-1.15	9606.ENSP00000258962	3556
Q08211	ATP-dependent RNA helicase A	140.9	6.84	-0.34	9606.ENSP00000356520	722
Q08752	Peptidyl-prolyl cis-trans isomerase D	40.7	7.21	-0.43	9606.ENSP00000303754	188
Q08J23	tRNA (cytosine(34)-C(5))-methyltransferase	86.4	6.77	-0.57	9606.ENSP00000264670	135
Q09028	Histone-binding protein RBBP4	47.6	4.89	-0.56	9606.ENSP00000362592	655
Q09161	Nuclear cap-binding protein subunit 1	91.8	6.43	-0.33	9606.ENSP00000364289	68.1
Q0VDF9	Heat shock 70 kDa protein 14	54.8	5.59	-0.07	9606.ENSP00000367623	n.a.

Q10567	AP-1 complex subunit beta-1	104.6	5.06	-0.05	9606.ENSP00000350199	45.5
Q10570	Cleavage and polyadenylation specificity factor subunit 1	160.8	6.4	-0.21	9606.ENSP00000339353	3.84
Q12756	Kinesin-like protein KIF1A	190.9	6.21	-0.50	9606.ENSP00000322791	n.a.
Q12789	General transcription factor 3C polypeptide 1	238.7	7.3	-0.54	9606.ENSP00000348510	1.12
Q12824	SWI/SNF-related matrix-associated actin-dependent regulator of chromatin subfamily B member 1	44.1	6.23	-0.58	9606.ENSP00000263121	44.5
Q12874	Splicing factor 3A subunit 3	58.8	5.38	-0.92	9606.ENSP00000362110	360
Q12888	Tumor suppressor p53-binding protein 1	213.4	4.7	-0.70	9606.ENSP00000371475	17.5
Q12904	Aminoacyl tRNA synthase complex-interacting multifunctional protein 1	34.3	8.43	-0.52	9606.ENSP00000378191	137
Q12996	Cleavage stimulation factor subunit 3	82.9	8.12	-0.48	9606.ENSP00000315791	23.6
Q13033	Striatin-3	87.2	5.36	-0.56	9606.ENSP00000350071	13.5
Q13043	Serine/threonine-protein kinase 4	55.6	5.07	-0.61	9606.ENSP00000361892	n.a.
Q13045	Protein flightless-1 homolog	144.7	6.05	-0.44	9606.ENSP00000324573	2.78
Q13057	Bifunctional coenzyme A synthase	62.3	6.99	-0.06	9606.ENSP00000464814	32.1
Q13085	Acetyl-CoA carboxylase 1	265.4	6.37	-0.25	9606.ENSP00000344789	37.4
Q13123	Protein Red	65.6	6.64	-1.43	9606.ENSP00000396301	277
Q13126	S-methyl-5'-thioadenosine phosphorylase	31.2	7.18	-0.15	9606.ENSP00000369519	2.91
Q13148	TAR DNA-binding protein 43	44.7	6.19	-0.53	9606.ENSP00000240185	440
Q13155	Aminoacyl tRNA synthase complex-interacting multifunctional protein 2	35.3	8.22	-0.14	9606.ENSP00000223029	105
Q13185	Chromobox protein homolog 3	20.8	5.33	-0.97	9606.ENSP00000336687	1354
Q13200	26S proteasome non-ATPase regulatory subunit 2	100.1	5.2	-0.17	9606.ENSP00000310129	356
Q13247	Serine/arginine-rich splicing factor 6	39.6	11.43	-1.55	9606.ENSP00000244020	500
Q13263	Transcription intermediary factor 1-beta	88.5	5.77	-0.39	9606.ENSP00000253024	1626
Q13283	Ras GTPase-activating protein-binding protein 1	52.1	5.52	-0.83	9606.ENSP00000348578	538
Q13310	Polyadenylate-binding protein 4	70.7	9.26	-0.44	9606.ENSP00000361949	280
Q13330	Metastasis-associated protein MTA1	80.7	9.26	-0.62	9606.ENSP00000333633	n.a.
Q13347	Eukaryotic translation initiation factor 3 subunit I	36.5	5.64	-0.42	9606.ENSP00000362688	741
Q13409	Cytoplasmic dynein 1 intermediate chain 2	71.4	5.2	-0.64	9606.ENSP00000380308	69
Q13428	Treacle protein	152	9.04	-0.91	9606.ENSP00000421655	127
Q13435	Splicing factor 3B subunit 2	100.2	5.67	-0.99	9606.ENSP00000318861	179
Q13451	Peptidyl-prolyl cis-trans isomerase FKBP5	51.2	5.9	-0.68	9606.ENSP00000338160	47.1
Q13547	Histone deacetylase 1	55.1	5.48	-0.71	9606.ENSP00000362649	504
Q13561	Dynactin subunit 2	44.2	5.21	-0.52	9606.ENSP00000408910	n.a.
Q13564	NEDD8-activating enzyme E1 regulatory subunit	60.2	5.4	-0.33	9606.ENSP00000290810	87.8
Q13576	Ras GTPase-activating-like protein IQGAP2	180.5	5.64	-0.48	9606.ENSP00000274364	10.7
Q13596	Sorting nexin-1	59	5.15	-0.65	9606.ENSP00000453785	n.a.
Q13616	Cullin-1	89.6	8	-0.52	9606.ENSP00000326804	129
Q13625	Apoptosis-stimulating of p53 protein 2	125.5	6.07	-0.76	9606.ENSP00000341957	n.a.
Q13685	Angio-associated migratory cell protein	46.7	4.42	-0.24	9606.ENSP00000248450	28.3
Q13765	Nascent polypeptide-associated complex subunit alpha	23.4	4.56	-0.66	9606.ENSP00000448035	507
Q13885	Tubulin beta-2A chain	49.9	4.89	-0.41	9606.ENSP00000369703	1234
Q13907	Isopentenyl-diphosphate Delta-isomerase 1	26.3	6.34	-0.45	9606.ENSP00000370748	n.a.
Q14008	Cytoskeleton-associated protein 5	225.4	7.8	-0.36	9606.ENSP00000432768	8.68
Q14137	Ribosome biogenesis protein BOP1	83.6	6.19	-0.50	9606.ENSP00000304151	10.7
Q14157	Ubiquitin-associated protein 2-like	114.5	7.11	-0.74	9606.ENSP00000355343	183
Q14160	Protein scribble homolog	174.8	5.07	-0.45	9606.ENSP00000349486	0.458
Q14166	Tubulin--tyrosine ligase-like protein 12	74.4	5.53	-0.39	9606.ENSP00000216129	85.8
Q14203	Dynactin subunit 1	141.6	5.81	-0.56	9606.ENSP00000354791	31.9
Q14204	Cytoplasmic dynein 1 heavy chain 1	532.1	6.4	-0.34	9606.ENSP00000348965	95.5
Q14498	RNA-binding protein 39	59.3	10.1	-0.65	9606.ENSP00000253363	87.6
Q14558	Phosphoribosyl pyrophosphate synthase-associated protein 1	39.4	7.2	-0.01	9606.ENSP00000414624	n.a.
Q14566	DNA replication licensing factor MCM6	92.8	5.41	-0.38	9606.ENSP00000264156	245
Q14669	E3 ubiquitin-protein ligase TRIP12	220.3	8.48	-0.51	9606.ENSP00000283943	0.136
Q14677	Clathrin interactor 1	68.2	6.42	-0.65	9606.ENSP00000429824	291
Q14683	Structural maintenance of chromosomes protein 1A	143.1	7.64	-0.97	9606.ENSP00000323421	51.3
Q14691	DNA replication complex GINS protein PSF1	23	7.39	-0.53	9606.ENSP00000262460	n.a.
Q14697	Neutral alpha-glucosidase AB	106.8	6.14	-0.36	9606.ENSP00000340466	316
Q14738	Serine/threonine-protein phosphatase 2A 56 kDa regulatory subunit delta isoform	69.9	8.13	-0.53	9606.ENSP00000417963	6.76
Q14839	Chromodomain-helicase-DNA-binding protein 4	217.9	5.86	-0.83	9606.ENSP00000349508	66.8
Q14974	Importin subunit beta-1	97.1	4.78	-0.09	9606.ENSP00000290158	173
Q14980	Nuclear mitotic apparatus protein 1	238.1	5.78	-0.92	9606.ENSP00000377298	30.4
Q14997	Proteasome activator complex subunit 4	211.2	6.9	-0.17	9606.ENSP00000384211	2.36
Q14C86	GTPase-activating protein and VPS9 domain-containing protein 1	164.9	5.22	-0.47	9606.ENSP00000377665	3.66
Q15003	Condensin complex subunit 2	82.5	5.06	-0.67	9606.ENSP00000240423	52
Q15007	Pre-mRNA-splicing regulator WTAP	44.2	5.19	-1.00	9606.ENSP00000351141	n.a.
Q15008	26S proteasome non-ATPase regulatory subunit 6	45.5	5.62	-0.36	9606.ENSP00000295901	145
Q15019	Septin-2	41.5	6.6	-0.53	9606.ENSP00000353157	127
Q15021	Condensin complex subunit 1	157.1	6.61	-0.26	9606.ENSP00000325017	42.5
Q15029	116 kDa U5 small nuclear ribonucleoprotein component	109.4	5	-0.25	9606.ENSP00000392094	289
Q15042	Rab3 GTPase-activating protein catalytic subunit	110.5	5.55	-0.44	9606.ENSP00000411418	3.43
Q15046	Lysine--tRNA ligase	68	6.35	-0.45	9606.ENSP00000325448	379
Q15054	DNA polymerase delta subunit 3	51.4	9.35	-0.85	9606.ENSP00000263681	41.3
Q15102	Platelet-activating factor acetylhydrolase IB subunit gamma	25.7	6.84	-0.35	9606.ENSP00000262890	51.6
Q15126	Phosphomevalonate kinase	22	5.73	-0.43	9606.ENSP00000357452	23.2
Q15181	Inorganic pyrophosphatase	32.6	5.86	-0.52	9606.ENSP00000362329	5188

Q15185	Prostaglandin E synthase 3	18.7	4.54	-1.05	9606.ENSP00000262033	410
Q15287	RNA-binding protein with serine-rich domain 1	34.2	11.84	-1.57	9606.ENSP00000301730	1006
Q15365	Poly(rC)-binding protein 1	37.5	7.09	-0.11	9606.ENSP00000305556	1496
Q15366	Poly(rC)-binding protein 2	38.6	6.79	-0.14	9606.ENSP00000352438	693
Q15382	GTP-binding protein Rheb	20.5	5.92	-0.09	9606.ENSP00000262187	n.a.
Q15393	Splicing factor 3B subunit 3	135.5	5.26	-0.17	9606.ENSP00000305790	152
Q15398	Disks large-associated protein 5	95.1	9	-0.79	9606.ENSP00000247191	0.479
Q15418	Ribosomal protein S6 kinase alpha-1	82.7	7.83	-0.36	9606.ENSP00000435412	0.087
Q15428	Splicing factor 3A subunit 2	49.2	9.64	-0.72	9606.ENSP00000221494	49.7
Q15436	Protein transport protein Sec23A	86.1	7.08	-0.24	9606.ENSP00000306881	190
Q15459	Splicing factor 3A subunit 1	88.8	5.22	-0.74	9606.ENSP00000215793	587
Q15555	Microtubule-associated protein RP/EB family member 2	37	5.57	-0.77	9606.ENSP00000300249	97.9
Q15631	Translin	26.2	6.44	-0.19	9606.ENSP00000374332	158
Q15691	Microtubule-associated protein RP/EB family member 1	30	5.14	-0.43	9606.ENSP00000364721	59.6
Q15717	ELAV-like protein 1	36.1	9.17	-0.36	9606.ENSP00000385269	679
Q15773	Myeloid leukemia factor 2	28.1	6.9	-0.88	9606.ENSP00000203630	n.a.
Q15785	Mitochondrial import receptor subunit TOM34	34.5	8.98	-0.61	9606.ENSP00000361900	n.a.
Q15813	Tubulin-specific chaperone E	59.3	6.76	-0.33	9606.ENSP00000355560	107
Q15819	Ubiquitin-conjugating enzyme E2 variant 2	16.4	8.09	-0.57	9606.ENSP00000428209	267
Q15836	Vesicle-associated membrane protein 3	11.3	8.79	-0.06	9606.ENSP00000054666	n.a.
Q15907	Ras-related protein Rab-11B	24.5	5.94	-0.44	9606.ENSP00000333547	135
Q16181	Septin-7	50.6	8.63	-0.79	9606.ENSP00000381992	30
Q16222	UDP-N-acetylhexosamine pyrophosphorylase	58.7	6.33	-0.31	9606.ENSP00000356903	4.64
Q16512	Serine/threonine-protein kinase N1	103.9	6.37	-0.38	9606.ENSP00000343325	n.a.
Q16513	Serine/threonine-protein kinase N2	112	6.3	-0.50	9606.ENSP00000359552	66.5
Q16539	Mitogen-activated protein kinase 14	41.3	5.78	-0.26	9606.ENSP00000229794	n.a.
Q16543	Hsp90 co-chaperone Cdc37	44.4	5.25	-0.97	9606.ENSP00000222005	31.4
Q16555	Dihydropyrimidinase-related protein 2	62.3	6.38	-0.26	9606.ENSP00000309539	228
Q16576	Histone-binding protein RBBP7	47.8	5.05	-0.53	9606.ENSP00000369424	755
Q16629	Serine/arginine-rich splicing factor 7	27.4	11.82	-1.40	9606.ENSP00000325905	4038
Q16630	Cleavage and polyadenylation specificity factor subunit 6	59.2	7.15	-0.97	9606.ENSP00000391774	46.5
Q16637	Survival motor neuron protein	31.8	6.55	-0.77	9606.ENSP00000370119	5.68
Q16644	MAP kinase-activated protein kinase 3	43	7.28	-0.58	9606.ENSP00000350639	n.a.
Q16658	Fascin	54.5	7.24	-0.45	9606.ENSP00000371798	96.6
Q16740	ATP-dependent Clp protease proteolytic subunit, mitochondrial	30.2	8.09	-0.07	9606.ENSP00000245816	52.3
Q16763	Ubiquitin-conjugating enzyme E2 S	23.8	8.38	-0.42	9606.ENSP00000264552	n.a.
Q16881	Thioredoxin reductase 1, cytoplasmic	70.9	7.39	-0.22	9606.ENSP00000434516	188
Q1KMD3	Heterogeneous nuclear ribonucleoprotein U-like protein 2	85.1	4.91	-1.08	9606.ENSP00000301785	453
Q27J81	Inverted formin-2	135.5	5.38	-0.40	9606.ENSP00000376410	0.207
Q29RF7	Sister chromatid cohesion protein PDS5 homolog A	150.7	7.91	-0.34	9606.ENSP00000303427	12.6
Q2NKX8	DNA excision repair protein ERCC-6-like	141	5.31	-0.55	9606.ENSP00000334675	13.1
Q2NL82	Pre-rRNA-processing protein TSR1 homolog	91.8	7.42	-0.59	9606.ENSP00000301364	n.a.
Q2TAL8	Glutamine-rich protein 1	86.4	5.87	-0.46	9606.ENSP00000350094	2.97
Q2VPK5	Cytoplasmic tRNA 2-thiolation protein 2	56.1	6.32	-0.23	9606.ENSP00000388320	n.a.
Q3LXA3	Triokinase/FMN cyclase	58.9	7.49	0.22	9606.ENSP00000378360	n.a.
Q52LJ0	Protein FAM98B	37.2	6.29	-0.32	9606.ENSP00000380734	35
Q53H96	Pyrroline-5-carboxylate reductase 3	28.6	7.72	0.25	9606.ENSP00000220966	37
Q5H9R7	Serine/threonine-protein phosphatase 6 regulatory subunit 3	97.6	4.6	-0.48	9606.ENSP00000377390	10.3
Q5JSH3	WD repeat-containing protein 44	101.3	5.45	-0.67	9606.ENSP00000254029	4.14
Q5JSZ5	Protein PRRC2B	242.8	8.34	-0.97	9606.ENSP00000349856	2.12
Q5RKV6	Exosome complex component MTR3	28.2	6.28	-0.17	9606.ENSP00000398597	n.a.
Q5SRE5	Nucleoporin NUP188 homolog	195.9	6.73	-0.01	9606.ENSP00000361658	0.423
Q5SW79	Centrosomal protein of 170 kDa	175.2	7.11	-0.93	9606.ENSP00000355500	9.85
Q5T4S7	E3 ubiquitin-protein ligase UBR4	573.5	6.04	-0.20	9606.ENSP00000364403	11.6
Q5TBB1	Ribonuclease H2 subunit B	35.1	9.13	-0.46	9606.ENSP00000337623	107
Q5VT52	Regulation of nuclear pre-mRNA domain-containing protein 2	155.9	7.42	-0.65	9606.ENSP00000358064	6.15
Q5VTR2	E3 ubiquitin-protein ligase BRE1A	113.6	5.94	-1.04	9606.ENSP00000373772	18.6
Q5VYK3	Proteasome-associated protein ECM29 homolog	204.2	7.12	-0.13	9606.ENSP00000259335	15.7
Q641Q2	WASH complex subunit FAM21A	147.1	4.81	-0.91	9606.ENSP00000351259	n.a.
Q68E01	Integrator complex subunit 3	118	5.8	-0.26	9606.ENSP00000318641	0.056
Q68EM7	Rho GTPase-activating protein 17	95.4	7.62	-0.66	9606.ENSP00000289968	n.a.
Q6IN85	Serine/threonine-protein phosphatase 4 regulatory subunit 3A	95.3	4.94	-0.44	9606.ENSP00000337125	11.5
Q6NW29	RWD domain-containing protein 4	21.2	5.31	-0.77	9606.ENSP00000388920	54.8
Q6NXE6	Armadillo repeat-containing protein 6	54.1	6.24	-0.09	9606.ENSP00000376148	75.7
Q6NYC1	Bifunctional arginine demethylase and lysyl-hydroxylase JMJD6	46.4	8.69	-0.88	9606.ENSP00000394085	27.5
Q6NZ67	Mitotic-spindle organizing protein 2B	16.2	10.15	-0.31	9606.ENSP00000281871	n.a.
Q6P1J9	Parafibromin	60.5	9.61	-0.58	9606.ENSP00000356405	10.1
Q6P1N0	Coiled-coil and C2 domain-containing protein 1A	104	8.09	-0.64	9606.ENSP00000313601	12.3
Q6P1N9	Putative deoxyribonuclease TATDN1	33.6	6.96	-0.32	9606.ENSP00000276692	n.a.
Q6P2E9	Enhancer of mRNA-decapping protein 4	151.6	5.86	-0.31	9606.ENSP00000351811	67
Q6P2Q9	Pre-mRNA-processing-splicing factor 8	273.4	8.84	-0.47	9606.ENSP00000304350	189
Q6P996	Pyridoxal-dependent decarboxylase domain-containing protein 1	86.7	5.38	-0.28	9606.ENSP00000379691	11.2
Q6PD62	RNA polymerase-associated protein CTR9 homolog	133.4	6.77	-0.89	9606.ENSP00000355013	11.3
Q6PGP7	Tetratricopeptide repeat protein 37	175.4	7.53	-0.27	9606.ENSP00000351596	n.a.
Q6PID6	Tetratricopeptide repeat protein 33	29.4	5.44	-0.50	9606.ENSP00000338533	n.a.
Q6PJG6	BRCA1-associated ATM activator 1	88.1	5.27	0.11	9606.ENSP00000339637	n.a.
Q6PKG0	La-related protein 1	123.4	8.82	-1.04	9606.ENSP00000336721	165

Q6VMQ6	Activating transcription factor 7-interacting protein 1	136.3	4.7	-0.65	9606.ENSP00000261168	n.a.
Q6Y7W6	PERQ amino acid-rich with GYF domain-containing protein 2	150	5.54	-1.23	9606.ENSP00000387170	60.8
Q6YP21	Kynurenine--oxoglutarate transaminase 3	51.4	8.19	-0.18	9606.ENSP00000260508	2.6
Q70CQ2	Ubiquitin carboxyl-terminal hydrolase 34	404	5.82	-0.33	9606.ENSP00000381577	n.a.
Q71RC2	La-related protein 4	80.5	6.61	-0.75	9606.ENSP00000381490	2.74
Q71U36	Tubulin alpha-1A chain	50.1	5.06	-0.23	9606.ENSP00000301071	101
Q7KZ85	Transcription elongation factor SPT6	198.9	4.91	-0.86	9606.ENSP00000319104	42.5
Q7KZF4	Staphylococcal nuclease domain-containing protein 1	101.9	7.17	-0.43	9606.ENSP00000346762	527
Q7KZI7	Serine/threonine-protein kinase MARK2	87.9	9.72	-0.68	9606.ENSP00000385751	5.56
Q7L014	Probable ATP-dependent RNA helicase DDX46	117.3	9.29	-0.93	9606.ENSP00000346236	171
Q7L1Q6	Basic leucine zipper and W2 domain-containing protein 1	48	5.92	-0.39	9606.ENSP00000394316	102
Q7L2H7	Eukaryotic translation initiation factor 3 subunit M	42.5	5.63	-0.18	9606.ENSP00000436049	57.8
Q7L5D6	Golgi to ER traffic protein 4 homolog	36.5	5.41	-0.30	9606.ENSP00000265857	112
Q7LBC6	Lysine-specific demethylase 3B	191.5	7.18	-0.50	9606.ENSP00000326563	n.a.
Q7Z2Z2	Elongation factor Tu GTP-binding domain-containing protein 1	125.3	5.91	-0.36	9606.ENSP00000268206	5.62
Q7Z3K3	Pogo transposable element with ZNF domain	155.2	7.4	-0.39	9606.ENSP00000271715	10.1
Q7Z406	Myosin-14	227.7	5.6	-0.81	9606.ENSP00000262269	1.32
Q7Z460	CLIP-associating protein 1	169.3	9.03	-0.45	9606.ENSP00000263710	5.31
Q7Z4H7	HAUS augmin-like complex subunit 6	108.6	6.47	-0.54	9606.ENSP00000369871	1.16
Q7Z4Q2	HEAT repeat-containing protein 3	74.5	5.11	-0.08	9606.ENSP00000299192	n.a.
Q7Z4S6	Kinesin-like protein KIF21A	187.1	6.42	-0.68	9606.ENSP00000354878	12.6
Q7Z5K2	Wings apart-like protein homolog	132.9	5.44	-0.68	9606.ENSP00000298767	n.a.
Q7Z6Z7	E3 ubiquitin-protein ligase HUWE1	481.6	5.22	-0.39	9606.ENSP00000262854	25.7
Q86TI2	Dipeptidyl peptidase 9	98.2	6.46	-0.38	9606.ENSP00000262960	17.3
Q86U90	YrdC domain-containing protein, mitochondrial	29.3	8.57	0.07	9606.ENSP00000362135	n.a.
Q86UY6	N-alpha-acetyltransferase 40	27.2	7.39	-0.61	9606.ENSP00000367024	8.42
Q86VP6	Cullin-associated NEDD8-dissociated protein 1	136.3	5.78	-0.02	9606.ENSP00000299218	116
Q86X55	Histone-arginine methyltransferase CARM1	65.8	6.73	-0.05	9606.ENSP00000325690	139
Q86Y37	CDK2-associated and cullin domain-containing protein 1	41	5.19	-0.38	9606.ENSP00000358147	n.a.
Q86Y56	Dynein assembly factor 5, axonemal	93.5	6.42	0.07	9606.ENSP00000297440	n.a.
Q86YP4	Transcriptional repressor p66-alpha	68	9.94	-0.50	9606.ENSP00000351552	0.566
Q86YR5	G-protein-signaling modulator 1	74.5	6.54	-0.64	9606.ENSP00000392828	n.a.
Q8IU81	Interferon regulatory factor 2-binding protein 1	61.6	8.18	-0.42	9606.ENSP00000307265	n.a.
Q8IUR0	Trafficking protein particle complex subunit 5	20.8	9.66	-0.03	9606.ENSP00000316990	n.a.
Q8IVD9	NudC domain-containing protein 3	40.8	5.25	-0.61	9606.ENSP00000347626	10.1
Q8IWJ2	GRIP and coiled-coil domain-containing protein 2	195.8	5.14	-0.90	9606.ENSP00000307939	0.77
Q8IWZ3	Ankyrin repeat and KH domain-containing protein 1	269.3	5.73	-0.38	9606.ENSP00000432016	6.22
Q8IX12	Cell division cycle and apoptosis regulator protein 1	132.7	5.76	-1.03	9606.ENSP00000265872	14.2
Q8IXM2	Chromatin complexes subunit BAP18	17.9	7.33	-0.32	9606.ENSP00000448598	n.a.
Q8IZ83	Aldehyde dehydrogenase family 16 member A1	85.1	6.79	0.01	9606.ENSP00000293350	7.64
Q8N0X7	Spartin	72.8	5.91	-0.56	9606.ENSP00000347314	12.5
Q8N163	Cell cycle and apoptosis regulator protein 2	102.8	5.22	-0.52	9606.ENSP00000310670	57.5
Q8N1F7	Nuclear pore complex protein Nup93	93.4	5.72	-0.37	9606.ENSP00000310668	14.6
Q8N1G2	Cap-specific mRNA (nucleoside-2'-O-)-methyltransferase 1	95.3	7.05	-0.45	9606.ENSP00000362550	36.1
Q8N1G4	Leucine-rich repeat-containing protein 47	63.4	8.28	-0.40	9606.ENSP00000367498	1.66
Q8N335	Glycerol-3-phosphate dehydrogenase 1-like protein	38.4	7.02	0.06	9606.ENSP00000282541	n.a.
Q8N3U4	Cohesin subunit SA-2	141.2	5.43	-0.42	9606.ENSP00000218089	27.3
Q8N5M4	Tetratricopeptide repeat protein 9C	20	8.92	-0.89	9606.ENSP00000325266	n.a.
Q8N684	Cleavage and polyadenylation specificity factor subunit 7	52	8	-0.78	9606.ENSP00000345412	64
Q8N6R0	Methyltransferase-like protein 13	78.7	6.73	-0.22	9606.ENSP00000354920	0.328
Q8N7H5	RNA polymerase II-associated factor 1 homolog	59.9	4.63	-1.16	9606.ENSP00000221265	77.2
Q8NB37	Parkinson disease 7 domain-containing protein 1	23.3	6.61	0.18	9606.ENSP00000321691	n.a.
Q8NBF2	NHL repeat-containing protein 2	79.4	5.55	-0.14	9606.ENSP00000358307	43.3
Q8NBJ5	Procollagen galactosyltransferase 1	71.6	7.31	-0.41	9606.ENSP00000252599	0.094
Q8NBJ7	Sulfatase-modifying factor 2	33.8	8	-0.56	9606.ENSP00000341938	9.74
Q8NBT2	Kinetochore protein Spc24	22.5	4.7	-0.53	9606.ENSP00000465075	n.a.
Q8NCW5	NAD(P)H-hydrate epimerase	31.7	7.66	-0.10	9606.ENSP00000357218	n.a.
Q8NDI1	EH domain-binding protein 1	139.9	5.35	-0.92	9606.ENSP00000263991	0.074
Q8NE71	ATP-binding cassette sub-family F member 1	95.9	6.8	-0.95	9606.ENSP00000313603	52.6
Q8NFF5	FAD synthase	65.2	6.93	-0.23	9606.ENSP00000292180	83.1
Q8NFH3	Nucleoporin Nup43	42.1	5.63	-0.36	9606.ENSP00000342262	n.a.
Q8NI27	THO complex subunit 2	182.7	8.44	-0.77	9606.ENSP00000245838	17.9
Q8TAQ2	SWI/SNF complex subunit SMARCC2	132.8	5.69	-0.74	9606.ENSP00000267064	37.6
Q8TAT6	Nuclear protein localization protein 4 homolog	68.1	6.38	-0.37	9606.ENSP00000331487	46.9
Q8TBC4	NEDD8-activating enzyme E1 catalytic subunit	51.8	5.45	-0.17	9606.ENSP00000354340	95.7
Q8TC07	TBC1 domain family member 15	79.4	5.67	-0.41	9606.ENSP00000448182	26.5
Q8TD19	Serine/threonine-protein kinase Nek9	107.1	5.74	-0.34	9606.ENSP00000238616	28.8
Q8TDP1	Ribonuclease H2 subunit C	17.8	5.03	-0.30	9606.ENSP00000308193	n.a.
Q8TEQ6	Gem-associated protein 5	168.5	6.62	-0.40	9606.ENSP00000285873	66.5
Q8TEX9	Importin-4	118.6	4.96	0.07	9606.ENSP00000346453	29.3
Q8WUM0	Nuclear pore complex protein Nup133	128.9	5.1	-0.24	9606.ENSP00000261396	8.76
Q8WUM4	Programmed cell death 6-interacting protein	96	6.52	-0.47	9606.ENSP00000411825	278
Q8WVB6	Chromosome transmission fidelity protein 18 homolog	107.3	7.21	-0.41	9606.ENSP00000262315	n.a.
Q8WVD3	E3 ubiquitin-protein ligase RNF138	28.2	6.93	-0.63	9606.ENSP00000261593	n.a.
Q8WVJ2	NudC domain-containing protein 2	17.7	5.07	-0.56	9606.ENSP00000304854	243
Q8WVK7	Spindle and kinetochore-associated protein 2	14.2	7.33	-0.72	9606.ENSP00000333433	n.a.
Q8WVY7	Ubiquitin-like domain-containing CTD phosphatase 1	36.8	6.46	-0.44	9606.ENSP00000296786	n.a.

Q8WWM7	Ataxin-2-like protein	113.3	8.59	-0.73	9606.ENSP00000378917	87.8
Q8WXI9	Transcriptional repressor p66-beta	65.2	9.7	-0.61	9606.ENSP00000357644	10.3
Q92499	ATP-dependent RNA helicase DDX1	82.4	7.23	-0.40	9606.ENSP00000233084	437
Q92538	Golgi-specific brefeldin A-resistance guanine nucleotide exchange factor 1	206.3	5.73	-0.26	9606.ENSP00000359000	4.16
Q92572	AP-3 complex subunit sigma-1	21.7	5.39	-0.01	9606.ENSP00000325369	185
Q92598	Heat shock protein 105 kDa	96.8	5.39	-0.57	9606.ENSP00000318687	698
Q92600	Cell differentiation protein RCD1 homolog	33.6	8.03	-0.02	9606.ENSP00000273064	n.a.
Q92615	La-related protein 4B	80.5	6.92	-0.72	9606.ENSP00000326128	1
Q92616	Translational activator GCN1	292.6	7.47	0.06	9606.ENSP00000300648	14.1
Q92620	Pre-mRNA-splicing factor ATP-dependent RNA helicase PRP16	140.4	6.54	-0.82	9606.ENSP00000268482	16.4
Q92621	Nuclear pore complex protein Nup205	227.8	6.19	-0.09	9606.ENSP00000285968	26.5
Q92793	CREB-binding protein	265.2	8.53	-0.69	9606.ENSP00000262367	5.15
Q92797	Symplekin	141.1	6.13	-0.20	9606.ENSP00000245934	8.83
Q92841	Probable ATP-dependent RNA helicase DDX17	80.2	8.27	-0.61	9606.ENSP00000380033	924
Q92878	DNA repair protein RAD50	153.8	6.89	-0.92	9606.ENSP00000265335	0.702
Q92888	Rho guanine nucleotide exchange factor 1	102.4	5.66	-0.58	9606.ENSP00000337261	3.59
Q92900	Regulator of nonsense transcripts 1	124.3	6.61	-0.35	9606.ENSP00000262803	149
Q92917	G patch domain and KOW motifs-containing protein	52.2	6.15	-0.69	9606.ENSP00000156109	n.a.
Q92922	SWI/SNF complex subunit SMARCC1	122.8	5.76	-0.81	9606.ENSP00000254480	37.8
Q92945	Far upstream element-binding protein 2	73.1	7.3	-0.77	9606.ENSP00000381216	2430
Q92973	Transportin-1	102.3	4.98	-0.12	9606.ENSP00000336712	59.6
Q93008	Probable ubiquitin carboxyl-terminal hydrolase FAF-X	292.1	5.8	-0.36	9606.ENSP00000316357	30.5
Q93009	Ubiquitin carboxyl-terminal hydrolase 7	128.2	5.55	-0.64	9606.ENSP00000343535	14.1
Q969G3	SWI/SNF-related matrix-associated actin-dependent regulator of chromatin subfamily E member 1	46.6	4.88	-1.14	9606.ENSP00000323967	62.7
Q969T4	Ubiquitin-conjugating enzyme E2 E3	22.9	7.18	-0.70	9606.ENSP00000376215	132
Q969T7	7-methylguanosine phosphate-specific 5'-nucleotidase	34.4	6.38	-0.31	9606.ENSP00000389948	n.a.
Q96A49	Synapse-associated protein 1	39.9	4.53	-0.75	9606.ENSP00000369500	767
Q96BW5	Phosphotriesterase-related protein	39	6.52	-0.22	9606.ENSP00000298942	n.a.
Q96C23	Aldose 1-epimerase	37.7	6.65	-0.32	9606.ENSP00000272252	n.a.
Q96C86	m7GpppX diphosphatase	38.6	6.38	-0.47	9606.ENSP00000263579	n.a.
Q96CS2	HAUS augmin-like complex subunit 1	31.8	5.53	-0.58	9606.ENSP00000282058	n.a.
Q96DE0	U8 snoRNA-decapping enzyme	21.3	6.89	-0.07	9606.ENSP00000422375	n.a.
Q96EA4	Protein Spindly	70.1	5.47	-0.85	9606.ENSP00000265295	n.a.
Q96EK5	KIF1-binding protein	71.8	5.49	-0.45	9606.ENSP00000354848	n.a.
Q96EY5	Multivesicular body subunit 12A	28.8	8.91	-0.10	9606.ENSP00000324810	31.1
Q96FW1	Ubiquitin thioesterase OTUB1	31.3	4.94	-0.55	9606.ENSP00000402551	682
Q96FZ2	Embryonic stem cell-specific 5-hydroxymethylcytosine-binding protein	40.5	8.15	-0.75	9606.ENSP00000372955	21.7
Q96G25	Mediator of RNA polymerase II transcription subunit 8	29.1	7.44	-0.55	9606.ENSP00000290663	n.a.
Q96G61	Diphosphoinositol polyphosphate phosphohydrolase 3-beta	18.5	5.99	-0.76	9606.ENSP00000365160	68.2
Q96GK7	Fumarylacetoacetate hydrolase domain-containing protein 2A	34.6	8.24	-0.02	9606.ENSP00000233379	16.6
Q96GX5	Serine/threonine-protein kinase greatwall	97.3	5.99	-0.50	9606.ENSP00000365107	n.a.
Q96H20	Vacuolar-sorting protein SNF8	28.8	6.65	-0.25	9606.ENSP00000421380	n.a.
Q96H79	Zinc finger CCCH-type antiviral protein 1-like	32.9	8.13	-0.26	9606.ENSP00000275766	n.a.
Q96JH7	Deubiquitinating protein VCIP135	134.2	7.2	-0.47	9606.ENSP00000309031	n.a.
Q96K76	Ubiquitin carboxyl-terminal hydrolase 47	157.2	5.08	-0.62	9606.ENSP00000339957	2.99
Q96KB5	Lymphokine-activated killer T-cell-originated protein kinase	36.1	5.12	-0.39	9606.ENSP00000301905	18.1
Q96KP4	Cytosolic non-specific dipeptidase	52.8	5.97	-0.28	9606.ENSP00000325548	26.4
Q96N67	Dedicator of cytokinesis protein 7	242.4	6.8	-0.35	9606.ENSP00000340742	4.08
Q96P16	Regulation of nuclear pre-mRNA domain-containing protein 1A	35.7	7.55	-0.64	9606.ENSP00000349955	n.a.
Q96P48	Arf-GAP with Rho-GAP domain, ANK repeat and PH domain-containing protein 1	162.1	6.23	-0.42	9606.ENSP00000377233	n.a.
Q96PU8	Protein quaking	37.6	8.56	-0.39	9606.ENSP00000355094	n.a.
Q96Q15	Serine/threonine-protein kinase SMG1	410.2	6.46	-0.22	9606.ENSP00000402515	n.a.
Q96QK1	Vacuolar protein sorting-associated protein 35	91.6	5.49	-0.31	9606.ENSP00000299138	3.39
Q96S44	TP53-regulating kinase	28.1	9.54	-0.29	9606.ENSP00000361186	n.a.
Q96S55	ATPase WRNIP1	72.1	6.1	-0.47	9606.ENSP00000370150	1.91
Q96T76	MMS19 nucleotide excision repair protein homolog	113.2	6.35	0.16	9606.ENSP00000359818	n.a.
Q99426	Tubulin-folding cofactor B	27.3	5.15	-0.54	9606.ENSP00000221855	361
Q99459	Cell division cycle 5-like protein	92.2	8.18	-0.96	9606.ENSP00000360532	3.88
Q99460	26S proteasome non-ATPase regulatory subunit 1	105.8	5.39	-0.23	9606.ENSP00000309474	203
Q99471	Prefoldin subunit 5	17.3	6.33	-0.27	9606.ENSP00000334188	n.a.
Q99497	Protein deglycase DJ-1	19.9	6.79	0.01	9606.ENSP00000340278	2194
Q99504	Eyes absent homolog 3	62.6	5.21	-0.45	9606.ENSP00000362978	n.a.
Q99536	Synaptic vesicle membrane protein VAT-1 homolog	41.9	6.29	-0.04	9606.ENSP00000347872	97.9
Q99543	DnaJ homolog subfamily C member 2	72	8.7	-1.08	9606.ENSP00000368565	89.7
Q99598	Translin-associated protein X	33.1	6.55	-0.56	9606.ENSP00000355599	90.6
Q99613	Eukaryotic translation initiation factor 3 subunit C	105.3	5.68	-0.79	9606.ENSP00000332604	93.7
Q99615	DnaJ homolog subfamily C member 7	56.4	6.96	-0.72	9606.ENSP00000406463	385
Q99627	COP9 signalosome complex subunit 8	23.2	5.38	-0.08	9606.ENSP00000346340	0.278
Q99700	Ataxin-2	140.2	9.57	-0.83	9606.ENSP00000366843	2.24
Q99707	Methionine synthase	140.4	5.58	-0.20	9606.ENSP00000355536	n.a.
Q99714	3-hydroxyacyl-CoA dehydrogenase type-2	26.9	7.78	0.23	9606.ENSP00000168216	69.2
Q99733	Nucleosome assembly protein 1-like 4	42.8	4.69	-0.78	9606.ENSP00000369915	136
Q99798	Aconitate hydratase, mitochondrial	85.4	7.61	-0.34	9606.ENSP00000216254	113
Q99829	Copine-1	59	5.83	-0.24	9606.ENSP00000317257	364

Q99832	T-complex protein 1 subunit eta	59.3	7.65	-0.10	9606.ENSP00000258091	289
Q99873	Protein arginine N-methyltransferase 1	41.5	5.43	-0.22	9606.ENSP00000406162	1442
Q99956	Dual specificity protein phosphatase 9	41.8	6.11	-0.23	9606.ENSP00000345853	n.a.
Q99961	Endophilin-A2	41.5	5.43	-0.73	9606.ENSP00000269886	n.a.
Q9BPU6	Dihydropyrimidinase-related protein 5	61.4	7.2	-0.15	9606.ENSP00000288699	10.1
Q9BPX3	Condensin complex subunit 3	114.3	5.59	-0.15	9606.ENSP00000251496	21.8
Q9BPX5	Actin-related protein 2/3 complex subunit 5-like protein	16.9	6.6	-0.39	9606.ENSP00000259477	6.29
Q9BQ52	Zinc phosphodiesterase ELAC protein 2	92.2	7.9	-0.32	9606.ENSP00000337445	10.7
Q9BQ67	Glutamate-rich WD repeat-containing protein 1	49.4	4.92	-0.47	9606.ENSP00000253237	n.a.
Q9BQ70	Transcription factor 25	76.6	6.35	-0.60	9606.ENSP00000263346	2.05
Q9BQA1	Methylosome protein 50	36.7	5.17	-0.01	9606.ENSP00000235090	266
Q9BQE3	Tubulin alpha-1C chain	49.9	5.1	-0.23	9606.ENSP00000301072	102
Q9BR76	Coronin-1B	54.2	5.88	-0.32	9606.ENSP00000340211	171
Q9BRG1	Vacuolar protein-sorting-associated protein 25	20.7	6.34	-0.46	9606.ENSP00000253794	n.a.
Q9BRS2	Serine/threonine-protein kinase RIO1	65.5	6.19	-0.89	9606.ENSP00000369162	5.84
Q9BRT9	DNA replication complex GINS protein SLD5	26	4.98	-0.51	9606.ENSP00000276533	n.a.
Q9BRX2	Protein pelota homolog	43.3	6.34	-0.37	9606.ENSP00000274311	n.a.
Q9BRX5	DNA replication complex GINS protein PSF3	24.5	5.34	-0.49		n.a.
Q9BSD7	Cancer-related nucleoside-triphosphatase	20.7	9.54	-0.13	9606.ENSP00000355587	50.2
Q9BSV6	tRNA-splicing endonuclease subunit Sen34	33.6	8.43	-0.44	9606.ENSP00000305524	n.a.
Q9BT78	COP9 signalosome complex subunit 4	46.2	5.83	-0.31	9606.ENSP00000264389	71.7
Q9BTE3	Mini-chromosome maintenance complex-binding protein	72.9	5.87	-0.34	9606.ENSP00000353098	19.9
Q9BTE6	Alanyl-tRNA editing protein Aarsd1	45.5	6.42	-0.40	9606.ENSP00000386621	n.a.
Q9BTE7	DCN1-like protein 5	27.5	5.58	-0.46	9606.ENSP00000260247	n.a.
Q9BTT0	Acidic leucine-rich nuclear phosphoprotein 32 family member E	30.7	3.85	-1.18	9606.ENSP00000324074	n.a.
Q9BTW9	Tubulin-specific chaperone D	132.5	6.19	-0.01	9606.ENSP00000347719	28.4
Q9BTY7	Protein HGH1 homolog	42.1	4.81	-0.13	9606.ENSP00000321320	n.a.
Q9BU89	Deoxyhypusine hydroxylase	32.9	4.83	-0.18	9606.ENSP00000250937	n.a.
Q9BUF5	Tubulin beta-6 chain	49.8	4.88	-0.33	9606.ENSP00000318697	509
Q9BUJ2	Heterogeneous nuclear ribonucleoprotein U-like protein 1	95.7	6.92	-1.08	9606.ENSP00000375863	54.6
Q9BUL8	Programmed cell death protein 10	24.7	8.19	-0.42	9606.ENSP00000376506	0.439
Q9BUT1	3-hydroxybutyrate dehydrogenase type 2	26.7	7.65	-0.02	9606.ENSP00000296424	23.5
Q9BV86	N-terminal Xaa-Pro-Lys N-methyltransferase 1	25.4	5.52	-0.24	9606.ENSP00000361558	59.5
Q9BVA1	Tubulin beta-2B chain	49.9	4.89	-0.41	9606.ENSP00000259818	1273
Q9BVM2	Protein DPCD	23.2	9.03	-0.61	9606.ENSP00000359170	n.a.
Q9BW83	Intraflagellar transport protein 27 homolog	20.5	5.41	-0.06	9606.ENSP00000393541	n.a.
Q9BWD1	Acetyl-CoA acetyltransferase, cytosolic	41.3	6.92	0.20	9606.ENSP00000356015	298
Q9BWH6	RNA polymerase II-associated protein 1	152.7	6.38	-0.07	9606.ENSP00000306123	n.a.
Q9BWJ5	Splicing factor 3B subunit 5	10.1	6.35	-0.84	9606.ENSP00000356541	n.a.
Q9BXJ9	N-alpha-acetyltransferase 15, NatA auxiliary subunit	101.2	7.42	-0.62	9606.ENSP00000296543	63.8
Q9BXP5	Serrate RNA effector molecule homolog	100.6	5.96	-1.13	9606.ENSP00000314491	60.3
Q9BXS5	AP-1 complex subunit mu-1	48.6	7.3	-0.28	9606.ENSP00000388996	144
Q9BXW9	Fanconi anemia group D2 protein	164	5.88	-0.17	9606.ENSP00000287647	1.94
Q9BY32	Inosine triphosphate pyrophosphatase	21.4	5.66	-0.17	9606.ENSP00000369456	n.a.
Q9BZX2	Uridine-cytidine kinase 2	29.3	6.7	-0.41	9606.ENSP00000356853	n.a.
Q9C0B1	Alpha-ketoglutarate-dependent dioxygenase FTO	58.2	5.22	-0.54	9606.ENSP00000418823	3.05
Q9C0C9	(E3-independent) E2 ubiquitin-conjugating enzyme	141.2	5.12	-0.54	9606.ENSP00000323687	42.3
Q9GZS3	WD repeat-containing protein 61	33.6	5.47	-0.19	9606.ENSP00000267973	384
Q9GZT3	SRA stem-loop-interacting RNA-binding protein, mitochondrial	12.3	10.24	-0.58	9606.ENSP00000450909	456
Q9GZZ9	Ubiquitin-like modifier-activating enzyme 5	44.8	4.84	-0.25	9606.ENSP00000348565	18
Q9H0A8	COMM domain-containing protein 4	21.8	7.31	0.07	9606.ENSP00000267935	n.a.
Q9H0B6	Kinesin light chain 2	68.9	7.15	-0.73	9606.ENSP00000314837	12.2
Q9H0C8	Integrin-linked kinase-associated serine/threonine phosphatase 2C	42.9	7.09	-0.48	9606.ENSP00000254654	30.8
Q9H0F7	ADP-ribosylation factor-like protein 6	21.1	8.54	-0.19	9606.ENSP00000337722	n.a.
Q9H0U4	Ras-related protein Rab-1B	22.2	5.73	-0.31	9606.ENSP00000310226	555
Q9H0W8	Protein SMG9	57.6	7.01	-0.48	9606.ENSP00000270066	1.46
Q9H1A4	Anaphase-promoting complex subunit 1	216.4	6.3	-0.13	9606.ENSP00000339109	2.13
Q9H223	EH domain-containing protein 4	61.1	6.76	-0.38	9606.ENSP00000220325	10.7
Q9H2G2	STE20-like serine/threonine-protein kinase	142.6	5.15	-0.99	9606.ENSP00000358770	10.4
Q9H2H8	Peptidyl-prolyl cis-trans isomerase-like 3	18.1	6.79	-0.46		n.a.
Q9H2M9	Rab3 GTPase-activating protein non-catalytic subunit	155.9	5.62	-0.18	9606.ENSP00000351832	3.99
Q9H2P9	Diphthine methyl ester synthase	31.6	5.31	-0.06	9606.ENSP00000359127	n.a.
Q9H2U2	Inorganic pyrophosphatase 2, mitochondrial	37.9	7.39	-0.52	9606.ENSP00000343885	68
Q9H307	Pinin	81.6	7.14	-1.41	9606.ENSP00000216832	90.8
Q9H3P2	Negative elongation factor A	57.2	9.03	-0.42	9606.ENSP00000372335	23.2
Q9H3P7	Golgi resident protein GCP60	60.6	5.06	-0.92	9606.ENSP00000355777	71.2
Q9H3U1	Protein unc-45 homolog A	103	6.07	-0.11	9606.ENSP00000407487	21.8
Q9H4A3	Serine/threonine-protein kinase WNK1	250.6	6.34	-0.39	9606.ENSP00000313059	17.7
Q9H4A4	Aminopeptidase B	72.5	5.74	-0.21	9606.ENSP00000295640	154
Q9H4L7	SWI/SNF-related matrix-associated actin-dependent regulator of chromatin subfamily A containing DEAD/H box 1	117.3	5.55	-0.59	9606.ENSP00000351947	6.26
Q9H4M9	EH domain-containing protein 1	60.6	6.83	-0.36	9606.ENSP00000320516	9.61
Q9H6T3	RNA polymerase II-associated protein 3	75.7	6.84	-0.80	9606.ENSP00000005386	0.622
Q9H773	dCTP pyrophosphatase 1	18.7	5.03	-0.46	9606.ENSP00000322524	420
Q9H8Y8	Golgi reassembly-stacking protein 2	47.1	4.82	-0.14	9606.ENSP00000234160	8.25
Q9H944	Mediator of RNA polymerase II transcription subunit 20	23.2	6.87	0.01	9606.ENSP00000265350	n.a.
Q9H9A6	Leucine-rich repeat-containing protein 40	68.2	6.43	-0.21	9606.ENSP00000359990	n.a.

Q9H9Q2	COP9 signalosome complex subunit 7b	29.6	6.15	-0.34	9606.ENSP00000272995	n.a.
Q9HAV4	Exportin-5	136.2	5.8	-0.05	9606.ENSP00000265351	13.7
Q9HB07	UPF0160 protein MYG1, mitochondrial	42.4	6.67	-0.41	9606.ENSP00000267103	n.a.
Q9HB71	Calcyclin-binding protein	26.2	8.25	-0.79	9606.ENSP00000356652	2714
Q9HBM1	Kinetochore protein Spc25	26.1	8	-0.72	9606.ENSP00000282074	n.a.
Q9HC35	Echinoderm microtubule-associated protein-like 4	108.8	6.4	-0.54	9606.ENSP00000320663	44.1
Q9HCK8	Chromodomain-helicase-DNA-binding protein 8	290.3	6.47	-0.67	9606.ENSP00000382863	0.138
Q9HCN8	Stromal cell-derived factor 2-like protein 1	23.6	7.03	-0.35	9606.ENSP00000248958	169
Q9NP79	Vacuolar protein sorting-associated protein VTA1 homolog	33.9	6.29	-0.52	9606.ENSP00000356602	n.a.
Q9NPA3	Mid1-interacting protein 1	20.2	5.5	-0.46	9606.ENSP00000338706	10.3
Q9NPD8	Ubiquitin-conjugating enzyme E2 T	22.5	7.99	-0.68	9606.ENSP00000356243	n.a.
Q9NPF4	Probable tRNA N6-adenosine threonylcarbamoyltransferase	36.4	6.35	0.00	9606.ENSP00000206542	116
Q9NQG5	Regulation of nuclear pre-mRNA domain-containing protein 1B	36.9	5.97	-0.67	9606.ENSP00000362532	n.a.
Q9NQR4	Omega-amidase NIT2	30.6	7.21	-0.19	9606.ENSP00000377696	9.49
Q9NQT5	Exosome complex component RRP40	29.6	8.1	-0.07	9606.ENSP00000323046	5.88
Q9NQW7	Xaa-Pro aminopeptidase 1	69.9	5.67	-0.25	9606.ENSP00000421566	41.1
Q9NR31	GTP-binding protein SAR1a	22.4	6.68	-0.08	9606.ENSP00000362335	n.a.
Q9NR45	Sialic acid synthase	40.3	6.74	-0.33	9606.ENSP00000210444	0.465
Q9NR50	Translation initiation factor eIF-2B subunit gamma	50.2	6.47	-0.11	9606.ENSP00000353575	0.822
Q9NRF9	DNA polymerase epsilon subunit 3	16.8	4.74	-1.20	9606.ENSP00000363284	n.a.
Q9NRY4	Rho GTPase-activating protein 35	170.4	6.64	-0.49	9606.ENSP00000385720	1.43
Q9NRZ9	Lymphoid-specific helicase	97	7.93	-0.55	9606.ENSP00000239027	18.7
Q9NSD9	Phenylalanine--tRNA ligase beta subunit	66.1	6.84	-0.12	9606.ENSP00000281828	71.7
Q9NTJ3	Structural maintenance of chromosomes protein 4	147.1	6.79	-0.69	9606.ENSP00000341382	80.1
Q9NTK5	Obg-like ATPase 1	44.7	7.81	-0.40	9606.ENSP00000284719	1096
Q9NTX5	Ethylmalonyl-CoA decarboxylase	33.7	8.21	-0.16	9606.ENSP00000436585	39.2
Q9NU22	Midasin	632.4	5.68	-0.37	9606.ENSP00000358400	5.98
Q9NUQ8	ATP-binding cassette sub-family F member 3	79.7	6.34	-0.39	9606.ENSP00000411471	13.9
Q9NUU7	ATP-dependent RNA helicase DDX19A	53.9	6.58	-0.38	9606.ENSP00000306117	14.5
Q9NV35	Probable 8-oxo-dGTP diphosphatase NUDT15	18.6	6.14	-0.57	9606.ENSP00000258662	1.17
Q9NVA2	Septin-11	49.4	6.81	-0.70	9606.ENSP00000264893	96.7
Q9NVE7	Pantothenate kinase 4	85.9	6.28	-0.20	9606.ENSP00000367727	1.01
Q9NVI1	Fanconi anemia group I protein	149.2	6.74	-0.10	9606.ENSP00000310842	5.08
Q9NVS9	Pyridoxine-5'-phosphate oxidase	30	7.06	-0.65	9606.ENSP00000225573	137
Q9NWS0	PIH1 domain-containing protein 1	32.3	5.14	-0.44	9606.ENSP00000262265	23.4
Q9NWY4	UPF0609 protein C4orf27	39.4	6.8	-0.53	9606.ENSP00000406598	3.13
Q9NX46	Poly(ADP-ribose) glycohydrolase ARH3	38.9	5.07	-0.16	9606.ENSP00000362273	7.92
Q9NXF7	DDB1- and CUL4-associated factor 16	24.2	6.04	-0.53	9606.ENSP00000371682	n.a.
Q9NY27	Serine/threonine-protein phosphatase 4 regulatory subunit 2	46.9	4.54	-1.07	9606.ENSP00000349124	95.6
Q9NY33	Dipeptidyl peptidase 3	82.5	5.1	-0.32	9606.ENSP00000353701	90
Q9NYF8	Bcl-2-associated transcription factor 1	106.1	9.98	-1.63	9606.ENSP00000435210	197
Q9NYL9	Tropomodulin-3	39.6	5.19	-0.58	9606.ENSP00000308753	157
Q9NYU2	UDP-glucose:glycoprotein glucosyltransferase 1	177.1	5.63	-0.33	9606.ENSP00000259253	32.5
Q9NYV4	Cyclin-dependent kinase 12	164.1	9.44	-0.91	9606.ENSP00000398880	4.09
Q9NZL9	Methionine adenosyltransferase 2 subunit beta	37.5	7.36	-0.34	9606.ENSP00000325425	138
Q9NZT2	Opioid growth factor receptor	73.3	4.84	-1.08	9606.ENSP00000290291	0.48
Q9P000	COMM domain-containing protein 9	21.8	5.88	0.01	9606.ENSP00000263401	n.a.
Q9P016	Thymocyte nuclear protein 1	25.7	9.25	-0.86	9606.ENSP00000341657	122
Q9P258	Protein RCC2	56	8.78	-0.42	9606.ENSP00000364582	38.5
Q9P287	BRCA2 and CDKN1A-interacting protein	36	4.61	-0.69	9606.ENSP00000357748	31.9
Q9P289	Serine/threonine-protein kinase 26	46.5	5.29	-0.46	9606.ENSP00000377867	46.8
Q9P2I0	Cleavage and polyadenylation specificity factor subunit 2	88.4	5.11	-0.39	9606.ENSP00000298875	28.5
Q9P2J5	Leucine--tRNA ligase, cytoplasmic	134.4	7.3	-0.40	9606.ENSP00000377954	164
Q9UBB4	Ataxin-10	53.5	5.25	-0.08	9606.ENSP00000252934	42.4
Q9UBB9	Tuftelin-interacting protein 11	96.8	5.67	-0.64	9606.ENSP00000383892	12.1
Q9UBE0	SUMO-activating enzyme subunit 1	38.4	5.3	-0.30	9606.ENSP00000270225	469
Q9UBF2	Coatomer subunit gamma-2	97.6	5.81	-0.11	9606.ENSP00000393912	30.6
Q9UBI1	COMM domain-containing protein 3	22.1	5.99	-0.37	9606.ENSP00000366032	n.a.
Q9UBL3	Set1/Ash2 histone methyltransferase complex subunit ASH2	68.7	5.69	-0.61	9606.ENSP00000340896	57.6
Q9UBQ5	Eukaryotic translation initiation factor 3 subunit K	25	4.93	-0.17	9606.ENSP00000248342	150
Q9UBQ7	Glyoxylate reductase/hydroxypyruvate reductase	35.6	7.39	-0.01	9606.ENSP00000313432	19.1
Q9UBT2	SUMO-activating enzyme subunit 2	71.2	5.29	-0.44	9606.ENSP00000246548	540
Q9UBV8	Peflin	30.4	6.54	-0.53	9606.ENSP00000362807	n.a.
Q9UBW8	COP9 signalosome complex subunit 7a	30.3	8.22	-0.27	9606.ENSP00000229251	n.a.
Q9UG63	ATP-binding cassette sub-family F member 2	71.2	7.37	-0.50	9606.ENSP00000222388	141
Q9UHB9	Signal recognition particle subunit SRP68	70.7	8.56	-0.55	9606.ENSP00000312066	167
Q9UHD1	Cysteine and histidine-rich domain-containing protein 1	37.5	7.87	-0.73	9606.ENSP00000319255	1121
Q9UHD8	Septin-9	65.4	8.97	-0.66	9606.ENSP00000391249	107
Q9UHI6	Probable ATP-dependent RNA helicase DDX20	92.2	6.95	-0.46	9606.ENSP00000358716	3.24
Q9UHJ6	Sedoheptulokinase	51.5	6.83	0.04	9606.ENSP00000225519	11.9
Q9UHV9	Prefoldin subunit 2	16.6	6.58	-0.59	9606.ENSP00000356989	787
Q9UHX1	Poly(U)-binding-splicing factor PUF60	59.8	5.29	-0.16	9606.ENSP00000434359	268
Q9UI12	V-type proton ATPase subunit H	55.8	6.48	-0.37	9606.ENSP00000352522	12.3
Q9UI26	Importin-11	112.5	5.25	-0.04	9606.ENSP00000386992	2
Q9UI30	Multifunctional methyltransferase subunit TRM112-like protein	14.2	5.26	-0.15	9606.ENSP00000438349	76.2
Q9UJ70	N-acetyl-D-glucosamine kinase	37.4	6.24	0.00	9606.ENSP00000389087	2.09
Q9UJC3	Protein Hook homolog 1	84.6	5.15	-0.81	9606.ENSP00000360252	4.06

Q9ULT8	E3 ubiquitin-protein ligase HECTD1	289.2	5.35	-0.45	9606.ENSP00000382269	12.4
Q9ULV4	Coronin-1C	53.2	7.08	-0.35	9606.ENSP00000261401	340
Q9UM54	Unconventional myosin-VI	149.6	8.53	-0.68	9606.ENSP00000358994	20.3
Q9UMS4	Pre-mRNA-processing factor 19	55.1	6.61	-0.17	9606.ENSP00000227524	664
Q9UN37	Vacuolar protein sorting-associated protein 4A	48.9	7.8	-0.53	9606.ENSP00000254950	n.a.
Q9UNE7	E3 ubiquitin-protein ligase CHIP	34.8	5.87	-0.81	9606.ENSP00000219548	46.4
Q9UNF0	Protein kinase C and casein kinase substrate in neurons protein 2	55.7	5.2	-1.03	9606.ENSP00000263246	17.1
Q9UNF1	Melanoma-associated antigen D2	64.9	9.32	-0.53	9606.ENSP00000218439	31.8
Q9UNH7	Sorting nexin-6	46.6	6.16	-0.60	9606.ENSP00000355217	53.2
Q9UNM6	26S proteasome non-ATPase regulatory subunit 13	42.9	5.81	-0.18		n.a.
Q9UNS1	Protein timeless homolog	138.6	5.4	-0.52	9606.ENSP00000450607	n.a.
Q9UP83	Conserved oligomeric Golgi complex subunit 5	92.7	6.6	-0.18	9606.ENSP00000297135	0.328
Q9UPN9	E3 ubiquitin-protein ligase TRIM33	122.5	6.67	-0.54	9606.ENSP00000351250	11.7
Q9UPU5	Ubiquitin carboxyl-terminal hydrolase 24	294.2	6.14	-0.24	9606.ENSP00000294383	3.64
Q9UQ35	Serine/arginine repetitive matrix protein 2	299.4	12.06	-1.36	9606.ENSP00000301740	23
Q9UQ80	Proliferation-associated protein 2G4	43.8	6.55	-0.50	9606.ENSP00000302886	948
Q9UQE7	Structural maintenance of chromosomes protein 3	141.5	7.18	-0.87	9606.ENSP00000354720	101
Q9Y224	UPF0568 protein C14orf166	28.1	6.65	-0.46	9606.ENSP00000261700	0.244
Q9Y230	RuvB-like 2	51.1	5.64	-0.23	9606.ENSP00000473172	135
Q9Y248	DNA replication complex GINS protein PSF2	21.4	5.44	-0.41	9606.ENSP00000253462	n.a.
Q9Y262	Eukaryotic translation initiation factor 3 subunit L	66.7	6.34	-0.47	9606.ENSP00000416892	166
Q9Y265	RuvB-like 1	50.2	6.42	-0.25	9606.ENSP00000318297	595
Q9Y266	Nuclear migration protein nudC	38.2	5.38	-1.04	9606.ENSP00000319664	924
Q9Y285	Phenylalanine--tRNA ligase alpha subunit	57.5	7.8	-0.45	9606.ENSP00000320309	39.2
Q9Y295	Developmentally-regulated GTP-binding protein 1	40.5	8.9	-0.16	9606.ENSP00000329715	26
Q9Y2L1	Exosome complex exonuclease RRP44	108.9	7.14	-0.47	9606.ENSP00000366997	54
Q9Y2Q3	Glutathione S-transferase kappa 1	25.5	8.41	-0.13		n.a.
Q9Y2W1	Thyroid hormone receptor-associated protein 3	108.6	10.15	-1.63	9606.ENSP00000346634	280
Q9Y2Z0	Protein SGT1 homolog	41	5.16	-0.60	9606.ENSP00000367208	103
Q9Y314	Nitric oxide synthase-interacting protein	33.2	8.82	-0.52	9606.ENSP00000375726	12.3
Q9Y371	Endophilin-B1	40.8	6.04	-0.42		n.a.
Q9Y383	Putative RNA-binding protein Luc7-like 2	46.5	10.01	-1.49	9606.ENSP00000347005	40.2
Q9Y3A5	Ribosome maturation protein SBDS	28.7	8.75	-0.50	9606.ENSP00000246868	49.9
Q9Y3B2	Exosome complex component CSL4	21.4	8.24	-0.12	9606.ENSP00000359939	1.74
Q9Y3B4	Splicing factor 3B subunit 6	14.6	9.38	-0.59	9606.ENSP00000233468	186
Q9Y3C6	Peptidyl-prolyl cis-trans isomerase-like 1	18.2	7.99	-0.30	9606.ENSP00000362803	685
Q9Y3D0	Mitotic spindle-associated MMXD complex subunit MIP18	17.7	5.19	-0.16	9606.ENSP00000387471	3.58
Q9Y3D8	Adenylate kinase isoenzyme 6	20	4.58	-0.58		n.a.
Q9Y3F4	Serine-threonine kinase receptor-associated protein	38.4	5.12	-0.32	9606.ENSP00000392270	96.5
Q9Y3I0	tRNA-splicing ligase RtcB homolog	55.2	7.23	-0.23	9606.ENSP00000216038	507
Q9Y3U8	60S ribosomal protein L36	12.2	11.59	-0.83	9606.ENSP00000252543	2160
Q9Y3Z3	Deoxynucleoside triphosphate triphosphohydrolase SAMHD1	72.2	7.14	-0.53	9606.ENSP00000262878	78.1
Q9Y450	HBS1-like protein	75.4	6.61	-0.38	9606.ENSP00000356811	3.66
Q9Y490	Talin-1	269.6	6.07	-0.24	9606.ENSP00000316029	73.1
Q9Y4B6	Protein VPRBP	168.9	5.06	-0.34	9606.ENSP00000393183	32.5
Q9Y4C2	TRPM8 channel-associated factor 1	102.1	6.54	-0.04	9606.ENSP00000419235	n.a.
Q9Y4L1	Hypoxia up-regulated protein 1	111.3	5.22	-0.55	9606.ENSP00000384144	24.8
Q9Y4U1	Methylmalonic aciduria and homocystinuria type C protein	31.7	7.81	-0.36	9606.ENSP00000383840	n.a.
Q9Y5K5	Ubiquitin carboxyl-terminal hydrolase isozyme L5	37.6	5.33	-0.43	9606.ENSP00000356425	53.6
Q9Y5L4	Mitochondrial import inner membrane translocase subunit Tim13	10.5	8.18	-0.51	9606.ENSP00000215570	426
Q9Y5N6	Origin recognition complex subunit 6	28.1	8.66	-0.33	9606.ENSP00000219097	3.61
Q9Y5P6	Mannose-1-phosphate guanyltransferase beta	39.8	6.61	0.07		n.a.
Q9Y5Q8	General transcription factor 3C polypeptide 5	59.5	6.9	-0.61	9606.ENSP00000361180	15.8
Q9Y5Y2	Cytosolic Fe-S cluster assembly factor NUBP2	28.8	5.83	0.13	9606.ENSP00000262302	39.7
Q9Y613	FH1/FH2 domain-containing protein 1	126.5	6.39	-0.30	9606.ENSP00000258201	1.53
Q9Y617	Phosphoserine aminotransferase	40.4	7.66	0.02	9606.ENSP00000365773	433
Q9Y678	Coatomer subunit gamma-1	97.7	5.47	-0.14	9606.ENSP00000325002	39.8
Q9Y6B6	GTP-binding protein SAR1b	22.4	6.11	-0.07	9606.ENSP00000385432	n.a.
Q9Y6D9	Mitotic spindle assembly checkpoint protein MAD1	83	5.92	-0.87	9606.ENSP00000265854	n.a.
Q9Y6E2	Basic leucine zipper and W2 domain-containing protein 2	48.1	6.68	-0.39	9606.ENSP00000258761	60.2
Q9Y6G9	Cytoplasmic dynein 1 light intermediate chain 1	56.5	6.42	-0.40	9606.ENSP00000273130	384
Q9Y6K9	NF-kappa-B essential modulator	48.2	5.71	-0.86	9606.ENSP00000358622	n.a.
Q9Y6Y8	SEC23-interacting protein	111	5.54	-0.42	9606.ENSP00000358071	95.7

Identified interactors of the Hsp16 core family

UniProtID	Hsp16.11	Hsp16.2	Hsp16.41	Hsp16.48	MW [kDa]	calc. pI	GRAVY index	String ID	abundance [ppm]
Q95Y90	x	x	x	x	21.508	10.08	-0.22	6239.R13A5.8.1	2950
Q18115	x	x	x	x	106.008	7.55	-0.20	6239.C23G10.4b.2	260
P34574	x	x	x	x	191.542	5.67	-0.29	6239.T20G5.1.1	341
Q07750	x	x	x	x	23.578	5.59	-0.34	6239.C38C3.5b.1	1995
Q19564	x	x	x	x	37.608	8.13	-0.41	6239.F18E3.7a.2	109
Q93235	x	x	x	x	36.672	7.47	-0.48	6239.C17E4.9.3	401
P27798	x	x	x	x	45.616	4.57	-1.07	6239.Y38A10A.5.1	1889
Q18823	x	x	x	x	181.213	4.71	-0.63	6239.C54D1.5.1	144
P49405	x	x	x	x	33.386	9.76	-0.71	6239.F54C9.5.1	3464
P10299	x	x	x	x	23.901	5.91	-0.41	6239.R107.7.2	841
Q09545	x	x	x	x	32.891	UNDEFINED	-0.21	6239.F42A8.2.1	268
O44480	x	x	x	x	20.959	10.38	-0.58	6239.E04A4.8.1	3269
O02485	x	x	x	x	35.591	6.86	-0.10	6239.ZK1073.1.1	392
P29355	x	x	x	x	26.21	6.08	-0.63	6239.C14F5.5	54.5
Q9NEN6	x	x	x	x	28.136	10.26	-0.79	6239.Y71A12B.1.2	4153
P41932	x	x	x	x	28.191	4.72	-0.59	6239.M117.2.1	1754
Q22494	x	x	x	x	54.213	5.90	-0.43	6239.T14F9.1.3	335
Q9XTI0	x	x	x	x	31.217	8.20	0.15	6239.B0250.5	359
Q27464	x	x	x	x	60.215	8.19	-0.40	6239.B0035.5.1	115
Q17820	x	x	x	x	38.738	5.26	-0.21	6239.C08B6.9.2	94.5
Q17761	x	x	x	x	53.196	6.44	-0.09	6239.T25B9.9.2	277
P47209	x	x	x	x	59.406	5.41	-0.16	6239.C07G2.3a.1	781
O01802	x	x	x	x	28.132	10.16	-0.67	6239.F53G12.10.2	2156
Q09450	x	x	x	x	56.114	6.53	-0.09	6239.C05C10.3.2	310
Q18801	x	x	x	x	44.489	5.99	-0.23	6239.C53B4.7b	73.3
D0PV95	x	x	x	x	76.343	6.60	-0.83	6239.Y71H2AM.19.1	199
O16259	x	x	x	x	36.962	6.58	-0.77	6239.R09E12.3	309
O16520	x	x	x	x	62.165	6.93	-0.23	6239.T05H4.6.1	223
Q27522	x	x	x	x	43.949	6.12	-0.13	6239.T13A10.11a.1	52.7
Q22782	x	x	x	x	23.365	5.93	-0.36	6239.T25G12.4	164
P34686	x	x	x	x	30.786	5.02	-0.69	6239.M106.5.1	212
G5EGK8	x	x	x	x	36.302	5.06	-0.40	6239.F38H4.9.1	257
Q9N4J8	x	x	x	x	60.457	7.96	-0.23	6239.F54A3.3	481
Q9U2G0	x	x	x	x	243.831	5.84	-0.33	6239.Y46G5A.4	80.6
G5ED41	x	x	x	x	141.726	5.49	-0.08	6239.Y102A5A.1	152
O18178	x	x	x	x	61.835	6.93	-0.26	6239.W08G11.4	148
Q9U2X0	x	x	x	x	39.771	5.44	-0.31	6239.Y113G7B.17.1	497
Q19722	x	x	x	x	61.186	5.94	-0.37	6239.F22D6.3a.1	481
Q7JKC3	x	x	x	x	131.597	5.44	-0.45	6239.H19N07.2c	116
Q19052	x	x	x	x	64.02	9.24	-0.50	6239.E04D5.1a.1	118
P34685	x	x	x	x	32.181	6.02	-0.63	6239.D2024.6.2	582
P18948	x	x	x	x	193.318	6.76	-0.70	6239.K07H8.6c	1689
Q21215	x	x	x	x	35.83	6.47	-0.32	6239.K04D7.1.4	2350
P41988	x	x	x	x	58.803	6.08	0.04	6239.T05C12.7.1	540
Q8WTM6	x	x	x	x	34.48	7.76	-0.46	6239.Y6D11A.2.2	277
Q94148	x	x	x	x	22.712	6.96	-0.35	6239.T23H2.5.1	168
P52013	x	x	x	x	21.927	9.20	-0.12	6239.F31C3.1.2	1021
P51875	x	x	x	x	40.451	5.28	-0.36	6239.C26C6.2.2	180
Q17602	x	x	x	x	147.968	8.78	-0.42	6239.C03D6.4	52
P48154	x	x	x	x	28.961	9.62	-0.56	6239.F56F3.5.2	3372
Q22169	x	x	x	x	21.563	9.05	-0.04	6239.T04G9.5.1	104
Q18688	x	x	x	x	80.283	4.96	-0.54	6239.C47E8.5.4	1825
Q21693	x	x	x	x	25.727	5.79	-0.57	6239.R04A9.4	96.4
O45218	x	x	x	x	66.559	6.36	-0.19	6239.Y50D7A.7	185
Q93714	x	x	x	x	38.466	UNDEFINED	-0.06	6239.F43G9.1.2	760
Q23670	x	x	x	x	172.334	8.63	-0.73	6239.K12D12.1	162
P40614	x	x	x	x	36.674	9.10	0.20	6239.F01G4.6b.2	503
Q9U332	x	x	x	x	14.261	10.10	-0.84	6239.W09C5.6a.1	640
P02567	x	x	x	x	223.323	5.79	-0.82	6239.R06C7.10.1	761
Q17345	x	x	x	x	33.838	5.16	-0.06	6239.Y56A3A.20.2	77
Q22799	x	x	x	x	10.344	6.81	-0.38	6239.T26A5.9.2	1599
P34690	x	x	x	x	49.913	4.93	-0.26	6239.C47B2.3.1	995
P21137	x	x	x	x	46.346	5.85	-0.31	6239.ZK909.2c	42.3
Q9GZH4	x	x	x	x	65.737	6.30	-0.27	6239.T22D1.4	274
P50093	x	x	x	x	32.668	9.75	-0.24	6239.T24H7.1.2	455
Q18040	x	x	x	x	46.454	UNDEFINED	-0.09	6239.C16A3.10a.1	814
O62431	x	x	x	x	88.262	7.58	-0.36	6239.Y41E3.4a.2	348
Q18787	x	x	x	x	48.611	6.08	-0.44	6239.C52E4.4.2	475
Q9U1Q4	x	x	x	x	118.921	6.26	-0.40	6239.Y87G2A.5	268
Q93572	x	x	x	x	33.774	6.29	-0.13	6239.F25H2.10.2	3227
P34545	x	x	x	x	222.415	8.63	-0.85	6239.R10E11.1b	25.5

Q18211	x	x	x	x	61.485	5.32	-0.46	6239.C26D10.1.1	238
Q17361	x	x	x	x	55.878	5.38	-0.55	6239.C13B4.2.1	286
Q17963	x	x	x	x	40.393	6.30	-0.31	6239.C14B1.4	38.6
O45495	x	x	x	x	15.921	7.84	-0.66	6239.F39B2.2.1	340
Q21219	x	x	x	x	94.109	5.97	0.01	6239.K04E7.2.1	6.76
Q07749	x	x	x	x	17.046	6.31	-0.39		
P02566	x	x	x	x	224.755	5.57	-0.87	6239.F11C3.3.2	1555
P50880	x	x	x	x	45.659	10.41	-0.67	6239.F13B10.2a.1	3852
O17622	x	x	x	x	21.202	5.41	-0.27	6239.C29F7.3	307
P12845	x	x	x	x	223.048	5.99	-0.82	6239.T18D3.4	633
P47991	x	x	x	x	24.313	10.99	-0.43	6239.R151.3.1	3294
P34575	x	x	x	x	51.54	UNDEFINED	-0.09	6239.T20G5.2.2	1092
P48152	x	x	x	x	27.314	9.63	-0.32	6239.C23G10.3.2	3122
Q22235	x	x	x	x	87.112	4.95	-0.57	6239.T05E11.3a.2	529
P27639	x	x	x	x	45.408	5.00	-0.25	6239.F57B9.6a.2	681
Q21313	x	x	x	x	404.23	5.19	-0.49	6239.K08C7.3a.1	89.7
P34462	x	x	x	x	28.786	9.23	-0.39	6239.F55H2.2.1	387
P43510	x	x	x	x	42.404	5.40	-0.49	6239.C25B8.3a	292
P34334	x	x	x	x	18.31	11.15	-0.66	6239.C14B9.7.1	3075
P34409	x	x	x	x	67.942	6.57	-0.55	6239.F22B7.6a	0.08
Q19869	x	x	x	x	16.075	11.28	-0.73	6239.F28C6.7a.2	1969
P46975	x	x	x	x	85.122	8.92	0.17	6239.T12A2.2.2	25.1
Q94218	x	x	x	x	66.581	6.96	-0.37	6239.F38A5.1a	85.8
P53013	x	x	x	x	50.668	9.07	-0.30	6239.R03G5.1a.3	2984
Q9N4A7	x	x	x	x	34.692	6.55	-0.43	6239.Y77E11A.13a	88.2
Q18212	x	x	x	x	48.493	5.55	-0.36	6239.C26D10.2a.2	301
P52011	x	x	x	x	18.55	8.88	-0.31	6239.Y75B12B.5.1	1418
G5EBN9	x	x	x	x	67.391	6.87	0.47	6239.T13B5.1.1	33.5
Q95XX1	x	x	x	x	63.347	6.19	-0.13	6239.Y54G2A.17b	61.2
P12844	x	x	x	x	225.51	5.51	-0.82	6239.K12F2.1	499
Q9BI88	x	x	x	x	19.411	4.69	-0.57	6239.F46B6.12.2	63.6
P17343	x	x	x		37.406	5.62	-0.22	6239.F13D12.7a.1	386
O01692	x	x	x		14.938	9.85	-0.79	6239.T08B2.10.2	4319
P34313	x	x	x		17.123	8.80	-0.60	6239.C07A9.2.2	181
Q02335	x	x	x		64.867	6.05	-0.33	6239.ZK370.8.1	71.3
P52709	x	x	x		84.417	7.11	-0.59	6239.C47D12.6a	199
P52819	x	x	x		14.946	9.80	-0.65	6239.C27A2.2a.3	3251
Q95ZJ1	x	x		x	71.382	6.46	-0.54	6239.Y39E4B.12a.1	8.46
Q95QW0	x	x		x	62.476	5.22	-0.37	6239.C17G10.9a.1	216
O44199	x	x		x	150.396	7.45	-0.84	6239.T04H1.4b.1	14.7
Q9U2A8	x	x		x	10.102	10.41	-0.42	6239.Y48B6A.2.2	1978
P46576	x	x		x	47.127	9.23	-0.04	6239.C34E10.1.1	45.5
O01803	x	x		x	23.429	6.44	-0.39	6239.F53G12.1.2	173
P36573	x	x		x	31.81	6.12	-0.60	6239.W09H1.6b	1155
P34460	x	x		x	22.704	4.38	-0.09	6239.F54H12.6	3684
P47207	x	x		x	56.975	5.65	-0.05	6239.T21B10.7.1	585
Q9N4X8	x	x		x	24.796	5.51	-0.34	6239.Y45G12C.2	108
Q17335	x	x		x	41.292	5.96	0.06	6239.H24K24.3b.1	127
P46769	x	x		x	30.703	5.48	-0.29	6239.B0393.1.2	2211
Q09531	x	x		x	57.911	7.94	-0.72	6239.F07F6.4.2	99.9
Q09289	x	x		x	39.773	4.75	-0.56	6239.C56G2.7.1	751
Q17688	x	x		x	47.197	5.60	-0.46	6239.C06A6.5	78.3
P48158	x		x	x	14.955	10.55	-0.14	6239.B0336.10.1	2310
Q18143	x		x	x	120.199	7.96	-0.29	6239.C25A8.4	5.82
Q93873	x		x	x	54.563	UNDEFINED	-0.21	6239.K09A9.5	86.2
Q21752	x		x	x	29.961	9.20	-0.19	6239.R05G6.7.2	2550
Q23381	x		x	x	81.683	UNDEFINED	-0.24	6239.ZK1058.1.1	245
Q18090	x		x	x	32.386	7.10	-0.09	6239.C18E9.6	121
Q09517	x		x	x	34.309	9.53	0.15	6239.C56G2.6b	172
Q07085	x		x	x	61.825	5.87	-0.35	6239.F13H6.3.2	89.8
Q09533	x		x	x	24.749	10.36	-0.67	6239.F10B5.1.2	2348
Q10454	x		x	x	44.168	6.83	-0.36	6239.F46H5.3a.2	1868
P53596	x		x	x	33.798	8.83	-0.09	6239.C05G5.4.1	1303
P46554	x		x	x	37.816	5.65	-0.33	6239.B0285.4	50.1
Q18678	x		x	x	55.22	5.97	-0.42	6239.C47E12.1.2	364
O45933	x		x	x	41.726	8.05	-0.33	6239.Y43F4B.4.2	82.4
Q9N358	x		x	x	59.734	5.84	-0.18	6239.Y55F3AR.3	685
Q8MXS1	x		x	x	22.62	5.49	-0.29	6239.Y92C3B.3b	80.8
Q05036	x		x	x	86.897	5.30	-0.45	6239.C30C11.4.2	555
Q04908	x		x	x	57.507	7.14	-0.41	6239.C30C11.2.1	368
Q9XV52	x		x	x	83.654	6.15	-0.40	6239.F29C12.4.2	133
Q20655	x		x	x	28.067	4.78	-0.64	6239.F52D10.3a.2	2464
Q27888	x		x	x	36.065	6.42	0.10	6239.F13D12.2.2	249
P29691	x		x	x	94.796	6.10	-0.22	6239.F25H5.4a.2	2156
O45903	x		x	x	38.195	8.51	-0.26	6239.W09H1.5	116
Q17632	x		x	x	108.786	6.04	-0.38	6239.C04G2.6	44.2
Q09581	x		x	x	33.641	7.17	-0.64	6239.ZK892.1d	421

O45228	x		x	x	69.823	UNDEFINED	-0.46	6239.B0513.5.1	91.2
Q95YF3	x		x	x	48.713	8.27	-0.24	6239.C07H6.5.2	272
P17331	x		x	x	36.427	7.68	-0.03	6239.F33H1.2	714
Q23500	x		x	x	96.66	5.49	-0.05	6239.ZK455.1.2	654
Q10039		x	x	x	84.15	8.38	-0.34	6239.T10F2.1a	433
O62146		x	x	x	66.638	6.11	-0.42	6239.F09B12.3	278
Q17426		x	x	x	64.631	6.07	-0.44	6239.B0024.11	24.3
Q10943		x	x	x	20.522	6.19	-0.22	6239.B0336.2.1	595
Q21554		x	x	x	125.718	5.13	-0.03	6239.M18.5.1	35.7
Q9N5R9	x	x			116.865	5.54	-0.65	6239.F55A3.3.1	75.8
P45969	x	x			37.36	4.88	-0.35	6239.T09A5.9.2	188
Q17334	x	x			37.697	6.07	0.09	6239.K12G11.3	1581
P34540	x	x			91.894	6.04	-0.68	6239.R05D3.7	162
G5EFP5	x	x			45.744	8.25	-0.29	6239.F59E12.13.3	27.2
Q03598	x	x			18.537	5.95	-0.38	6239.C40H1.6.1	28.6
O44857	x	x			85.422	5.75	-0.42		
P46550	x	x			58.905	5.88	-0.16	6239.F01F1.8a.1	677
Q09475	x	x			194.097	6.34	-0.36	6239.C28H8.3.1	108
O01510	x	x			265.479	7.91	-0.29	6239.C48B6.6a	1.66
P05690	x	x			187.722	6.19	-0.59	6239.C42D8.2a	1644
P06125	x	x			186.439	6.55	-0.55	6239.C04F6.1	995
P46548	x		x		50.889	7.21	-0.30	6239.T17E9.2b	208
Q95XP9	x		x		71.096	5.33	-0.25	6239.Y39G10AR.2a	47.3
P02513	x		x		16.299	5.52	-0.57	6239.T27E4.9	57.8
O61820	x		x		50.72	5.80	-0.27	6239.B0511.10.2	127
P91374	x		x		24.125	11.64	-1.11	6239.K11H12.2.1	2356
Q20875	x		x		84.389	8.27	-0.42	6239.F56D2.6a.1	82
Q9TZC4	x		x		52.26	6.23	-0.16	6239.C29F9.7	61.5
Q20585	x			x	47.584	6.36	-0.38	6239.F49C12.8.1	380
Q9N3X2	x			x	29.044	10.47	-0.35	6239.Y43B11AR.4.1	3482
Q10901	x			x	54.676	8.22	0.57	6239.C12D12.2a.1	49.9
P06581	x			x	16.252	5.94	-0.59	6239.Y46H3A.2	34
P34346	x			x	27.925	8.98	-0.42	6239.C29E4.8.1	469
Q20970	x			x	101.714	8.00	-0.38	6239.F58B3.5a	127
P49049	x			x	52.794	8.99	0.25	6239.T05E11.5	68.4
O62327	x			x	18.152	6.73	-0.27	6239.R05H10.5	288
O44451	x			x	38.141	5.24	0.04	6239.C04C3.3.2	478
G5EEH9	x			x	180.454	9.17	-0.47	6239.ZK328.5b	66.9
Q10657	x			x	26.574	6.23	0.00	6239.Y17G7B.7.2	926
Q965S8	x			x	36.873	5.29	-0.46	6239.Y74C10AR.1	134
P48727	x			x	37.792	6.34	-0.32	6239.F56C9.1.1	215
Q18803	x			x	14.834	9.73	-0.08	6239.C53B7.4.2	336
Q95Q95	x			x	306.529	8.57	-0.31	6239.B0261.2a.2	24.2
P49029	x			x	17.637	5.15	-0.62	6239.R09B3.5.1	542
P90795	x			x	80.807	7.45	-0.31	6239.T25G3.4.2	137
Q94051	x			x	26.291	5.34	-0.08	6239.T13F2.8a	587
Q18685	x			x	82.355	6.52	-0.55	6239.C47E8.7.2	97.3
Q9U2D9	x			x	76.459	5.84	-0.34	6239.Y46G5A.31	216
Q20390	x			x	33.984	8.15	-0.25	6239.F44C4.5	49.9
P53585	x			x	121.616	6.60	-0.19	6239.D1005.1.2	114
Q09996	x			x	134.52	6.17	-0.37	6239.R74.1.2	206
P41956	x			x	19.982	UNDEFINED	0.44	6239.T07C4.7.1	48.6
Q9BKU4	x			x	29.988	6.94	-0.05	6239.Y37E3.9.1	1037
Q23232	x			x	43.639	5.70	-0.28	6239.Y102E9.2b.1	200
Q9XWH0	x			x	38.127	7.71	-0.30	6239.Y54G9A.6	92.5
P53588	x			x	47.419	5.70	-0.02	6239.F47B10.1.1	532
P34563	x			x	17.867	5.15	-0.44	6239.T05G5.10a	1095
Q23312		x	x		22.058	9.90	-0.36	6239.ZC434.2.2	3052
P19826		x	x		111.922	6.20	-0.49	6239.ZC477.9a	196
Q23280			x	x	19.431	4.34	-0.89	6239.ZC395.10.2	1871
Q9XWI6			x	x	83.065	5.67	-0.57	6239.Y54E2A.11a.1	134
P47208			x	x	58.391	6.13	-0.08	6239.K01C8.10.3	905
Q27535			x	x	40.382	8.57	-0.46	6239.ZC434.8.2	413
O61742	x				37.348	4.54	-0.40	6239.B0205.3.2	567
Q04457	x				63.722	4.90	-0.33	6239.R12A1.4.2	47.1
P53489	x				44.841	6.15	-0.23	6239.K07C5.1.2	164
Q22633	x				44.383	5.40	-0.30	6239.T21C12.2	389
O17732	x				129.285	6.53	-0.20	6239.D2023.2a.3	348
P41847	x				25.551	4.63	-0.24	6239.T20B12.7.2	400
Q9TXP0	x				9.347	9.44	-0.15	6239.F56E10.4.1	389
P91427	x				44.113	6.53	-0.05	6239.T03F1.3.1	1288
P90747	x				131.973	7.25	0.08	6239.C10C6.6.1	34.6
Q9XUY5	x				35.75	6.75	-0.41	6239.F55F3.3.2	175
P51403	x				28.96	10.12	-0.36	6239.C49H3.11.3	1995
Q9U2M7	x				15.889	5.96	-0.51	6239.Y37H9A.6.1	85.2
Q86S66	x				22.078	4.97	-0.76	6239.Y65B4BR.5b.1	2269
P34183	x				58.559	8.50	-0.33	6239.T11G6.1b.1	441

Q17693	x				75.487	5.26	-0.37	6239.C06A8.1a.2	109
P49180	x				13.768	11.26	-0.39	6239.F10E7.7.1	3229
Q23449	x				28.795	5.56	-0.22	6239.ZK20.5.1	170
O18229	x				30.414	5.16	-0.37	6239.Y57G11C.3a	176
Q18493	x				53.497	5.96	-0.26	6239.C36A4.4.1	168
Q9XXU9	x				43.459	7.68	-0.26	6239.Y38F2AL.3a	498
Q9Y194	x				61.097	7.02	-0.11	6239.Y66H1B.4	130
Q21153	x				79.595	8.26	-0.18	6239.K02F3.2	149
P54412	x				44.388	6.29	-0.36	6239.F17C11.9a	1056
Q9XUE6	x				28.839	5.34	-0.40	6239.F52B11.2a	64.7
Q22021	x				18.75	10.04	-0.41	6239.R53.4.1	419
Q968Y9	x				207.124	6.50	-0.48	6239.Y55D5A.5a	6.83
P11141	x				70.845	5.61	-0.32	6239.C37H5.8	1016
O62106	x				26.308	4.71	0.25	6239.C47B2.5.2	228
Q11067		x			47.728	5.70	-0.31	6239.B0403.4	505
O01541		x			106.782	5.51	-0.35	6239.F28H1.3.3	399
Q20228		x			21.957	10.53	-0.63	6239.F40F8.10.1	2415
Q18359		x			17.335	9.33	-0.57	6239.C33A12.1	350
Q09278		x			36.018	5.17	-0.54	6239.C45G9.5	48.4
Q09580			x		82.606	5.95	-0.20	6239.M106.4b	88.4
Q19338			x		181.546	6.01	0.08	6239.F11A10.4b	15.1
P91079			x		52.085	6.63	-0.31	6239.C23H3.4a.3	73.2
Q22099			x		65.136	5.71	-0.44	6239.T02G5.9b	286
P90980				x	78	6.99	-0.48	6239.E01H11.1c	5.67
Q22307				x	144.214	6.63	-0.39	6239.T07D4.3.2	40.9
P34519				x	34.219	UNDEFINED	-0.02	6239.K11H3.3	172
O44750				x	69.34	6.19	-0.31	6239.W03G9.4.2	188
Q93353				x	41.553	6.56	-0.09	6239.C37E2.1.1	307
O02621				x	18.424	6.34	-0.38	6239.F26E4.12	59.2
Q27497				x	37.205	5.77	-0.28	6239.F29F11.6b	169
Q27257				x	33.135	9.07	0.16	6239.F49E8.5.1	128
G5EDP2				x	44.386	7.55	-0.14	6239.Y57A10C.6.1	361

Publications

Mymrikov, E. V., M. Daake, B. Richter, M. Haslbeck and J. Buchner (2017). "The Chaperone Activity and Substrate Spectrum of Human Small Heat Shock Proteins." J Biol Chem **292**(2): 672-684.

Schneider, M., M. Rosam, M. Glaser, A. Patronov, H. Shah, K. C. Back, M. A. Daake, J. Buchner and I. Antes (2016). "BiPPred: Combined sequence- and structure-based prediction of peptide binding to the Hsp70 chaperone BiP." Proteins **84**(10): 1390-1407.

Schoppner, P., G. Csaba, T. Braun, M. Daake, B. Richter, O. F. Lange, M. Zacharias, R. Zimmer and M. Haslbeck (2016). "Regulatory Implications of Non-Trivial Splicing: Isoform 3 of Rab1A Shows Enhanced Basal Activity and Is Not Controlled by Accessory Proteins." J Mol Biol **428**(8): 1544-1557.

Eckl, J. M., M. Daake, S. Schwartz and K. Richter (2016). "Nucleotide-Free sB-Raf is Preferentially Bound by Hsp90 and Cdc37 In Vitro." J Mol Biol **428**(20): 4185-4196.

Lerchner, A., M. Daake, A. Jarasch and A. Skerra (2016). "Fusion of an alcohol dehydrogenase with an aminotransferase using a PAS linker to improve coupled enzymatic alcohol-to-amine conversion." Protein Eng Des Sel **29**(12): 557-562.

Fleckenstein, T., A. Kastenmuller, M. L. Stein, C. Peters, M. Daake, M. Krause, D. Weinfurtner, M. Haslbeck, S. Weinkauf, M. Groll and J. Buchner (2015). "The Chaperone Activity of the Developmental Small Heat Shock Protein Sip1 Is Regulated by pH-Dependent Conformational Changes." Mol Cell **58**(6): 1067-1078.

Eckl, J. M., M. J. Scherr, L. Freiburger, M. A. Daake, M. Sattler and K. Richter (2015). "Hsp90.Cdc37 Complexes with Protein Kinases Form Cooperatively with Multiple Distinct Interaction Sites." J Biol Chem **290**(52): 30843-30854.

Danksagung

An erster Stelle möchte ich mich bei meinem Doktorvater Prof. Dr. Johannes Buchner für die Betreuung meiner Doktorarbeit bedanken. Die interessanten und fordernden Fragestellungen und Diskussionen in Kombination mit der hervorragenden Infrastruktur am Lehstuhl und dem nötigen kreativen Freiraum haben im wesentlichen zum Gelingen dieser Arbeit beigetragen.

Dr. Martin Haslbeck möchte ich für die Einführung in die spannende Welt der sHsps, die wissenschaftlichen Diskussionen dazu und die Unterstützung bei organisatorischen Problemen danken. Ein weitere besonderer Dank gilt Fr. Rubinstein für ihre immerzu freundliche Art und ihre Hilfe in allen bürokratischen Angelegenheiten.

Großer Dank gebührt außerdem Bettina Richter für die großartige Unterstützung bei der MS-Probenvorbereitung und die generelle Unterstützung im Laboralltag.

Des weiteren möchte ich mich bei Katja Bäuml, Matthial Stahl, Anja Fux und Dr. Nina Bach für die gute Zusammenarbeit an den Orbitraps und den Austausch in MS-Fragen bedanken. Danke auch an Gina Feind für die MALDI-Messungen.

Vielen Dank auch an Dr. Hyun-Seo Kang für die Durchführung und Analyse der NMR-Experimente, sowie Dr. Beate Rockel für die EM Analysen zu Hsp26. Außerdem danke ich Prof. Dr. Sevil Weinkauf und Prof. Dr. Michael Sattler für die wissenschaftlichen Diskussionen zu Hsp26.

Besonderer Dank gilt Dr. Evgeny Mymrikov für die großartige Zusammenarbeit an dem Projekt zu den humanen sHsps sowie für die Durchführung der CoIP-Experimente.

Ein großes Dankeschön auch an Regina Rettenmaier für ihre Unterstützung bei der Analyse der Hsp26 Phosphomutanten und später auch im Hsp16er-Projekt.

Dr. Christine John und Philipp Schmid danke ich für die Durchführung der AUC Messungen.

Ganz besonders bedanken möchte ich mich außerdem bei allen „Office2-Generationen“, die ich durchlebt habe. Vielen Dank an Christine, Katrin, Chris, Betty, Moritz, Pamina und Jannis für die schöne gemeinsame Zeit. Danke auch an Chrissy, Patzi, Sabine, Mathias, Katha, Mareike, Bene, Franzi und Philipp für die entspannten Mittags- und Gummibärchenpausen sowie die ein oder andere Jogging-Einheit und allen anderen Mitgliedern des Buuuuuuchner-Lehrstuhl, durch die ich die Zeit hier sicherlich immer in guter Erinnerung behalten werde.

Ein riesiger Dank gilt außerdem Martin und meinen Eltern, die mich immer unterstützt und gefördert haben! Danke!!!

Eidesstattliche Erklärung

Hiermit erkläre ich an Eides statt, dass ich die vorliegende Arbeit selbstständig verfasst und keine anderen als die angegebenen Quellen und Hilfsmittel verwendet habe. Die aus fremden Quellen übernommenen Gedanken sind als solche kenntlich gemacht. Die vorliegende Arbeit wurde noch keiner anderen Prüfungsbehörde vorgelegt. Teile dieser Arbeit wurden in wissenschaftlichen Journalen veröffentlicht.

Garching, den ....

Marina Kreuzeder